UNIVERSITY OF LIVERPOOL

Investigating Mitochondrial Impairment as a Mechanism of Statin-Induced Muscle Toxicity

Thesis submitted in accordance with the requirements of the University of Liverpool for the degree of Doctor in Philosophy

by

Samantha Wendy Jones

June 2019

Declaration

This thesis is the result of my own work. The material contained within this thesis has not been presented, nor is currently being presented, either wholly or in part for any other degree or qualification.

Samantha Wendy Jones

This research was carried out in the Department of Molecular and Clinical Pharmacology, in the Institute of Translational Medicine, at the University of Liverpool.

Acknowledgements

It would be impossible to not first thank my supervisors, Professor Ana Alfirevic, Dr Amy Chadwick and Dr Dan Carr as well as the Medical Research Council (MRC) and the PREDICTION-ADR Consortium for providing me with the opportunity and the funding to undertake this PhD project. A special mention should also be extended to both Ana and Amy. I'll always be extremely grateful for the support, guidance and encouragement that you've given me over the past four years, you truly are a supervisory dream team.

I would also like to give my thanks to all the past and present members of Team Bioenergetics, particularly Amy, Sophie, Carol and Laleh. Thank you for always knowing how to make me laugh, being a shoulder to cry on and listening to me complain for four years straight, your patience knows no bounds. This journey would not have been the same without you and you've helped me to grow as a person and a scientist in so many ways.

Most importantly, I'd like to dedicate this thesis to my grandparents. You've always worked to give me the best possible opportunities in life and I appreciate you more than you'll ever know. Whilst you may not understand any of this work, I hope that you'll still try to humour me and read it, but most of all I hope that I have made you proud.

Contents Table

Acknowledgements iii

Research Communications v

Abstract vi

Abbreviations viii

Chapter 1 General Introduction 1

Chapter 2 Assessing the Differential Effects of Simvastatin Lactone and β-Hydroxy Acid upon Mitochondrial Respiratory Chain Function 53

Chapter 3 The Generation of Three-Dimensional, Tissue-Engineered Skeletal Myobundles to Assess Drug-Induced Mitochondrial Dysfunction 97

Chapter 4 Utilising Myobundles to Investigate Inter-individual Susceptibility to Statin-Induced Mitochondrial Dysfunction 130

Chapter 5 Mitochondrial DNA Haplogroup-Disease Association Study for Statin-Related Myopathy 153

Chapter 6 General Discussion 179

Appendices 188

Bibliography 220

Research Communications

Publications

A.L. Ball, **S.W. Jones**, A. Alfirevic, J.J. Lyon, A.E. Chadwick, The Role of MtDNA Variation in Drug Response: A Systematic Review**.** *Manuscript in preparation (2019).*

S.W. Jones, K. Bloch, A.L. Ball, A.E. Chadwick, A. Alfirevic, Mitochondrial Genome Sequencing of a Statin Myopathy Case-Control Cohort. *Manuscript in preparation* (2019).

S.W. Jones, G. Truskey, A.E Chadwick, A. Alfirevic, The Generation of Miniaturised, Tissue-Engineered Skeletal Micro-Tissues to Assess Statin-Mediated Mitochondrial Impairment. *Manuscript in preparation (2019).*

Conference Communications

2016: Poster presentation, Chemical biology approaches to assessing and modulating mitochondria, The Royal Society, Milton Keynes.

2016: Poster presentation, MiTOX Annual Meeting, University of Oxford.

2017: Poster presentation, British Toxicological Society Annual Congress, Liverpool.

2017: Poster presentation, MiTOX Annual Meeting, University of Oxford.

2018: Invited Speaker, UK MYONET, King's Collage, London.

2018: Poster presentation, British Pharmacological Society Annual Congress, London.

Training Placements

2016: Professor Hans Zischka, Helmholtz Centre for Environmental Research, Institute of Molecular Toxicology and Pharmacology, Munich, Germany. Techniques: Semi-automated mitochondrial isolations.

2017: Professor George Truskey, Pratt School of Engineering, Department of Biomedical Engineering, Duke University, North Carolina, USA. Techniques: Skeletal muscle micro-tissue engineering.

Abstract

Statins, also known as 3-hydroxy-3-methylglutaryl coenzyme A reductase (HMG-CoAR) inhibitors, are currently the pharmaceutical intervention strategy of choice for the primary and secondary prevention of atherosclerotic disorders that are related to hypercholesterolemia. In most recipients, statin therapy is effective and well tolerated, however the most significant barrier to cardiovascular disease (CVD) risk reduction is the development of adverse effects, of which statin-related myopathies (SRM) are the most frequently reported. The aetiological basis of SRM is both complex and multifaceted, with no clear dose-response relationship and a plethora of generalised and genetic risk factors identified to date. However, the deleterious effects of statins upon mitochondrial function has been implicated as one of several putative mechanisms by which myopathic symptoms may be potentiated in some patients.

Therefore, the aim of this research was to establish the effects of statin chemical species (i.e. inactive lactones versus active β-hydroxy acids) upon the functionality of the mitochondrial electron transport chain using high resolution respirometry. Thereafter, the remainder of the thesis focussed upon the development of three-dimensional, bioengineered micro-tissue models of human skeletal muscle to identify functional bioenergetic factors which may confer enhanced or diminished risk of statin-mediated mitochondrial dysfunction. Finally, due to the governance of respiratory chain assembly, stability and functionality by the mitochondrial genome, next generation sequencing (NGS) of patient mitochondrial DNA was performed for a statin myopathy case-control cohort to determine if there was an association between mitochondrial genotype and patient phenotype.

Preliminary *in vitro* investigations performed using the L6 myoblast cell line identified succinate dehydrogenase (complex II) driven respiration as a major, but not an exclusive target of simvastatin-mediated mitochondrial dysfunction over acute and extended dosing regimens. Following the assessment of simvastatin-mediated mitochondrial dysfunction in a murine cell line, a cohort of statin-naïve, statin-tolerant and statin-intolerant patients were recruited via the Liverpool Musculoskeletal Biobank (LMB) before isolation of satellite cells from skeletal muscle biopsy samples. The satellite cells were then used to generate biomimetic, engineered micro-tissues known as myobundles. Examination of baseline bioenergetic parameters in patient derived myobundles showed that individuals belonging to the statin-tolerant group exhibited a greater spare respiratory capacity than both the

statin-naïve and statin-intolerant patients, a trait linked to increased succinate dehydrogenase activity and cell survival.

Finally, the mitochondrial DNA haplogroups of 264 statin myopathy cases, 291 statin-tolerant controls and 342 healthy volunteers were resolved using NGS and HaploGrep2 software (phylotree build 17) before performing a haplogroup-disease association study. Within this study, a significant association between mitochondrial macro-haplogroup assignment and statin related myopathy was not identified. The distribution of mitochondrial haplogroups in both the case and control groups resembled that of the healthy volunteer cohort and the Northern European population.

To conclude, statin-mediated mitochondrial dysfunction has a role to play in the development of myopathic symptoms amongst susceptible patients. However, this research has also identified enhanced spare respiratory capacity as a potential protective factor amongst statin-tolerant individuals. What is less clear is the relative contributions of direct respiratory inhibition and/or modulation of peripheral pathways which interact with the wider mitochondrial signalling network, to the overall pathophysiological mechanism.

Abbreviations

A-band	Anisotropic band
ABC	ATP-binding cassette
ACA	6-aminocaproic acid
ACAD	Acyl-CoA dehydrogenase
ACC	American College of Cardiology
ACE	Angiotensin converting enzyme
ADP	Adenosine diphosphate
ADR	Adverse drug reaction
AHA	American Heart Association
AKT	Protein kinase B
ALF	Acute liver failure
ALR	ATP-linked respiration
ALT	Alanine transaminase
AMPK	5' AMP-activated protein kinase
ANOVA	Analysis of Variance
ATCC	American Type Culture Collection
ATP	Adenosine triphosphate
AVA	Atorvastatin β-hydroxy acid
BCA	Bicinchoninic acid
BMI	Body mass index
BR	Basal respiration
BSA	Bovine serum albumin
BWA-MEM	Burrows-Wheeler Alignment
Ca^{2+}	Calcium ion
CACT	Carnitine acylcarnitine translocase

CGR	Centre for Genomic Research
CK	Creatine kinase
CLC-1	Chloride channel 1
C_{max}	Maximum serum concentration
CoA	Coenzyme A
CO_2	Carbon dioxide
CoQ10	Ubiquinone
$CoQ10H_2$	Ubiquinol
COX	Cytochrome oxidase
CPTI/II	Carnitine palmitoyltransferase I/II
CRF	Case report form
$Cu^{1+/2+}$	Copper (I) oxide/ Cupric ion
CVA	Cerivastatin β-hydroxy acid
CVD	Cardiovascular disease
CVL	Cerivastatin lactone
CYP450	Cytochrome P450
Cyt *c*	Cytochrome *c*
DCI	Dodecenoyl-CoA delta isomerase
DILI	Drug-induced liver injury
D-loop	Displacement loop
DM	Diabetes mellitus
DMEM	Dulbecco's modified eagle medium
DMSO	Dimethyl sulfoxide
DNA	Deoxyribonucleic acid
dNTPs	Deoxyribonucleotide triphosphate
dsDNA	Double-stranded DNA
ECAR	Extracellular acidification rate

ECL	Enhanced chemiluminescence reagent
ECM	Extracellular matrix
EDTA	Ethylenediaminetetraacetic acid
EFG	Elongation factors
EGTA	Ethylene glycol-bis (β-aminoethyl ether)-N,N,N′,N′-tetraacetic acid
ER	Endoplasmic reticulum
ETC	Electron transport chain
FAD	Flavin adenine dinucleotide
$FADH_2$	Reduced flavin adenine dinucleotide
FAO	Fatty acid oxidation
FATPs	Fatty acid transport proteins
FBS	Foetal bovine serum
FCCP	Carbonyl cyanide 4-(trifluoromethoxy) phenylhydrazone
FDA	Food and Drug Administration
$Fe^{2+/3+}$	Ferrous ion (II/III)
FMN	Flavin mononucleotide
FOG	Fast oxidative/glycolytic
FPP	Farnesyl pyrophosphate
GATK	Genome Analysis Tool Kit
GFR	Growth factor reduced
GGPP	Geranylgeranyl pyrophosphate
GLUT	Glucose transporter
GSPx	Glutathione peroxidases
G3PDH	Glycerol-3-phosphate dehydrogenase
HBSS	Hank's buffered saline solution
HCl	Hydrochloric acid
HDL-C	High density lipoprotein cholesterol

HEPES	4-(2-hydroxyethyl)-1-piperazineethanesulfonic acid
HMG-CoAR	3-hydroxy-3-methylglutaryl coenzyme A reductase
hPSC	Human pluripotent stem cells
HRP	Horseradish peroxidase
HSKMDC	Human skeletal muscle derived cells
HSP	Heavy strand promotors
H-strand	Heavy strand
H_2O_2	Hydrogen peroxide
I-band	Isotropic band
IC_{50}	Half maximal inhibitory concentration
IF	Initiation factor
IFC	Integrated fluidic circuit
IGF1	Insulin-like growth factor
IMM	Inner mitochondrial membrane
IMS	Inter-membrane space
ISP	Reiske iron-sulphur protein
KCl	Potassium chloride
KH_2PO_4	Potassium phosphate monobasic
LDH	Lactate dehydrogenase
LDL	Low density lipoprotein
LDL-C	Low density lipoprotein cholesterol
LDL-R	Low density lipoprotein receptor
LMB	Liverpool Musculoskeletal Biobank
LSP	Light strand promoter
L-strand	Light strand
MAS	Mitochondrial assay solution
MCAD	Medium chain acyl-CoA dehydrogenase

MCHAD	Medium chain hydroxyacyl-CoA dehydrogenase
MCKAT	Medium chain 3-ketoacyl-CoA thiolase
MCT1/4	Monocarboxylate transporter 1/4
Mg^{2+}	Magnesium ion
$MgCl_2$	Magnesium chloride
MHC	Myosin heavy chain
MMP	Mitochondrial membrane potential
MnSOD	Manganese superoxide dismutase
MOPS	3-(N-morpholino)propanesulfonic acid
MPTP	Mitochondrial permeability transition pore
MRCA	Most recent common ancestor
MRC	Maximal respiratory capacity
MRF	Myogenic regulatory factor
mtDNA	Mitochondrial DNA
MTERF1	Mitochondrial transcription termination factor 1
MTOR	Mechanistic target of rapamycin
MTP	Mitochondrial trifunctional protein
mtRRF	Mitochondrial ribosome recycling factors
mtSSB	Mitochondrial single stranded binding protein
MuRF1	Muscle RING-finger protein 1
MyoG	Myogenin
NAD	Nicotinamide adenine dinucleotide
NADH	Reduced nicotinamide adenine dinucleotide
NaOH	Sodium hydroxide
nDNA	Nuclear DNA
NGS	Next generation sequencing
NHLBI	National Heart, Lung and Blood Institute

NHS	National Health Service
NICE	The National Institute for Health and Care Excellence
NO	Nitric oxide
NSAID	Non-steroidal anti-inflammatory drug
OCR	Oxygen consumption rate
O_H	Heavy strand origin
O_L	Light strand origin
OMI	Non-linear optical molecular imaging
OMM	Outer mitochondrial membrane
OR	Odds ratio
OSCP	Oligomycin sensitive conferral protein
OXPHOS	Oxidative phosphorylation
O2K	Oxygraph-2K
O_2^{-}.	Superoxide radical
PBS	Phosphate buffered saline
PCCR	Pump-controlled cell rupture
PCR	Polymerase chain reaction
PDH	Pyruvate dehydrogenase
PDK	Pyruvate dehydrogenase kinase
PDMS	Polydimethylsiloxane
PGC1-α	Peroxisome proliferator-activated receptor gamma coactivator 1-alpha
P_i	Inorganic phosphate
POLG	DNA polymerase gamma
POLMT	Mitochondrial RNA polymerase
PPR_{gly}	Proton pumping rate (glycolysis)
PTFE	Polytetrafluoroethylene
PVA	M-polyvinyl alcohol

QC	Quality control
qPCR	Quantitative PCR
rCRS	Revised Cambridge reference sequence
REC	Research Ethics Committee
Rho 0	Cells lacking mitochondrial DNA
Rho123	Rhodamine 123
RIPA	Radioimmunoprecipitation buffer
RLBUHT	Royal Liverpool and Broadgreen University Hospital Trust
RNA	Ribonucleic acid
RNS	Reactive nitrogen species
ROS	Reactive oxygen species
rPFO	Recombinant perfringolysin O
rRNA	Ribosomal RNA
SAA	Sarcomeric alpha actinin
SAM	Sequence alignment/map
SCAD	Short chain acyl-CoA dehydrogenase
SCHAD	Short chain hydroxyacyl-CoA dehydrogenase
SDS	Sodium dodecyl sulphate
SIRT3	NAD-dependent deacetylase sirtuin-3
SLCO1B1	Solute carrier organic anion transporter
SMTE	Skeletal muscle tissue engineering
SNP	Single nucleotide polymorphism
SO	Slow oxidative
SOP	Standard operating procedure
SRC	Spare respiratory capacity
SRM	Statin-related myopathy
SVA	Simvastatin β-hydroxy acid

SVL	Simvastatin lactone
TBS	Tris buffered saline
TCA	Tricarboxylic acid cycle
TEFM	Transcriptional elongation factor
TES	2-((1,3-dihydroxy-2-(hydroxymethyl)propan-2yl)amino) ethanesulfonic acid
TFAM	Mitochondrial transcription factor A
TMPD	N,N,N',N'-tetramethyl-p-phenylenediamine
tRNA	Transfer RNA
UCP	Uncoupling protein
UDP	Uridine diphosphate
UGT	Uridine diphosphate (UDP)-glucuronosyl-transferase
ULN	Upper limit of normal
VCF	Variant calling format
VDAC	Voltage gated anion channel
VLCAD	Very long chain acyl-CoA dehydrogenase
VLDL	Very low density lipoprotein
XF	Extracellular flux analyser
2D	Two-dimensional
3D	Three-dimensional
ΔP	Proton motive force
Δψ	Mitochondrial membrane potential

Chapter 1

General Introduction

Contents

1.1 Cardiovascular Disease and Statin Therapy 4

1.1.1 The Statin Drug Class 4

1.1.2 Physicochemical Characteristics 4

1.1.3 Chemical Species Interconversion 6

1.1.4 Statin Pharmacokinetics 7

1.1.5 Regulation of Cholesterol Biosynthesis by Statins 8

1.2 The Safety of Statins 10

1.2.1 The Economical and Clinical Significance of Adverse Drug Reactions 10

1.2.2 Statin-Related Hepatic Injury 11

1.2.3 New Onset Type 2 Diabetes Mellitus 11

1.2.4 Statin-Related Myopathy 12

1.2.5 Pathomechanisms of Statin-Related Myopathy 15

1.2.6 Mitochondria and Statin-Related Myopathy 16

1.3 Drug-Induced Myopathies of Skeletal Muscle 20

1.3.1 Compounds Associated with Drug-Induced Myopathies 21

1.4 Skeletal Muscle and Skeletal Muscle Modelling 24

1.4.1 Ultrastructural Arrangement 24

1.4.2 Muscle Fiber Types 26

1.4.3 Muscle Plasticity 28

1.4.4 Developmental Myogenesis and Regeneration 29

1.4.5 Modelling Skeletal Muscle *In Vitro* 30

1.5 Mitochondrial Structure and Respiration 34

1.5.1 Mitochondrial Structure 34

1.5.2 Oxidative Phosphorylation 35

1.5.3 Beta-Oxidation of Fatty Acids 40

1.5.4 Reactive Oxygen Species 42

1.5.5 Regulation of Oxidative Phosphorylation 43

1.6 The Mitochondrial Genome 43

1.6.1 Basic Structure 43

1.6.2 Inheritance 44

1.6.3 Nucleoid Packaging 45

1.6.4 MtDNA Maintenance: Replication, Transcription and Translation 45

1.6.5 Heteroplasmy 47

1.6.6 MtDNA Mutations 48

1.6.7 Mitochondrial Haplogroups 48

1.6.8 MtDNA Variation and Functional Consequence 49

1.7 Models to Assess Mitochondrial Dysfunction 50

1.7.1 Whole Cell Models 50

1.7.2 Isolated Mitochondria 51

1.7.3 Permeabilised Cells 51

1.8 Thesis Aims 51

1.1 Cardiovascular Disease and Statin Therapy

Atherosclerotic cardiovascular disease (CVD) is the leading cause of morbidity and mortality worldwide, accounting for > 17 million deaths globally per annum, a figure currently projected to rise to > 23 million by 2030 (Forouzanfar *et al.*, 2016). Studies conducted in the mid 1900's first identified the relationship between hypercholesterolemia and the onset of cardiovascular disease by utilising ultracentrifugation to separate the different lipoproteins present in patient plasma by floatation (Egom and Hafeez, 2016). It was found that not only did CVD correlate with elevations in plasma cholesterol but that the cholesterol was associated with low density lipoprotein (LDL) specifically. Assimilation of epidemiological studies underpinning this concept have been meta-analysed by The Emerging Risk Factors Collaboration to implicate LDL-cholesterol as one of the main risk factors for developing CVD and high dietary lipid intake as a cause of pathological LDL-cholesterol levels (Danesh *et al.*, 2007). The results of such studies provided the impetus for the discovery of cholesterol and lipid lowering medications.

1.1.1 The Statin Drug Class

Statins, also known as 3-hydroxy-3-methylglutaryl coenzyme A reductase (HMG-CoAR) inhibitors, have been the treatment of choice for atherosclerotic disorders that are related to elevated cholesterol levels (hypercholesterolemia) since their introduction to the clinic in 1987 (Sathasivam, 2012; Feng *et al.*, 2012; Golomb and Evans, 2008). The drug class is extremely effective in reducing both the morbidity and mortality associated with adverse cardiovascular and cerebrovascular events, particularly CVD and stroke in high-risk populations (Silva *et al.*, 2006).

Statins represent the most popular prescription drug class in the developed world, with an estimated 25 % of the global population > 65 years taking statins to manage CVD (Sathasivam, 2012; du Souich *et al.*, 2017). In the UK, the number of patients prescribed statins is increasing due to a review of the eligibility guidelines in 2014 by the National Institute for Health and Care Excellence (NICE). The review broadened eligibility for statin prescription from ≥ 20 % 10-year risk of cardiovascular disease to ≥ 10 % 10-year risk. Ultimately this has the potential to increase the number of patients receiving statin therapy from ~7 million to ~11.5 million (Matthews *et al.*, 2016; Trusler, 2011).

1.1.2 Physicochemical Characteristics

Statins are comprised of two principle components; a β-hydroxy heptanoic acid pharmacophore which is conserved across all statins, and a covalently bonded hydrophobic

ring which is crucial for the close binding to HMG-CoA reductase (Figure 1.1) (Hamelin, 1998; Gazzerro *et al.*, 2012). The pharmacophore is a 'HMG-like' moiety and is able to competitively and reversibly bind to HMG-CoAR with three times more affinity than that of its natural substrate HMG-CoA (Tiwari and Khokhar, 2014).

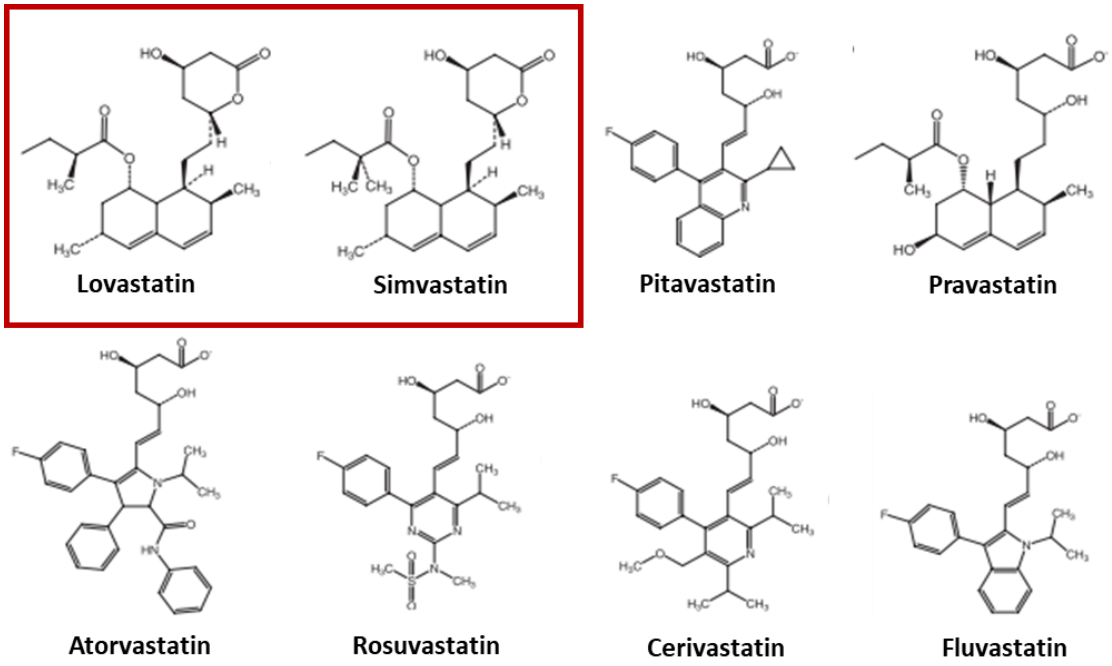

Figure 1.1 Chemical structures of the 8 HMG-CoAR inhibitors. All compounds are represented in their open β-hydroxy heptanoic acid conformation except for lovastatin and simvastatin (red box) which are in their closed lactone ring conformation.

The chemical makeup of the hydrophobic ring structure defines both the solubility of the statin along with many of the pharmacological properties. Simvastatin, lovastatin and pravastatin have a partially reduced naphthalene rings, whereas atorvastatin has a pyrrole, fluvastatin an indole, rosuvastatin a pyrimidine, cerivastatin a pyridine and pitavastatin a quinoline (Gazzerro *et al.*, 2012).

Statins are generally grouped into two types based on their origin. Type 1 statins are natural/fungal derived statins (lovastatin, simvastatin and pravastatin) whereas type 2 statins are synthetically derived. The major functional differences between the two groups are their ability to interact with HMG-CoAR and their overall lipophilicity. Type 2 statins are able to form more interactions with the HMG-CoAR enzyme thus rendering them (rosuvastatin in particular) extremely efficient in reducing enzymatic activity in relation to dosage (Gazzerro *et al.*, 2012; Davidson, 2002).

1.1.3 Chemical Species Interconversion

Unlike the other statins, both simvastatin and lovastatin are administered as inactive lactone 'pro-drugs' which must undergo either enzymatic or non-enzymatic hydrolysis to form an active β-hydroxy acid (Figure 1.2) (Hamelin, 1998; Skottheim *et al.*, 2008).

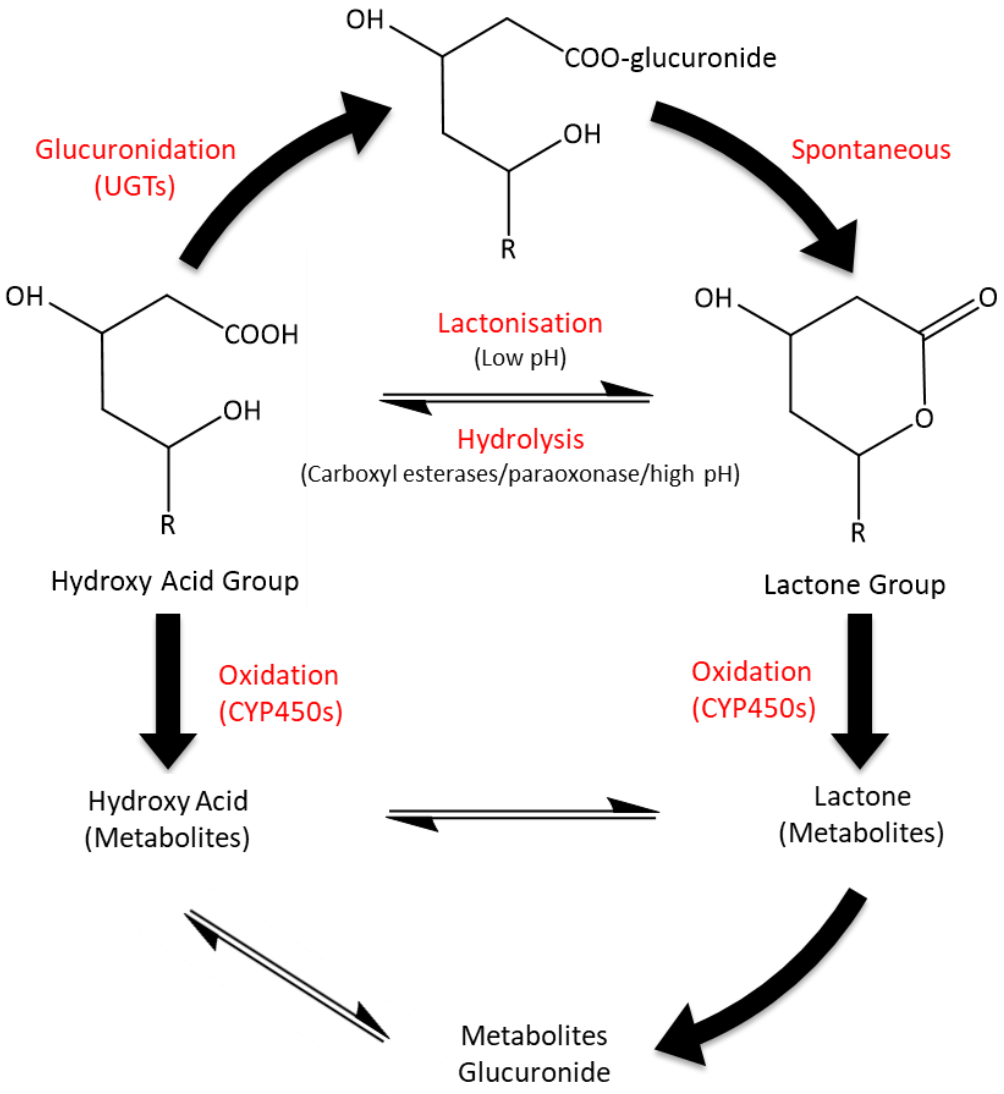

Figure 1.2 Summary of statin chemical species interconversion. Diagram adapted from (Shitara and Sugiyama, 2006). Abbreviations: CYP450, cytochrome P450; UGT, uridine diphosphate (UDP)-glucuronosyl-transferase.

The open acid molecular conformation is essential for the interaction and subsequent inhibition of HMG-CoAR. *In vivo,* all statins whether administered as an active acid or inactive lactone have the potential to interconvert between the two chemical conformations, as well as forming several short lived active metabolites (Prueksaritanont, Subramanian, *et al.*, 2002; Hoffmann and Nowosielski, 2008; Shitara and Sugiyama, 2006).

In the case of simvastatin and lovastatin particularly, the primary mechanism of lactone hydrolysis is thought to be mediated by microsomal carboxyl esterases in the liver, however there is also evidence to suggest that at near physiological or alkaline pH, statin lactones are less stable and equilibrium will substantially favour hydrolysis of the lactone ring and formation of the β-hydroxy acid (Taha *et al.*, 2016, 2017).

Conversely, the lactonisation of active statins *in vivo* has been hypothesised to serve as an intermediate step in statin metabolism whereby the drugs interconvert between the acid and lactone forms until an equilibrium is established. A potential reason for this occurrence is that lactonisation provides a more suitable substrate for the action of cytochrome P450 (CYP) isoform 3A4, an enzyme heavily implicated in the phase I metabolism of lipophilic statins, ultimately aiding in overall drug clearance (Schirris *et al.*, 2015).

The mechanistic basis of statin lactonisation is still under debate, the active β-hydroxy acid is thought to undergo lactonisation non-enzymatically in the presence of low pH conditions such as those in the gastrointestinal tract. However, the leading theory which appears to be conserved across multiple species is the conversion of the statin hydroxy acids to lactones by uridine diphosphate (UDP)-glucuronosyl-transferase (UGTs) conjugation in the liver. UGTs can catalyse the formation of coenzyme A or acyl glucuronide intermediates that, due to instability, rapidly decay to lactones (Schirris *et al.*, 2015; Hoffmann and Nowosielski, 2008).

1.1.4 Statin Pharmacokinetics

At the pharmacokinetic level (i.e. the absorption, distribution, metabolism and excretion of a given drug), the statin class exhibits several important differences between compounds, including half-life, systemic exposure, maximum plasma concentration (C_{max}), bioavailability, lipophilicity, metabolism and excretion routes (Table 1.1). The liver is the primary site of biotransformation for all statins. Their low overall systemic bioavailability is consequential of an important hepatic first-pass effect. With the exception of pravastatin, which is enzymatically transformed in the cytosol of hepatocytes, all other statins undergo microsomal metabolism by the cytochrome P450 (CYP450) isoenzyme family (Bellosta *et al*, 2004).

Statins are generally hepato-selective with respect to inhibition of HMG-CoAR, an important property given that the majority of endogenous cholesterol biosynthesis takes place in the liver. The mechanisms contributing to the hepato-selective nature of statins are governed by the relative solubility of the compound. Lipophilic statins are able to passively diffuse

through the hepatocyte cell membrane whilst hydrophilic statins are reliant upon carrier-mediated uptake (Schachter, 2005).

Table 1.1 Summary of statin pharmacokinetic properties adapted from (Stefano *et al.*, 2004).

	Statin						
	Atorva	**Fluva**	**Lova**	**Pitava**	**Prava**	**Rosuva**	**Simva**
T_{max} (h)	2-3	0.5-1	2-4	1-1.8	0.9-1.6	3	1.3-2.4
***C*max (ng/mL)**	27-66	448	10-20	~60	45-55	37	34-920
Bioavailability (%)	12	19-29	5	>60	18	20	5
Lipophilicity (Log P)	1.11	1.27	1.70	1.49	-0.84	-0.33	1.60
Protein Binding (%)	80-90 %	>99	>95	>99 %	43-55	88	94-98
Metabolism	CYP3A4	CYP2C9	CYP3A4	CYP2C9	Sulfation	CYP2C9/2C19	CYP3A4
Metabolites	Active	Inactive	Active	Inactive	Inactive	Active (minor)	Active
Transporter Protein Substrate	Yes	No	Yes	Yes	Yes	Yes	Yes
$T_{½}$ (h)	15-30	0.5-2.3	2.9	8-9	1.3-2.8	20.8	2-3
Urinary excretion (%)	2	6	10	15	20	10	13
Fecal excretion (%)	70	90	83	79	71	90	58

Based on a 40 mg oral dose, with the exception of pitavastatin (2 mg) and simvastatin (7.5 mg/kg). Table generated using data compiled from (Stefano *et al.*, 2004; Catapano, 2010; Jung *et al.*, 2012; Morgan *et al.*, 2012; Corsini *et al.*, 1999; White, 2002; Ahmed *et al.*, 2013).

Whilst the lipophilicity of the compound promotes efficient hepatic shunting, the same property results in the increased potential for permeation of extra-hepatic tissues. For this reason, hydrophilic statins exhibit greater hepato-selectivity than their lipophilic counterparts (Schachter, 2005).

1.1.5 Regulation of Cholesterol Biosynthesis by Statins

The liver is the primary site of *de novo* cholesterol synthesis in the body, accounting for up to two thirds of endogenous cholesterol production (Hamelin, 1998). Endogenous cholesterol is produced in the endoplasmic reticulum (ER) of hepatocytes via the mevalonate

pathway. Statins are used for the rational therapeutic manipulation of the mevalonate pathway through the competitive inhibition of HMG-CoAR. HMG-CoAR is a key enzymatic regulator at the apex of the biosynthetic pathway, dictating the rate limiting step that catalyses the conversion of HMG-CoA to mevalonic acid. In addition to cholesterol, the mevalonate pathway is responsible for the synthesis of isoprenoids, steroid hormones and bile acid precursors (Figure 1.3).

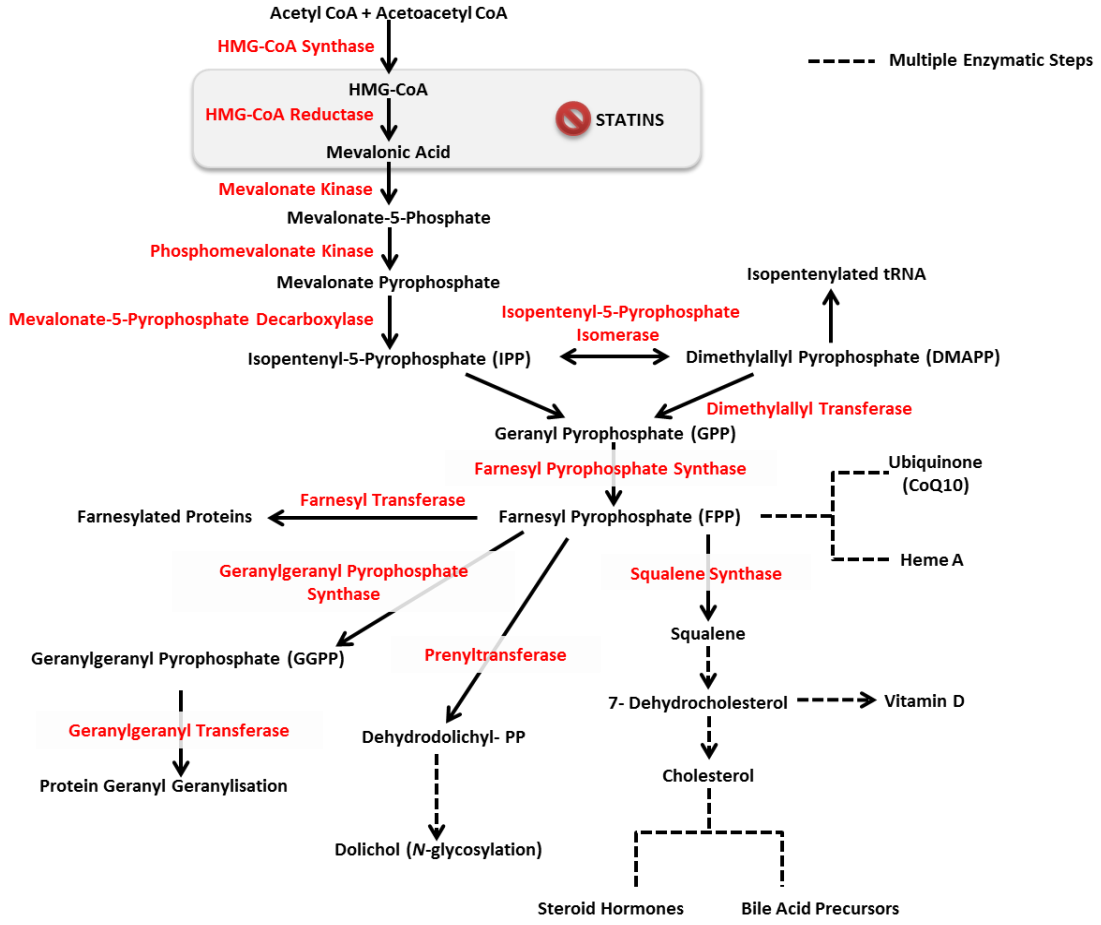

Figure 1.3 HMG-CoAR catalyses the conversion of HMG-CoA to mevalonic acid, the rate limiting step of the biosynthetic pathway. Mevalonic acid is an intermediary metabolite of cholesterol and several other sterol isoprenoids including dolichol (transmembrane carrier of glycosyl units), electron transport chain proteins Heme A and ubiquinone (CoQ10), Geranylgeranyl pyrophosphate (GGPP) and farnesyl pyrophosphate (FPP). GGPP and FPP are also implicated in the post-translational modification of up to 2 % of total cellular proteins including small GTPases and nuclear lamins.

Isoprenoids are an essential by-product of the pathway, required for the post-translational modification of proteins (i.e prenylation, farnesylation, geranyl geranylisation). Inhibition of the pathway and subsequent isoprenoid deficiency is thought to have a plethora of heterogeneous downstream effects such as impaired synthesis of transfer RNAs, glycoproteins, respiratory chain proteins heme A and ubiquinone (CoQ10) and small GTPases (i.e. RhoA, RAP1, Ras) essential for both cell signalling, intracellular protein trafficking and

attenuation of apoptotic signalling (Baer and Wortmann, 2007; Flint *et al.*, 1997b; Tricarico *et al.*, 2015).

Secondary to the reduction of *de novo* cholesterol synthesis, decreased intracellular cholesterol activates low density lipoprotein receptor (LDL-R) gene transcription, instigating the over expression of LDL-R on the hepatocyte plasma membrane. Overexpression of LDL-R increases the reuptake of LDL-cholesterol from systemic circulation, decreasing the total LDL-cholesterol plasma concentration (Duriez, 2003).

1.2 The Safety of Statins

Statin treatment is one of the most effective pharmaceutical intervention strategies available for the primary and secondary prevention of atherosclerotic cardiovascular and cerebrovascular disease. In the majority of recipients, statin therapy is safe and well tolerated. However, statins are associated with rare, life-threatening side effects, such as rhabdomyolysis and hepatotoxicity and have been linked to an increased incidence of new-onset, type 2 diabetes mellitus (Sakamoto and Kimura, 2013; Thapar *et al.*, 2013; Sattar and Taskinen, 2012). Patients increasingly report symptomatic side effects such as joint pain or proximal muscle pain and/or weakness which prevent the continuation of treatment, a condition collectively referred to as statin intolerance.

1.2.1 The Economical and Clinical Significance of Adverse Drug Reactions

Adverse drug reactions (ADRs) are defined as “an appreciably harmful or unpleasant reaction, resulting from an intervention related to the use of a medicinal product, which predicts hazard from future administration and warrants prevention or specific treatment, or alteration of the dosing regimen, or withdrawal of the product” (Edwards and Aronson, 2000).

ADRs have been estimated to be responsible for the attrition of ~30 % of candidate pharmaceuticals. Consequently, this has contributed to the high economical cost of drug development, especially when adverse effects are not recognised until late phase clinical trials or post marketing (Guengerich, 2011). The cost of profitable drug development has been increasing for many years, with recent research and development outlay estimates approaching $1.4 billion per new compound (DiMasi *et al.*, 2016).

Drug withdrawal during the research and development phase has been most commonly associated with hepatic, cardiovascular and to a lesser extent skeletal muscle liabilities (Guengerich, 2011; Waring *et al.*, 2015). However, xenobiotic-induced myopathies have

become an area of increasing concern due to the widespread and prolific use of hypolipidemic medications such as statins and fibrates. The problem was highlighted by the withdrawal of cerivastatin from the market in 2001 due to an unacceptable incidence of rhabdomyolysis resulting in ~100 patient deaths (Thompson *et al.*, 2003; Baker and Tarnopolsky, 2001).

From a clinical standpoint, ADRs increase the burden upon the healthcare system by promoting non-adherence to medications, increasing hospitalisation, prolonging hospital stays and increasing the need for additional clinical investigations in more serious cases. Furthermore, ADRs may elicit prescription cascades whereby new medications are prescribed to treat conditions which are consequential of another drug. Not only does this increase the cost of pharmacotherapy but it also compounds the risk of further ADRs occurring (Sultana *et al.*, 2013).

1.2.2 Statin-Related Hepatic Injury

Clinical trials have demonstrated that statin therapy is associated with elevations in serum alanine aminotransferase (ALT) levels in approximately 3 % of recipients. In most cases, these elevations are not clinically significant, indeed ALT levels 3X the upper limit of normal (ULN) are rarely observed. However with continued administration, mild elevations in serum ALT generally resolve (Thapar *et al.*, 2013). In contrast, clinically important drug-induced liver injury (DILI) is rarely seen with statin use. The spectrum of hepatic abnormalities observed include: (1) asymptomatic elevations in ALT: usually transient (ALT <3X ULN) as previously described; (2) hepatitis with ALT >3X ULN and clinical symptoms of liver disease; (3) cholestatic or mixed hepatitis; and (4) autoantibody-associated DILI (Thapar *et al.*, 2013).

Acute liver failure (ALF) develops in a very small minority of statin recipients, with the incidence not differing from that of the general population. The overall risk of developing DILI from statin therapy is estimated to be 1 in 100,000, whereas the estimated risk of ALF is 1 in 1,000,000 (Russo *et al.*, 2009).

1.2.3 New Onset Type 2 Diabetes Mellitus

The risk of developing type 2 diabetes mellitus (DM) through statin use has been studied in both randomised controlled clinical trials and via meta-analyses (Navarese *et al.*, 2013; Sattar *et al.*, 2010; Baker *et al.*, 2010; Rajpathak *et al.*, 2009). Based upon the results of the aforementioned studies, risk of new onset DM has been added to the labels of statins by the US Food and Drug Administration (FDA). However, it is important to consider that DM is often

associated with dyslipidaemia, hypertension, obesity and elevated glucose levels, therefore it remains unclear if only patients who are pre-disposed to developing DM are susceptible to statin-induced DM or if it also extends to individuals who are at low risk for type 2 DM. Despite the mounting evidence for a higher incidence of DM with statin use, the pathomechanism remains unclear. Statins may directly decrease insulin biosynthesis or reduce secretion, thus exacerbating insulin resistance or modifying signalling to peripheral tissues (Sattar and Taskinen, 2012; Koh *et al.*, 2012). Conversely, others have suggested that the inhibition of the mevalonate pathway by statins and the consequential reduction in cholesterol synthesis induces DM and not the drug itself (White *et al.*, 2016).

1.2.4 Statin-Related Myopathy

The most significant barrier to atherosclerotic disease risk reduction is the development of statin-related myopathy (SRM). Whilst mild myotoxicity from the use of statins is generally self-limiting and will resolve itself with the cessation of treatment, it can foster poor patient compliance, reduced quality of life and reduced treatment efficacy. The clinical spectrum of musculoskeletal complications from statin therapy can vary significantly from patient to patient. At one end of the scale, individuals can be asymptomatic with elevated CK levels, or possess mild proximal muscle pain and weakness teamed with elevated CK. Conversely, patients can present with biopsy affirmed inflammatory myositis or in extremely rare cases (0.003-0.1 %) rhabdomyolysis with elevated CK and potential for acute kidney injury (Apostolopoulou *et al.*, 2015).

The reported incidence of statin-linked muscle complaints of varying severities are thought to range between 1-5 % in randomised clinical trials (Kashani *et al.*, 2006), however the true case rate of myopathy may fall between 7-29 % when all disease phenotypes are taken into consideration (Stroes *et al.*, 2015). Unfortunately the lack of a unifying classification system for the report of myopathic symptoms results in discrepancies in these figures, thus a truly representative case rate is particularly difficult to quantify. To address this Alfirevic *et al*., proposed an algorithm to standardise nomenclature, outline phenotypic definitions and rank severity to aid both clinicians and researchers (Table 1.2) (Alfirevic *et al.*, 2014).

Table 1.2 Statin-related myopathy (SRM) phenotype classification adapted from (Alfirevic *et al*., 2014).

SRM Classification	Phenotype	Definition
SRM 0	CK elevation < 4X ULN	No muscle symptoms
SRM 1	Myalgia, tolerable	Muscle symptoms without CK elevation
SRM 2	Myalgia, intolerable	Muscle symptoms, CK < 4X ULN, complete resolution upon dechallenge
SRM 3	Myopathy	CK elevation > 4X ULN < 10X ULN ± muscle symptoms, complete resolution upon dechallenge
SRM 4	Severe myopathy	CK elevation > 10X ULN < 50X ULN ± muscle symptoms, complete resolution upon dechallenge
SRM 5	Rhabdomyolysis	CK elevation > 10X ULN with evidence of renal impairment + muscle symptoms or CK > 50X ULN
SRM 6	Autoimmune-mediated necrotising myositis	HMG-CoAR antibodies, HMG-CoAR expression in the muscle biopsy, incomplete resolution upon dechallenge

Abbreviations: SRM, statin-related myopathy; CK, creatine kinase; ULN, upper limit of normal; HMG-CoAR, 3-hydroxy-3-methylglutaryl-coenzyme A reductase.

1.2.4.1 Patient Risk Factors for Statin-Related Myopathy

The identification of patients with an increased proclivity for developing myopathic symptoms when challenged with statins could allow the clinician to make more cost effective decisions and improve patient safety. Several generalised factors have been uncovered which have been shown to confer an elevated risk of SRM in statin recipients (Table 1.3) (Harper and Jacobson, 2007).

Table 1.3 Compilation of general risk factors for the development of statin-related myopathy (Feng *et al.*, 2012; Harper and Jacobson, 2007).

Type	Risk Factor
Generalised	Advanced age (>80 years)
	Female gender
	Hypertension
	Low body mass index (BMI)
	Strenuous exercise
	Alcohol abuse
	Drug abuse
	Low vitamin D levels
	Familial history of myopathy
	Smoking
	Surgery
	Renal disease
	Hepatic disease
	High drug dose
	Lipophilicity of statin
Metabolic	Diabetes mellitus
	Hypothyroidism
	Metabolic muscle disease
	McArdle disease
	Carnitine palmitoyl transferase II deficiency
	Myoadenylate deaminase deficiency
Co-medications	Fibrates
	Nicotinic acid
	Cyclosporine
	Azole antifungals
	Macrolide antibiotics
	Protease inhibitors
	Nefazadone
	Verapamil
	Amiodarone
	Warfarin
	Grapefruit Juice
Genetic Polymorphisms	CYP450 isoenzymes
	SLCO1B1
	ABCB1/ABCC2

Abbreviations: CYP450, cytochrome-P450, SLCO1B1, solute carrier organic anion transporter family member 1B1; ABCB1/C2, ATP-binding cassette subfamily B1/C2; UGT1, UDP-glucuronosyltransferase 1.

In addition, there are suggestions within the literature that patients with subclinical mitochondrial insufficiencies or fully realised metabolic disorders are more likely to manifest myopathic symptoms following the administration of a statin (Antons *et al.*, 2006; Apostolopoulou *et al.*, 2015).

1.2.5 Pathomechanisms of Statin-Related Myopathy

The pathomechanistic nature of SRM is as yet unresolved, however there are numerous hypotheses which have been proposed in order to rationalise their manifestation. Cholesterol is a key structural and functional component of the cell plasma membrane, therefore modulation of the mevalonate pathway by statins may result in changes to both membrane fluidity and ion channel conductance, altering muscle membrane excitability (Pierno *et al.*, 1995).

Isoprenoids are yet another essential by-product of the mevalonate pathway, required for the post-translational modification of proteins (i.e prenylation, farnesylation, geranyl geranylisation, N-glycosylation). Inhibition of the pathway and subsequent isoprenoid deficiency is thought to have heterogeneous downstream effects such as impaired synthesis of tRNAs, glycoproteins, respiratory chain cofactors, and small GTPases (i.e. RhoA, RAP1, Ras) essential for both cell signalling, intracellular protein trafficking and attenuation of apoptotic signalling (Flint *et al.*, 1997b; Baer and Wortmann, 2007).

Indeed, defects associated with the proximal mevalonate pathway are considered to be more closely associated with myopathy, whilst those of the distal pathway appear to be of lesser importance (Baer and Wortmann, 2007). This idea is substantiated when paired with studies demonstrating that mevalonate pathway blockade *in vitro* at the point of squalene synthesis, the first committed step in cholesterol synthesis, does not result in cytotoxicity (Flint *et al.*, 1997b). Squalene synthesis is downstream from the formation of isoprenoid precursors such as farnesyl pyrophosphate (FPP) and geranylgeranyl pyrophosphate (GGPP), indicating that impaired post-translational modification of proteins and not altered membrane cholesterol content, may be more important in the development of myopathy (Flint *et al.*, 1997a). Furthermore, supplementation of mevalonic acid, the product of HMG-CoAR, in to the media of statin treated myocytes has been shown to abrogate the loss of cell viability (Sacher *et al.*, 2005). However, only 30-50 % of the reduction in viable cells was attributable to the inhibition of HMG-CoAR which is indicative of additional underlying toxicity mechanisms which may be independent of the inhibition of the mevalonate pathway (Dirks and Jones, 2006; Sacher *et al.*, 2005).

It has also been reported that statins may have a direct effect on the sarcoplasmic chloride concentration by modulating ClC-1 chloride channel activity and altering resting chloride conductance (gCl) in the muscle. Decreased ClC-1 mRNA expression has been detected in

rats receiving fluvastatin or atorvastatin resulting in a 30 % reduction in gCl (Pierno *et al.*, 2009).

In skeletal muscle, MCT1 and MCT4 are responsible for mediating lactate flux relative to the lactate concentration and proton gradient, either into or out of the myocyte. MCT1 is thought to be predominantly expressed in type I oxidative fibers whilst MCT4 is expressed primarily in type II glycolytic fibers (Bonen, 2001). Both transporters are located on the sarcolemmal and mitochondrial membranes. Several studies have demonstrated that lipophilic statins in particular may block MCT1/4, thereby increasing sarcoplasmic lactate concentrations (Kobayashi *et al.*, 2006, 2005; Kobayashi, 2015).

A role for the activation of atrophy related genes have been identified in statin mediated muscle fiber damage. In particular the upregulation of two E3 ubiquitin ligases, Atrogin-1 and MuRF1, which are members of the muscle-specific ubiquitin proteasome (Hanai *et al.*, 2007; Goodman *et al.*, 2015). Atrogin-1 expression is thought to be upregulated early in the induction of atrophy, preceding the loss of muscle mass. Patients who exhibit SRM demonstrate elevated Atrogin-1 mRNA expression in biopsies of quadriceps muscle (Cao *et al.*, 2009).

1.2.6 Mitochondria and Statin-Related Myopathy

Mitochondrial dysfunction is now one of the most widely accepted and well-studied pathomechanisms of SRM. However, the exact nature, extent and type of mitochondrial dysfunction(s) elicited by statin therapy still remains unclear. Previous studies seeking to establish the aetiological basis of SRM have demonstrated impairment of multiple mitochondrial process.

1.2.6.1 Drug-induced Mitochondrial Dysfunction

Recognition of the ability for specific compounds to perturb mitochondrial function (e.g. oligomycin, carbon monoxide and 2,4,-dinitrophenol) dates back more than 60 years. It wasn't until 2007 and the release of several landmark papers spearheaded by Yvonne Will and James Dykens, that the appreciation for the role of mitochondrial dysfunction in the aetiology of adverse drug reactions was truly recognised (Dykens and Will, 2007; Marroquin *et al.*, 2007). Compounds that induced mitochondrial dysfunction can do so through multiple mechanisms, encompassing both direct (e.g. respiratory complex inhibition) and indirect (e.g. altered cross-talk with the nucleus) targets.

Growing understanding of chemical-induced mitochondrial dysfunction has also been paralleled with an increased awareness of the implication of mitochondrial dysfunction in disease. Many metabolic diseases are caused by mutations in both the nuclear and mitochondrial genomes, affecting roughly 1 in every 4,300 individuals (Gorman *et al.*, 2015). An even greater proportion of people are affected by diseases which are associated with, yet may not necessarily be directly caused by, mitochondrial dysfunction (e.g. Parkinson's disease).

This raises the question, are individuals suffering from mitochondrial disease or harbouring subclinical mitochondrial insufficiencies more susceptible to mitochondrial toxicants? This topic has been reviewed in the context of drug-induced liver injury (DILI) as a means to explain its often idiosyncratic nature (Boelsterli and Lim, 2007). Later work using murine embryonic fibroblasts with distinct mitochondrial DNA (mtDNA) polymorphisms supported significant variability in response to mitochondrial toxicants, however this has yet to be reviewed in the context of drug-induced skeletal muscle injury (Pereira *et al.*, 2012).

1.2.6.2 Indirect Mitochondrial Effects

Statin-associated mitochondrial dysfunction was originally thought to be mediated by the inhibition of CoQ10 synthesis, an important respiratory chain co-factor and a by-product of the mevalonate pathway. Lower CoQ10 levels were observed in the circulation and skeletal muscle of patients receiving statin treatment in tandem with higher lactate/pyruvate ratios, a clinical indicator of mitochondrial dysfunction (Laaksonen *et al.*, 1994; De Pinieux *et al.*, 1996).

A systematic review of the literature identified several studies that reported a decrease in plasma CoQ10 levels in statin myopathy cases. However, the reported decrease may have been due to the simultaneous decrease in circulating LDL-cholesterol, the primary transporter of CoQ10 to peripheral tissues (Marcoff and Thompson, 2007). CoQ10 does not circulate in any appreciable concentration as an unbound free molecule (Deichmann *et al.*, 2010). Furthermore, whilst circulating levels of CoQ10 may routinely decrease with statin treatment, this does not always correlate to changes in CoQ10 levels in skeletal muscle or to mitochondrial dysfunction (Laaksonen *et al.*, 1996).

Multiple clinical trials have evaluated the impact of oral CoQ10 supplementation as a means to prevent or treat statin myopathy, however these have yielded inconclusive results (Table 1.4).

Table 1.4 List of placebo-controlled CoQ10 supplementation trials for the treatment of SRM. ↓ decrease, ↔ no change.

Reference	CoQ10 Dose (Duration)	Statin (Dose)	Study Outcome
(Caso *et al.*, 2007)	100 mg/day, 30 days	Variety	↓ Muscle pain
(Young *et al.*, 2007)	200 mg/day, 12 weeks	Simvastatin (10-40 mg)	↔ Muscle pain, statin tolerance
(Bookstaver *et al.*, 2012)	60 mg/2x day, 3 months	Variety	↔ Pain at 1 month
(Bogsrud *et al.*, 2013)	400 mg/day 12 weeks	Atorvastatin (10 mg)	↔ Symptoms
(Fedacko *et al.*, 2013)	200 mg/day, 3 months	Variety	↓ Muscle pain, SRM cases
(Skarlovnik *et al.*, 2014)	50 mg/2x day, 30 days	Variety	↓ Muscle pain
(Taylor *et al.*, 2015)	600 mg/day, 8 weeks	Simvastatin (20 mg)	↔ Muscle pain, SRM cases

Abbreviations: SRM, statin-related myopathy

1.2.6.3 Direct Mitochondrial Effects

Next to lowering CoQ10 levels in the skeletal muscle, statins were suggested to directly impair the functionality of the respiratory chain. A number of studies investigating statin mediated mitochondrial dysfunction have been conducted across a variety of platforms including *in vitro* culture, animal models and human trials.

1.2.6.3.1 In Vitro and Ex Vivo Studies

In 2005, Sirvent and colleagues demonstrated that acute application of high doses of simvastatin β-hydroxy acid to isolated human skeletal muscle fibers caused depolarisation of the inner mitochondrial membrane and Ca^{2+} release into the cytoplasm. This was followed by a larger Ca^{2+} release by the sarcoplasmic reticulum which precipitated the injurious effects of simvastatin (Sirvent *et al.*, 2005b; Sirvent *et al.*, 2005a). The same group later identified that inhibition of complex I of the respiratory chain initiated these effects in both human and rat skeletal muscle samples (Sirvent *et al.*, 2005b). Subsequent studies have supported the described mitochondria/Ca^{2+} mechanism of acute *in vitro* toxicity in both rat and human skeletal muscle (Sacher *et al.*, 2005; Liantonio *et al.*, 2007; Nadanaciva *et al.*, 2007a). Experiments using isolated mitochondria and high-throughput immune-capture assays have

also identified additional sites of respiratory complex inhibition which varied depending upon the statin administered (Nadanaciva *et al.*, 2007a).

The effect of statins on respiratory parameters has also been investigated using various cell lines. Application of lipophilic statins (100 μM) to the L6 rat skeletal muscle cell line impaired both mitochondrial membrane potential and phosphorylating respiration, whilst inducing mitochondrial swelling, DNA fragmentation and cytochrome *c* release (Kaufmann *et al.*, 2006). Similar deleterious effects on viability were observed in response to 5 μM simvastatin in rhabdomyosarcoma cells (Vaughan *et al.*, 2013). Studies performed using the C2C12 murine skeletal muscle cell line have also demonstrated perturbations in mitochondrial function, an effect which was not paralleled in the HepG2 hepatocarcinoma cell line. The differences between the two cell types was later found to be attributable to decreased phosphorylation of protein kinase B (Akt) in the C2C12 line, suggesting that modulation of the IGF-1/Akt signalling axis may be instrumental to the development of myotoxicity (Mullen *et al.*, 2010, 2011).

In addition, Skottheim and colleagues showed differential cytotoxicity between statin lactones and statin β-hydroxy acids in human skeletal muscle cells (Skottheim *et al.*, 2008). Follow up studies suggested that respiratory complex III was a likely target for the reversible binding of statin lactones specifically. This was supplemented with *in silico* docking analyses which supported the possibility that lactones could bind to and inhibit the Q_0 site of complex III. (Schirris *et al.*, 2015).

Whilst *in vitro* investigations such as these have proved insightful for elucidating the potential mechanistic basis of statin mediated mitochondrial dysfunction, it is important to acknowledge that the concentrations used in most cases are in excess of the plasma C_{max}, thus the translational utility of the data is often called into question (Björkhem-Bergman *et al.*, 2011).

1.2.6.3.2 In Vivo Studies

Although studies using animal models have shown muscle injury as a result of statin treatment, they do not consistently support a role for direct respiratory dysfunction. For example, treatment of male rabbits with simvastatin and pravastatin resulted in a decrease in muscle CoQ10 content but did not affect respiratory enzyme activity (Nakahara *et al.*, 1998). Similarly, female rats treated with cerivastatin for 15 days exhibited elevated CK levels, necrosis and swollen mitochondria whilst respiratory complex activities remained

unchanged (Schaefer *et al.*, 2004). Nevertheless, there are studies which support mitochondrial involvement in SRM, documenting changes in mitochondrial morphology before the onset of necrosis (Obayashi *et al.*, 2011), increased ROS production and decreased PGC-1α expression (Bouitbir *et al.*, 2012).

Mitochondrial involvement in the pathophysiological mechanism of SRM has also been investigated in statin treated patients. Elevated lactate/pyruvate ratio in statin treated patients versus controls provided the initial evidence that statin therapy may perturb mitochondrial function and provided the impetus for further investigation (De Pinieux *et al.*, 1996). Observations performed on four patients experiencing SRM without CK elevation showed increased lipid storage (oil red O staining), ragged red fibers (Gomori trichrome staining) and cytochrome *c* oxidase (COX) negative fibers. Parameters which are considered to be clinical characteristics of mitochondrial disease and respiratory chain dysfunction (Phillips *et al.*, 2002). Further studies have shown impaired complex I driven respiration in symptomatic patients versus asymptomatic and control groups (Sirvent *et al.*, 2012), whilst others demonstrate impaired complex II driven respiration in response to high dose simvastatin in combination with altered calcium homeostasis (Galtier *et al.*, 2012). These data support the possibility that complex I may not be the only respiratory complex targeted by statins and that different statins may affect mitochondrial function in different ways (Sirvent *et al.*, 2012).

1.3 Drug-Induced Myopathies of Skeletal Muscle

Drug-induced myopathies represent both a clinically and pathologically diverse group of musculoskeletal disorders, which can be caused by a variety of recreational and medicinal compounds, venoms, and biological toxins (Mastaglia and Needham, 2012). Drug –induced myopathy is classically defined as a subacute or rarely acute manifestation of myopathic symptoms (Table 1.5) which occur in patients without prior muscle disease when exposed to therapeutic doses of certain drugs (Husband, 2009).

Table 1.5 Definitions of various terms used in the literature to describe drug-induced muscle injury. Myositis definition is based upon the recommendation of the ACC/AHA/NHLBI clinical advisory of the use and safety of statins. Myositis may also be defined as biopsy affirmed muscle inflammation (Pasternak *et al.*, 2002)

Terminology	Definition
Myopathy	Blanket term for a disease of the musculoskeletal system
Myositis	Muscle symptoms accompanied by elevated creatine kinase (CK) levels < 10X upper limit of normal (ULN).
Myalgia	Muscle pain without elevation of CK
Rhabdomyolysis	Severe muscle symptoms, elevation of CK 10X ULN, myoglobinuria and renal failure.
Asymptomatic Myopathy	Elevated CK in the absence of muscle symptoms.

Myotoxic agents are capable of inducing myopathy in a number of ways by (a) directly and focally affecting the muscle tissue at the injection site; (b) targeting subcellular organelle such as the mitochondria, endoplasmic reticulum, lysosomes and myofibrillar proteins; (c) altering muscle antigens and inducing an inflammatory response; and (d) inducing general systemic effects such as electrolyte imbalance (e.g potassium or phosphorous) and malabsorption which may extend to have secondary effects on the muscle tissue (Dalakas, 2009).

In contrast to many other pathologies of skeletal muscle, drug-induced myopathies can be self-limiting and potentially resolved with the cessation of the offending compound. However, in other instances toxicity may be irreversible as was the case with fialuridine, a nucleoside analogue that caused irreversible neuromuscular damage due its successive incorporation into the mtDNA of recipients (Johnson, 2008).

1.3.1 Compounds Associated with Drug-Induced Myopathies

The clinical manifestation and mechanisms of drug-induced muscle toxicity can vary significantly between different compounds. Drug-induced myopathies are relatively uncommon in clinical practice with the exception of those that are associated with lipid-lowering compounds and glucocorticoids. However, it is still critical to understand toxic myopathies in order to facilitate timely diagnosis, cessation of treatment with the offending compound and patient recovery. There are a wide variety of compounds which are known to illicit detrimental effects on the skeletal muscle, therefore they are often categorised according to the type of injury induced in the muscle fiber or to the subcellular organelle.

Table 1.6 provides a list of both medicinal and recreational compounds which are more commonly associated with the onset of myopathic symptoms in recipients along with their injury categorisation (Pasnoor *et al.*, 2014).

Table 1.6 Table of compounds associated with drug-induced skeletal muscle injury.

Compound Class	Compound(s)	Classification	Reference(s)
Lipid lowering	Statins	• Necrotising myopathy • Rhabdomyolysis • Mitochondrial myopathy • Inflammatory myopathy	(Sathasivam, 2012; Mammen *et al.*, 2012; Sakamoto and Kimura, 2013; Vaklavas *et al.*, 2009)
	Fibrates	• Necrotising myopathy • Rhabdomyolysis	(Guis *et al.*, 2003; Pasnoor *et al.*, 2014; Prueksaritanont, Tang, *et al.*, 2002),
Recreational	Cocaine	• Rhabdomyolysis	(Goldstein *et al.*, 2009; Richards, 2000; Welch *et al.*, 1991; Pasnoor *et al.*, 2014)
	Amphetamines	• Rhabdomyolysis	(Green *et al.*, 2004; Carvalho *et al.*, 2012)
	Phencyclidine	• Rhabdomyolysis	(Richards, 2000; Kuncl and Meltzer, 1974; Patel *et al.*, 1979; Cogen *et al.*, 1978)
	Ethanol	• Necrotising myopathy • Hypokalaemic myopathy	(Richards, 2000; Thapaliya *et al.*, 2014; Fernandez-Solà *et al.*, 2007; Chawla, 2011)
Anti-retroviral	Zidovudine	• Mitochondrial myopathy	(Mammen, 2012; Scruggs and Dirks Naylor, 2008; Chawla, 2011)

	Fialuridine	• Mitochondrial myopathy	(Mammen, 2012; Johnson, 2008)
Anti-malarial	Chloroquine	• Amphiphilic cationic drug myopathy • Lysosomal storage myopathy	(Mammen, 2012; Guis *et al.*, 2003)
Anti-gout	Colchicine	• Anti-microtubular myopathy	(Mammen, 2012; Guis *et al.*, 2003)
Immunosuppressants	Glucocorticoids	• Hypokalaemic myopathy • Type II muscle fiber atrophy	(Valiyil and Christopher-Stine, 2010; Dirks-Naylor and Griffiths, 2009; Gruver-Yates and Cidlowski, 2013)
General anaesthetics	Volatile anaesthetics or succinylcholine	• Malignant hyperthermia	(Mammen, 2012; Pasnoor *et al.*, 2014)
Anxiolytics	Barbiturates	• Rhabdomyolysis	(Mastaglia, 1982)
Opiate analgesics	Opiate overdose (Morphine, dihydrocodiene & heroin)	• Rhabdomyolysis	(Villalba Garcia *et al.*, 1994; Sahni *et al.*, 2008; Blain *et al.*, 1985)
Antipsychotics	Neuroleptic compounds (clozapine, risperidone, melperone, olanzapine, haloperidol, loxapine)	• Type II fiber atrophy	(Meltzer, 2000; Sieb and Gillessen, 2003)
Other	Ipecac (Emetine Hydrochloride)	• Hypokalaemic myopathy • Myofibrillar myopathy	(Silber, 2005)
	Interferon-α	• Inflammatory myopathy	(Mammen, 2012; Valiyil and Christopher-Stine, 2010; Greenberg *et al.*, 2005)
	D-penicillamine	• Inflammatory myopathy	(Sieb and Gillessen, 2003)

1.4 Skeletal Muscle and Skeletal Muscle Modelling

Skeletal muscle is one of three major muscle types within the body, the others being cardiac and smooth muscle. Skeletal muscle is a form of striated muscle that is under the control of the somatic nervous system and constitutes the effector organs of the locomotor system. In most healthy adults, skeletal muscle is thought to account for roughly 45 % of the total body mass and is characterised by its highly organised ultrastructural arrangement, extensive vasculature and high metabolic rate (Pette and Staron, 2000; Ostrovidov *et al.*, 2014).

Skeletal muscle is fundamental for the execution of dynamic events such as prehension, ocular movements, directional motion as well as gravitational tasks such as postural support. Skeletal muscle is also a remarkably heterogeneous tissue, diverse in fiber composition and capable of extensive metabolic reprogramming in response to changing physiological demands (Vainshtein *et al.*, 2015).

1.4.1 Ultrastructural Arrangement

Single skeletal muscle fibers (Figure 1.4), when isolated from muscle tissue and examined microscopically are comprised of multinucleated syncytia of fused myotubes. The muscle fiber itself is enclosed within a plasma membrane, which in turned is sheathed by an extracellular basement membrane, the two compartments being collectively termed the

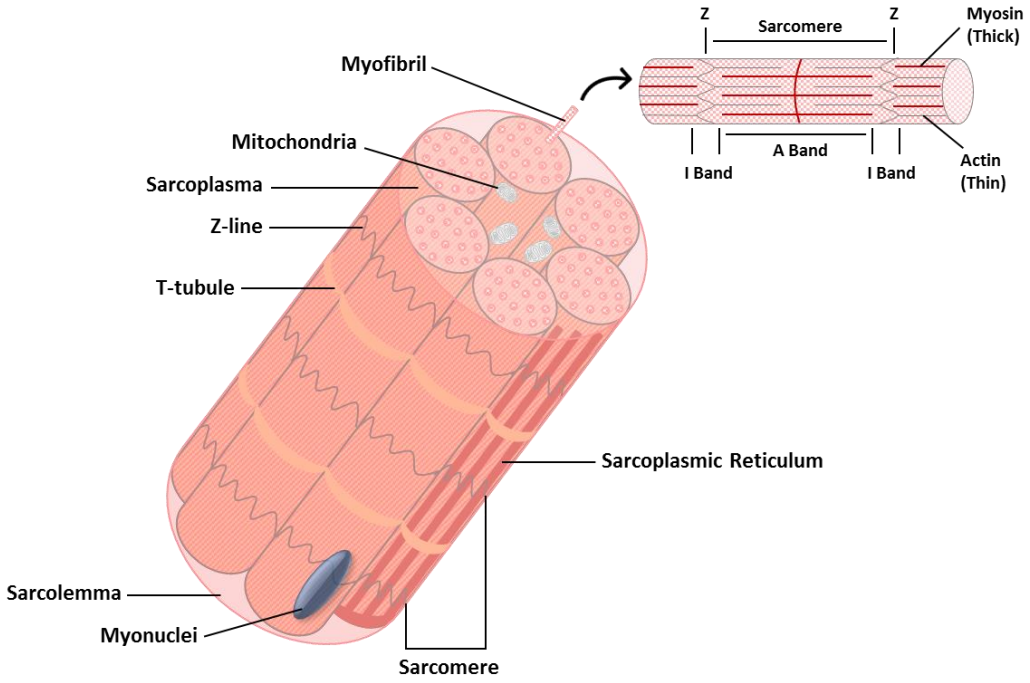

Figure 1.4 Schematic representation of the ultrastructural arrangement of individual skeletal muscle fibers (Lieber, 2002).

sarcolemma. Myonuclei are positioned along the length of the fiber, immediately beneath the sarcolemmal layer (Vye, 1976).

The cytoplasm of the muscle fiber is occupied by numerous cylindrical filaments called myofibrils which run parallel to the long axis of the fiber. Myofibrils consititue the basic structural unit of the muscle fiber and are the smallest component to retain the striated or 'banded' patterning owing to the presence of repeating contractile modules called sarcomeres. Within the sarcomere unit, the larger dark band is known as the anisotropic band (A-band), the smaller lighter bands the isotropic bands (I-band). The I-band is bisected by the Z-line, with two adjacent Z-lines enclosing the sarcomere (Vye, 1976; Pette and Staron, 1990).

Both the A- and I-bands are comprised of an array of highly ordered filamentous, contractile protein complexes. The interaction between the two sets of myofilaments is responsible for the force generation required to execute muscle contractions. The thinner of the filaments is found predominantly in the I-band and is made up from the protein actin and to a lesser extent, tropomyosin and troponin. The thicker of the filaments, which is located exclusively in the A-band, is an aggregate of arranged myosin subunits (Lieber, 2002; Vye, 1976).

Mitochondria, essential subcellular organelle implicated in the generation of adenosine triphosphate (ATP), are located in both the sub-sarcolemmal space and between myofibrils in the I-bands. Sub-sarcolemmal mitochondria occur in clusters often occupying the perinuclear space. Within the I-bands, paired mitochondria are located between myofibrils on either side of the Z-line. Mitochondria located within the I-band display a highly convoluted structure in order to conform to the spatial restrictions between myofibrils. The number of mitochondria per muscle fiber can be extremely variable. For example, fibers which are more reliant on aerobic respiration for energy generation may be rich in mitochondria, whereas those which are more dependent on anaerobically generated energy from glycolysis may have fewer or smaller mitochondrial networks. Muscle fibers which have prolonged or sustained energy demands may possess numerous mitochondria, each of which display extensive infolding of cristae (Lieber, 2002; Vye, 1976).

Muscle fibers possess a highly modified smooth endoplasmic reticulum, which is arranged into an extensive and ordered system of tubules referred to as the sarcoplasmic reticulum. The tubules of the sarcoplasmic reticulum are in close contact with the myofibrils and are primarily implicated in the storage of calcium ions (Ca^{2+}). Transverse tubules (T-tubules),

which are extensions of the sarcolemmal membrane that protrude into the interior of the fiber, are closely associated with specific regions of the sarcoplasmic reticulum known as the terminal cisternae, the primary site of Ca^{2+} release (Vye, 1976).

1.4.2 Muscle Fiber Types

Within the muscle tissue, different groups of fibers are charged with carrying out different roles, ranging from low intensity gravitational tasks to bursts of vigorous activity. To achieve such diversity in function, individual muscle groups possess a range of biophysical and bioenergetic properties as summarised in Table 1.7 (Arany, 2008; Vainshtein *et al.*, 2015).

Table 1.7 Summary of the major biophysical properties of mammalian skeletal muscle fiber types. Abbreviations: OXPHOS, Oxidative Phosphorylation.

	Slow Oxidative (SO)	**Fast Oxidative/Glycolytic (FOG)**	**Fast Twitch Glycolytic**
MHC Type	I	IIa	IIx/IIb
Fiber Size	Small	Intermediate	Large
Myoglobin Content	High (Red)	High (Red)	Low (White)
Glycogen Content	Low	Intermediate	High
Mitochondrial Density	High	High/Intermediate	Low
ATP Source	OXPHOS	OXPHOS/Glycolysis	Glycolysis
Major Substrate Store	Triglycerides	Phosphocreatine/ Glycogen	Phosphocreatine/ Glycogen
Contraction Velocity	Slow	Moderate/Fast	Fast
Fatigue Resistance	High	Moderate	Moderate/low

In adult mammalian skeletal muscle, there are four major muscle fiber types: I, IIa, IIx and IIb, defined by both the type of myosin heavy chain (MHC) predominantly expressed and the contraction-relaxation profile. It is the myosin ATPases that are the driving force behind the actin/myosin cycling machinery in tandem with ancillary sarcomeric/sarcolemmal proteins which regulate Ca^{2+} flux. Thus, the MHC type dictates the overall biophysical properties of a muscle fiber (Arany, 2008; Obayashi *et al.*, 2011; Neunhäuserer *et al.*, 2011).

Under resting conditions, it is widely accepted that the energetic demands of muscle tissue are predominantly met by the catabolism of fatty acids through the β-oxidation metabolic pathway. In *vivo,* skeletal muscle has limited permeability to glucose due to the expression of the primary glucose transporter GLUT4 on intracellular vesicles. Translocation of GLUT4 to the cell membrane is promoted by elevated circulating insulin levels or during exercise, thereby increasing glucose flux into the muscle. The glucose transporter GLUT1 is thought to be important for basal uptake of glucose into myocytes, however other hexose transporters such as GLUT3, GLUT5 and GLUT12 are also present (Cheng *et al.*, 2014; Leone *et al.*, 2005).

Once internalised, glucose can be utilised for ATP generation, be stored as glycogen in order to meet long-term energy demands or to be used when β-oxidation of fatty acids is reduced. During routine, low intensity activity, skeletal muscle is capable of consuming significant amounts of ATP through two main mechanism; ATP hydrolysis by the S1 head of the myosin protein and the Ca^{2+} ATPase which returns calcium ions to the sarcoplasmic reticulum following contraction of the muscle. It is therefore essential for the ATP pool to be continuously replenished. Medications that disrupt the cellular pathways of energy generation in skeletal muscle, can often lead to toxic outcomes (Westerblad *et al.*, 2010; Jones *et al.*, 2014; Richter and Hargreaves, 2013).

MHC type I fibers, classically known as slow oxidative (SO) or slow twitch fibers are characterised by a slower contraction-relaxation profile. Type I fibers are known to be rich in myoglobin, mitochondria and mitochondrial networks, favouring aerobic modalities of ATP production such as β-oxidation of fatty acids over anaerobic glycolysis (Arany, 2008). Type I fibers acquire fatty acids for metabolism from three principle sources, the first and most important is from adipose tissue by hormone-sensitive lipases. Sources of lesser importance include plasma very low density lipoprotein (VLDL) mobilised by lipoprotein lipase and fatty acids formed by the hydrolysis of intramuscular triacylglycerol (Salway, 2004).

MHC type II fibers, otherwise known as fast twitch fibers can be further sub-categorised into three types, type IIa, IIb and IIx. Whilst type IIb fibers (fast glycolytic) are present in most mammalian species, it is important to note that they are absent in humans. Therefore, only three fiber types: type I and types IIa/IIx meet the functional needs of the musculoskeletal system. Type IIa fibers are fast oxidative/glycolytic (FOG) fibers and possess intermediate biophysical properties whereas type IIx have the fastest contraction-relaxation profiles (Westerblad *et al.*, 2010; Neunhäuserer *et al.*, 2011). Type II muscle fibers have a greater reliance on anaerobic modalities of ATP production, especially during ‘explosive’ bursts of

muscle activity such as sprinting. Much of the ATP produced during this period is derived from the catabolism of the phosphagen, phosphocreatine and a 1000 fold increase in glycolysis (Salway, 2004).

In addition to the 'pure' fiber types, which express only a single MHC isoform, hybrid fibers also exist. Such fibers are comprised of two or more MHC isoforms, bridging the gap between the pure fiber types and forming a continuum within the musculoskeletal system (Pette and Staron, 2000).

1.4.3 Muscle Plasticity

One of the key features of skeletal muscle is its 'plasticity' or ability to adapt in the face of enhanced or diminished physical activity, exogenous stimuli or disease. Whilst basal muscle fiber type is largely determined during embryonic development, adult skeletal muscle retains a significant capacity for fiber type transition (Arany, 2008).

The transcriptional co-activator, peroxisome proliferator–activated receptor (PPAR)-γ coactivator 1α (PGC-1α), regulates the molecular mechanism by which muscle plasticity and oxidative fiber transitions are mediated. The PGC-1 family have a number of biological functions as outlined in Figure 1.5, most of which are linked to the promotion of oxidative metabolism, mitochondrial biogenesis and fatty acid oxidation (Wende *et al.*, 2007). Transgenic expression of PGC-1α in murine fast-twitch muscle fibers at physiological levels results in the activation of genetic pathways and the transcription of myofibrillar proteins characteristic of slow oxidative muscle fibers (Lin *et al.*, 2002). The skeletal muscle of the mice are more resistant to contraction-induced fatigue, which is indicative of an oxidative fiber type transition mediated by PGC-1α. In contrast, PGC-1α deficient murine muscle is prone to contraction-induced fatigue and exercise intolerance (Leone *et al.*, 2005).

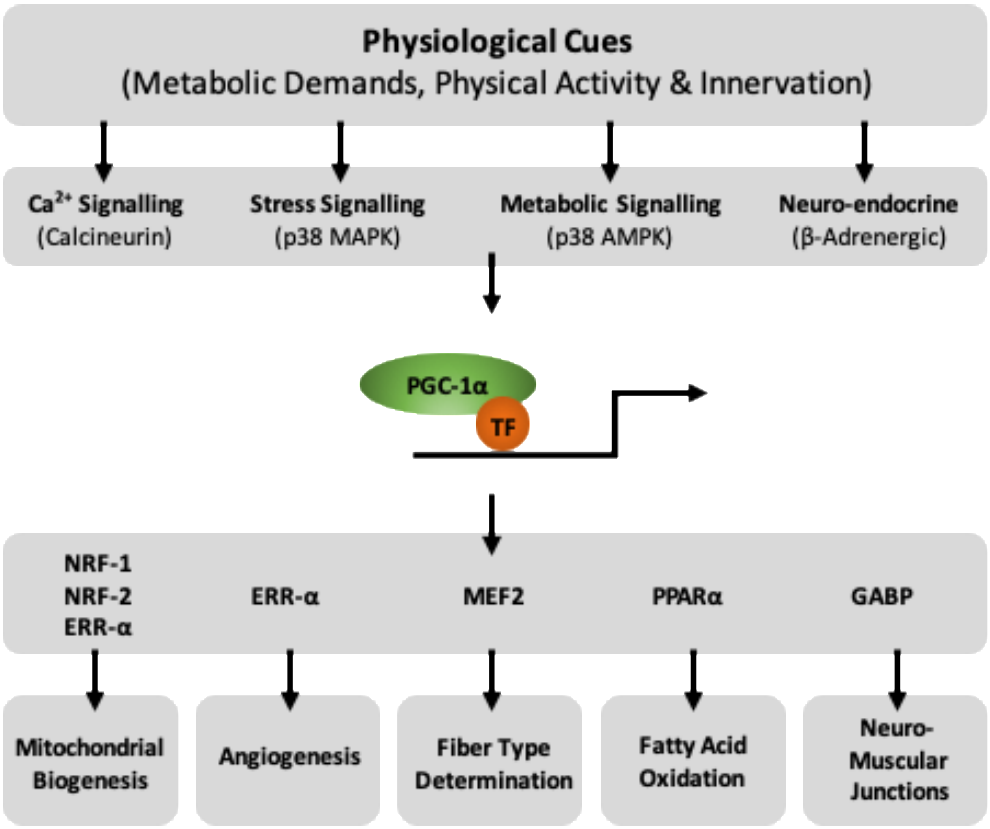

Figure 1.5 Schematic diagram illustrating the role of PGC-1α in muscle plasticity. Physiological cues (row 1) initiate key signalling pathways (row 2), promoting the expression of PGC-1α mRNA and the synthesis of the PGC-1α protein. In turn, PGC-1α co-activates a number of key transcription factors (row 3), leading to the activation of broad genetic programmes (row 4). Diagram adapted from Arany, 2008.

Therefore, PGC-1α acts to drive a complex phenotypic switch which couples both the metabolic and contractile phenotypes of mammalian skeletal muscle fibers, functionally transitioning glycolytic fast-twitch fibers into oxidative slow-twitch fibers and increasing mitochondrial biogenesis (Lin *et al.*, 2002, 2005).

1.4.4 Developmental Myogenesis and Regeneration

Mammalian skeletal muscle possesses an impressive capacity for regeneration after injury, a process which shares many parallels with muscle development during embryogenesis. In order to gain an appreciation for the regeneration process, it is important to first understand the basics of myogenesis (Figure 1.6).

During development, progenitor cells derived from the paraxial mesoderm (somites) give rise to skeletal muscle. The activation of the *Pax3/7* genes is instrumental to the migration of progenitor cells and their eventual commitment to the satellite cell lineage. Satellite cells

then receive signals from peripheral tissues, initiating the expression of transcription factors known as myogenic regulatory factors (MRFs).

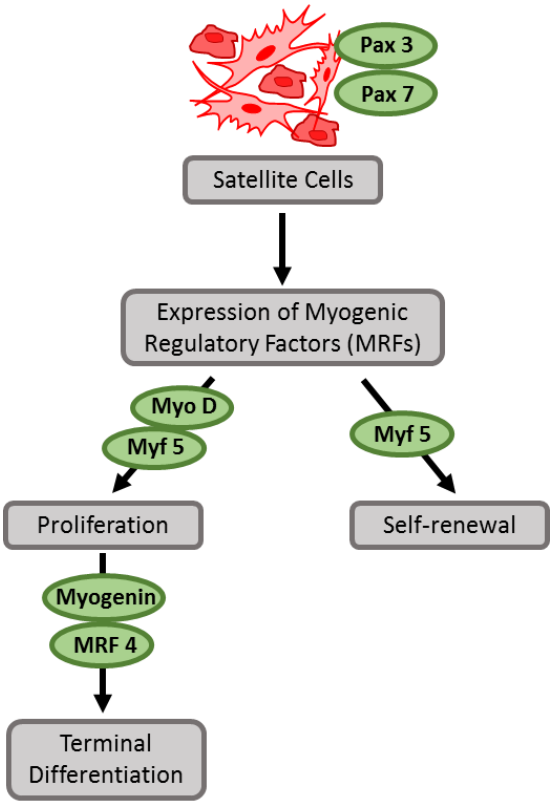

Figure 1.6 Activation and commitment of satellite cells to a myogenic fate during muscle development and regeneration. Diagram adapted from Karalaki *et al.*, 2009.

Myogenic cells which express the MRFs myf5 and MyoD are otherwise known as myoblasts. Upregulation of second tier MRFs, myogenin (MyoG) and MRF4 promotes the terminal differentiation of myoblasts into myotubes. Myotubes are characterised by the expression of mature muscle proteins such as myosin heavy chain (MHC) and creatine kinase (CK) and will eventually fuse, giving rise to adult skeletal muscle fibers (Karalaki *et al.*, 2009).

During the late stages of myogenesis, a pool of satellite cells fail to differentiate and remain closely associated with the muscle fiber in a quiescent state. This reservoir of undifferentiated *Pax7* positive satellite cells is central to muscle regeneration after injury, during routine maintenance or in response to increased functional demand. Moreover, the pool of quiescent satellite cells are capable of self-renewal in order to re-establish the population for subsequent rounds of regeneration (Karalaki *et al.*, 2009).

1.4.5 Modelling Skeletal Muscle *In Vitro*

As with all human organ systems, there is a need to develop physiologically relevant *in vitro*, drug screening platforms that can reliably predict *in vivo* effects in both rodent models and

human patients. The use of cell lines and primary cells to develop functional (i.e. contractile) models of skeletal muscle has been desirable for some time. However, due to the inherent architectural complexity of skeletal muscle, loss of key ion channel and receptor expression *in vitro* and a lack of processes which contribute to the mechanical activation of myocytes in culture, progress has been limited (Allen *et al.*, 2005). Hence, cells that can reliably reproduce myogenesis in culture i.e. the fusion and terminal differentiation of myoblasts into mature multinucleated myotubes have been the mainstay of skeletal muscle modelling for some time.

1.4.5.1 Two Dimensional Monoculture: Cell lines

As highlighted in prior discussion, skeletal muscle cells that can successfully recapitulate myogenesis in culture are preferential as they more closely mimic a mature myocyte phenotype. One of the most notable and widely used examples is the mouse derived C2C12 myoblast line, originally established by Yaffe and Saxel in 1977 (Yaffe and Saxel, 1977). The C2C12 line is capable of rapid differentiation upon serum reduction, forming contractile myotubes which express myogenic regulatory factors (MRFs) such as MyoG, MyoD and MRF4 (Wei and Paterson, 2001). However, one of the most significant caveats of C2C12 myocytes is that they require intense surveillance as they undergo terminal differentiation upon reaching confluence, consequently depleting the proliferative myoblast population. A similar model, the L6 rat neonatal myoblast line was originally isolated by Yaffe in 1968 (Yaffe, 1968), whereby primary cultures of rat quadriceps were maintained for the first two passages in methyl cholanthrene. L6 cells are capable of fusing in culture upon serum reduction to form multinucleated myotubes and striated fibers. However, the fusion potential of the cells declines with serial passages, resulting in the need for periodic re-cloning and selection for fusion competent cells (Allen *et al.*, 2005).

1.4.5.2 Two Dimensional Monoculture: Primary Cells

Satellite cells can be isolated from biopsy samples of adult, mammalian skeletal muscle and cultivated to generate a proliferating myoblast population, which can subsequently be differentiated into myotubes in culture (Aas *et al.*, 2013).

Primary myocyte cultures are an essential model in the biomedical field; often facilitating the effective therapeutic translation of results generated using clonal animals or cell lines. They possess the most relevant genetic background for the investigation of human disease, closely mimic the protein expression patterns of mature muscle and allow for the investigation of the innate characteristics of the donor (Aas *et al.*, 2013). The most prominent drawbacks of

using primary cell cultures derived from human muscle biopsy samples are their purity post isolation, their limited proliferative capacity and variation in phenotype when amplified *in vitro* due to progressive cellular senescence with successive population expansions (Mamchaoui *et al.*, 2011). Human myotubes from myoblast cultures undergoing senescence exhibit defects in both lipid and glucose metabolism and a diminished fusion potential (Nehlin *et al.*, 2011).

Further developments in myocyte culture have allowed for the creation of stably immortalised cell lines from myoblasts isolated from human biopsies. This has been instrumental in creating a robust collection of cell lines produced from pathological tissues that can be used to study a variety of neuromuscular disorders (Mamchaoui *et al.*, 2011).

1.4.5.3 Three Dimensional Muscle Tissue Engineering

The concept of skeletal muscle tissue engineering (SMTE) focuses upon the culture of myocytes that are isolated from patients, donors or preclinical species, with or without the aid of scaffolds to generate functional micro-tissues *in vitro* (Figure 1.7).

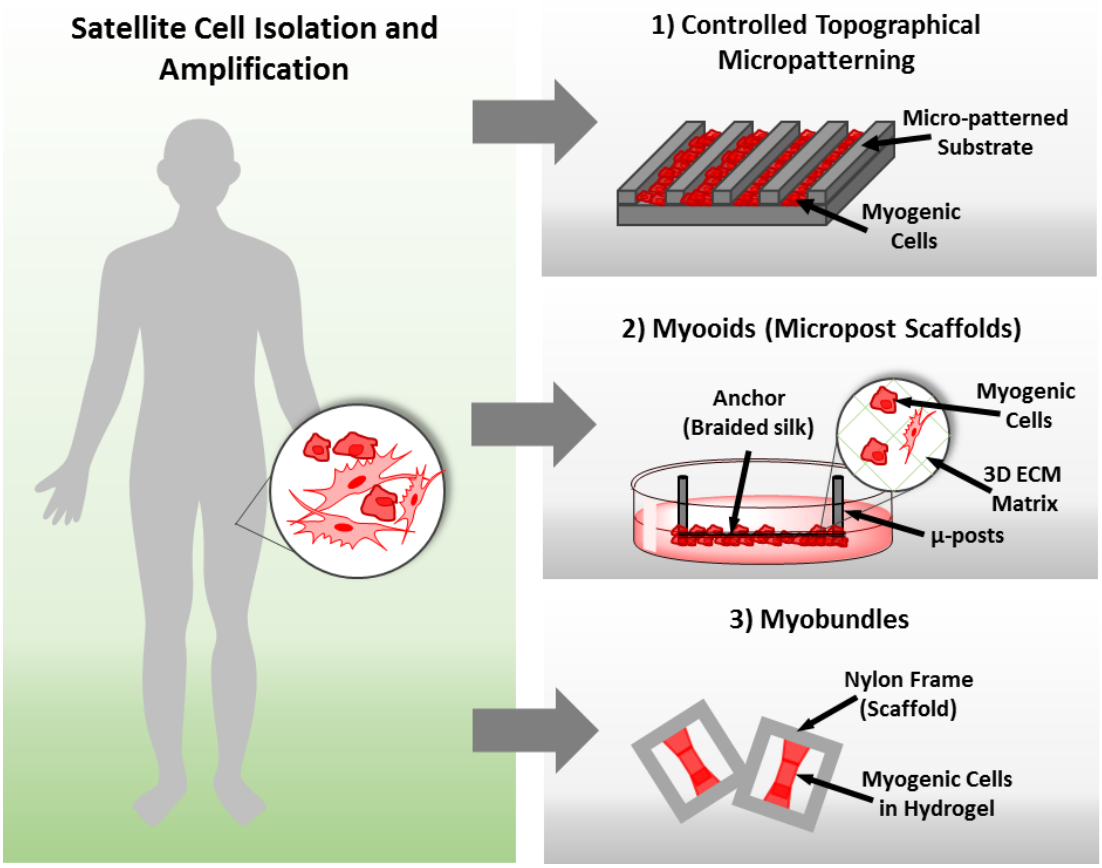

Figure 1.7 Representation of the concept of skeletal muscle micro-tissue engineering from biopsy derived myocytes. The diagram illustrates the isolation of proliferative satellite cells, their amplification *in vitro* as well as three different established methods of generating fabricated micro-tissue constructs. Adapted from (Ostrovidov *et al.*, 2014; Kwee and Mooney, 2017).

The goal of SMTE is to produce tissues as structurally similar to their *in vivo* counterparts so function is optimised as it is within the body (Lam *et al.*, 2009). With this in mind, SMTE was originally developed in order to repair or replace the normal function of defective muscle by creating micro-tissues from the donor's own cells for eventual re-implantation (Ostrovidov *et al.*, 2014). However, SMTE has shown great promise for a number of applications, not limited to predictive pharmaceutical testing, hybrid mechanical/muscle actuators and engineered meat production.

In the early 1990s, Strohman (Strohman *et al.*, 1990), described the first three dimensional skeletal muscle constructs produced from murine myoblasts grown on top of Saran wrap. After differentiation, the myocytes would 'roll up' to form a 3D contractile muscle tissue, later termed myooids by Dennis (Dennis and Kosnik, 2000), who incorporated stainless steel μ-posts and braided silk sutures coated in laminin to act as artificial tendons, aiding cellular anchorage (Figure 1.7).

More recent developments by Lam (Lam *et al.*, 2009), showed that by pre-aligning murine myoblasts by topographical micro-patterning on a 'wavy' polydimethylsiloxane (PDMS) surface before incorporating a fibrin hydrogel solution, they could produce a free-standing 3D muscle construct with superior muscle fiber content and force production capacity. More importantly, they demonstrated that pre-alignment of myocytes was pivotal to the successful engineering of skeletal muscle with increased muscle fiber formation. To this end, many nano/microfabrication techniques such as soft lithography, photolithography, electrospinning, passive and active stretching or electrical field stimulation have been employed to promote cell alignment (Ostrovidov *et al.*, 2014; Zorlutuna *et al.*, 2012; Ostrovidov *et al.*, 2013).

In 2015, Madden and co-workers described the development and validation of the 'myobundle' model, a biomimetic human micro-tissue platform with potential applications in clinically relevant *in vitro* studies of muscle physiology and pharmaceutical testing (Madden *et al.*, 2015). The purpose of the model was to recapitulate key functional aspects of human skeletal muscle, in logical progression from previous iterations of the myobundle platform using cells derived from pre-clinical species (Juhas and Bursac, 2014). The system is reliant on the encapsulation of myogenic cells within a fibrin hydrogel formed in a PDMS mould. Within the mould sits a nylon frame to which the cell/hydrogel mixture anchors, acting as an artificial tendon and keeping the myobundle under passive tension (Madden *et al.*, 2015). Further studies have demonstrated their utility in long-term pharmacological

examination of contractile force measurement, monitoring of calcium transients and oxygen consumption rate due to their increased culture lifespan of ~42 days (Madden *et al.*, 2015; Davis *et al.*, 2017; Cheng *et al.*, 2014).

1.5 Mitochondrial Structure and Respiration

Mitochondria are ubiquitous intracellular organelle whose dominant function is to produce energy in the form of adenosine triphosphate (ATP). Mitochondria can vary vastly in shape, size and number, ranging from a few discrete organelle per cell to the formation of interconnected and dynamic networks known as the mitochondrial reticulum (Glancy *et al.*, 2015). Despite the variance in number and morphology of mitochondria between cell types, all mitochondria share several highly conserved fundamental characteristics (Wojtczak and Zabłocki, 2008).

1.5.1 Mitochondrial Structure

As shown in Figure 1.8, two distinct lipid bilayer membranes bind all mitochondria. The outer mitochondrial membrane (OMM) forms the interface between the mitochondrion itself and the rest of the cellular metabolic network. The outer membrane is rich in cholesterol and is permeable to solutes and ions up to 10 kDa in size due to the presence of mitochondrial porin, also termed voltage-dependent anion channels (VDAC). The inner mitochondrial membrane (IMM) encapsulates an aqueous compartment, better known as the matrix, where the mitochondrial DNA (mtDNA) and enzymes of the tricarboxylic acid (TCA), and β-oxidation pathways are located. The IMM is not freely permeable to ions or metabolites and instead requires the use of transport proteins in order to translocate select metabolites across the membrane. The impermeable nature of the inner membrane is pivotal for the structural and functional integrity of the mitochondrion and accounts for the generation of

the electrochemical gradient that provides the proton motive force for ATP generation (Scatena *et al.*, 2007; Wallace and Starkov, 2000; Wojtczak and Zabłocki, 2008).

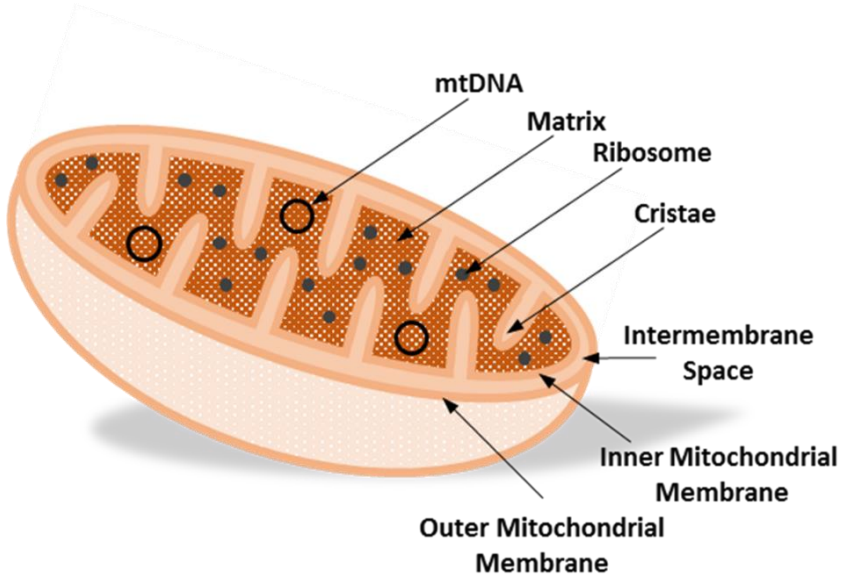

Figure 1.8 Simplified cross sectional diagram of the ultrastructural arrangement of a 'typical' mitochondrion**.** Cristae are presented as invaginations of the inner mitochondrial membrane however they are 'bag-like' structures separated from the intermembrane space by narrow tubular junctions (Colgliati *et al*., 2016).

Unlike the lipid composition of the outer membrane, the inner membrane is distinctive in that it is virtually devoid of cholesterol and is abundant in a molecule called cardiolipin. Cardiolipin (diphosphatidylglycerol) is a unique, anionic phospholipid found only in cell membranes that function in electron transport. It is not a passive component of the IMM but in fact interacts with a number of inner membrane proteins and has been shown to be important for maximal electron transfer activity (Robinson, 1993).

1.5.2 Oxidative Phosphorylation

Greater than 90 % of the energy produced by organisms that utilise aerobic metabolism occurs by oxidative phosphorylation (OXPHOS). The mitochondria are often considered as cellular 'powerhouses', converting the energy released during substrate oxidation into ATP for use in other cellular processes. OXPHOS consists of two functionally independent processes: the oxidation of reduced substrates by the enzymatic complexes of the proximal respiratory chain and the phosphorylation of ADP to ATP by in inorganic phosphate and ATP synthase (F_o/F_1 ATPase) (Figure 1.9). The coupling of the two processes is highly dependent upon the impermeability of inner mitochondrial membrane and the generation of a proton motive force (Δp) (Wojtczak and Zabłocki, 2008).

The mitochondrial respiratory chain is composed of more than 85 proteins that are assembled into four enzymatic complexes. Complex I (NADH: ubiquinone oxidoreductase), complex III (ubiquinol: cytochrome *c* oxidoreductase) and complex IV (cytochrome *c* oxidase) are all located within the IMM whereas complex II (succinate dehydrogenase), which catalyses a step in the tricarboxylic acid (TCA) cycle is located on the matrix side of the IMM. The four complexes, along with diffusible electron donors/acceptors ubiquinone (CoQ10), ubiquinol ($CoQ10H_2$) and cytochrome *c* (cyt *c*), function to catalyse electron transfer from reduced electron donors NADH and $FADH_2$ to molecular oxygen (1/2 0_2) (Wojtczak and Zabłocki, 2008).

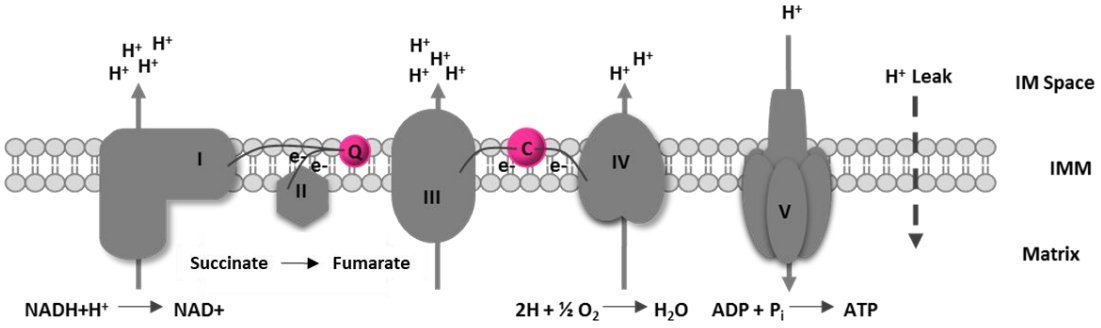

Figure 1.9 Schematic diagram of the mitochondrial respiratory chain. The inner mitochondrial membrane houses the enzymatic components of the respiratory chain that translocate protons from the mitochondrial matrix into the intermembrane (IM) space, thus generating an electrochemical gradient (proton motive force, **Δp**). Δp consists of two principle components – the electrical component (**Δψ,** positive in IM space**)** and a chemical component (**ΔpH,** acidic in IM space). Δp drives protons from the IM space to the matrix through F_o/F_1 ATP Synthase (Complex V), generating ATP from the phosphorylation of ADP.

Due to a large difference in redox potential between the electron donors and the final electron acceptor, passage of electrons down the respiratory chain is accompanied by a large increase in free energy (decreased Gibbs potential). The majority of the free energy is used to pump protons across the IMM into the IM space. The remaining energy is dissipated as heat. The proportion of energy that is dedicated to proton pumping or thermogenesis depends greatly upon the type and physiological status of the tissue from which the mitochondria were originally derived (Wojtczak and Zabłocki, 2008).

1.5.2.1 The Electrochemical Gradient

1.5.2.1.1 Complex I (NADH: ubiquinone oxidoreductase)

Complex I is responsible for catalysing the oxidation of NADH concomitantly with the reduction of CoQ10 to $CoQ10H_2$.

Reaction: $NADH + H^+ + CoQ10 + 4H^+_{in} \rightarrow NAD^+ + CoQ10H_2 + 4H^+_{out}$

Number of Protons Translocated to IMS: 4

Complex I binds NADH, transferring two electrons to the flavin mononucleotide (FMN) prosthetic group to produce NAD^+ and $FMNH_2$. Electrons are passed through a series of seven iron-sulphur (Fe-S) clusters and are finally delivered to the electron acceptor CoQ10. $4H^+$ are pumped into the intermembrane space for every two electrons donated from NADH (Hirst, 2005).

1.5.2.1.2 Complex II (succinate dehydrogenase)

Complex II resides on the matrix side of the IMM, providing the second electron entry point into the respiratory chain. In addition to its role in the respiratory chain, complex II is a component of the tricarboxylic acid cycle catalysing the oxidation of succinate to fumarate in tandem with the reduction of FAD to $FADH_2$.

Reaction: Succinate + CoQ10 → fumarate + $CoQ10H_2$

Number of Protons Translocated to IMS: 0

Two electrons are transferred from $FADH_2$ through three Fe-S clusters before being passed onto CoQ10. The transfer of electrons from $FADH_2$ to CoQ10 does not result in the translocation of protons from the matrix to the IM space, therefore complex II does not directly contribute to Δp generation (Rutter *et al.*, 2010).

1.5.2.1.3 Complex III (ubiquinol: cytochrome c oxidoreductase)

The reaction catalysed by complex III involves the oxidation of one molecule of $CoQ10H_2$ and the reduction of two molecules of cytochrome *c*. Unlike CoQ10, which can accept two electrons per molecule, cytochrome *c* can accept only one thus the reaction mechanism is more elaborate than that of the other respiratory enzymes.

Reaction: $CoQ10H_2$ + 2 cytochrome *c* (Fe^{3+}) + $2H^+_{in}$ → CoQ10 + 2 cytochrome *c* (Fe^{2+}) + $4H^+_{out}$

Number of Protons Translocated to IMS: 4

Diffusible $CoQ10H_2$ binds to the Q_O site on complex III, donating one electron to the 2Fe-2S cluster known as the Reiske Iron-Sulphur Protein (ISP). The ISP donates the electron to cytochrome *c*1, allowing for the extrusion of two protons into the IM space whilst $CoQ10H_2$ (now ubisemiquinone) remains bound to the Q_O site. The second electron from $CoQ10H_2$ is passed to a lower potential chain containing the b_L and b_H hemes of cytochrome *b.* This chain delivers electrons to a second CoQ10 processing site, the Q_i site. At this site, CoQ10 is

reduced to $CoQ10H_2$. The reaction requires two electrons, therefore the Q_O site must turn over twice, oxidising two $CoQ10H_2$ molecules and releasing four protons into the IMM. If the complex starts with a CoQ10 molecule already bound, the first electron at the Q_i is stored on a ubisemiquinone which reduced to $CoQ10H_2$ by the second electron (Crofts, 2004).

1.5.2.1.4 Complex IV (cytochrome c oxidase)

Complex IV is the terminal oxidase of the respiratory chain, catalysing the transfer of electrons from reduced cytochrome *c* to molecular oxygen forming two molecules of water.

Reaction: 4 cytochrome c (Fe^{2+}) + $4H^+$ + 0_2 → 4 cytochrome *c* Fe^{3+} + $2H_2O$

Number of Protons Translocated to IMS: 2

Cytochrome *c* transfers its electron to the redox centre of subunit II (Cu_A) then subsequently to heme *a* allowing cytochrome *c* to dissociate. Heme *a* then transfers its electron to the redox centre Cu_B associated with heme *a*3. A second molecule of cytochrome *c* then binds and transfers its electron to heme *a*3. With two electrons bound, heme *a*3 binds with molecular oxygen. A third molecule of cytochrome *c* donates its electron to heme *a*3, this electron together with two protons from the matrix leads to the cleavage of the O=O bond and the generation of a Fe^{4+} centre. A fourth molecule of cytochrome *c* donates its electron to the heme *a*3 Cu_B centre reducing Fe^{4+} =O to Fe^{3+}. The free oxygen atom picks up two protons simultaneously to produced H_2O (Blomberg, 2016).

1.5.2.2 Mitochondrial ATP Synthase and ATP Production

Mitochondrial ATP Synthase (F_o/F_1 ATPase) is a large protein complex partially embedded into matrix side of the inner mitochondrial membrane (Figure 1.10). Although not formally part of the respiratory chain, it is often referred to as complex V. Its primary function is to synthesise ATP from ADP and P_i using Δp generated by the proximal respiratory chain. The protein is bipartite as indicated by its name and is comprised of a F_1 portion (α_3, β_3, γ, OSCP and ε subunits), and a F_O portion made up by a, b and c subunits in the stoichiometry 1:2:10-14. Two stalks, a peripheral one involving the b and OSCP subunits and a central one containing the γ and ε subunits link F_1 and F_O (Capaldi and Aggeler, 2002) .

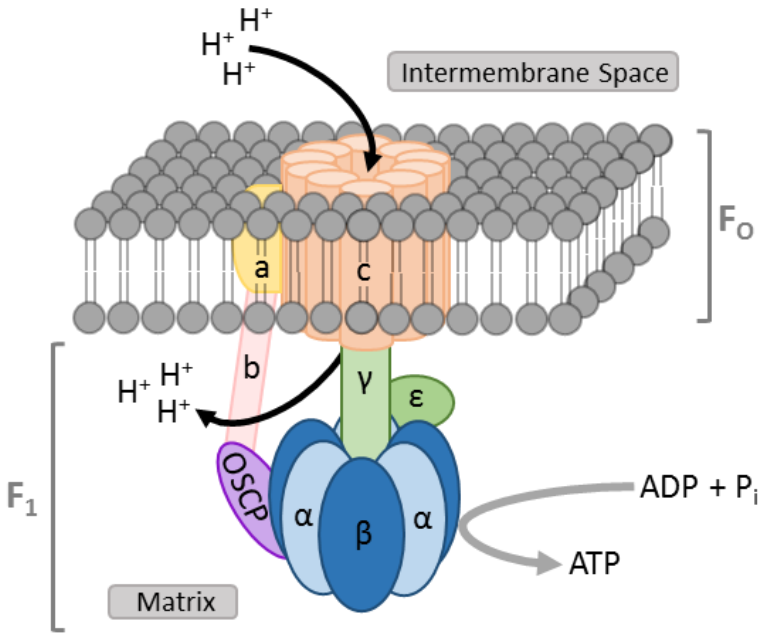

Figure 1.10 Structure of ATP Synthases (F_o/F_1 ATPase). The F_o region of ATP synthase is composed of a ring structure embedded into the inner mitochondrial membrane. It acts as a proton pore allowing H^+ ions to return to the matrix. The F_1 region of ATP synthase is responsible for catalysing ATP synthesis.

1.5.2.2.1 Conformational Model of ATP Synthesis

The most widely accepted mechanistic model of ATP synthesis is the 'conformational change' or 'alternating site' hypothesis proposed by Boyer (Boyer, 1993). The key feature of this model is that the catalytic domains housed on the three β-subunits of F_1 are in one of three different conformational states at any given time. The conformational states act to vary the binding affinity of the β-subunits for substrates (ADP+P_i) and products (ATP). Conformation 'O', meaning open, is characterised by a low affinity for ATP; conformation 'L' meaning loose, loosely binds ADP and P_i; conformation 'T', meaning tight, tightly binds ADP and P_i.

Under physiological conditions, protons flowing from the IM space into the matrix via the membrane embedded F_O force the γ subunit to rotate whilst subunit b holds the αβ dimers stationary. For one complete 360° turn of subunit γ, one proton must return to the matrix for every c subunit present (10-14 H^+). In simplified terms, rotation of the γ subunit by 120° results in a switch from conformation to the next. As depicted in Figure 1.11, if a β subunit starts at conformation 'O', after rotating 120° it will change its conformation to L, after rotating another 120° it will now sit in the T conformation. One 360° revolution of the γ

subunit constitutes one full cycle in which three molecules of ATP are synthesised (Wojtczak and Zabłocki, 2008; Capaldi and Aggeler, 2002)

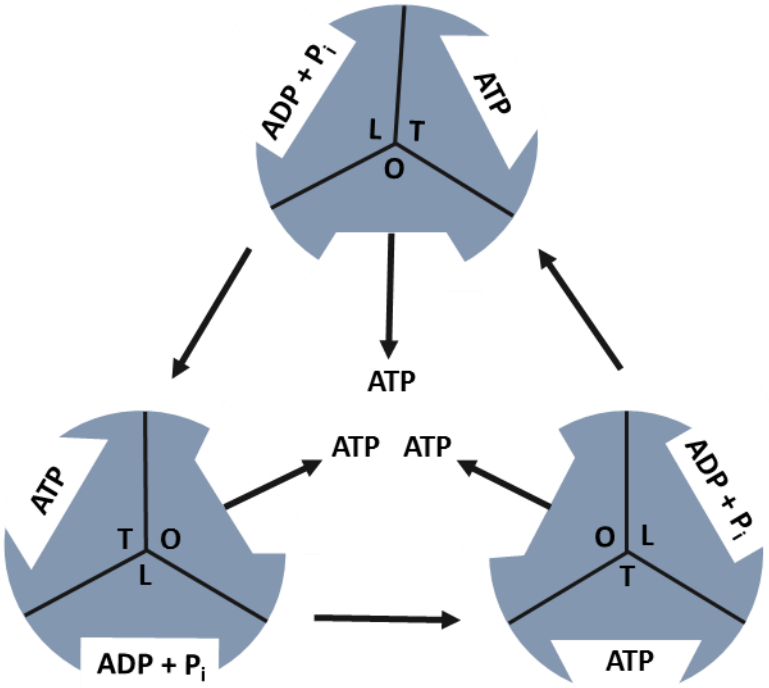

Figure 1.11 Conformational model of ATP synthesis. O, L and T represent the three different conformational states of the catalytic domain of the β subunit. The revolution of the γ subunit drives the changes in conformational state. ADP and P_i bind loosely (L), followed by tight binding (T) resulting in ATP synthesis, before being released (O). From Wojtczak and Zablocki, 2008.

1.5.3 Beta-Oxidation of Fatty Acids

The principle pathway used for the catabolism of fatty acids is mitochondrial fatty acid β-oxidation (FAO). FAO is of particular importance in organs such as the liver for the production of ketone bodies and in the heart and skeletal muscle as a substrate for OXPHOS (Houten and Wanders, 2010). Fatty acid transport proteins (FATPs) mediate the uptake of fatty acids into the cell. FATPs have acyl-CoA synthetase activity and rapidly convert fatty acids to acyl-CoAs after translocation across the plasma membrane (Figure 1.12). Acyl-CoAs are unable to cross the outer mitochondrial membrane and require import via the carnitine shuttle. The first step, performed by carnitine palmitoyltransferase I (CPT1) converts acyl-CoA to acylcarnitine. Carnitine acylcarnitine translocase (CACT) then exchanges acylcarnitines for free carnitine molecules at the inner mitochondrial membrane. Once acylcarnitines have entered the mitochondrial matrix, carnitine palmitoyltransferase II (CPT2) converts acylcarnitines into their CoA esters, which then undergo β-oxidation (Houten and Wanders, 2010; Bartlett and Eaton, 2004).

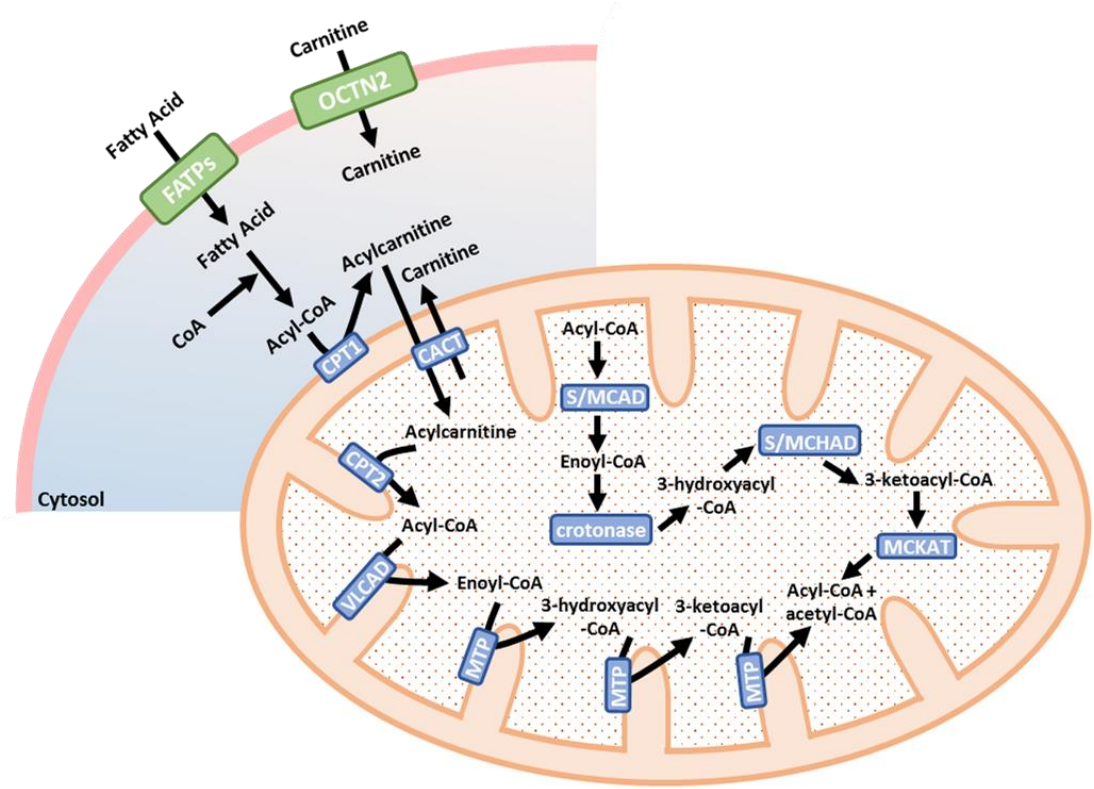

Figure 1.12 Overview of the mitochondrial carnitine shuttle and fatty acid β-oxidation pathway in humans.

Once within the mitochondrial matrix, acyl-CoAs are broken down into acetyl-CoA molecules via a four-step series of enzymatic reactions called β-oxidation. The process is cyclic whereby acyl-CoA molecules are shortened, releasing two carboxy-terminal carbon atoms after the completion of each full cycle. Each cycle begins with an acyl-CoA ester that is dehydrogenated by an acyl-CoA dehydrogenase (ACAD) to produce a trans-2-enoyl-CoA. Following hydration of the double bond to produce $_{L}$-3-hydroxy-acyl-CoA, a dehydrogenation step generates 3-keto-acyl-CoA. Finally, 3-keto-acyl-CoA undergoes thiolytic cleavage to produce a chain-shortened acyl-CoA, an acetyl-CoA, NADH and $FADH_2$. The chain-shortened acyl-CoA enters another cycle of β-oxidation whilst the acetyl-CoA enters the TCA cycle and NADH/$FADH_2$ donate their electrons to the respiratory chain (Bartlett and Eaton, 2004).

Directly after import, long chain acyl-CoA molecules undergo 2-3 FAO cycles to produced medium chain acyl-CoAs. Metabolism of long chain acyl-CoAs is perfomed by membrane bound very long chain acyl-CoA dehydrogenase (VLCAD) and mitochondrial trifunctional protein (MTP). Medium and short chain acyl-CoAs are metabolised by a series of matrix-soluble enzymes. The initial steps are catalysed by medium chain acyl-CoA dehydrogenase (MCAD) for 3-4 cycles then subsequently by short chain acyl-CoA dehydrogenase (SCAD) for the final 1-2 cycles (Houten and Wanders, 2010).

Three enzymes perform steps 2-4 of the oxidation of both medium and short chain acyl-CoAs: enoyl–CoA hydratase (crotonase), medium and short chain hydroxyacyl-CoA dehydrogenase (M/SCHAD) and medium chain 3-ketoacyl-CoA thiolase (MCKAT). The enzymes have broad substrate specificity to accommodate for acyl-esters with chain lengths of up to ten carbon atoms. The oxidation of unsaturated fatty acids such as oleic acid requires an additional isomerase step performed by dodecenoyl-CoA delta isomerase (DCI) (Houten and Wanders, 2010).

1.5.4 Reactive Oxygen Species

The production of reactive oxygen species (ROS) by mammalian mitochondria is an inevitable consequence of aerobic metabolism. The proximal respiratory chain produces superoxide (O_2^{-}.) anions when single electrons leak to O_2 as electron pairs are passed from one complex to the next. There are seven widely accepted sites of O_2^{-}. production in the mitochondria, however the two sites with the greatest maximal capacities to produce ROS are situated within complexes I and III (Brand, 2010). Though, the relative contribution of each complex to ROS production is as yet unresolved and may be tissue or condition specific.

Under physiological conditions O_2^{-}. can readily dismutate to form hydrogen peroxide (H_2O_2), a reaction catalysed by manganese superoxide dismutases (MnSODs) (Brand, 2010; Murphy, 2009). Glutathione peroxidases (GSPx), peroxiredoxins and catalase (peroxisomes) along with a number of low molecular weight antioxidants (e.g. ascorbic acid, β-carotene, α-tocopherol) constitute the antioxidant defence system, converting H_2O_2 to H_2O thus completely scavenging the ROS produced by the mitochondria (Wojtczak and Zabłocki, 2008).

Whilst O_2^{-}. and H_2O_2 are not strong oxidants themselves, they are the precursor molecules of most reactive oxygen species and are involved in the propagation of oxidative chain reactions within the cell. H_20_2 may be partially reduced to a hydroxyl radical ($^{\cdot}OH$) by transition metal ions (Fe^{2+} or Cu^{+}) whilst O_2^{-}. can react with other radicals such as nitric oxide (NO) to form reactive nitrogen species (RNS) (Turrens, 2003).

Imbalance between ROS/RNS production and endogenous antioxidant defences due to disease or toxic agents results in oxidative stress and the initiation of cell death. Whilst small fluctuations in steady-state ROS concentration is thought to play a role in mitochondrial signalling, excessive free radical production can lead to the indiscriminate targeting of proteins, lipids, polysaccharides and DNA (Vuda and Kamath, 2016; Turrens, 2003).

1.5.5 Regulation of Oxidative Phosphorylation

The rate of OXPHOS is primarily governed by substrate feedback as electron transport, in most cases, is tightly coupled to oxidative phosphorylation. OXPHOS requires a source of electrons at high potential (NADH and $FADH_2$), O_2, ADP and P_i. However, the most important factor determining respiratory rate is the abundance of ADP. Addition of ADP markedly increases mitochondrial oxygen consumption which subsequently returns to its initial value once converted to ATP. The regulation of OXPHOS by ADP availability is known as respiratory control (Hüttemann *et al.*, 2007; Berg *et al.*, 2007).

In higher organisms, additional mechanisms have evolved in order to 'fine tune' aerobic metabolism. These regulatory mechanisms include the expression of isoenzyme variants for tissue-specific requirements, intracellular allosteric control (e.g. phosphorylation) and extracellular cell signalling (e.g. glucagon and insulin).

1.6 The Mitochondrial Genome

In mammals the mitochondrial genome represents the only source of essential cellular proteins outside of the nucleus. Within the mitochondrion, mitochondrial DNA (mtDNA) is arranged as a circular, double-stranded DNA molecule. The two strands are distinguishable due to their nucleotide composition, the heavy strand (H-strand) is rich in guanine whilst the light strand (L-strand) is rich in cytosine. The length of mtDNA is variable amongst species, however in humans it is ~16,569 bp. Depending upon their energetic demands, somatic cells can contain anywhere between 100-10,000 copies of mtDNA (Chinnery and Hudson, 2013).

1.6.1 Basic Structure

MtDNA encodes a total of 37 genes, 28 of which reside on the H-strand and 9 on the L-strand (Figure 1.13). Thirteen of the genes encode for integral structural subunits of the mitochondrial respiratory chain, whilst the remaining 24 genes encode 22 tRNA molecules, 16s ribosomal RNA and 12s ribosomal RNA. Unlike nuclear DNA (nDNA), mtDNA lacks intronic regions and some genes, most notably MT-ATP6/MT-ATP8 which code for subunits within the F_o complex of ATP synthase, possess overlapping reading frames (Chinnery and Hudson, 2013). The displacement loop (D-loop), is the only major non-coding region within the mtDNA. It also represents the start site of mtDNA replication, containing both the origin of H-strand synthesis (OH) and H-strand transcription factors (heavy strand promotors (HSP) 1/2) (Chinnery and Hudson, 2013).

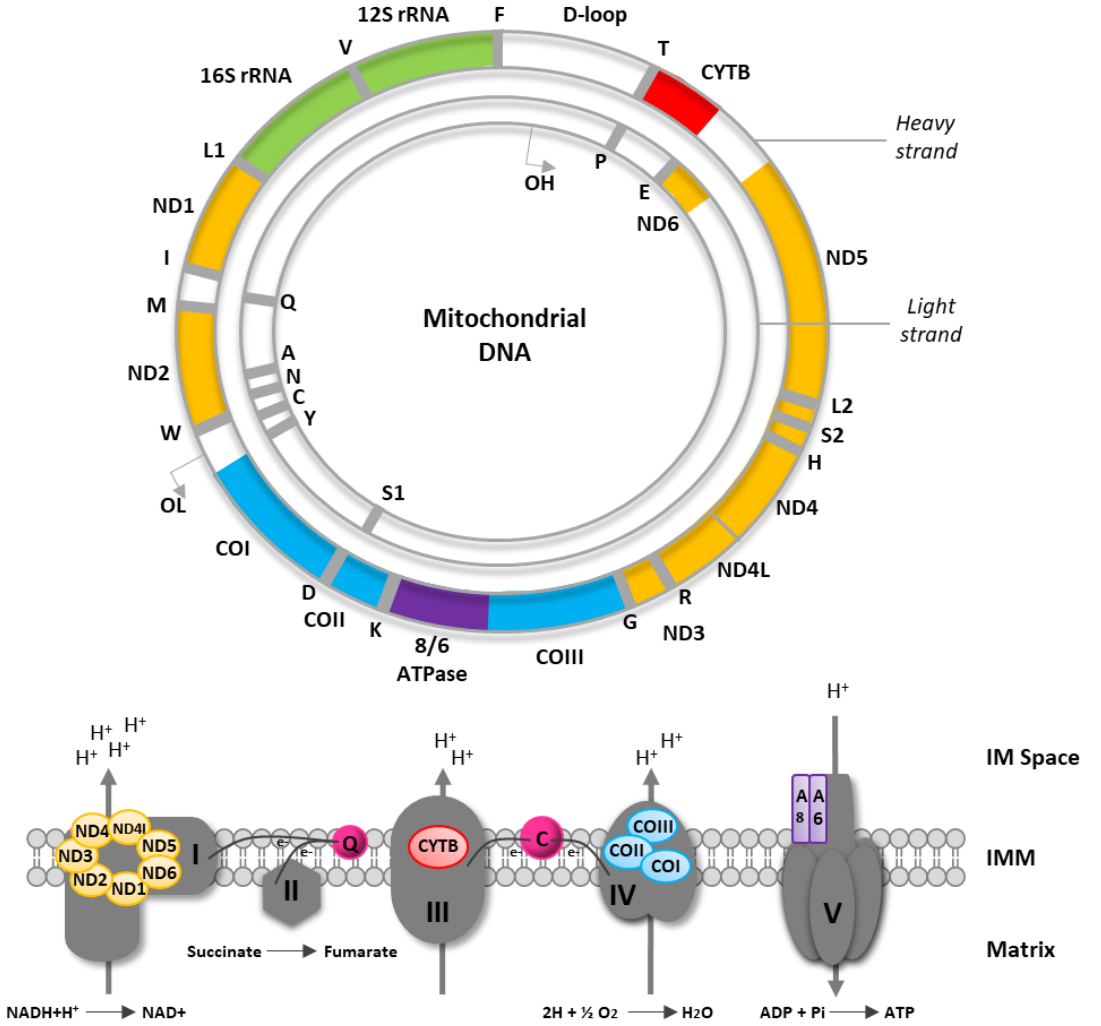

Figure 1.13 Basic structure of a human mitochondrial DNA molecule. Mitochondrial DNA encoded subunits of the respiratory chain are colour coded to the corresponding genes.

Human mtDNA does not strictly adhere to the genetic code of the nuclear genome. MtDNA uses only two stop codons 'AGA' and 'AGG' as opposed to 'UAA', 'UGA and 'UAG' used in nDNA (Temperley *et al.*, 2010). 'UGA' in the mitochondria encodes tryptophan whilst 'AUA', the codon for isoleucine in nDNA, encodes for methionine in the mtDNA (Chinnery and Hudson, 2013).

1.6.2 Inheritance

The DNA of cytoplasmic organelle such as the mitochondria are inherited in a non-Mendelian manner. It is generally accepted that in most multicellular organsims, mtDNA is inherited solely from the maternal germ line. This inheritance pattern is also known as 'uniparental inheritance'.

In human spermatozoa the mtDNA copy number is relatively low (50-100 copies), whereas in the oocyte it is extremely high (~100,000 copies). Thus maternal inheritance was originally thought to be due to dilution of the paternal mtDNA contribution beyond detection. More recent studies have unveiled that paternal mitochondria are selectively targeted for proteolysis once they enter the cytoplasm of the oocyte due to the presence of polyubiquinated prohibitin, an inner mitochondrial membrane protein expressed during spermatogenesis (Sutovsky *et al.*, 2004; W. E. Thompson *et al.*, 2003).

1.6.3 Nucleoid Packaging

The organisation of mtDNA is consequential of the endosymbiotic origin of the mitochondrion. Like bacterial DNA, mtDNA is compacted into ~100 nm DNA-protein complexes called nucleoids (Kukat *et al.*, 2011). Without nucleoid packaging, a completely relaxed 16.6 kb circular DNA molecule would have a diameter of ~5 µm (Gilkerson *et al.*, 2013). It has been estimated that each nucleoid houses 1.4 copies of mtDNA in human mitochondria and 1.5 copies in murine mitochondria, arguing the point that most mammalian nucleoids probably contain only a single copy of mtDNA (Kukat *et al.*, 2011).

The mitochondrial nucleoid comprises a variety of different proteins with diverse functions of which the most abundant are TFAM (mitochondrial transcription factor A). These functions range from the packaging, transcription and replication of mtDNA to communication and integration with the wider cellular signalling network. The condensation of mtDNA into nucleoids ensures distribution of genetic material throughout the mitochondrion and responsiveness to the metabolic needs of the cell (Gilkerson *et al.*, 2013).

Nucleoids are often found in close contact with the inner mitochondrial membrane, an attachment which is speculated to serve in the segregation of mtDNA during fission events or to aid insertion of mtDNA transcribed proteins into the IMM (Scheffler, 2008).

1.6.4 MtDNA Maintenance: Replication, Transcription and Translation

Replication of the mitochondrial genome takes place within the mitochondrial matrix. As opposed to the nuclear genome, mtDNA replication can occur in terminally differentiated cells which have exited the cell cycle (i.e. neurons and skeletal muscle) as well as proliferating cells. The ability of mtDNA to replicate in post mitotic cells highlights the importance of continuous mtDNA turnover throughout the life of an organism.

The mechanistic basis of mitochondrial replication has not yet been fully resolved however the ‘traditional’ model describes replication as an asynchronous strand displacement

mechanism involving two independent origins. Briefly, mtDNA synthesis begins at the origin of H-strand replication (O_H), downstream of the light strand promoter (LSP) within the non-coding D-loop domain. Upon displacement of the L-strand, synthesis proceeds along the parental H-strand until it reaches the origin of L-strand replication (O_L). Exposure of the L-strand initiation site allows replication to progress in the opposite direction to generate the daughter L-strand (Fernández-silva *et al.*, 2003; Clayton, 1982).

A second model of mtDNA replication has been suggested in which coupled leading-lagging strand replication initiated at the O_H is coordinated. In this model, lagging L-strand synthesis begins shortly after the initiation of H-strand synthesis and is the result of Okazaki fragment generation and subsequent conversion to DNA. (Holt *et al.*, 2000; Yasukawa *et al.*, 2006; Pohjoismäki *et al.*, 2010; Tuppen *et al.*, 2010).

Replication of the mitochondrial genome is accomplished by nuclear encoded proteins. Core components of the replisome include mitochondrial DNA polymerase γ (POLG), mitochondrial transcription factor A (TFAM) and mitochondrial single stranded binding protein (mtSSB) (Tuppen *et al.*, 2010).

1.6.4.1 Transcription

In mammalian mitochondria, mtDNA transcription is regulated at the D-loop. The D-loop possess two H-strand promoters (HSP1/2) along with the LSP and the O_H. Transcription initiated from the L-strand promoter is necessary for the generation of the primer for H-strand replication, therefore mtDNA replication is considered to be inherently linked to transcription. Bi-directional transcription gives rise to transcripts which encode several proteins (polycistronic transcripts). Transcription of both the L- and H-strand is achieved by the mitochondrial transcriptional core (TFAM, mitochondrial RNA polymerase (POLMT) and mitochondrial transcription factor B2) (Rebelo *et al.*, 2011). After transcriptional activation, elongation steps are performed by the mitochondrial transcriptional elongation factor (TEFM) through interaction with POLMT. MtDNA transcription, when initiated from the HSP1 promoter is terminated by the specific binding of mitochondrial transcription termination factor 1 (MTERF1) (Tuppen *et al.*, 2010).

1.6.4.2 Translation

The mitochondrial translation system is responsible for the production of 13 essential subunits of the respiratory chain complexes (I-IV) and ATP synthase. Whilst critical for respiratory function, the existence and biogenesis of mitochondria is not dependent upon

mitochondrial protein synthesis as demonstrated by the generation of rho0 cells which are devoid of mtDNA (Kukat *et al.*, 2008; Scheffler, 2008).

Mitochondrial protein synthesis mechanisms are poorly resolved in comparison to their cytoplasmic counterparts. The basic machinery required to perform mitochondrial translation includes mtDNA encoded rRNA and tRNAs as well as nuclear encoded factors which are imported into the mitochondria. These include two initiation factors (IF2 and IF3), four elongation factors (EFG1, EFG2, EFTs and ETFu) and one termination factor (mtRF1a) along with mitochondrial ribosomal proteins, aminoacyl-tRNA synthetases, methionyl-tRNA transformylase and ribosome recycling factors (mtRRF) (Van Den Heuvel *et al.*, 2010).

The mitochondrial translation system is distinct from its cytoplasmic counterpart due to the presence of polycistronic transcripts, polyadenylated partial stop codons, deviation from the standard genetic code and RNA-poor mitoribosomes (Tuppen *et al.*, 2010).

1.6.5 Heteroplasmy

Mutations in mtDNA cannot always be linked to phenotypic consequence due to the presence of multiple copies of mtDNA within a cell (polyploidy). Whilst in most cases the polymorphisms present in mtDNA molecules are homoplasmic (i.e. present in all copies), mutations can affect a subset of the mtDNA population, leading to the presence of multiple distinct sequences which can be both inter or intra-mitochondrial. This phenomenon is known as heteroplasmy (Wallace and Chalkia, 2013).

The majority of pathogenic mtDNA mutations are recessive and the mutational load can differ significantly between tissues of the same individual (Tam *et al.*, 2008) or may be entirely tissue specific. The segregation of mtDNA during cell division is a random process resulting in the potential for daughter cells to receive different copies of mtDNA in an event called replicative segregation (Diez-Juan and Simón, 2015). Replicative segregation can lead to the continuous propagation of bioenergetic defects however, a minimum critical proportion of mutant mtDNA is required before a phenotypic consequence is apparent. Typically this threshold value can range anywhere between 60-90 % mutant to wild-type mtDNA and may be lower in cell types which are particularly reliant on OXPHOS for ATP generation (Tuppen *et al.*, 2010). Conversely, mtDNA mutants may be reduced or lost via replicative segregation, particularly in highly proliferative cell types (Rahman *et al.*, 2001).

In post mitotic cells, mtDNA is continuously being turned over in a process referred to as relaxed replication. In a heteroplasmic cell, it is plausible that by chance a mutant mtDNA

copy may be replicated more frequently than a wild-type molecule. This has the potential to change the mutational load of a cell over time (Stewart and Chinnery, 2015).

1.6.6 MtDNA Mutations

MtDNA genes have a very high sequence evolution rate, in the order of 10-17 fold greater than that of nuclear genes. This is a by-product of an exceptionally high mutational rate and a comparatively low endogenous repair capacity (Wallace and Chalkia, 2013). The high mutational rate of mtDNA is attributable to errors accrued during genome replication rather than oxidative damage as previously assumed (Larsson, 2010).

Rearrangements (deletions) of the genome are thought to be a result of inherited mutations in nuclear genes whose products are involved in mtDNA maintenance (e.g. POLG or TWINKLE) (Tuppen *et al.*, 2010). Point mutations may be the result of imbalances in the levels of different nucleotides within the mitochondria and not the fidelity of POLG specifically (Flintoft, 2005; Song *et al.*, 2005).

There are three types of clinically relevant mtDNA mutations: functional variants associated with ancient mtDNA lineages, recent deleterious mutations that can result in maternally inherited disease and somatic mutations which accumulate in tissues over time. The phenotypic consequences of mtDNA mutations may be further modulated by interactions with the nuclear genome and the environment (Wallace, 2013).

1.6.7 Mitochondrial Haplogroups

A mitochondrial 'haplotype' is defined as a group of polymorphisms within an organism that have been inherited together from a single parent. A mitochondrial haplogroup represents

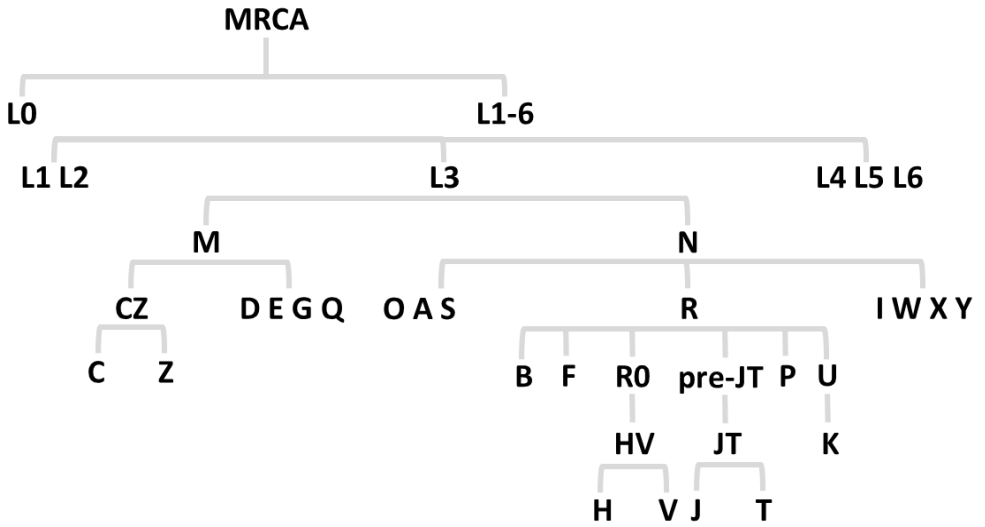

Figure 1.14 Simplified phylogenetic tree of major human mitochondrial DNA haplogroups. The tree is based upon mtDNA phylotree build 17 (van Oven, 2015)**.**

a group of similar haplotypes that share a common ancestor but are distinguishable by the addition of functionally significant single nucleotide polymorphisms (SNPs).

Each mitochondrial haplogroup originates from, and remains a part of a preceding single haplogroup. As such, related haplogroups can be modelled as a nested hierarchy, relating to the sequential accumulation of mutations since the most recent common ancestor (MRCA) (Figure 1.14). Macro-haplogroups are identified by an initial letter of the alphabet with sub-clade refinements consisting of additional letter and number combinations. As haplogroups were named in the order of their discovery, the alphabetical ordering does not pertain to any genetic relationships.

1.6.8 MtDNA Variation and Functional Consequence

The central role of the mitochondrial genome in OXPHOS and cellular physiology means that functional variants in mtDNA genes can have considerable consequences at the tissue or systemic level. In the past it has been difficult to evaluate the contribution of mtDNA variation to molecular processes. However, with the advent of the cybrid (cytoplasmic hybrid) model, questions relating to the functional importance of mtDNA variation and mitochondria-nuclear interactions can now be answered. The cybrid model relies on the fusion of rho0 zero cells (devoid of mtDNA) with mitochondria rich cytoplasts (anucleate) from different donors, creating cells with an identical nuclear background whilst varying the mtDNA haplogroup.

This technique has been instrumental in identifying key functional differences between different mitochondrial haplogroups. For example, recent studies have demonstrated differences in mtDNA copy number and mtDNA coded respiratory complex expression between African haplogroup L and European haplogroup H. Haplogroup L exhibited decreased ATP turnover and lower levels of ROS production, attributes which are consistent with greater OXPHOS efficiency (Kenney *et al.*, 2014).

Importantly, work such as this has paved the way for studies into the effects of mitochondrial genome variability upon susceptibility to complex diseases such as breast cancer, metabolic syndrome and sepsis (Tanaka *et al.*, 2007; Bai *et al.*, 2007; Yang *et al.*, 2008; Jiménez-Sousa *et al.*, 2015). Furthermore, several studies have also investigated a causal linkage between mitochondrial genome variation and the development of adverse reactions in response to certain drugs, particularly antiretroviral agents (Hendrickson *et al.*, 2009; Canter *et al.*, 2010; Kampira *et al.*, 2013; Micheloud *et al.*, 2011).

1.7 Models to Assess Mitochondrial Dysfunction

Interrogations of mitochondrial function *in vitro* are typically performed using isolated mitochondria or whole cells. Both approaches are accompanied by their own set of advantages and disadvantages; particularly, the use of isolated mitochondria allows for the direct delivery of respiratory substrates to the organelle but suffers from limited physiological relevance. In contrast, intact cells have greater physiological relevance yet are constrained as a model by impermeability to some mitochondrial substrates (Salabei *et al.*, 2014; Brand and Nicholls, 2011). Therefore, to facilitate the selection of an appropriate model, one must first consider both the chemical characteristics of the drug in question and the overall aim of the study (Figure 1.15).

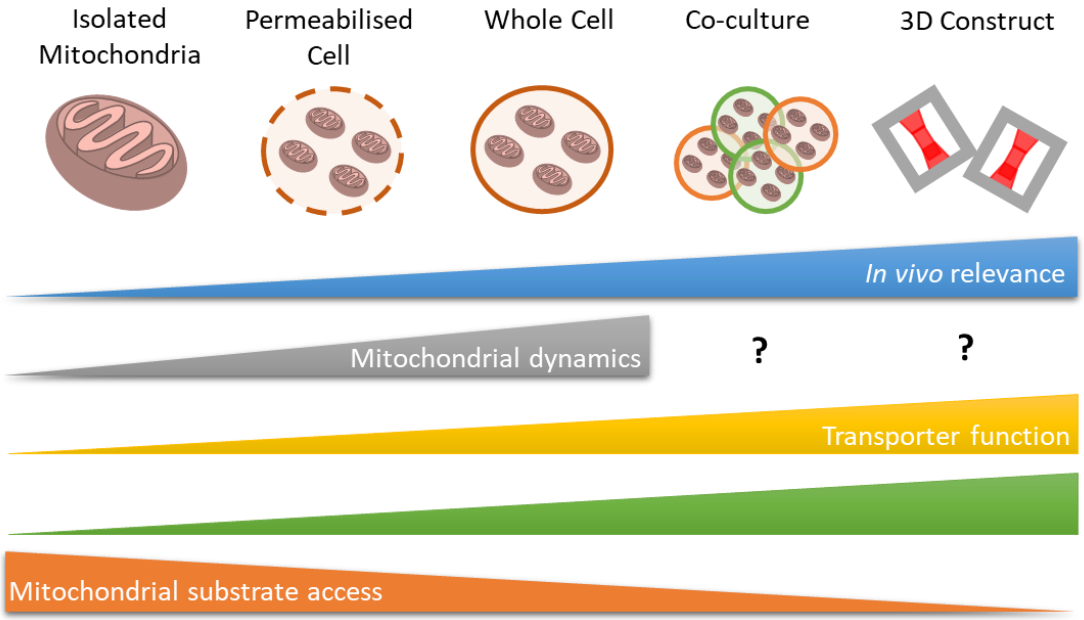

Figure 1.15 Comparison of different models used to assess drug-induced mitochondrial dysfunction, ranging from isolated mitochondria to 3D cell models.

1.7.1 Whole Cell Models

Whole cell models are frequently used to indirectly assess mitochondrial function, via the measurement of cellular ATP abundance for example. They also have the additional benefit of only requiring a relatively small amount of biological material to perform a plethora of plate-based assays, thus improving through-put. Importantly, intact cells provide a more physiologically relevant environment from which to study mitochondria *in situ*. Maintenance of the native cellular environment preserves inter-mitochondrial communications, mitochondrial dynamics and interactions with other organelle. As such, cell-based systems

are more appropriate when examining multi-mechanistic toxicity or indirect mitochondrial dysfunction (Brand and Nicholls, 2011)

1.7.2 Isolated Mitochondria

The isolation of mitochondria from cells has long been a mainstay in the field of drug-induced mitochondrial dysfunction, a technique necessitated by the impermeability of the plasma membrane to mitochondrial substrates (Salabei *et al.*, 2014). However, there are practical limitations associated with the method, namely the amount of cellular material required to generate a sufficient yield of mitochondria for study, structural disruption during isolation, and limited functionality of the organelle post-isolation (Kuznetsov *et al.*, 2008).

The isolation of mitochondria does indeed allow for the study of direct mitochondrial interactions with exogenously supplied compounds and substrates; however, these interactions are less physiologically relevant due to a lack of competing toxicity or protective mechanisms which would otherwise be present in a 'whole cell' setting (Perry *et al.*, 2013; Kuznetsov *et al.*, 2008). Furthermore, compound screening performed using isolated organelle may increase the likelihood that drug-induced dysfunction remains undetected, particularly in scenarios whereby multi-mechanistic toxicity is at play or biotransformation of a compound is required to see an effect.

1.7.3 Permeabilised Cells

The caveats associated with both isolated mitochondria and whole cells can be, in part, ameliorated using permeabilised cells. This technique enables the simultaneous delivery of mitochondrial substrates past the plasma membrane whilst maintaining the integrity of mitochondrial-protein and mitochondrial-organelle contacts *in situ* (Brand and Nicholls, 2011). The cellular material requirements are far more conservative than those needed to perform comparable studies in isolated mitochondria. Furthermore, the technique avoids any bias mediated by the sub-selection of mitochondrial populations during isolation and the functional decline of mitochondria removed from their native environment (Kuznetsov *et al.*, 2008; Brand and Nicholls, 2011).

1.8 Thesis Aims

The deleterious effects of statins upon the mitochondrial respiratory chain has been implicated as one of several putative mechanism by which myopathic symptoms may be potentiated in some statin recipients. Furthermore, inter-individual variation in

mitochondrial genotype and by extension, bioenergetic function, may in part underpin susceptibility to statin-related myopathy.

Therefore, the overall aim of this research was to first establish the effects of statin chemical species (i.e. inactive lactone pro-drugs versus active β-hydroxy acids) upon the functionality of the mitochondrial respiratory chain using high-resolution respirometry. Thereafter, the remainder of the thesis focussed upon the development of a three-dimensional, bioengineered, micro-tissue model of human skeletal muscle to identify functional bioenergetic factors which may confer enhanced or diminished risk of statin-mediated mitochondrial dysfunction. Finally, due to the governance of respiratory chain assembly, stability and functionality by the mitochondrial genome, next generation sequencing (NGS) of patient mitochondrial DNA was performed on a statin myopathy case-control cohort to determine if there was an association between mitochondrial genotype and patient status.

Chapter 2

Assessing the Differential Effects of Simvastatin Lactone and β-Hydroxy Acid upon Mitochondrial Respiratory Chain Function

Contents

2.1 Introduction 56

2.1.1 Summary of Chapter Aims 58

2.2 Materials and Methods 60

2.2.1 Materials 60

2.2.2 General Cell Culture Maintenance 60

2.2.3 Differentiation Procedure 60

2.2.4 Combined Lactate Dehydrogenase (LDH) and ATP Assays 61

2.2.5 Extracellular Flux Analysis 65

2.2.6 Semi-Automated Pump Controlled Cell (PCC) Rupture System for the Isolation of Mitochondria from Cultured Cells 70

2.2.7 Simultaneous Assessment of Membrane Potential and Swelling in Isolated Mitochondria 72

2.2.8 Western Blots 73

2.2.9 Statistical Analyses 74

2.3 Results 75

2.3.1 Acute Metabolic Manipulation of L6 Myocytes using Galactose Media ... 75

2.3.2 Examining the Post-Translational Farnesylation of RAS GTPase in L6 Myocytes via Western Blot. 78

2.3.3 Extracellular Flux Analysis of Acute Statin-Induced Changes in Mitochondrial Function 79

2.3.4 Assessing Acute Simvastatin-Induced Respiratory Complex Dysfunction 82

2.3.5 Assessment of Mitochondrial Membrane Potential and Swelling in Isolated Mitochondria 83

2.3.6 Chronic Metabolic Manipulation of L6 Myocytes using Galactose Media 85

2.3.7 Extracellular Flux Analysis of Chronic Statin-Induced Changes in Mitochondrial Function 86

2.3.8 Assessing Chronic Simvastatin-Induced Respiratory Complex Dysfunction 88

2.3.9 Investigating the Impact of Chronic Simvastatin Treatment upon Acyl-Carnitine Driven Respiration 90

2.4 Discussion 91

2.5 Conclusions 96

2.1 Introduction

The deleterious effect of statins upon muscular energy metabolism appears to represent both an important and frequently cited feature of the mechanism through which they impart their cytotoxic effects (Apostolopoulou *et al.*, 2015; Golomb and Evans, 2008). However, despite continued research within the field, the precise nature of the mitochondrial toxicity is still widely debated. To add further complexity, statins are administered as either a lactone pro-drug or a pharmacologically active β-hydroxy acid. Both lactones and acids of a given statin can be detected in systemic circulation, indicating the interconversion of the chemical species *in vivo* (Prueksaritanont, Subramanian, *et al.*, 2002; Hoffmann and Nowosielski, 2008). It has been reported, across a limited number of studies, that the lactone species of statins have a greater propensity for mediating acute cytotoxicity when directly compared, at equimolar concentrations, with their corresponding β-hydroxy acid (Skottheim *et al.*, 2008; Schirris *et al.*, 2015). However, this has yet to be investigated under extended time points or at concentration ranges which are more reflective of the plasma C_{max} in patients (Table 2.1).

Table 2.1 Plasma C_{max} ranges for each statin in its administered form i.e. lovastatin and simvastatin values are calculated for the lactone species whilst all remaining values are calculated for the β-hydroxy acid species.

	Statin							
	Atorva	**Ceriva**	**Fluva**	**Lova**	**Pitava**	**Prava**	**Rosuva**	**Simva**
Plasma C_{max} (nM)	48-118	15.4-19.5	1000	24	142.3	105.9-129.5	76.8	80-2200

Based on a 40 mg oral dose, with the exceptions of pitavastatin (2 mg) and cerivastatin (0.8 mg) and simvastatin (7.5 mg/kg). Table generated using data compiled from (Stefano *et al.*, 2004; Catapano, 2010; Jung *et al.*, 2012; Morgan *et al.*, 2012; Corsini *et al.*, 1999; White, 2002; Mück, 2000; Ahmed *et al.*, 2013).

Previous *in vitro* studies within this area have been typically performed using immortalised, cancer-derived cell lines of either human or rodent origin. One of the key aspects by which immortalised cells differ from those within living systems or those maintained in primary culture is that of their bioenergetic profile. Whilst is it typical of most cells, under physiological conditions, to generate ATP preferentially through oxidative phosphorylation within the mitochondria, it is characteristic of some cancer cells to undergo extensive metabolic adaptations in order to meet the energetic demands imposed by an enhanced proliferative capacity (Diaz-Ruiz *et al.*, 2011). Specifically, the repression of oxidative metabolism in cancer cells can occur despite the presence of saturating oxygen

concentrations and a full complement of functional mitochondria, a phenomenon known as 'aerobic glycolysis' or the 'Warburg effect'. This change is thought to be a long-term compensatory mechanism which allows for cellular proliferation in hypoxic environments, such as those found in solid tumours (Diaz-Ruiz *et al.*, 2011; Warburg, 1956). It has also been demonstrated that some cell lines are capable of reversibly switching between fermentation and oxidative metabolism depending on the exogenous glucose supply, a transient event known as the 'Crabtree effect' (Diaz-Ruiz *et al.*, 2011, 2009).

In cells that exhibit an enhanced reliance on aerobic glycolysis, direct mitochondrial toxicants have little observable effect on cell viability or ATP content, which in turn diminishes their utility as predictors of mitochondrial dysfunction. Resistance to mitochondrial perturbations is exacerbated by modern cell culture practice whereby cells are often grown in media containing glucose concentrations five-fold greater than physiological levels, thus supressing oxidative metabolism via the Crabtree effect (Marroquin *et al.*, 2007; Rodríguez-Enríquez *et al.*, 2001) . To circumvent this effect and allow for the identification of mitochondrial toxins in an otherwise resistant system, an elegant solution was developed in 2007 by Marroquin *et al*. The culturing of cells in the presence of galactose and L-glutamine, with the simultaneous exclusion of glucose, impels anaerobically poised cells to oxidise pyruvate and glutamine via oxidative phosphorylation due to insufficient ATP gain from the oxidation of galactose to pyruvate (Marroquin *et al.*, 2007; Reitzer *et al.*, 1979).

This method has been increasingly employed as a means of screening for compound associated mitochondrial toxicity in tissue specific systems. Indeed, subsequent studies conducted by Dott *et al*., have demonstrated that the L6 rat skeletal myocyte line exhibits increased susceptibility to classic mitochondrial toxicants when supported by galactose and L-glutamine supplementation, as opposed to glucose (Dott *et al.*, 2014). Therefore, by utilising simvastatin as an archetypical representative of a lipophilic statin which causes myopathy in both human and animal models (Kwak *et al.*, 2012), this chapter shall assess the differential toxic effects of simvastatin, in both its inactive lactone (SVL) and pharmacologically active β-hydroxy acid (SVA) conformations, upon mitochondrial function. Initially this shall be assessed by comparing measurements of cytotoxicity and ATP content in L6 myotubes which have been metabolically conditioned to media containing either glucose or galactose and L-glutamine.

Assessment of mitochondrial respiratory function *in vitro* has typically been performed by measuring the rate of oxygen consumption in isolated organelles or cells in suspension using

an oxygen electrode. Whilst this method has proved extremely effective in delineating aspects of mitochondrial physiology, it is not suitable for all cell types. Conversely, the use of isolated organelle lacks the cellular regulation of mitochondrial function and may overstate drug toxicity (Dranka *et al.*, 2011). In order to bridge this gap, methods have been developed to assess the behaviour of mitochondria within a cellular setting using real time extracellular flux analysis (XF). XF analysers are capable of simultaneously measuring the oxygen consumption rate (OCR) and extracellular acidification rate (ECAR) of adherent cell cultures, facilitating the simultaneous assessment of oxidative and glycolytic flux with the capacity to sequentially inject a variety of respiratory inhibitors (Hill *et al.*, 2012).

In this chapter, extracellular flux analyser technology (XF^e96) shall be employed so that the bioenergetic performance of SVL and SVA treated L6 myocytes may be ascertained. Using sequential injections of respiratory inhibitors, whilst monitoring the resultant variations in OCR/ECAR in real time, it is possible to determine the efficiency at which oxidative phosphorylation is coupled to oxygen consumption whilst concurrently measuring parameters such as maximal respiratory capacity, ATP-linked respiration, proton leak and spare respiratory capacity. Furthermore, this technology shall be used to examine the mechanistic nature of any observed perturbations. This will be achieved by means of *in situ* cell permeabilisation, using recombinant perfringolysin O (rPFO), and controlled substrate provision so that the functionality of each independent respiratory complex and the fatty acid β-oxidation pathway may be interrogated (Divakaruni *et al.*, 2014).

Investigations within this chapter have been performed over a range of drug concentrations and time courses in order to examine the relationship between the onset of mitochondrial dysfunction and the emergence of cell death. It is intended that through these experiments, the hypothesis that simvastatin and its active hydroxy acid can exert direct and independent deleterious effects on the mitochondrial respiratory chain, may be fully examined.

2.1.1 Summary of Chapter Aims

1) To examine the differential impact of simvastatin lactone and β-hydroxy acid upon ATP content and cell viability in both acutely and chronically treated L6 myocytes.
2) To examine the differential impact of simvastatin lactone and β-hydroxy acid application upon respiratory functionality in whole and permeabilised L6 cells at acute and chronic time points.

3) To examine the differential impact of acute simvastatin lactone and β-hydroxy acid application upon mitochondrial swelling and inner membrane potential in isolated mitochondria.

2.2 Materials and Methods

2.2.1 Materials

All forms of Dulbecco's Modified Eagle Medium (DMEM), media supplements and cell culture reagents were purchased from Life Technologies (Paisley, UK). L6 myoblasts were obtained as a cryopreserved stock (1 x 10^6 cells) from the American Type Culture Collection (ATCC, VA, USA). Anti-actin and anti-VDAC 1 antibodies were purchased from Abcam (Cambridge, UK). Anti-Ras antibody was purchased from BD Biosciences (London, UK). Lactate dehydrogenase cytotoxicity detection kit was purchased from Roche Diagnostics Ltd (West Sussex, UK). Extracellular flux analyser (XF^{e}96) consumables and base medium were purchased from Agilent Technologies (CA, USA). Simvastatin hydroxy acid ammonium salt and cerivastatin hydroxy acid sodium salt were purchased from Toronto Research Chemicals (LGC Promochem, Middlesex, UK). Cerivastatin lactone was purchased from Santa-Cruz Biotechnology Inc (TX, USA). All other reagents and chemicals were purchased from Sigma Aldrich (Dorset, UK) unless otherwise stated.

2.2.2 General Cell Culture Maintenance

L6 rat skeletal myoblasts were routinely maintained in a complete growth medium consisting of high glucose DMEM (25 mM), supplemented with 4 mM L-glutamine (1 % v/v), 10 % (v/v) foetal bovine serum (FBS), 5 mM HEPES (4-(2-hydroxyethyl)-1-piperazineethanesulfonic acid) (1 % v/v) and 1 mM sodium pyruvate (1 % v/v). Cells were cultured in vented T75 flasks and incubated in a humidified environment at 37 °C with 5 % (v/v) CO_2. In order to prevent the decline of cell fusion properties, L6 myoblasts were maintained at sub-70 % confluence and were used between passages 3-15 as per the vendor instructions. Cell populations were frozen using a standard cryopreservation mix which consisted of complete growth medium supplemented with 10 % DMSO (v/v) and stored at -180 °C under the liquid nitrogen vapour phase.

2.2.3 Differentiation Procedure

Cells were dissociated using 0.25 % trypsin-EDTA and seeded into collagen coated (50 µg/mL in 0.02 M acetic acid) tissue culture plates at the specified densities. Cells were incubated for 24 hours in complete growth medium to promote adherence (37 °C with 5 % (v/v) CO_2). The following day, the growth medium was removed and cells were washed twice with 1X HBSS. Cells were then cultured in a differentiation medium consisting of high glucose (25mM) DMEM supplemented with 4 mM L-glutamine (1 % v/v), 5 mM HEPES (1 % v/v), 1 mM sodium

pyruvate (1 % v/v) and 2 % (v/v) horse serum. Thereafter, the differentiation medium was changed every 48 hours for 7 days.

2.2.4 Combined Lactate Dehydrogenase (LDH) and ATP Assays

2.2.4.1 Acute Metabolic Manipulation using Galactose Media

Many highly proliferative cell types grown in supra-physiological glucose conditions generate the vast majority of their ATP via glycolysis despite being cultured in the presence of oxygen and possessing a full complement of functional mitochondria. This process is known as the crabtree effect (Marroquin *et al.*, 2007). Therefore, assessment of direct mitochondrial dysfunction in some cell types requires the replacement of glucose with galactose as the primary carbon source. By substituting glucose, glycolysis must be initiated by the oxidation of galactose to pyruvate, resulting in negligible net ATP gain via glycolysis and an increased reliance upon oxidative phosphorylation for ATP generation (Figure 2.1) (Reitzer *et al.*, 1979). This ultimately enables the detection of compounds which perturb mitochondrial function within an *in vitro* setting.

This method was later adapted by Kamalian *et al*., whereby acute conditioning to galactose media 2 hours prior to the addition of test compounds, rather than long-term culture, was deemed sufficient to detect mitochondrial liabilities in HepG2 cells (Kamalian *et al.*, 2015) and later in HepaRG cells (Kamalian *et al.*, 2018).

The assessment of ATP content in galactose media is used as an endpoint measure of mitochondrial function and is sensitive enough to be detected in the absence of cell death. When assessed in parallel to cytotoxicity, it can provide additional information on whether the mitochondrial liability is the cause or consequence of cytotoxicity (Kamalian *et al.*, 2015). Direct mitochondrial dysfunction can be defined as a significant difference between the ATP IC_{50} values in glucose and galactose media with a ratio ≥ 2 (IC_{50}ATPglu/IC_{50}ATPgal ≥ 2). Induction of mitochondrial dysfunction prior to the onset of cell death is defined as (IC_{50}LDHgal/ IC_{50}ATPgal ≥ 2) (Kamalian *et al.*, 2015; Swiss *et al.*, 2013).

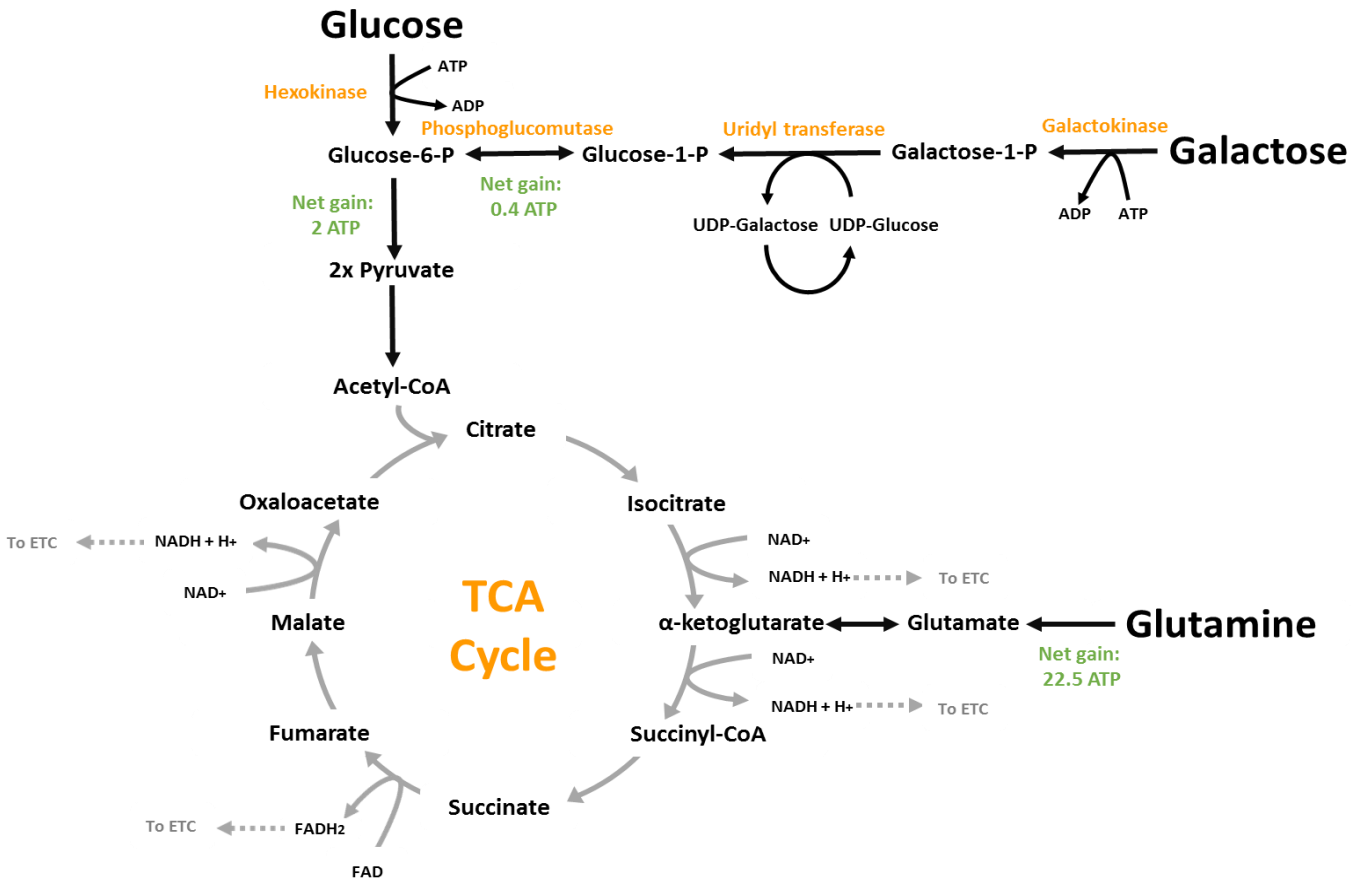

Figure 2.1 The principles behind galactose and L-glutamine supported respiration. There is zero net ATP gain from galactose oxidation until reaction equilibria is reached. At steady state, due to inefficiencies in the pathway, the net yield is 0.4 mol ATP per mol galactose i.e. 80 % less than with glucose. 22.5 mol ATP is derived from glutamine metabolism, accounting for > 98 % of the total ATP yield. This is sufficient to force cells to become aerobically poised (Reitzer *et al.*, 1979). Abbreviations: ETC, electron transport chain; TCA, tricarboxylic acid; CoA, Coenzyme A; UDP, uridine diphosphate; 1/6-P, 1/6-phosphate.

2.2.4.2 Experimental Design

L6 myoblasts were collected by trypsinisation and seeded into collagen coated (50 µg/mL in 0.02 M acetic acid) flat-bottomed 96-well plates in complete growth media ($1.6x10^4$ cells/100 µL/well) and differentiated for 7 days thereafter (37 °C with 5 % (v/v) CO_2). Resultant myotubes were washed three times in serum-free glucose or galactose media (DMEM supplemented with 25 mM glucose and 4 mM L-glutamine or 10 mM galactose and 6 mM L-glutamine respectively, plus 5 mM HEPES (1 % v/v) and 1 mM sodium pyruvate (1 % v/v)), before the addition of either glucose or galactose media (50 µL) and incubation for 2 hours (37 °C with 5 % (v/v) CO_2). For drug incubation periods which exceeded 48 hours, 2 % (v/v) horse serum was added to the assay medium.

After 2 hours of media conditioning, 200X drug stock solutions prepared in DMSO were diluted 1:100 into either glucose or galactose media before 50 µL was added to the relevant wells (final solvent concentration 0.5 %). Drug incubations were carried out for the stipulated time period, in the relevant assay media type (37 °C with 5 % (v/v) CO_2). Dosing medium was refreshed every 24 hours if culture time exceeded this period. All plates included both a vehicle control (0.5 % DMSO) and blank wells containing media alone.

2.2.4.3 ATP Assay

A bioluminescence assay kit was used for the quantitative determination of ATP content. The principle of the assay is based upon the hydrolysis of ATP and the emission of light when recombinant firefly luciferase catalyses the oxidation of D-luciferin. When ATP is the limiting factor, the light emitted during the assay is directly proportional to the amount of ATP present in the sample:

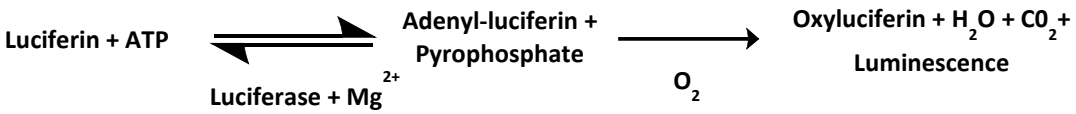

ATP content was assessed by the addition of sample lysates (5 µL) and ATP standards to a white-walled 96-well plate. The ATP reaction solution was prepared according to manufacturer's instructions by mixing ATP assay mix with ATP dilution buffer in a 1:25 ratio. 40 µL of the reaction solution was added to both samples and standards then read immediately on a Varioskan™ Flash multimode plate reader with SkanIt™ software to capture the peak luminescent signal.

2.2.4.4 Lactate Dehydrogenase (LDH) Assay

Detection of cytotoxicity was achieved using a lactate dehydrogenase (LDH) assay kit. LDH is a stable cytoplasmic enzyme present in most cell types. Upon rupture or damage of the plasma membrane, LDH is rapidly released into the surrounding supernatant. LDH activity is determined in a coupled reaction whereby L-lactate and pyruvate are interconverted concomitantly with NADH and NAD^+ by LDH. Diaphorase and NADH reduce the tetrazolium salt INT (2-(4-iodophenyl)-3-(4-nitrophenyl)-5-phenyl-2*H*-tetrazolium) to a red, water soluable formazan dye which is quantifiable at an absorbance of 492 nm (Figure 2.2).

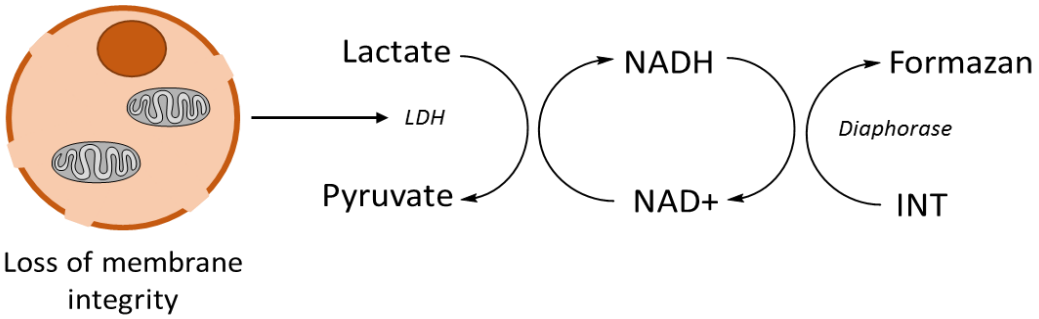

Figure 2.2 Upon rupture of the cell membrane, release of LDH into the surrounding supernatant can be detected using INT tetrazolium salts.

LDH retention was determined by extracting 25 µL supernatant and 10 µL cell lysate for each sample and incubating them with 50 µL LDH catalyst-dye solution (1:45 ratio), according to manufacturer's instructions. After 30 minutes incubation in the dark, samples were read at 490 nm on a Varioskan Flash multimode plate reader with SkanIt™ software. LDH retention was determined using the following equation:

$$\textbf{LDH Retention} = \frac{\textbf{Lysate}}{(\textbf{Supernatant} + \textbf{Lysate})}$$

2.2.4.5 Bicinchoninic Acid (BCA) Assay

The bicinchoninic acid (BCA) assay kit was used to normalise ATP data to total protein in order to account for potential variances in cell seeding density. The BCA assay works by combining the reduction of Cu^{2+} to Cu^{1+} by proteins in an alkaline medium, with the colorimetric detection of the cuprous oxide cation (Cu^{1+}) by BCA.

The first step, also known as the biuret reaction, involves the chelation of copper (II) sulphate with proteins containing 3 or more amino acid residues in an alkaline environment to produce a light blue coloured chelate complex with Cu^{1+}. The second step is a colour

development reaction whereby BCA reacts with reduced Cu^{1+} to produce an intense purple-coloured copper-BCA complex which exhibits a strong linear absorbance at 562 nm.

Protein content was determined using cell lysates (10 µL) and a bovine serum albumin (BSA) standard curve (10 µL). BCA reagent was prepared according to manufacturer's instructions by mixing BCA with copper (II) sulphate in a ratio of 50:1. 200 µL of the resultant reaction mixture was dispensed into each well. The plates were then incubated at 37 °C for 30 minutes before reading at 562 nm on a Varioskan™ Flash multimode plate reader with SkanIt™ software.

2.2.5 Extracellular Flux Analysis

One of the most commonly used instruments to measure respiratory function is the extracellular flux analyser (Agilent Technologies). The instrument uses a 96-well (XF^e96) or 24 well (XF24) cell culture microplate and a sensor cartridge which sits within the microplate to execute the assay. Each probe of the cartridge harbours two fluorophores, one of which is sensitive to oxygen (O_2) and the other to protons (H^+) (Figure 2.3).

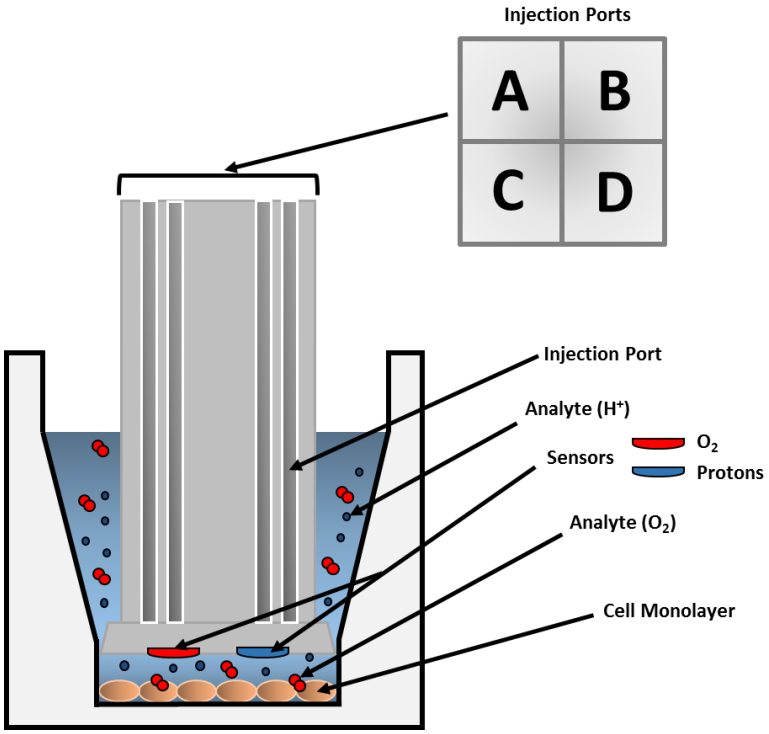

Figure 2.3 Schematic diagram depicting the detection of analytes (O_2 and H^+) by extracellular flux analysis. Measurement of changes in O_2 and H^+ within the extracellular medium occurs in real time by lowering a sensor cartridge containing fluorophores into a microplate containing a cell monolayer. Injection ports allow for the addition of substrates or inhibitors at user-defined intervals.

Fibre optic bundles are lowered into the sensor probes, creating a transient micro-chamber (200 µL) whilst emitting light and exciting the embedded fluorophores. Changes in the

emission of the fluorophores corresponds to changes in the concentration of O_2 and H^+ in the extracellular medium.

This relates to changes in the oxygen consumption rate (OCR) and extracellular acidification rate (ECAR) of the cells (Ferrick *et al.*, 2008; Perry *et al.*, 2013). In addition, the XF analyser cartridges have four injection ports which allow for the sequential incorporation of compounds or substrates at user defined intervals to determine various respiratory parameters as outlined in Table 2.2.

Table 2.2 Calculations for mitochondrial stress test respiratory parameters.

Bioenergetic Parameter	Calculation
Basal Respiration	Last OCR measurement before injection of oligomycin – non-mitochondrial OCR
ATP-Linked Respiration	Last OCR measurement before injection of oligomycin – lowest OCR measurement after oligomycin injection
Proton Leak	Lowest OCR measurement after injection of oligoycin- non-mitochondrial OCR
Maximal Respiratory Capacity	Highest OCR measurement after injection of FCCP – non-mitochondrial OCR
Spare Respiratory Capacity	Maximal respiratory capacity – basal respiration
Non-Mitochondrial OCR	Lowest OCR measurement after injection of rotenone and antimycin A
% Coupling Efficiency	ATP-linked respiration/basal respiration *100

Abbreviations: OCR, oxygen consumption rate; FCCP, carbonyl cyanide 4-(trifluoromethoxy) phenylhydrazone.

2.2.5.1 Assay Preparation and Normalisation

L6 myoblasts were collected by trypsinisation and seeded into collagen coated (50 µg/mL in 0.02 M acetic acid) XF^{e}96 cell culture microplates in complete growth media ($1x10^4$ cells/well/100 µL) and differentiated for 7 days (37 °C with 5 % (v/v) CO_2). Following the completion of XF assays, cells were lysed in somatic cell ATP releasing agent (20 µL). Lysates (10 µL) were transferred to a 96-well plate for quantification of protein content by BCA assay. Protein content per well was used as a means to normalise raw OCR and ECAR values.

2.2.5.2 Mitochondrial Stress Test

L6 myotubes were incubated for 1 hour (37 °C, 0 % CO_2) prior to the start of the assay. Culture medium was replaced with 175 µL unbuffered XF base medium supplemented with glucose (25 mM), L-glutamine (2 mM), sodium pyruvate (1 mM), pre-warmed to 37 °C (pH 7.4).

2.2.5.3 Compound Preparation

For the acute injection of test compounds (Table 2.3), serial dilutions of 200X drug stocks were prepared in DMSO. Each 200X stock was further diluted to 8X the final well concentration in unbuffered assay media. Injection solutions were buffered to pH 7.4 using 0.03 M HCl and/or NaOH before being loaded into injection port A of the sensor cartridge.

Table 2.3 Acute mitochondrial stress test injection port locations, compound stock concentrations, dilution factors and final well concentrations.

Injection Port	Compound	Stock Concentration	Well Dilution Factor	Final well concentration
A	Test Compound (x)	200X final concentration	8	0-300 µM
B	Oligomycin	2.5 mM	9	1 µM
C	FCCP	2.5 mM	10	0.75 µM
D	Rotenone/Antimycin A	2.5 mM	11	1 µM

Abbreviations: FCCP, carbonyl cyanide 4-(trifluoromethoxy) phenylhydrazone.

For the pre-treatment strategy (Table 2.4), serial dilutions of 200X drug stocks were performed in DMSO. Each 200X stock was further diluted 1:200 into L6 differentiation media and incubated with the cells in XF^{e}96 microplates for the stipulated time period. The dosing medium was refreshed every 24 hours where applicable.

Table 2.4 Pre-treatment mitochondrial stress test injection port locations, compound stock concentrations, dilution factors and final well concentrations.

Injection Port	Compound	Stock Concentration	Well Dilution Factor	Final well concentration
A	Oligomycin	2.5 mM	8	1 µM
B	FCCP	2.5 mM	9	0.75 µM
C	Rotenone/Antimycin A	2.5 mM	10	1 µM

Abbreviations: FCCP, carbonyl cyanide 4-(trifluoromethoxy) phenylhydrazone.

Each run included a pre-programmed calibration, an equilibration step and 3 cycles of mix/measure/wait (3 mins/3 mins/0 mins) to establish a baseline OCR/ECAR prior to the injection of any compounds. Where applicable, test compounds were acutely injected and ten OCR measurement cycles (54 minutes) were performed. Following this, a mitochondrial stress test was conducted, consisting of sequential injections of oligomycin (ATP synthase inhibitor), carbonyl cyanide 4-(trifluoromethoxy) phenylhydrazone (FCCP) (ionophore) and rotenone/antimycin A (complex I/III inhibitors respectively) (Figure 2.4).

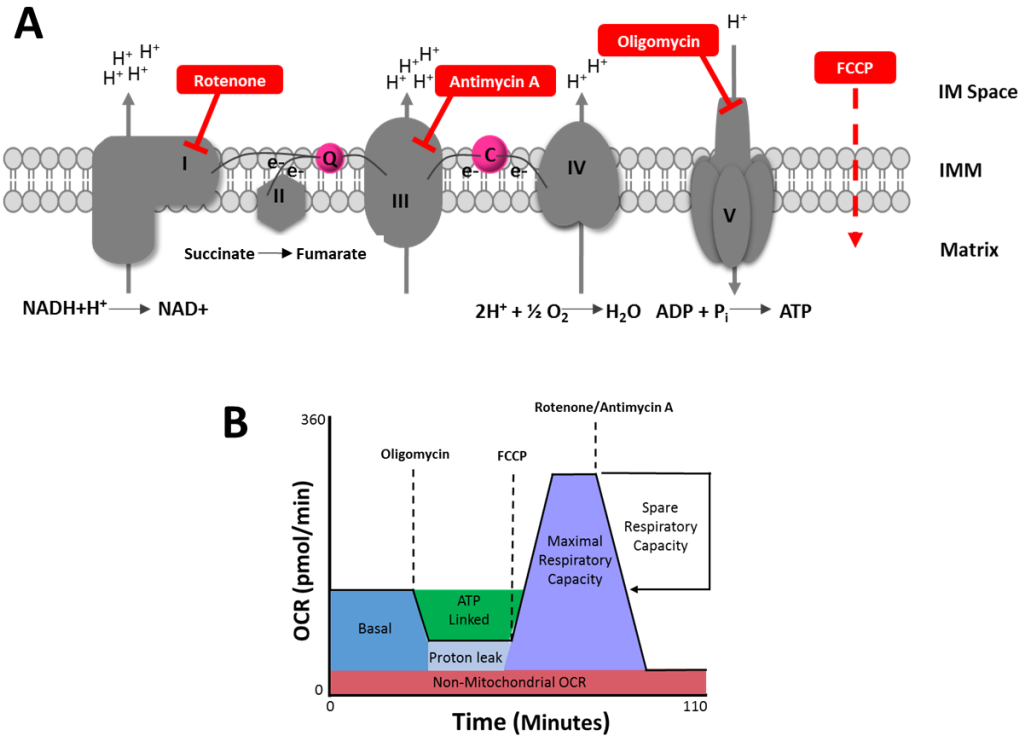

Figure 2.4 Fundamentals of the mitochondrial stress test. **(A)** Sites of action of the respiratory inhibitors used in the mitochondrial stress test. **(B)** Representative mitochondrial stress test trace including derived bioenergetic parameters: basal respiration, ATP-linked respiration, proton leak, maximal respiratory capacity and spare respiratory capacity. Abbreviations: FCCP, carbonyl cyanide 4-(trifluoromethoxy) phenylhydrazone; IM, intermembrane space; IMM, inner mitochondrial membrane.

2.2.5.4 Respiratory Complex Assays (I-IV)

The cell culture medium was replaced with mitochondrial assay solution (MAS) buffer (5 mM $MgCl_2$, 220 mM mannitol, 70 mM sucrose, 10 mM KH_2PO_4, 2 mM HEPES, 1 mM ethylene glycol-bis(β- aminoethyl ether)-N,N,N′,N′-tetraacetic acid (EGTA) and 0.4 % (w/v) fatty acid free bovine serum albumin (BSA), pH 7.2), supplemented with constituents to stimulate oxygen consumption via complex I (4.6 mM ADP, 30 mM malic acid, 22 mM glutamic acid, 0.2 % (w/v) BSA and 1 nM recombinant perfringolysin O (rPFO)), complex II (4.6 mM ADP, 20 mM succinic acid, 1 µM rotenone, 0.2 % (w/v) BSA and 1 nM rPFO), complex III (4.6 mM ADP, 500 µM duroquinol, 1 µM rotenone, 40 µM malonic acid, 0.2 % (w/v) BSA and 1 nM rPFO) or

complex IV (4.6 mM ADP, 20 mM ascorbic acid, 0.5 mM TMPD (N,N,N',N'-tetramethyl-p-phenylenediamine, 2 µM antimycin A, 0.2 % (w/v) BSA and 1 nM rPFO).

Each run included a pre-programmed calibration and 3 cycles of mix/measure/wait (30 secs/2 mins/ 30 secs) to establish a baseline OCR prior to the injection of any compounds. Where applicable, test compounds were acutely injected and three measurement cycles were performed. Following this, a mitochondrial stress test was conducted as previously described. The sites of action of complex specific substrate and inhibitors are illustrated in Figure 2.5.

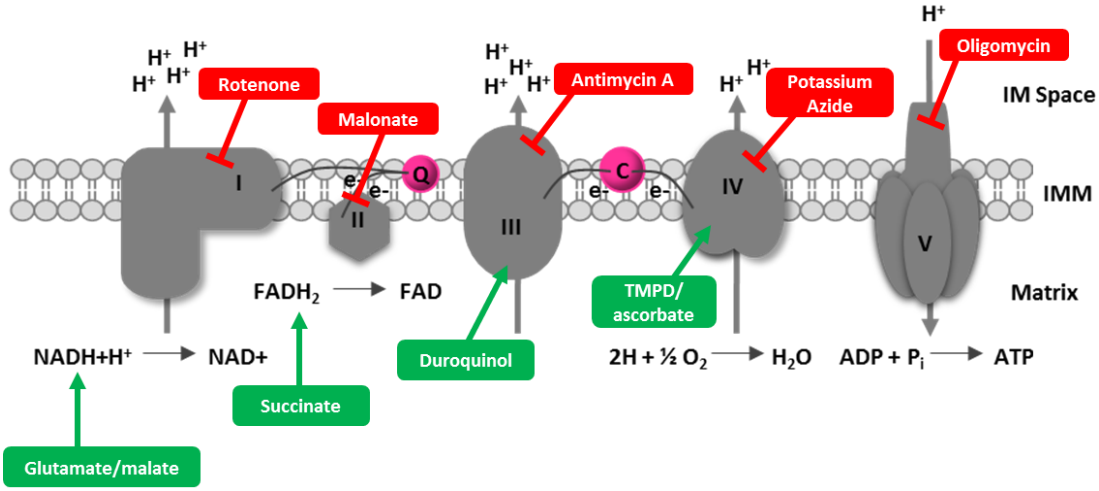

Figure 2.5 Sites of action of substrates (green) and inhibitors (red) used within the mitochondrial complex assays. Abbreviations: TMPD, N,N,N',N'-tetramethyl-p-phenylenediamine; IM, intermembrane space; IMM, inner mitochondrial membrane.

For the assessment of complex IV driven respiration, the final injection of rotenone/antimycin A was substituted with potassium azide (50 µM) (complex IV inhibitor), allowing for the calculation of non-mitochondrial OCR. This was of importance as TMPD/ascorbate undergoes redox cycling which 'consumes' oxygen within the medium, producing notable background signal which could be falsely interpreted as complex IV activity (Morgan and Wikstrom, 1991). Individual complex activities were defined as maximal respiratory capacity (as a % of basal respiration), normalised to the respective vehicle control.

2.2.5.5 Fatty Acid Oxidation Assays

The cell culture medium was replaced with mitochondrial assay solution (MAS) buffer (pH 7.2). Substrate injections were prepared by combining 36.8 mM ADP, 4 mM malic acid, 400 µM palmitoyl-L-carnitine or octanyl-L-carnitine and 8 nM rPFO in MAS buffer before loading into injection port A. Ports B and C contained oligomycin (final well concentration 1 µM) and rotenone/antimycin A (final well concentration 2 µM) respectively (Salabei *et al.*, 2014).

Following three cycles of mix/measure/wait (2 mins/ 3 mins/ 2 mins) to establish a baseline OCR, substrate solutions containing either palmitoyl-L-carnitine or octanyl-L-carnitine were injected and measured for two cycles. Subsequent injections were measured over two cycles. Respiratory activity supported by fatty acid oxidation was determined by deducting non-mitochondrial OCR from substrate driven OCR and normalising to the vehicle control.

2.2.6 Semi-Automated Pump Controlled Cell (PCC) Rupture System for the Isolation of Mitochondria from Cultured Cells

Functionally intact mitochondria were isolated from cultured cells using methods obtained from the laboratory of Professor Hans Zischka (Helmholtz Centre, Munich, Germany) and optimised for the L6 cell line (Schmitt *et al.*, 2013).

2.2.6.1 Assay Preparation

L6 myoblasts were seeded into T175 culture flasks ($1.2x10^6$ cells/flasks) in complete growth media before being differentiated for 7 days (37 °C with 5 % (v/v) CO_2). Cells were collected by trypsinisation before resuspension in mitochondrial isolation buffer (300 mM sucrose, 5 mM N-[Tris (hydroxymethyl) methyl]-2-aminoethanesulfonic acid (TES), 200 µM EGTA) at a density of $6x10^6$ cells/mL and chilled for 20 minutes on ice.

2.2.6.2 Semi-Automated Pump Controlled Cell Rupture

A Balch homogeniser containing a tungsten carbide ball (8 µm clearance) and 1 mL luer lock, gas-tight syringes (4.608 mm diameter) were pre-chilled to 4 °C. A high precision pump (Pump 11, Harvard apparatus, USA) was set with a flow rate of 700 µL/min. The syringes and homogeniser were primed with isolation buffer to flush air pockets from the system.

Homogenisation was achieved by taking up 1 mL of cell suspension in a syringe and attaching it to the first inlet of the homogeniser. The second inlet was occupied by an empty syringe. The pump was used to depress the plunger of the first syringe and ‘pass’ the cells through the homogeniser into the empty syringe at a constant rate (Figure 2.6).

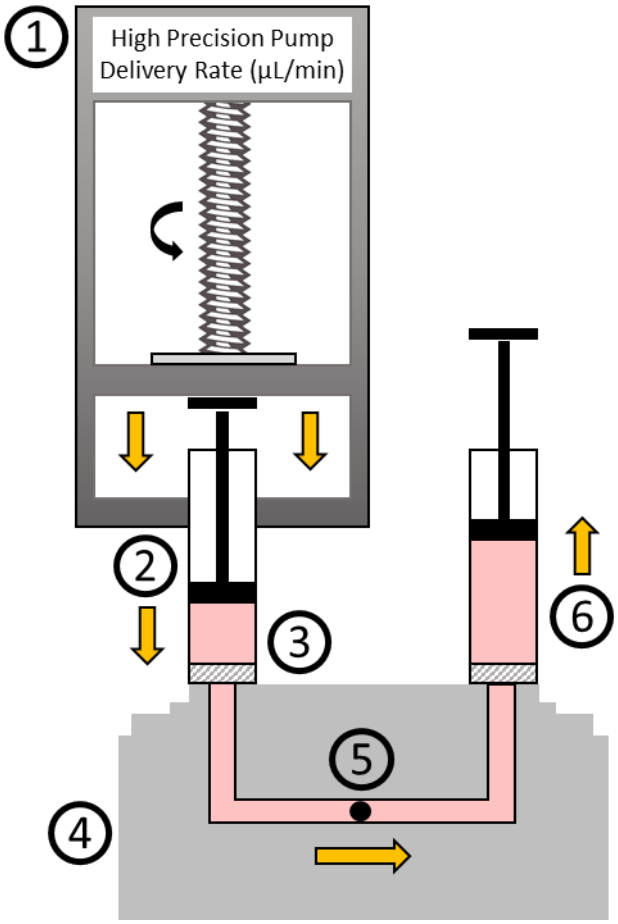

Figure 2.6 Schematic diagram of the pump controlled cell (PCC) rupture system. A high precision pump **(1)** was connected to gas tight syringes **(2)** to ensure the continuous delivery of sample **(3)** at a constant rate to the Balch homogeniser **(4)**. Rupture of cells occurred upon passage through a defined clearance (8 µm) which was dictated by the diameter of a tungsten carbide ball **(5).** Homogenates were collected in a second syringe **(6)** and were subject to further 'passes' through the homogeniser (Schmitt *et al.*, 2013).

The process was repeated 4 times before collecting the homogenate and centrifuging at 800 x g (4 °C) for 5 minutes to pellet the cell debris. The resultant supernatant was transferred to fresh tubes before centrifuging again at 9000 x g (4 °C) for 10 minutes to pellet the mitochondrial fraction. Total protein content of the mitochondrial fraction was determined by Bradford assay. Briefly, 20 µL BSA protein standards and mitochondria (diluted 1:20 in isolation buffer) were loaded into a plate in duplicate. Bradford reagent was diluted 1:5 in water and 200 µL of the reaction mix was added to each well. Plates were read immediately at 595 nm on a Varioskan™ Flash multimode plate reader with SkanIt™ software.

2.2.7 Simultaneous Assessment of Membrane Potential and Swelling in Isolated Mitochondria

Integrity of the mitochondrial membrane potential (MMP) was assessed using the cationic fluorescent dye, rhodamine 123 (Rho123) under quenching conditions. In polarised mitochondria, high concentrations of Rho123 (>100 nM) accumulate within the matrix and form aggregates, quenching the fluorescent signal. Depolarisation of the inner mitochondrial membrane by chemical uncouplers (e.g. FCCP) releases the dye from the matrix, thus resulting in a relative increase in fluorescent signal. This probe is preferentially used for its poor ability to interact with mitochondrial structures and inhibit electron transport compared with other lipophilic, cationic dyes (Perry *et al.*, 2011; Scaduto and Grotyohann, 1999).

The induction of the mitochondrial permeability transition pore (MPTP) under pathological conditions (e.g. Ca^{2+} overloading) promotes a non-specific increase in membrane permeability. The resultant influx of solutes to the matrix increases mitochondrial volume which can be detected by monitoring changes in the mitochondrial suspension pseudo-absorbance. Decreases in optical density correlate with increased matrix swelling and vice versa. Changes to optical density are monitored at 540 nm which falls within the range of mitochondrial isosbestic point (Fulda *et al.*, 2010).

2.2.7.1 Assay preparation

Freshly isolated mitochondria were diluted in chilled isolation buffer (2 µg/µL) before being dispensed (25 µL/well) into a black-walled 96-well plate with a transparent bottom. Neutral swelling buffer (200 mM sucrose, 10 mM MOPS (3-(*N*-morpholino)propanesulfonic acid) – Tris, 1 mM phosphoric acid, 10 µM EGTA) was supplemented with 5 mM succinate and 2 µM rotenone and chilled on ice. Test compounds (200X stocks in DMSO) were diluted 1:50 into succinate swelling buffer before being added to the plate (50 µL/well). Wells containing FCCP (500 nM) were used as a positive control for depolarisation of the MMP and Ca^{2+} (100-600 µM) for induction of mitochondrial swelling. Mitochondria (0.5 % DMSO) were used as a negative control.

Finally, 25 µL succinate swelling buffer and 50 µL rhodamine 123 (500 nM) were added to all wells (200 µL final well volume) before the plate was briefly agitated and placed on a Varioskan™ Flash multimode plate reader. Alternating photometric (540 nm) and fluorometric (500/20 nm excitation; 528/20 nm emission) reads were performed every 30

seconds for 1 hour, after which 1 µM FCCP was added to all wells to dissipate the MMP of any remaining functional mitochondria, serving as an internal control.

2.2.8 Western Blots

L6 myotubes were treated with SVL or SVA for the stipulated time periods and drug concentrations before being rinsed with 1X PBS (-/-) and lysed with RIPA buffer. All lysates were centrifuged at 13,000 rpm for 20 minutes (4 °C) to remove aggregates and insoluble components. Total protein quantification was performed by BCA assay.

Briefly, 20 µg of protein lysate was mixed with 5 µL of sample loading dye. Samples were heat denatured at 95 °C for 5 minutes before loading into NuPAGE® 4-12 % Bis-Tris pre-cast gels alongside 5 µL of Precisions Plus Protein™ molecular weight marker. Loaded samples were subject to electrophoretic separation by molecular weight under reducing conditions in 1X MOPS-SDS (50 mM MOPS, 50 mM Tris-base, 0.1 % (w/v) SDS, 1 mM EDTA) running buffer supplemented with 500 µL NuPAGE® antioxidant for 1 hour (170 V).

Separated proteins were transferred onto nitrocellulose membranes using an XCell II blotting module for 1 hour (220 V). The transfer stack was submerged in 1X transfer buffer (25 mM Tris-base, 192 mM glycine, 20 % (v/v) methanol). Resultant membranes were stained with ponceau red dye to ensure transfer uniformity before blocking for 1 hour in 10 % (w/v) non-fat milk 1X TBS-T (137 mM NaCl, 2.7 mM KCl, 19 mM Tris-base, 0.01 % (v/v) Tween 20, pH 7.4). Primary antibodies were diluted in 5 % (w/v) non-fat milk 1X TBS-T in accordance with Table 2.5 and incubated with membranes for 16 hours (4 °C).

Table 2.5 Summary of primary antibodies, dilution factors and complimentary secondary antibodies.

Primary Antibodies	Dilution Factor	HRP-Conjugated Secondary Antibodies
Anti- Ras	1: 500	Rabbit anti-mouse
Anti- β actin	1: 10,000	Rabbit anti-mouse
Anti- VDAC1	1: 1,000	Goat anti-rabbit

Following washes in 1X TBS-T, appropriate HRP-conjugated secondary antibodies were diluted 1:10,000 in 5 % (w/v) non-fat milk 1X TBS-T and incubated with membranes for 2 hours at room temperature. Band signals were detected using enhanced chemiluminescent reagent (ECL) and developed on film. Densitometry analyses were performed using ImageJ 1.48 software.

2.2.9 Statistical Analyses

Data are representative of at least three independent experiments (n=3) and all values are expressed as mean $\pm$ standard deviation (S.D.) as appropriate. Statistical analyses were performed using GraphPad Prism® 7 software (GraphPad Software, Inc, CA, USA). Data were tested for Guassian distribution using the Shapiro-Wilk normality test before statistical significance was determined using a student's t-test with Welch's correction, one-way Analysis of Variance (ANOVA) with Dunnett's correction for multiple comparisons or two-way ANOVA with Dunnett's or Sidak's correction for multiple comparisons. The non-parametric equivalents for each test were used where applicable. IC_{50} values for dose response curves were determined using non-linear regression analysis. A p value ≤ 0.05 was accepted as the significance threshold.

2.3 Results

2.3.1 Acute Metabolic Manipulation of L6 Myocytes Using Galactose Media.

The effects of simvastatin lactone and its pharmacologically active β-hydroxy acid on cellular ATP content and LDH retention were examined in L6 myotubes acutely conditioned to glucose or galactose media (Figure 2.7).

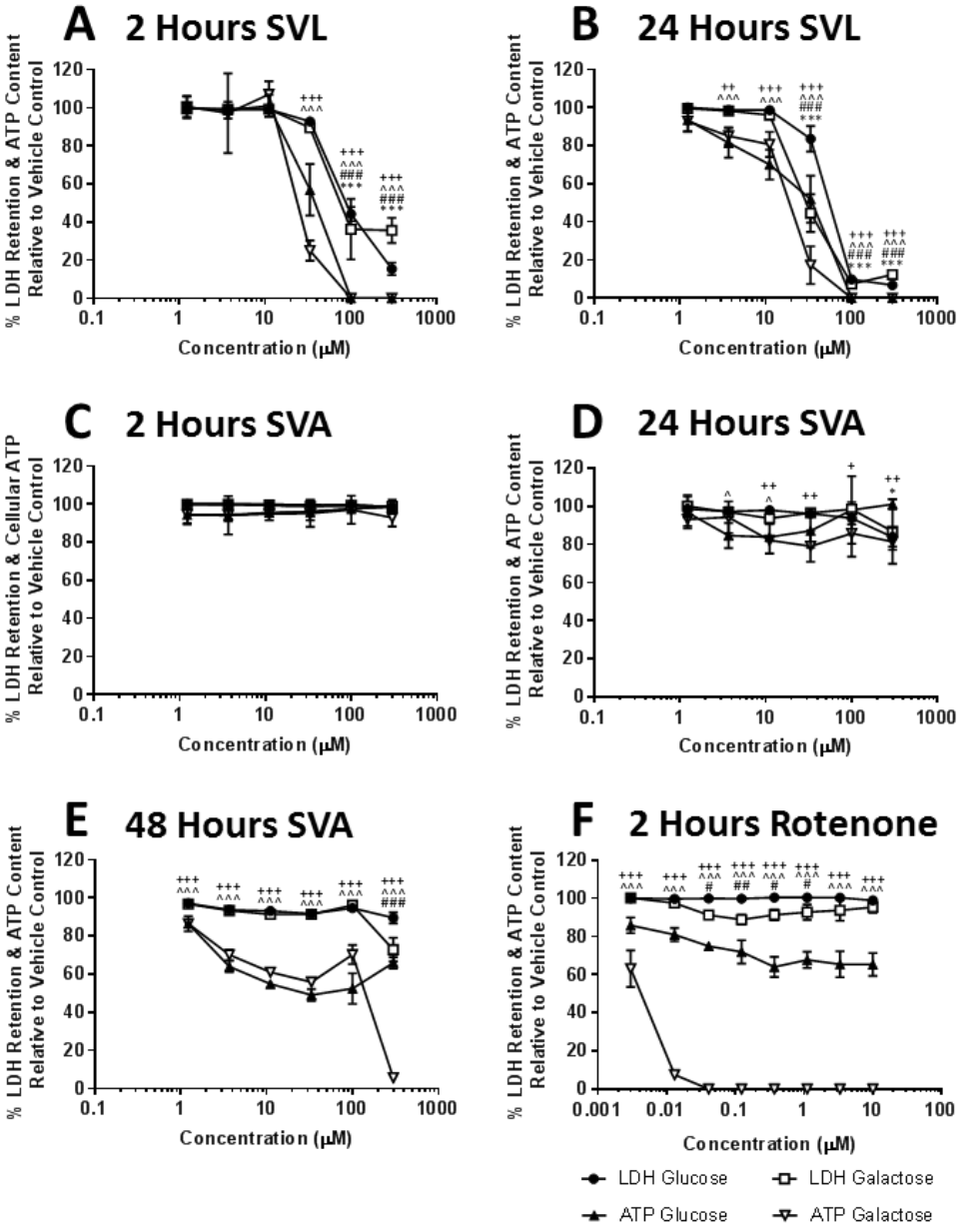

Figure 2.7 The effect of acute simvastatin lactone (0-300 µM), simvastatin β-hydroxy acid (0-300 µM) and rotenone (0-10 µM) exposure on ATP content and LDH retention in L6 myotubes compared with the vehicle control in glucose and galactose media. Results are expressed as a percentage of the corresponding media vehicle control and graphical values are displayed as mean ± S.D (n=3). Statistical significance compared to the vehicle control was determined by one-way ANOVA with Dunnett's correction for multiple comparisons. LDH glucose *p value < 0.05 **p value < 0.01 ***p value < 0.001, LDH galactose $^{\#}$p value < 0.05 $^{\#\#}$p value < 0.01 $^{\#\#\#}$p value < 0.001, ATP glucose ^p value < 0.05 ^^p value < 0.01 ^^^p value < 0.001, ATP galactose $^{+}$p value < 0.05 $^{++}$p value < 0.01 $^{+++}$p value < 0.001. Abbreviations: SVL, simvastatin lactone; SVA, simvastatin β-hydroxy acid.

Rotenone, a potent NADH dehydrogenase (complex I) inhibitor, was used as a positive control (Figure 2.7 **(F)**). Exposure of L6 myocytes to simvastatin lactone (SVL) for 2 and 24 hours at a supra-physiological concentration range (0-300 µM) reduced both cellular ATP content and LDH retention in glucose and galactose media (Figure 2.7 **(A-B)**). Conversely, exposure of cells to simvastatin β-hydroxy acid (SVA) for 2 and 24 hours did not induce any appreciable loss in ATP content or LDH retention in either media condition at equimolar concentrations (Figure 2.7 **(C-D)**). After an extended 48 hour incubation period, 300 µM SVA induced a significant reduction (94.3 %) in ATP content in the galactose media condition specifically, with an accompanying 27.2 % reduction in LDH retention (Figure 2.7 **(E)**).

Mitochondrial toxicity was defined by calculating the ratio between the IC_{50} values for ATPglu versus ATPgal, whereby a ratio ≥ 2 indicated that the test compound was a respiratory toxicant, thus had a more pronounced effect in galactose media. An IC_{50} ratio ≥ 2 for LDHgal versus ATPgal indicated that mitochondrial dysfunction preceded cell death, in line with previous definitions (Swiss *et al.*, 2013; Kamalian *et al.*, 2015). As indicated in Table 2.6, rotenone exceeded the threshold for a respiratory toxicant and induced mitochondrial dysfunction in the absence of cell death as expected.

Table 2.6 Summary of accompanying IC_{50} values for each compound as determined by non-linear regression analysis. Results are displayed as mean ± S.D (n=3). Statistical significance was determined by un-paired t-test with Welch's correction. *p value < 0.05, **p value < 0.01, ***p value < 0.001.

		ATP IC_{50} (µM) ± S.D		**LDH IC_{50} (µM) ± S.D**			
Compound	**Incubation (Hours)**	**Glucose**	**Galactose**	**Glucose**	**Galactose**	**IC_{50} ATP glu/ IC_{50} ATP gal**	**IC_{50} LDH gal/ IC_{50} ATP gal**
SVL	2	34.81 ± 2.02	29.28 ± 1.42	90.62 ± 6.13	39.60 ± 0.53	1.18 (*)	1.35 (*)
	24	29.62 ± 7.64	20.25 ± 1.99	48.82 ± 2.57	31.45 ± 2.46	1.48 (*)	1.55 (**)
SVA	2	>300	>300	>300	>300	~1 (n/d)	~1 (n/d)
	24	>300	>300	>300	>300	~1 (n/d)	~1 (n/d)
	48	>300	176.16 ± 22.69	>300	>300	>1.70 (n/d)	>1.70 (n/d)
Rotenone	2	>10	0.0094 ± 0.0018	>10	>10	>1059.45 (n/d)	>1059.45 (n/d)

Abbreviations: SVL, simvastatin lactone; SVA, simvastatin β-hydroxy acid; n/d, value not determined.

In contrast, neither SVL nor SVA met the screening threshold over the 2 or 24 hour incubation periods. After 48 hours, SVA displayed hallmarks of a positive mitochondrial toxicant, showing a dramatic loss of ATP content in galactose media which preceded loss of viability.

In order to assess whether the outcomes of the acute mitochondrial toxicity screening were specific to simvastatin, the same assay conditions were applied to cerivastatin lactone (CVL) and cerivastatin β-hydroxy acid (CVA) (Figure 2.8).

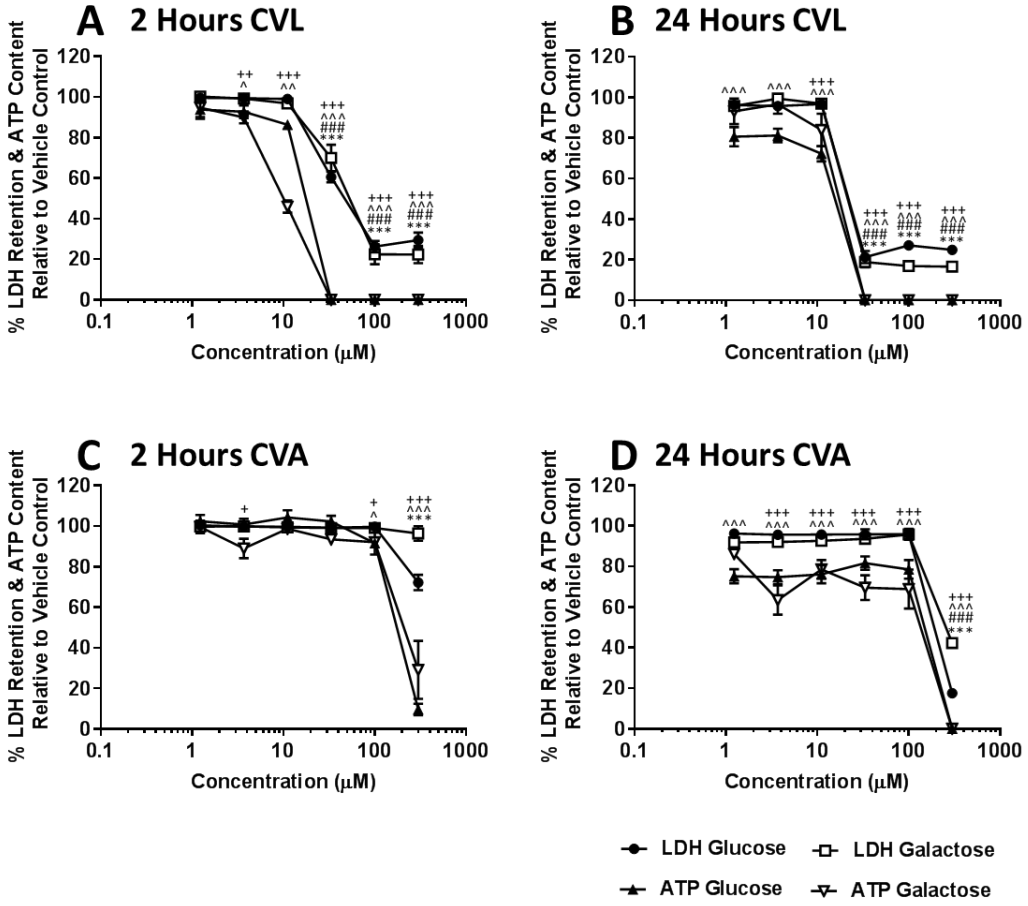

Figure 2.8 Examining the effect of acute cerivastatin lactone (0-300 μM) and cerivastatin β-hydroxy acid (0-300 μM) exposure on ATP content and LDH retention in L6 myotubes compared with the vehicle control in glucose and galactose media. Results are expressed as a percentage of the corresponding media vehicle control and graphical values are displayed as mean ± S.D (n=3). Statistical significance compared to the vehicle control was determined by one-way ANOVA with Dunnett's correction for multiple comparisons. LDH glucose *p value < 0.05 **p value < 0.01 ***p value < 0.001, LDH galactose $^{\#}$p value < 0.05 $^{\#\#}$p value < 0.01 $^{\#\#\#}$p value < 0.001, ATP glucose ^p value < 0.05 ^^p value < 0.01 ^^^p value < 0.001, ATP galactose $^{+}$p value < 0.05 $^{++}$p value < 0.01 $^{+++}$p value < 0.001. Abbreviations: CVL, cerivastatin lactone; CVA, cerivastatin β-hydroxy acid.

Incubation of L6 myocytes with CVL for 2 and 24 hours, at the same concentration range (0-300 μM), induced concomitant loss of ATP content and LDH retention more potently than SVL in both media conditions (Figure 2.8 **(A-B)**). Unlike SVA, reduced ATP content was evident after 2 hours of exposure to CVA (300 μM), which was accompanied by loss of LDH retention

after 24 hours (Figure 2.8 **(C-D)**). There was no differential toxicity between glucose and galactose.

In support of these observations, the ratios between IC_{50} ATP glu/ IC_{50} ATP gal for each of the compounds and time points did not breach the screening threshold of ≥ 2. However, a reduction in ATPgal preceded a reduction in LDHgal for CVL at the 2 hour time point as indicated by a ratio of 4.15 (Table 2.7).

Table 2.7 Summary of accompanying IC_{50} values for each compound as determined by non-linear regression analysis. Results are displayed as mean ± S.D. (n=3). Statistical significance was determined by un-paired t-test with Welch's correction. *p value < 0.05, **p value < 0.01, ***p value < 0.001.

		ATP IC_{50} (μM) ± S.D		**LDH IC_{50} (μM) ± S.D**			
Compound	**Incubation (Hours)**	**Glucose**	**Galactose**	**Glucose**	**Galactose**	**IC_{50} ATP glu/ IC_{50} ATP gal**	**IC_{50} LDH gal/ IC_{50} ATP gal**
CVL	2	13.59 ± 0.62	10.51 ± 0.40	34.77 ± 0.27	43.69 ± 3.26	1.29 (*)	4.15 (***)
	24	12.93 ± 0.30	12.98 ± 0.33	15.19 ± 2.20	21.33 ± 4.79	0.99 (NS)	1.64 (**)
CVA	2	187.50 ± 5.52	234.55 ± 44.63	>300	>300	0.79 (NS)	>1.27 (n/d)
	24	171.99 ± 6.30	152.34 ± 18.04	194.71 ± 3.01	192.74 ± 0.93	1.13 (NS)	1.27 (NS)

Abbreviations: CVL, cerivastatin lactone; CVA, cerivastatin β-hydroxy acid; n/d, value not determined; NS, not significant.

2.3.2 Examining the Post-Translational Farnesylation of RAS GTPase in L6 Myocytes via Western Blot.

Alterations in the post-translational farnesylation state of RAS GTPase were determined via western blot after simvastatin lactone and β-hydroxy acid treatment (10 μM) to detect modulation of the mevalonate pathway. Unfarnesylated RAS has a higher molecular weight than its farnesylated counterpart due to the cleavage of the last three carboxy terminal residues. The difference can be visualised as a band split using a single antibody (Mullen *et al.*, 2010).

After treatment, the higher molecular weight band was detected at the 24 hour time point for both compounds (Figure 2.9). As only the active β-hydroxy acid can inhibit HMG-CoAR, thus modulating the mevalonate pathway, the presence of a band split after exposure to SVL

is suggestive of the lactone ring undergoing either enzymatic or non-enzymatic hydrolysis *in vitro* during the 24 hour incubation period.

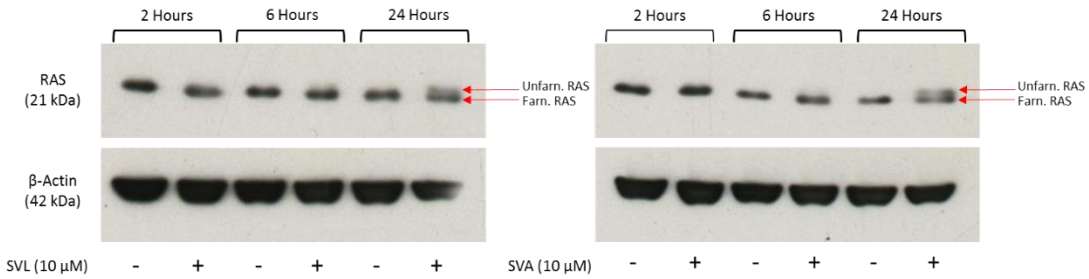

Figure 2.9 Representative blots demonstrating the effect of 10 μM simvastatin lactone and simvastatin β-hydroxy acid on the farnesylation state of RAS GTPase. β-actin was used as a loading control. Abbreviations: SVL, simvastatin lactone; SVA, simvastatin β-hydroxy acid.

2.3.3 Extracellular Flux Analysis of Acute Statin-Induced Changes in Mitochondrial Function

An extracellular flux analyser instrument (XF^{e}96) was utilised to specifically interrogate mitochondrial respiratory chain functionality via a mitochondrial stress test, a representative trace for the L6 cell line is displayed in Figure 2.10. Acute injection of SVA demonstrated respiratory uncoupling, promoting a non-significant increase in basal respiration paired with a significant decrease in coupling efficiency at the highest concentration (300 μM) (Figure 2.11, Figure 2.12 **(A-C)**). 300 μM SVA however, significantly increased proton leak in tandem with a decrease in ATP-linked respiration and spare respiratory capacity as standalone values and also as a proportion of the maximal respiratory capacity (Figure 2.11 **(E & G)**). In contrast, acute injection of SVL showed marginal changes in basal respiration, maximal respiration and coupling efficiency (Figure 2.11, Figure 2.12 **(A-C)**). However, when examining further respiratory parameters, there was a significant increase in proton leak at 30 μM (Figure 2.11 **(D & F)**) and 100 μM (Figure 2.11 **(F)**) when plotted alone or reported as a proportion of maximal respiratory capacity.

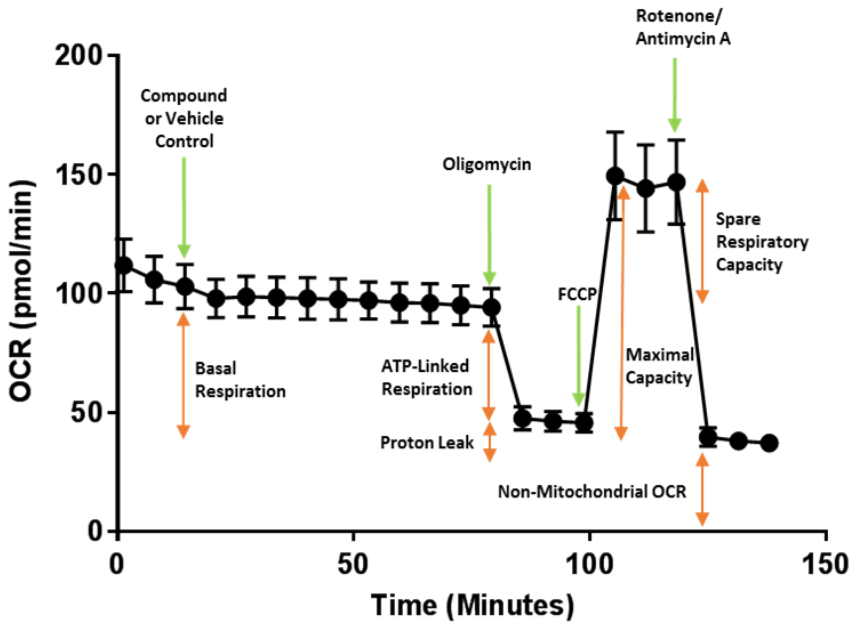

Figure 2.10 Representative control mitochondrial stress test trace for L6 myocytes. The mitochondrial stress test assay consisted of sequential injections of test compounds and respiratory inhibitors into the cell culture microplate to determine various respiratory parameters. After three basal measurement cycles, either a test compound or vehicle control was injected, followed by ten measurement cycles. The remaining injections of oligomycin, FCCP and rotenone/antimycin A were followed by three measurement cycles. Abbreviations: OCR, oxygen consumption rate; FCCP, carbonyl cyanide 4-(trifluoromethoxy) phenylhydrazone.

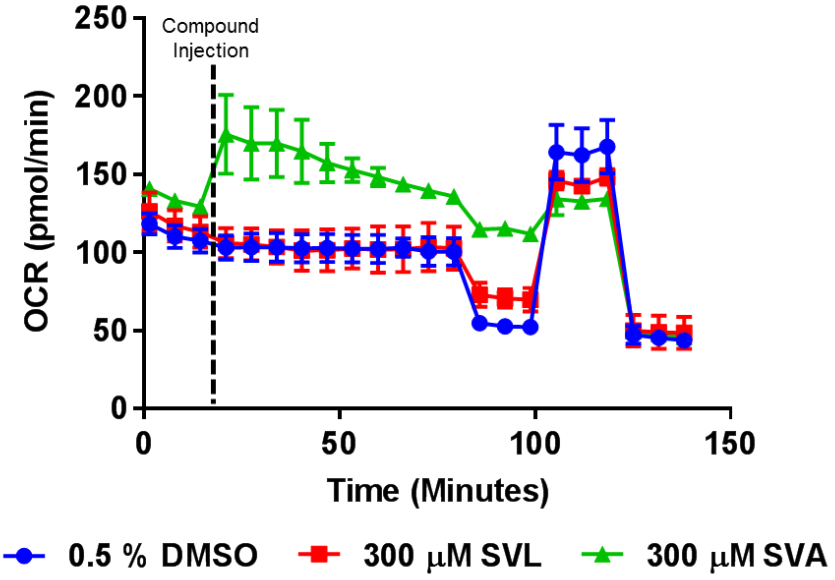

Figure 2.11 Representative mitochondrial stress test trace of vehicle control, simvastatin lactone and simvastatin β-hydroxy acid treated L6 myocytes. Following compound incubation, a mitochondrial stress test was performed via the sequential injection of respiratory inhibitors oligomycin (1 µM), carbonyl cyanide 4-(trifluoromethoxy) phenylhydrazone (FCCP) (0.75 µM) and rotenone/antimycin A (1 µM) whilst monitoring changes in oxygen consumption rate (OCR). Abbreviations: SVL, simvastatin lactone; SVA, simvastatin β-hydroxy acid.

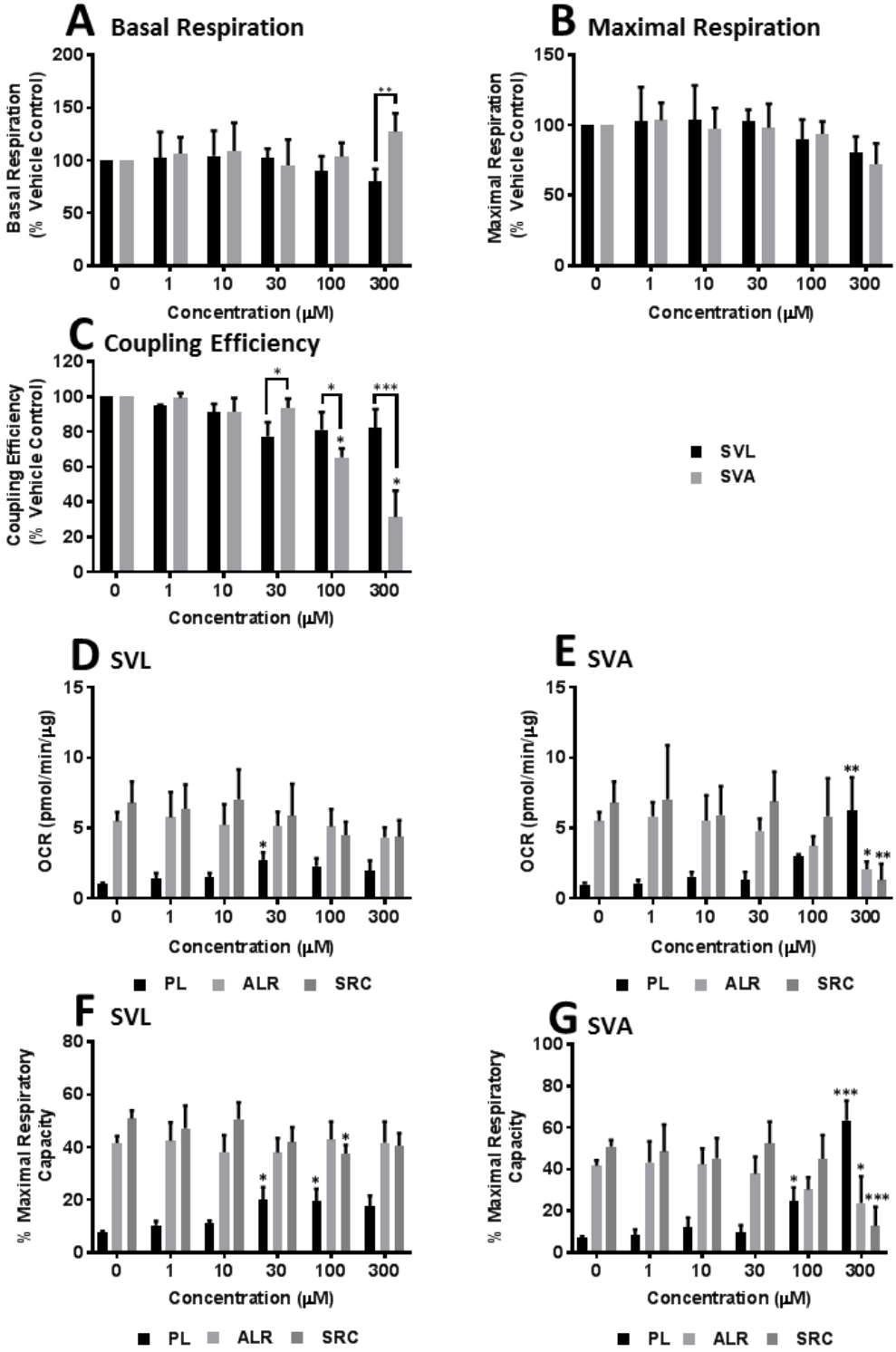

Figure 2.12 Examining the effect of acute simvastatin lactone (SVL) and β-hydroxy acid (SVA) (0-300 μM) exposure upon mitochondrial function in L6 myocytes compared with the vehicle control. **(A)** basal respiration, **(B)** maximal respiration, **(C)** coupling efficiency, **(D**-**E)** bioenergetic parameters as standalone values, (**F**-**G**) bioenergetic parameters as a percentage of maximal respiratory capacity. Graphical values are displayed as mean ± S.D. (n=3) and were normalised to μg protein per well. Statistical significance compared to the vehicle control and between drug treatments was determined by two-way ANOVA with Dunnett's or Sidak's correction for multiple comparisons *p value < 0.05 **p value < 0.01 ***p value < 0.001. Abbreviations: PL, proton leak; ALR, ATP-linked respiration; SRC, spare respiratory capacity; OCR, oxygen consumption rate.

2.3.4 Assessing Acute Simvastatin-Induced Respiratory Complex Dysfunction

For the assessment of individual respiratory complex driven respiration (I-IV), L6 myocytes were permeabilised *in situ* using recombinant perfringolysin O (rPFO) and assayed using solutions which contained specific substrate-inhibitor mixtures to support the function of the complex of interest. Cells were acutely treated with either SVL (0-300 µM) or SVA (0-300 µM) before conducting a mitochondrial stress test (Figure 2.13). A significant reduction in complex I driven respiration was observed in response to SVL (300 µM) and SVA (100-300 µM) with notable differential toxicity between the two compounds (Figure 2.13 **(A)**). A similar trend was observed for complex II, however considerable dysfunction was evident after only 30 µM SVA (Figure 2.13 **(B)**).

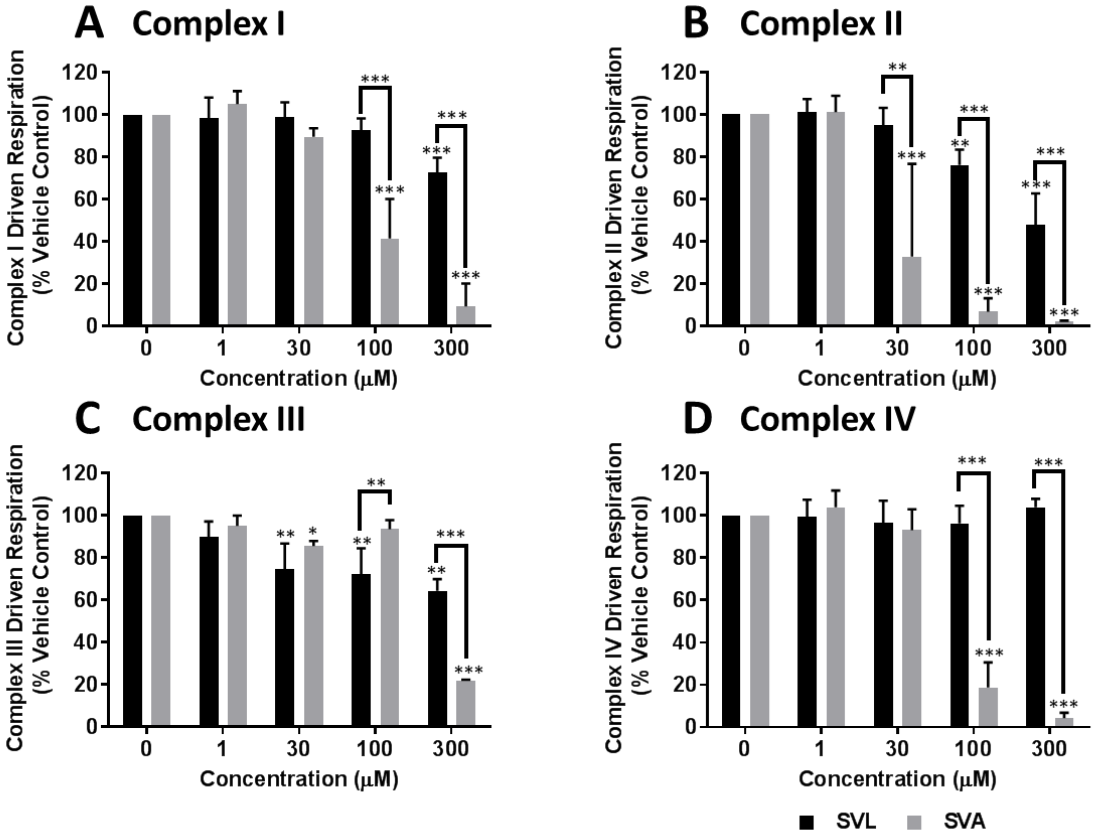

Figure 2.13 The effect of acute simvastatin lactone (SVL) and simvastatin β-hydroxy acid (SVA) exposure upon the activity of the mitochondrial respiratory complexes (I-IV). Permeablised L6 myocytes were treated with SVL or SVA (0-300 µM) before conducting a mitochondrial stress test using an extracellular flux analyser (XF^{e}96) instrument. Complex driven respiration (activity) was defined as maximal respiration (as a % of basal respiration) normalised to the vehicle control. Graphical values are displayed as mean ± S.D. (n=3) and results were normalised to µg protein per well. Statistical significance compared to the vehicle control and between drug treatments was determined by two-way ANOVA with Dunnett's or Sidak's correction for multiple comparisons *p value < 0.05 **p value < 0.01 ***p value < 0.001.

In addition, both SVL and SVA exerted inhibitory effects upon complex III driven respiration (25.4 % and 15.6 % respectively) starting at 30 µM (Figure 2.13 **(C)**). However, there were no significant changes to complex IV activity after SVL application at any concentration tested (Figure 2.13 **(D)**).

2.3.5 Assessment of Mitochondrial Membrane Potential and Swelling in Isolated Mitochondria

The integrity of the inner mitochondrial membrane potential was assessed using the cationic fluorescent dye, rhodamine 123 (Rho123) under quenching conditions in isolated mitochondria (Figure 2.14). Introduction of compounds that depolarise the inner mitochondrial membrane (e.g. FCCP) results in a relative increase in fluorescent signal due to the release of Rho123 from the mitochondrial matrix (Figure 2.14 **(A)**). Additionally, induction of the mitochondrial permeability transition pore (MPTP) (e.g. in the presence of high Ca^{2+} concentrations) perpetuates a large, non-specific increase in membrane permeability. The consequential influx of solutes into the mitochondrial matrix results in swelling of the organelle, which may be detected as a relative decrease in optical density at 540 nm (Figure 2.14 **(B)**).

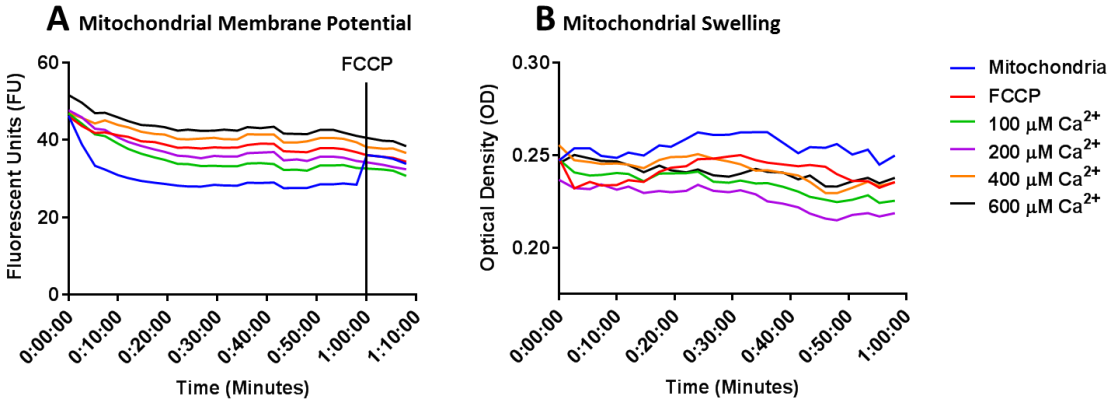

Figure 2.14 Representative kinetic traces for the assessment of mitochondrial membrane potential and swelling. Mitochondria isolated from L6 myocytes (50 µg/well) were incubated with a series of Ca^{2+} concentrations (100-600 µM) and FCCP (500 nM) in a succinate swelling buffer before assessing mitochondrial membrane integrity using rhodamine 123. Mitochondrial swelling was measured photometrically by monitoring changes in optical density at 540 nm. Abbreviations: FCCP carbonyl cyanide 4-(trifluoromethoxy) phenylhydrazone.

Exposure of isolated mitochondria to SVL (100 and 300 µM) caused a significant increase in fluorescent signal compared with the negative control, an observation consistent with membrane depolarisation (Figure 2.15 **(A & C)**). In addition, both the 30 µM and 100 µM conditions demonstrated a decrease in optical density, suggestive of mitochondrial swelling. This was not, however, recapitulated at 300 µM where there was a marked increase in the

optical density reading at 540 nm. Increased optical density compared with the negative control is considered to be characteristic of either mitochondrial shrinkage or rupture (Figure 2.15 (**B** & **D**). As illustrated in Figure 2.15 **(B)**, time to onset of mitochondrial swelling was delayed for the 30 µM (~30 minutes) and 100 µM (~20 minutes) conditions, exemplifying the need to sample from an appropriately 'stable' time point.

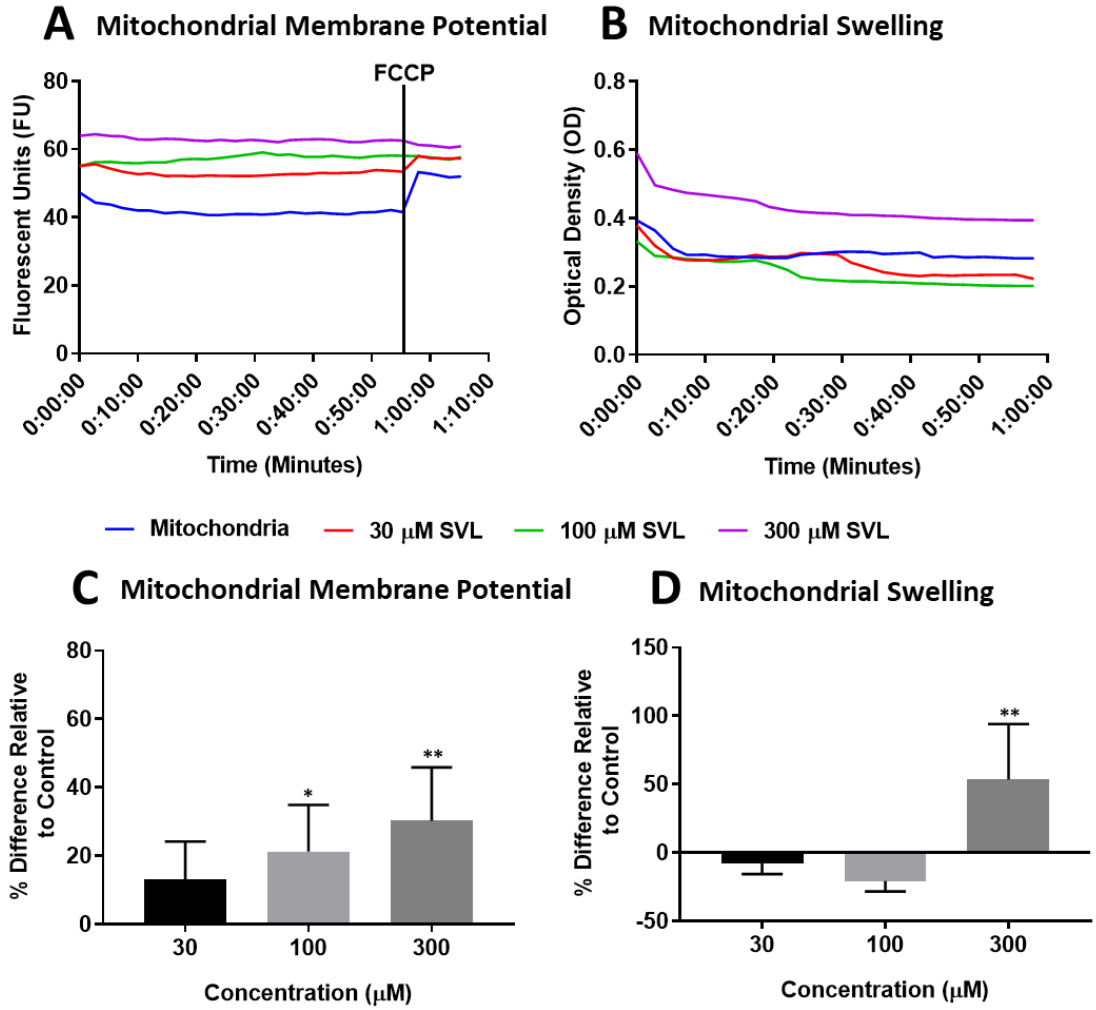

Figure 2.15 Representative kinetic traces for the assessment of mitochondrial membrane potential and swelling in response to simvastatin lactone treatment (**A-B**). Mitochondria isolated from L6 myocytes (50 µg/well) were treated with the test compound (0-300 µM) in a succinate swelling buffer before assessing mitochondrial membrane integrity using rhodamine 123 dye under quenching conditions (**C**). Mitochondrial swelling was measured by monitoring changes in optical density (**D**). Calculation of percentage change compared to mitochondria alone was performed at kinetic read 20 (46 minutes). Graphical values are displayed as mean ± S.D. (n=3). Statistical significance was determined by one-way AVOVA with Dunnet's correction for multiple comparisons *p value < 0.05 **p value < 0.01 ***p value < 0.001. Abbreviations: SVL, simvastatin lactone; FCCP carbonyl cyanide 4-(trifluoromethoxy) phenylhydrazone.

Conversely, simvastatin β-hydroxy acid caused significant membrane depolarisation at 300 µM (Figure 2.16 **(A & C)**), this was preceded by mitochondrial swelling which reached statistical significance at 30 µM (Figure 2.16 **(B & D)**).

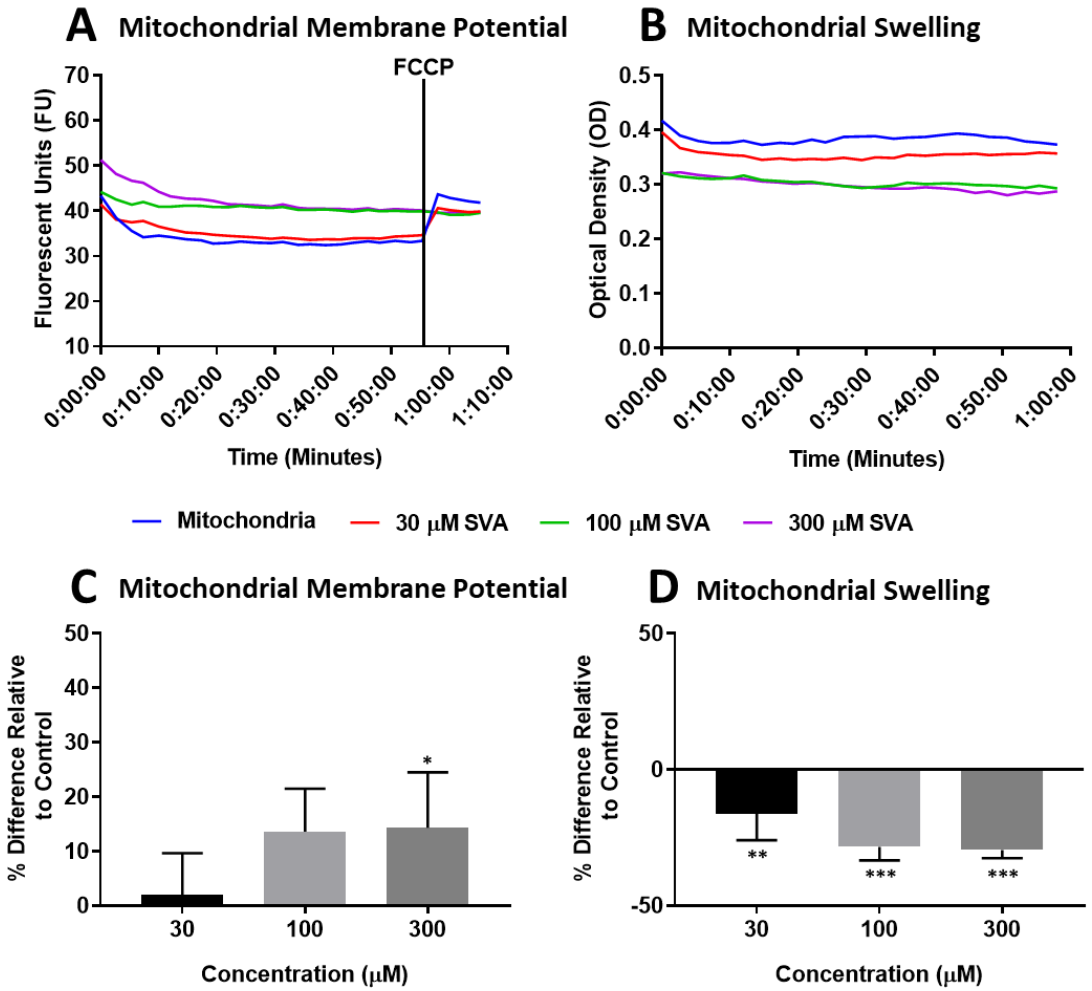

Figure 2.16 Representative kinetic traces for the assessment of mitochondrial membrane potential and swelling in response to simvastatin β-hydroxy acid treatment (**A-B**). Mitochondria isolated from L6 myocytes (50 μg/well) were treated with the test compound (0-300 μM) in a succinate swelling buffer before assessing mitochondrial membrane integrity using rhodamine 123 (**C**). Mitochondrial swelling was measured by monitoring changes in optical density (**D**). Calculation of percentage change compared to mitochondria alone was performed at kinetic read 20 (46 minutes). Graphical values are displayed as mean ± S.D. (n=3). Statistical significance was determined by one-way AVOVA with Dunnet's correction for multiple comparisons *p value < 0.05 **p value < 0.01 ***p value < 0.001. Abbreviations: SVA, simvastatin β-hydroxy acid; FCCP carbonyl cyanide 4-(trifluoromethoxy) phenylhydrazone.

2.3.6 Chronic Metabolic Manipulation of L6 Myocytes Using Galactose Media

To address the chronic effects of SVL and SVA upon mitochondrial function at a concentration range which better reflected the plasma C_{max} in patients (0-1000 nM), differentiated L6 myocytes were dosed every 24 hours for 120 hours in either glucose or galactose media before simultaneously assessing ATP content and LDH retention (Figure

2.17). These investigations were performed with the intention to detect changes in mitochondrial function (ATP content) which occur independently of significant cytotoxicity.

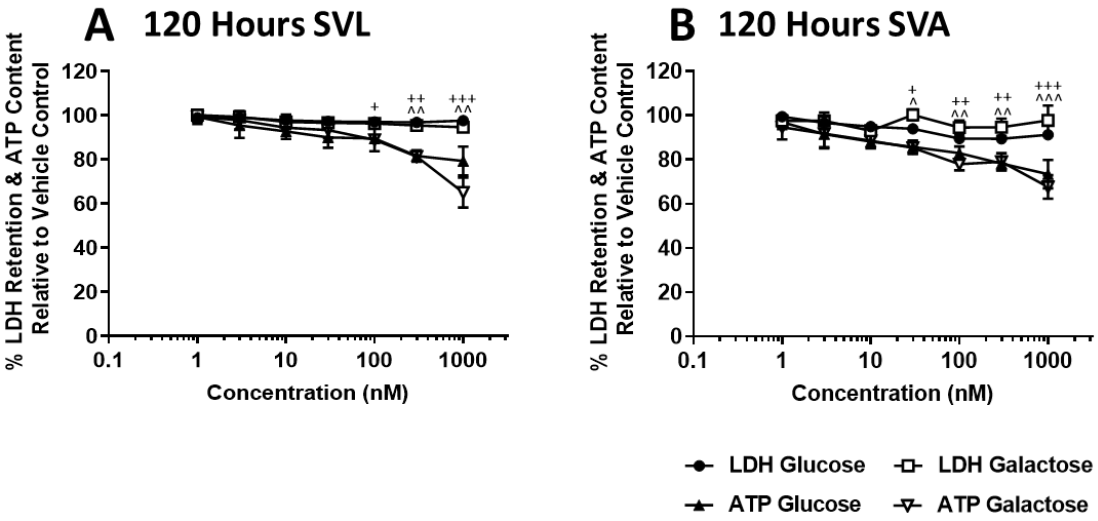

Figure 2.17 The effect of chronic (120 hours) simvastatin lactone (0-1000 nM) and simvastatin β-hydroxy acid (0-1000 nM) exposure on ATP content and LDH retention in L6 myotubes compared with the vehicle control in glucose and galactose media. Results are expressed as a percentage of the corresponding media vehicle control and graphical values are displayed as mean ± S.D (n=3). Statistical significance compared to the vehicle control was determined by one-way ANOVA with Dunnett's correction for multiple comparisons. LDH glucose *p value < 0.05 **p value < 0.01 ***p value < 0.001, LDH galactose $^{\#}$p value < 0.05 $^{\#\#}$p value < 0.01 $^{\#\#\#}$p value < 0.001, ATP glucose ^p value < 0.05 ^^p value < 0.01 ^^^p value < 0.001, ATP galactose $^{+}$p value < 0.05 $^{++}$p value < 0.01 $^{+++}$p value < 0.001. Abbreviations: SVL, simvastatin lactone; SVA, simvastatin β-hydroxy acid.

In response to long-term SVL treatment (Figure 2.17 **(A)**), there were no significant losses to cell viability in the glucose or galactose media conditions compared with the respective media controls. At 100 nM and above, ATP content declined in galactose media, followed by glucose at 300 nM. Simvastatin β-hydroxy acid exhibited a significant decline in ATP content in both media conditions starting from 30 nM (Figure 2.17 **(B)**).

2.3.7 Extracellular Flux Analysis of Chronic Statin-Induced Changes in Mitochondrial Function

Chronic exposure of L6 myocytes to both SVL and SVA at a physiological concentration range induced a dose dependent decline in basal respiration and maximal respiration with no notable differential toxicity between the two compounds (Figure 2.18 **(A-B)**).

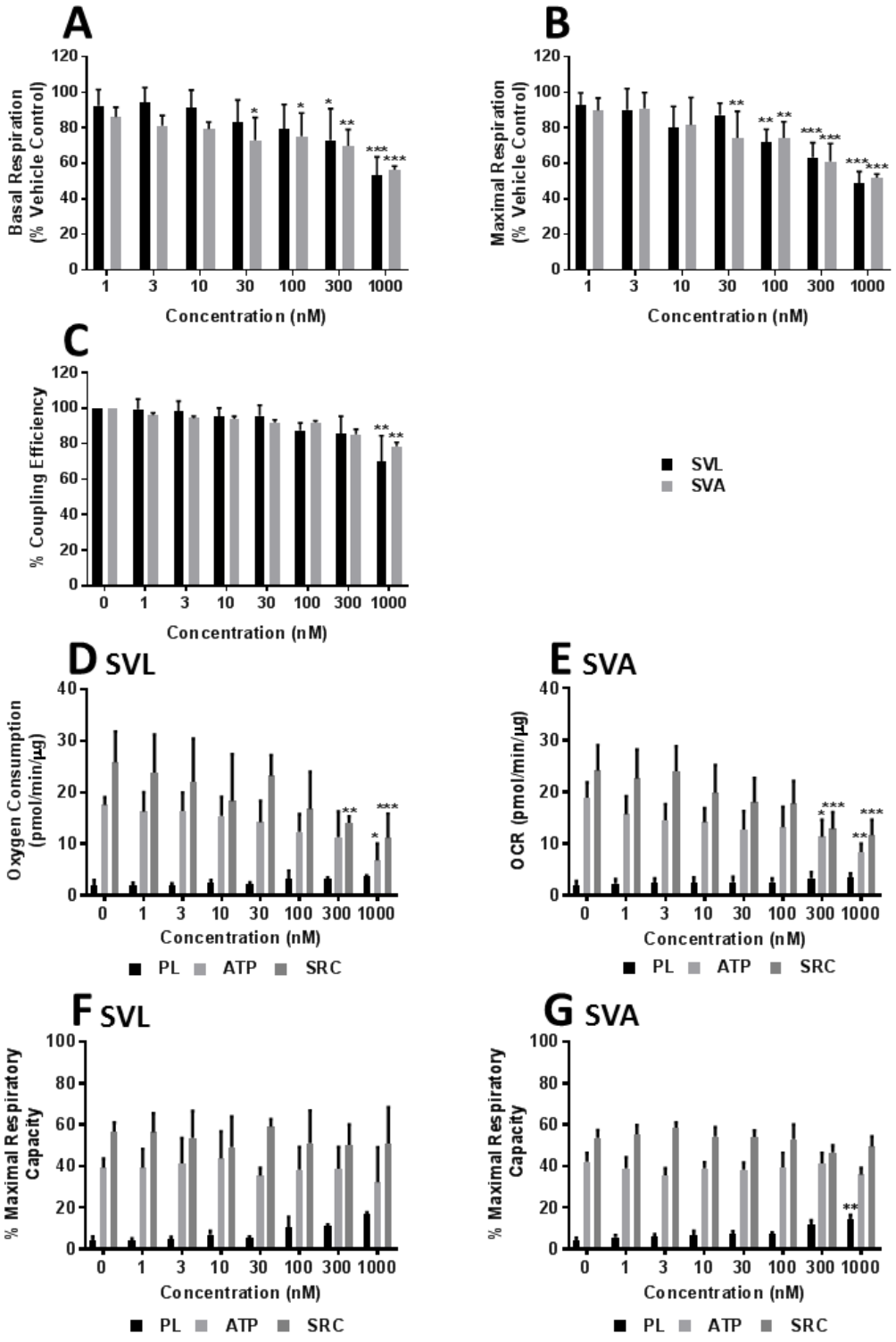

Figure 2.18 Examining the effect of chronic (120 hours) simvastatin lactone (SVL) and β-hydroxy acid (SVA) (0-1000 nM) exposure upon mitochondrial function in L6 myocytes compared with the vehicle control. **(A)** basal respiration, **(B)** maximal respiration, **(C)** coupling efficiency, **(D-E)** bioenergetic parameters as standalone values, **(F-G)** bioenergetic parameters as a percentage of maximal respiratory capacity. Graphical values are displayed as mean ± S.D. (n=3) and were normalised to µg protein per well. Statistical significance compared to the vehicle control and between drug treatments was determined by two-way ANOVA with Dunnett's or Sidak's correction for multiple comparisons *p value < 0.05 **p value < 0.01 ***p value < 0.001. Abbreviations: PL, proton leak; ALR, ATP-linked respiration; SRC, spare respiratory capacity; OCR, oxygen consumption rate.

When examining further metabolic parameters, the data illustrated a marked reduction in spare respiratory capacity and ATP-linked respiration as standalone values for both SVL and SVA at 300 and 1000 nM (Figure 2.18 **(D & E)**). However, when metabolic parameters were reported as a percentage of their respective maximal respiratory capacities, proton leak values increased dose dependently (Figure 2.18 **(F & G)**).

2.3.8 Assessing Chronic Simvastatin-Induced Respiratory Complex Dysfunction

As described in section 2.3.4, assessment of individual respiratory complex (I-IV) driven respiration was performed in permeabilised L6 myocytes using substrate-inhibitor mixtures specific to the complex of interest. Cells were chronically treated (120 Hours) with either simvastatin lactone or β-hydroxy acid (0- 1000 nM) before conducting a mitochondrial stress test (Figure 2.19).

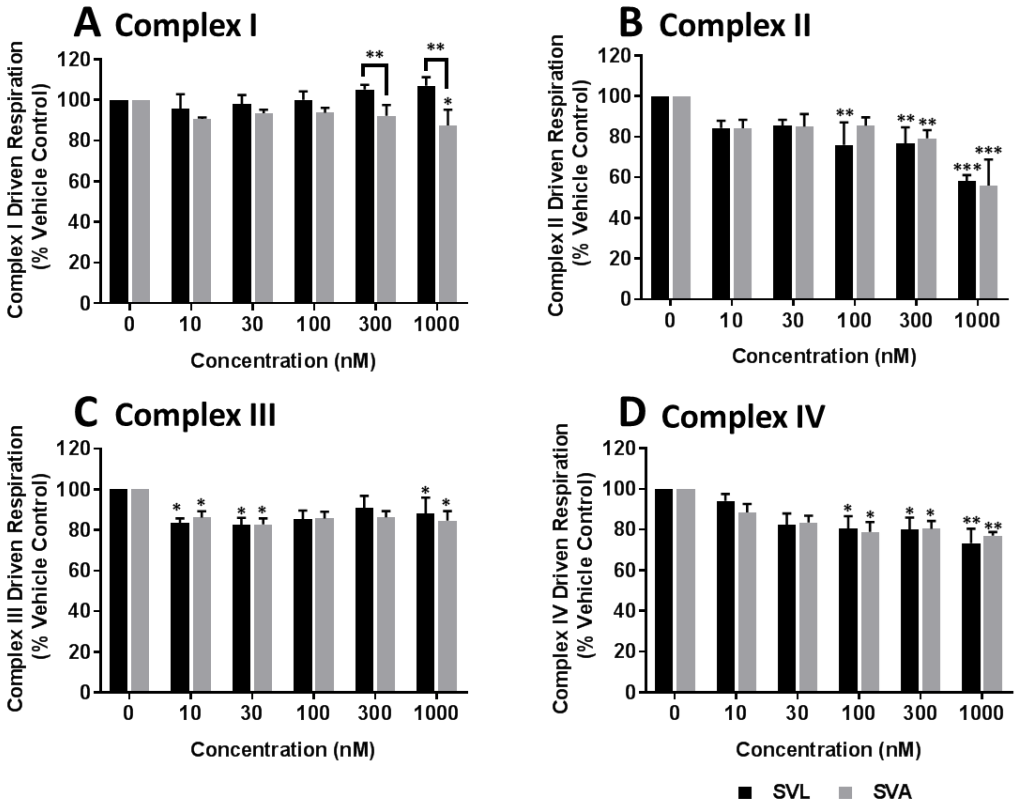

Figure 2.19 The effect of chronic (120 hours) simvastatin lactone (SVL) and simvastatin β-hydroxy acid (SVA) exposure upon the activity of the mitochondrial respiratory complexes (I-IV). L6 myocytes were pre-treated with SVL or SVA (0-1000 nM) before cell permeabilisation and delivery of complex specific substrate mixtures using an extracellular flux analyser (XF^{e}96) instrument. Complex driven respiration was defined as maximal respiration (as a % of basal respiration) normalised to the vehicle control. Graphical values are displayed as mean ± S.D. (n=3) and results were normalised to µg protein per well. Statistical significance compared to the vehicle control and between drug treatments was determined by two-way ANOVA with Dunnett's or Sidak's correction for multiple comparisons *p value < 0.05 **p value < 0.01 ***p value < 0.001.

The most significant change to respiratory complex function in response to prolonged simvastatin exposure was observed at complex II (Figure 2.19 **(B)**), an observation which was consistent with the acute toxicity screening results (section 2.3.4). At the highest concentration tested (1000 nM) both simvastatin lactone and β-hydroxy acid showed an almost equipotent inhibitory capacity, reducing complex II driven respiration by 42.7 % and 44.1 % respectively. Dose dependent decreases in substrate supported respiration were also noted at complexes III and IV to a lesser extent (Figure 2.19 **(C-D)**). Whilst there were no changes to complex I supported respiration compared with vehicle, with the exception of 1000 nM SVA, there were differential effects between the two compounds at 300 nM and 1000 nM (Figure 2.19 **(A)**).

To ensure that the changes in respiratory complex function after statin exposure were not due to a decrease in mitochondrial mass, mitochondrial voltage-dependent anion channel 1 (VDAC1) abundance was measured in whole cell lysates via western blot (Figure 2.20).

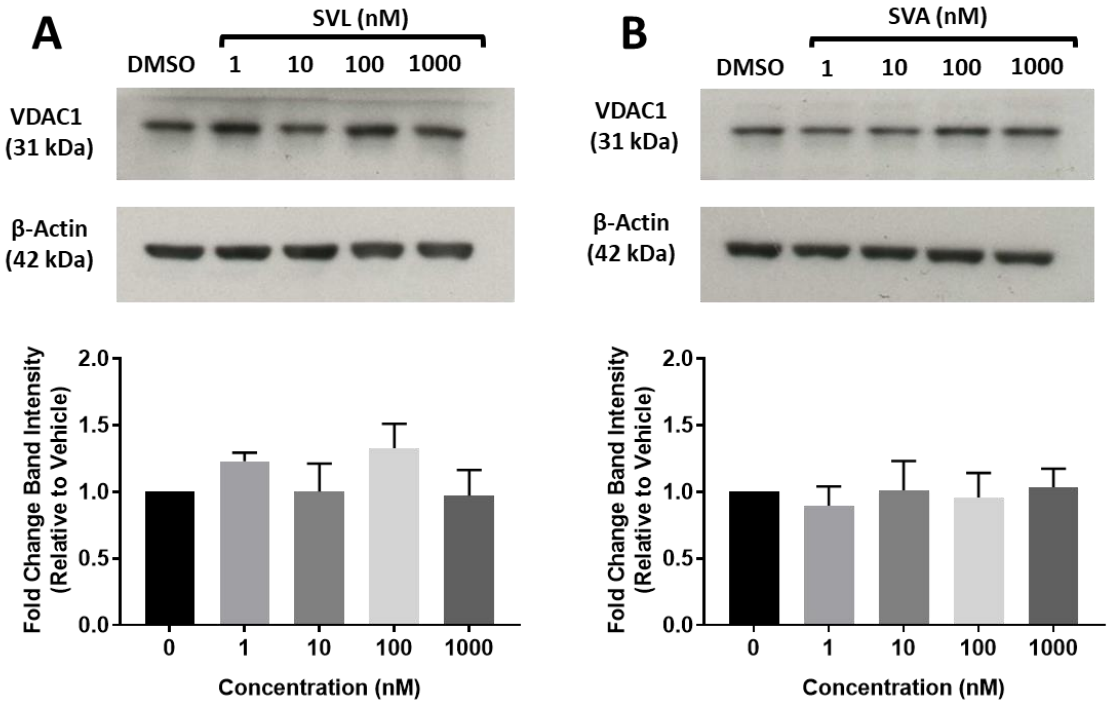

Figure 2.20 Examining the abundance of voltage-gated anion channel 1 (VDAC1) present in whole cell lysates pre-treated with simvastatin lactone (**A**) or simvastatin β-hydroxy acid (**B**) for 120 hours. Integrated band intensities were determined via densitometry using ImageJ 1.48 software and normalised to the loading control β-actin before presenting as fold change relative to the vehicle control. Graphical values are displayed as mean ± S.D. (n=3). Statistical significance compared to the vehicle control was determined by one-way ANOVA with Dunnett's correction for multiple comparisons *p value < 0.05 **p value < 0.01 ***p value < 0.001. Abbreviations: SVL, simvastatin lactone; SVA, simvastatin β-hydroxy acid.

There were no significant changes to mitochondrial mass in response to SVL (Figure 2.20 **(A)**) or SVA (Figure 2.20 **(B)**) treatment.

2.3.9 Investigating the Impact of Chronic Simvastatin Treatment upon Acyl-Carnitine Driven Respiration

Medium- (octanyl-L-carnitine; C8) and long- (palmitoyl-L-carnitine; C16) chain acyl-carnitine stimulated respiration was assessed using permeabilised L6 myocytes pre-treated with either SVL or SVA for 120 hours (Figure 2.21).

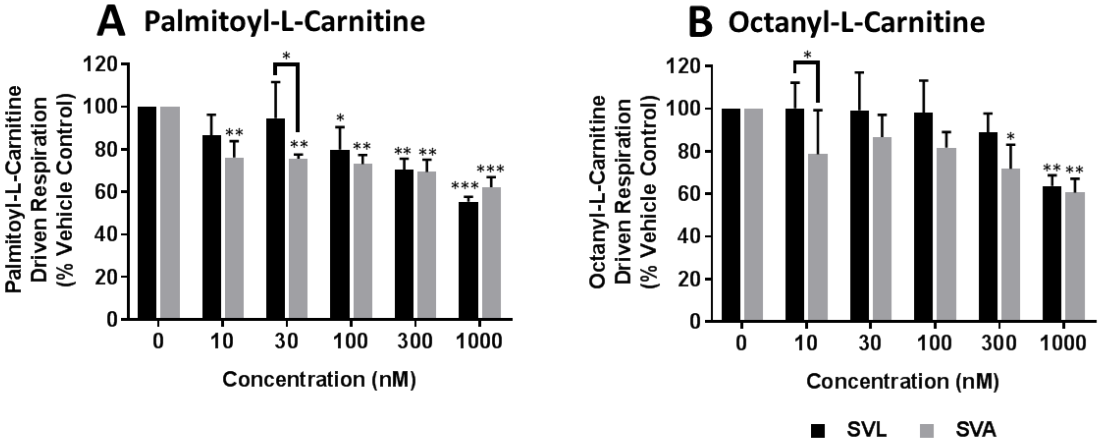

Figure 2.21 Examining the effect of chronic (120 hours) simvastatin lactone (SVL) and simvastatin β-hydroxy acid (SVA) exposure upon long- (**A**) and medium- (**B**) chain acyl-carnitine driven respiration. L6 myocytes were pre-treated with SVL or SVA (0-1000 nM) before cell permeablisation and delivery of specific substrate mixtures using an extracellular flux analyser instrument (XF^{e}96). Respiratory activity supported by acyl-carnitine oxidation was determined by deducting non-mitochondrial OCR from substrate driven OCR and normalising to the vehicle control. Graphical values are displayed as mean ± S.D. (n=3) and results were normalised to µg protein per well. Statistical significance compared to the vehicle control and between drug treatments was determined by two-way ANOVA with Dunnett's or Sidak's correction for multiple comparisons *p value < 0.05 **p value < 0.01 ***p value < 0.001. Abbreviations: SVL, simvastatin lactone; SVA, simvastatin β-hydroxy acid.

Simvastatin lactone and β-hydroxy acid promoted a dose dependent decrease in long-chain (Figure 2.21 **(A)**) and medium-chain (Figure 2.21 **(B)**) acyl-carnitine oxidation, exhibiting an almost equipotent reduction (~40 %) in substrate driven respiration at 1000 nM in both cases. In regard to palmitoyl-L-carnitine specifically, significant inhibitory effects to substrate-driven respiration were noted from 10 nM, though a similar trend was observed for octanyl-L-carnitine.

2.4 Discussion

Mitochondrial dysfunction is increasingly implicated as a contributing factor in many xenobiotic-induced organ toxicities, particularly in aerobically poised tissues. The ability to detect drug mediated mitochondrial liabilities pre-clinically has been propelled by the introduction of the glucose-galactose metabolic screening assay. However, whilst much work has been conducted using hepatocarcinoma (HepG2) and myocardiocyte (H9c2) cell lines, until recently this model had not been evaluated in a skeletal muscle cell line (Marroquin *et al.*, 2007; Rana *et al.*, 2011; Dykens *et al.*, 2008). Therefore to fill an unmet need, studies have since demonstrated that the L6 myogenic cell line is not only amenable to long-term culture supported by galactose and L-glutamine supplementation but also shows enhanced susceptibility to classic mitochondrial toxicants when compared to its glucose-conditioned counterpart (Dott *et al.*, 2014). However, no studies to date have assessed the long-term proteomic implications of culturing L6 cells in galactose versus glucose media.

Acute manipulation of L6 bioenergetics via the substitution of 25 mM glucose with 10 mM galactose and 6 mM L-glutamine in the culture medium increased cellular reliance upon oxidative metabolism for ATP generation. This was evidenced by a significant decrease in ATP content following rotenone treatment, a potent NADH dehydrogenase (complex I) inhibitor, in galactose-conditioned cells versus glucose-conditioned cells. Comparisons of the resultant IC_{50} values in both media types further confirmed that rotenone mediated direct mitochondrial dysfunction (IC_{50} ATPglu/IC_{50} ATPgal ratio ≥2) which preceded the induction of cytotoxic effects (IC_{50} LDHgal/ IC_{50} ATPgal ≥2) as expected (Kamalian *et al.*, 2015; Dott *et al.*, 2014).

Upon challenge with simvastatin lactone over a 2 and 24 hour time period, ATP depletion was observed in both media types accompanied by a loss of cellular LDH retention. Based upon the IC_{50} values, simvastatin lactone had a more pronounced effect upon galactose-conditioned cells. However, despite this difference reaching statistical significance, the resultant ratios were indicative of a multifactorial toxicity mechanism rather than mitochondrial dysfunction alone (Swiss *et al.*, 2013; Hynes *et al.*, 2013). Though it should be acknowledged that there are several examples of drugs (e.g. troglitazone, chlorpromazine and sertraline) which have known mitochondrial liabilities yet fall under the umbrella of multifactorial toxicity (Swiss *et al.*, 2013; Li *et al.*, 2012; Bullough *et al.*, 1985).

When examining an equimolar range of simvastatin β-hydroxy acid over a 2 and 24 hour period, there were no appreciable effects on ATP content or cell viability. Though this was

followed by a 94.34 % reduction in ATP content (300 µM) after 48 hours in galactose-conditioned cells. At the shorter incubation periods, it could be assumed that the compound harboured no mitochondrial liability, however extended modelling revealed that there was indeed considerable differential toxicity between the two media types. Importantly, these findings are in firm agreement with previous reports that statin lactones are more potent mediators of acute cytotoxicity than their β-hydroxy acid counterparts. This observation was replicated when examining the two chemical species of cerivastatin within this chapter and amongst several other statins in C2C12 myocytes and primary human myocytes (Schirris *et al.*, 2015; Skottheim *et al.*, 2008).

Although glucose-galactose assays are extremely useful as a first-line screening tool, a major caveat of the model is that it cannot be used to detect all forms of mitochondrial dysfunction and is often confounded by multifactorial toxicity mechanisms or insufficient incubation periods. For example, compounds with documented mitochondrial liabilities e.g. perhexilline can be incorrectly defined as negative for mitochondrial toxicity based upon the defined screening thresholds (Kamalian *et al.*, 2015; Swiss *et al.*, 2013; Deschamps *et al.*, 1994). In addition, the use of total ATP content as a surrogate measure of overall mitochondrial functionality is extremely simplistic, providing no deeper mechanistic insight to the nature of the perturbations taking place. Furthermore, it does not take into account depletion of ATP reserves due to the activation of cellular defence mechanisms or compensatory mechanisms which may maintain ATP levels despite the presence of respiratory dysfunction (Espinosa-Diez *et al.*, 2015). Crucially, it exemplifies the need to use supplementary techniques to determine the contribution of mitochondrial dysfunction to the overall cytotoxic effect of a compound. As such, extracellular flux analysis was used to provide further mechanistic information as monitoring changes to cellular oxygen consumption is known to be a more sensitive measure of mitochondrial function (Brand and Nicholls, 2011; Wu *et al.*, 2007).

Both simvastatin lactone and β-hydroxy acid differed considerably in their effects upon mitochondrial respiration in an acute setting; simvastatin lactone induced marginal, dose-dependent reductions in basal and maximal respiration, whereas the β-hydroxy acid increased basal respiration at 300 µM. These observations are consistent with mild ETC inhibition by the lactone and respiratory uncoupling by the β-hydroxy acid. The uncoupling of oxidative phosphorylation, particularly in the presence of weak acids, increases basal respiration as the rate-limiting step of ATP synthesis is no longer coupled to oxygen

consumption, enabling OCR to increase (Terada, 1990). This was substantiated by the concurrent increase in proton leak and decrease in coupling efficiency, ATP-linked respiration and spare respiratory capacity mediated by simvastatin β-hydroxy acid. Furthermore, acute respiratory uncoupling by simvastatin β-hydroxy warrants further investigation to determine the specific mechanism by which it disrupts the mitochondrial membrane potential.

In line with previous reports, extracellular flux analysis of permeabilised L6 myocytes in the presence of respiratory complex-specific substrates identified SVL as an inhibitor of complex I, and to a greater extent, complex II and III supported respiration (Sirvent *et al.*, 2005; Schirris *et al.*, 2015; Larsen *et al.*, 2013; Paiva *et al.*, 2005; Nadanaciva *et al.*, 2007; La Guardia *et al.*, 2013). However, simvastatin β-hydroxy acid caused global reductions in substrate driven respiration, particularly at complex II, demonstrating differential inhibitory potency when compared to the lactone species at equimolar concentrations. Whilst, reductions in complex I and II supported respiration have been noted in response to the β-hydroxy acid species in C2C12 myocytes, the precise concentrations used to see this effect were not fully disclosed (2-8 times IC_{50} of the corresponding lactone) (Schirris *et al.*, 2015). Encouragingly, a significant reduction in complex III driven respiration by SVL was seen at a 30 µM which is consistent with predictive *in silico* modelling and experimental data suggesting that simvastatin lactone is capable of reversibly binding to the Q_O site of complex III, the effects of which may be mitigated by enriching the reduced ubiquinol pool to compete with SVL for the binding site (Schirris *et al.*, 2015).

When examining the effect of both chemical species upon isolated mitochondria, in agreement with the respirometry data, 300 µM SVA increased rhodamine123 fluorescence indicating depolarisation of the inner mitochondrial membrane. In addition, an increase in mitochondrial volume was also detected starting from 100 µM as signified by a relative decrease in optical density. In contrast, the highest concentration of SVL (300 µM) promoted an increase in optical density compared with the vehicle, eluding to mitochondrial shrinkage or rupture with the simultaneous loss of membrane potential. These results are consistent with the effects of acute simvastatin application upon permeabilised human skeletal muscle fibers. Concentrations greater than 100 µM have been shown to cause mitochondrial membrane depolarisation and Ca^{2+} efflux into the cytoplasm via induction of the MPTP. The consequential increase in cytosolic Ca^{2+} promotes further Ca^{2+} release from the sarcoplasmic reticulum, precipitating the myotoxic effects of simvastatin. The initiation of this 'chain

reaction' was later linked to complex I inhibition in human and rat skinned skeletal muscle samples (Sirvent *et al.*, 2005a; Sirvent *et al.*, 2012; Sirvent *et al.*, 2005b).

Whilst experiments have illustrated acute differential effects mediated by the two chemical species of simvastatin upon respiratory function, it is important to acknowledge that the concentrations used in this setting are well in excess of the plasma C_{max} for each compound (0.08-2.2 µM SVL and 0.03-0.6 µM SVA), thus limiting the translational utility of the data (Björkhem-Bergman *et al.*, 2011; Ahmed *et al.*, 2013). However, it is documented that the doses of statin required to produce myopathic effects in rodents are high compared with therapeutic doses in humans, possibly due to differences in drug-biotransformation, basal metabolic rate, lipid metabolism or greater spare respiratory capacity (Sidaway *et al.*, 2009; Sanuki *et al.*, 2017).

To address this, further investigations endeavoured to define if simvastatin, in both its lactone and β-hydroxy acid conformation, when administered using a chronic and therapeutically relevant dosing regime *in vitro*, can have a similar negative impact upon mitochondrial respiratory function. In contrast to previous studies using acute high dose statin application in murine cell lines, reductions in cellular ATP content (SVL (1 µM) galactose: 40.9 %, SVA (1 µM) galactose: 24.51 %) were observed over a 120 hour dosing period which preceded the induction of cell death.

When assessing mitochondrial respiratory chain functionality using extracellular flux analyser technology in whole cells, significant decreases in basal respiration, maximal respiration and coupling efficiency were observed for both SVL and SVA (1 µM)**.** When compared to the respective vehicle controls there was no significant difference between the two drug treatments at equimolar concentrations. Respiratory uncoupling (i.e. an increase in basal respiration) as seen when acutely injecting SVA (300 µM) was not recapitulated in this model suggesting that this is a phenomenon only observed when 'overloading' the mitochondria with high concentrations of compound.

When examining the effect of simvastatin on the individual respiratory complexes in permeabilised cells, both SVL and SVA (1 µM) had the most profound effect on succinate dehydrogenase (complex II) function (41.7 % and 44.1 % reductions in complex activity respectively), which paralleled with the results garnered from the acute injection studies. Significant reductions in function were also observed for complexes I, III and IV to a lesser extent. Importantly, these changes were independent of changes to mitochondrial mass.

However, this could be further supported by examining citrate synthase activity or mtDNA copy number especially as these parameters have been reported to be perturbed by long-term statin treatment in human subjects (Stringer *et al.*, 2013; Larsen *et al.*, 2013; Schick *et al.*, 2007; Paiva *et al.*, 2005)

Interrogation of the mitochondrial β-oxidation pathway was also examined under the chronic modelling system. Consistent with reports that statins can exert inhibitory effects upon carnitine palmitoyl transferase II (CPT2) activity, the enzymatic mediator of medium- and long-chain fatty acid oxidation in the mitochondrion, significant reductions in acyl-carnitine driven respiration were observed in response to both SVL and SVA exposure (Vladutiu *et al.*, 2006; Hur *et al.*, 2014; Schirris *et al.*, 2015). This effect was particularly prominent in the presence of long-chain palmitoyl-L-carnitine (SVL >100 nM, SVA >10 nM), possibly due to the reliance upon the carnitine shuttle for mitochondrial entry (Vladutiu *et al.*, 2006). Medium-chain fatty acids, on the other hand, are only partially reliant upon facilitated transport due to the ability of molecules with ≤ 8 carbon atoms to permeate the inner mitochondrial membrane (Schönfeld and Wojtczak, 2016). Thus, there may be less of a substrate feeding 'bottle-neck' in the presence of octanyl-L-carnitine, delaying the onset of dysfunctional substrate-driven respiration under these conditions.

Lack of substantial differential toxicity between the two chemical conformations in most cases is likely reflective of the hydrolysis of the lactone ring *in vitro* over each 24 hour re-dosing period as evidenced by the modulation of RAS GTPase farnesylation by SVL. Indeed, it has been demonstrated, using liquid chromatography-mass spectrometry, that atorvastatin β-hydroxy acid is relatively stable in myocyte culture medium (< 10 % conversion to lactone) over a 72 hour period. In contrast, the majority of atorvastatin lactone is converted to the β-hydroxy acid species after 24 hours (Hermann *et al.*, 2005; Skottheim *et al.*, 2008). Therefore, it would be of merit to investigate if the same outcomes can be replicated with simvastatin.

Whilst beyond the scope of this thesis, aside from the induction of respiratory dysfunction, it is important to consider the implications that therapeutically relevant statin exposure may have upon the wider mitochondrial signalling network, particularly Ca^{2+} mediated cross-talk with the sarco/endoplasmic reticulum as the primary location of HMG-CoAR, attenuation of the Akt/mTOR/ULK1 signalling pathway, redox signalling, the homeostatic role of mitophagy and the induction of cell death pathways (Sirvent *et al.*, 2005b; Mullen *et al.*, 2011; du Souich *et al.*, 2017; Kwak *et al.*, 2012; Andres *et al.*, 2017). Further work should begin to integrate

the aforementioned themes to build a more holistic picture of the causes and consequences of statin-mediated mitochondrial dysfunction in skeletal muscle.

2.5 Conclusions

The data presented within this chapter demonstrate that simvastatin can mediate deleterious effects upon several pathways of mitochondrial energy metabolism which may, in turn, perpetuate the manifestation of myopathic symptoms in some patients receiving statin therapy. At supra-physiological concentrations and acute time points these perturbations appear to be discrete between the two chemical species, however the same outcomes are not recapitulated using chronic modelling at concentrations which reflect the plasma C_{max}. This is likely due to the hydrolysis of simvastatin lactone over extended culture periods, resulting in an inability to distinguish a significant differential impact upon mitochondrial function between the two chemical species. Though, this situation is perhaps more reflective of the behaviour of the compounds *in vivo*. Based upon these findings, the remainder of this thesis will focus upon the development of advanced *in vitro* models of human skeletal muscle and the identification of both functional and genetic (mtDNA) patient factors which may confer an enhanced or diminished risk of statin mediated mitochondrial perturbations and by extension, development of myopathic symptoms.

Chapter 3

The Generation of Three-Dimensional, Tissue-Engineered Skeletal Myobundles to Assess Drug-Induced Mitochondrial Dysfunction

Contents

3.1 Introduction 100

3.1.1 Summary of Chapter Aims 101

3.2 Materials and Methods 102

3.2.1 Materials 102

3.2.2 Isolation of Satellite Cells from Surgical Waste Tissue 103

3.2.3 General Cell Culture Maintenance 103

3.2.4 Differentiation Procedure for Monolayers 103

3.2.5 Fabrication of Myobundles 104

3.2.6 Fluorescent Imaging 106

3.2.7 Western Blots 107

3.2.8 Acute Metabolic Manipulation using Galactose Media 107

3.2.9 Combined Lactate Dehydrogenase (LDH) and ATP Assays 108

3.2.10 Extracellular Flux Analyser (XF24/XF^{e}96) Assays 109

3.2.11 Statistical Analysis 111

3.3 Results 112

3.3.1 Participant Characteristics 112

3.3.2 Characterisation of Isolated and Commercial Myocytes 113

3.3.3 Assessment of Myoblast Fusion Potential 114

3.3.4 Assessment of Myobundle Architecture and Composition 116

3.3.5 Longitudinal Assessment of Myobundle Stability 118

3.3.6 Acute Metabolic Modification of Monolayers with Galactose Media 118

3.3.7 Acute Metabolic Modification of Myobundles with Galactose Media ... 120

3.3.8 Examining the Oxidative and Glycolytic Profiles of Monolayers 121

3.3.9 Examining the Oxidative and Glycolytic Profiles of Myobundles 122

3.3.10 Assessing Respiratory Parameters Between Monolayers and Myobundles 123

3.4 Discussion 125

3.5 Conclusions 129

3.1 Introduction

Cell based assays have long been the backbone of the drug development process. They provide a simple, fast and economically viable tool to alleviate the ethical considerations demanding a reduction in the use of animals in biomedical research. Cultured cells represent the fundamental building blocks of such techniques, since the results of the assays are based upon the cellular responses to exogenously supplied compounds or stimuli. The vast majority of cell based assays are performed using a conventional monolayer of primary or immortalised cells grown on a flat, rigid substrate. Whilst two-dimensional (2D) culture has proven to be an extremely valuable tool for cell-based research, the limitations of the platform have been increasingly recognised as fields have advanced (Breslin and O'Driscoll, 2013; Edmondson *et al.*, 2014; Anton *et al.*, 2015).

In an *in vivo* setting, almost all cells are surrounded by, and interact with, an extracellular matrix (ECM) and cells from neighbouring tissues in a three-dimensional (3D) fashion. As such, monoculture cannot adequately reconstruct the environment from which these cells are originally derived. There are a number of reasons that this may occur, including but not limited to, differences in cellular morphology, receptor expression, polarity, ECM interactions, cell-cell signalling and lack of tissue architecture (Breslin and O'Driscoll, 2013; Edmondson *et al.*, 2014). When taken together, this may result in the generation of misleading or non-predictive data for *in vivo* or clinical responses.

Recently there has been a drive for the development of more sophisticated *in vitro* models which can accurately reflect the physiology and function of native tissues. There has been considerable progress made in the areas of liver and cardiac tissue modelling (Mathur *et al.*, 2016; Underhill and Khetani, 2018). However, functional skeletal muscle models are still in their infancy which, until recently, has posed a significant barrier to musculoskeletal research. This is particularly important as there exists a wide range of muscular diseases encompassing metabolic, neuromuscular and dystrophic disorders that are currently under investigation and lack effective therapeutic intervention strategies (Madden *et al.*, 2015; Truskey *et al.*, 2013). Tissue-engineered human skeletal muscle presents a promising candidate platform from which to study both the fundamentals of muscle physiology and perform high content screening of muscle-active compounds (Vandenburgh *et al.*, 2008).

The present chapter aims to utilise established tissue-engineering techniques to generate myobundles, a biomimetic and three-dimensional human skeletal micro-tissue model with improved physiological relevance and culture lifespan over conventional primary myocyte

culture (Madden *et al.*, 2015; Juhas and Bursac, 2014). The study will expand upon previous iterations of the model by taking a 'scaled-down' approach, producing myobundles which are 6.7x smaller in volume than the originally published design (Juhas and Bursac, 2014). This approach will be taken for two purposes; firstly to reduce the amount of cellular material required to make each myobundle and secondly to make the model amenable to a standard 96-well plate format, improving throughput and utility for drug screening applications. Myobundles will be generated using myogenic cells isolated from surgical waste tissue derived from two donors with an additional sample of primary human skeletal myoblasts purchased from a commercial source (Cook Myosite Ltd, PA, USA).

A recent study demonstrated the amenability of the myobundle model to interrogations of mitochondrial oxygen consumption polarographically in conjunction with measurements of contractile function (Davis *et al.*, 2017). Therefore, the aim of this chapter is to define the utility of the myobundles as a platform for detecting drug-induced mitochondrial dysfunction in skeletal muscle using compounds with known mitochondrial liabilities. This will be investigated using standard mitochondrial toxicity screening assays, including the acute glucose-galactose metabolic conditioning model (Kamalian *et al.*, 2015) and extracellular flux analyser technology (XF24), the principles of which are described in detail in Chapter 2.

3.1.1 Summary of Chapter Aims

1) To generate a down-scaled, tissue-engineered myobundle model amenable to a 96-well plate format, using primary proliferative myocytes derived from both commercial sources and donor tissue.
2) To characterise the structure and cellular composition of the myobundles.
3) To assess the predictive utility of the myobundle model for identifying known mitochondrial toxicants using glucose-galactose metabolic conditioning and extracellular flux analyser (XF24) technology.

3.2 Materials and Methods

3.2.1 Materials

3.2.1.1 Commercially Sourced Primary Cells

Human primary skeletal muscle derived cells (HSKMDC) (catalogue #SK-1111, Lot #P0100750F) were purchased from Cook Myosite Ltd, PA, USA as a cryopreserved stock of myoblasts ($5x10^5$ cells/ mL).

3.2.1.2 Human Skeletal Muscle Samples

Surgical waste tissue (500 mg - 2 g) was obtained from the quadriceps femoris of patients undergoing orthopaedic surgeries at the Royal Liverpool and Broadgreen University Hospital NHS Trust (RLBUHT). Tissue samples were collected by the Liverpool Musculoskeletal Biobank (LMB) in accordance with LMB approved standard operating procedures (SOPs) and covered by LMB study sponsorship (UoL001361) and ethical approval (Ref 15/NW/0661). All participants gave written, informed consent. Further details of patient inclusion/exclusion criteria are outlined in the LMB study sponsorship protocol (Appendix I).

3.2.1.3 Reagents and Consumables

All forms of DMEM, media supplements, Hoechst Fluoropure™, AlexaFluor® Phalloidin (568 nm), AlexaFluor® conjugated secondary antibodies and ProLong® Gold antifade mountant were purchased from Life Technologies (Paisley, UK). Matrigel and growth factor reduced (GFR) matrigel were purchased from Corning GmBH (Wiesbaden, Germany). Epidermal growth factor (10 µg/mL) was purchased from PeproTech (London, UK). Anti-sarcomeric α-actinin, anti-desmin, anti-vimentin and anti-β-actin antibodies were purchased from Abcam (Cambridge, UK). Anti-myogenin (MyoG) primary antibody was purchased from the Developmental Studies Hybridoma Bank (Iowa, USA). Lactate dehydrogenase cytotoxicity detection kit was purchased from Roche Diagnostics Ltd (West Sussex, UK). Extracellular flux analyser (XF24/XF^e96) consumables and base medium were purchased from Agilent Technologies (CA, USA). All other reagents and chemicals were purchased from Sigma Aldrich (Dorset, UK) unless otherwise stated.

3.2.1.4 Specialist Equipment

Precision milled polytetrafluoroethylene (PTFE) masters for the casting of polydimethylsiloxane (PDMS) moulds and laser cut Cerex® frames were kindly provided by Dr George Truskey, Department of Biomedical Engineering, Duke University, North Carolina.

Dow Corning Sylgard 184 PDMS kit was obtained from Ellsworth Adhesives Limited (East Kilbride, Scotland).

3.2.2 Isolation of Satellite Cells from Surgical Waste Tissue

Satellite cells were isolated from surgical waste tissue and expanded by outgrowth using methods similar to those described by Blau and Webster with amendments (Blau and Webster, 1981; Madden *et al.*, 2015). Upon receipt, tissue samples were washed with 1X PBS (-/-) supplemented with 2X gentamycin and amphotericin B (0.2% v/v) and weighed. The muscle tissue was carefully dissected to remove fat and connective tissue before being gently separated into smaller tissue fragments. Tissue fragments were enzymatically digested for 30 minutes in 0.05 % trypsin-EDTA (37 °C) under periodic agitation.

Following digestion, the trypsin was neutralised with an equal volume of complete growth medium and the tissue collected. Digested tissue fragments were pre-plated into uncoated T75 flasks for 2 hours to promote the adherence and subsequent disposal of remnant dermal fibroblasts. After two hours, the tissue fragments and media were transferred to growth factor reduced (GFR) matrigel coated flasks (5 μL/mL). Myogenic cell populations were observed daily to monitor cell outgrowth and expanded over a period of two weeks before bulk stocks were cryopreserved at passage 3 ($1x10^6$ cells/mL).

3.2.3 General Cell Culture Maintenance

Both commercial HSKMDC and isolated myocytes were routinely maintained in complete growth medium containing physiological glucose (5 mM) DMEM with sodium pyruvate (1 mM) and L-glutamine (4 mM), supplemented with 8 % (v/v) FBS, 0.4 μg/mL dexamethasone, 10 ng/mL epidermal growth factor, 50 μg/mL fetuin, 0.1 % (v/v) gentamycin and amphotericin B. Cells were kept in vented T75 flasks coated in GFR matrigel (5 μL/mL) and incubated in a humidified environment (37 °C with 5 % (v/v) CO_2), media changes were performed every 48 hours. All stock cultures were maintained at sub-60 % confluence and used between passages 3-5 (≤10 population doublings) to prevent the decline of cell fusion properties. Cell populations were frozen using a standard cryopreservation mix which consisted of complete growth medium supplemented with 10 % DMSO (v/v). All cryopreserved cell stocks were stored at -180 °C under the liquid nitrogen vapour phase.

3.2.4 Differentiation Procedure for Monolayers

Cells were dissociated using 0.05 % trypsin-EDTA and seeded into GFR-matrigel (5 μL/mL) coated tissue culture plates at specified densities before incubating in complete growth

media for 24 hours (37 °C, 5 % (v/v) CO_2). The following day, the growth media was removed and the cells were washed twice with 1X PBS (-/-). Cells were then cultured in a differentiation medium consisting of physiological glucose (5 mM) DMEM with sodium pyruvate and L-glutamine, supplemented with 2 % (v/v) horse serum, 10 nM human insulin, 0.1 % (v/v) gentamycin and amphotericin B. Thereafter, the differentiation media was changed every 48 hours for 5 days. Differentiation of cultures was confirmed through visual inspection under a light microscope.

3.2.5 Fabrication of Myobundles

Expanded myogenic cell populations maintained in complete growth medium were dissociated from T75 flasks in 0.05 % trypsin-EDTA to a single cell suspension and encapsulated in a fibrin hydrogel solution on to laser cut Cerex® frames (3.8 mm x 3.6 mm outer dimensions, 2.6 mm x 2.0 mm inner dimensions) within PDMS moulds (cast from machine milled PTFE masters and pre-treated with 0.2 % (w/v) pluronic® F127) at a density of $1x10^5$ cells/myobundle (Figure 3.1).

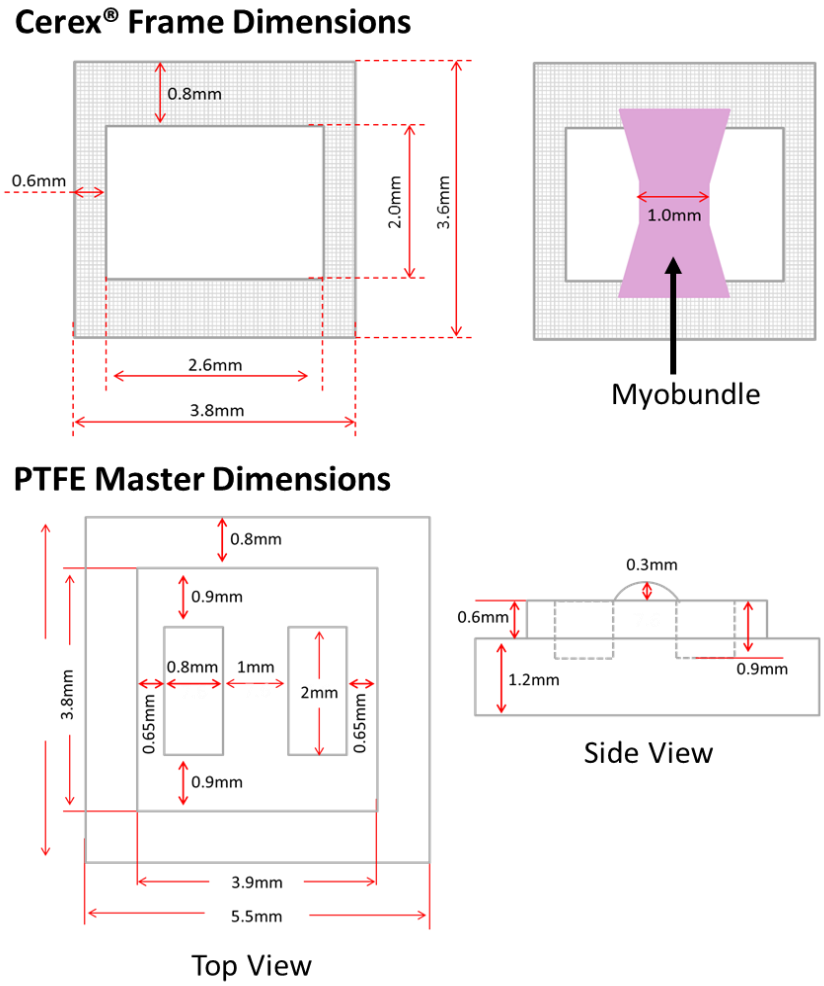

Figure 3.1 Schematic diagram depicting the dimensions of the Cerex® frames and PTFE masters used for casting PDMS moulds. All designs provided by the Truskey laboratory, Duke University, NC, USA.

Specifically, a cell solution (1x10^5 cells in 3.35 µL growth media per myobundle with 0.4 µL of 50 units/ mL thrombin (reconstituted in 1X PBS supplemented with 0.1 % fatty acid free BSA) and a hydrogel solution (0.75 µL growth medium, 1.5 µL fibrinogen (25 mg/mL) and 1.5 µL matrigel) were prepared in separate vials on ice for up to four myobundles per vial. The hydrogel solution was combined with the cell solution and pipetted vigorously on ice to mix. 7.5 µL of the cell/hydrogel mixture was individually pipetted into PDMS moulds ensuring end-to-end contact with the Cerex® frames (Figure 3.2).

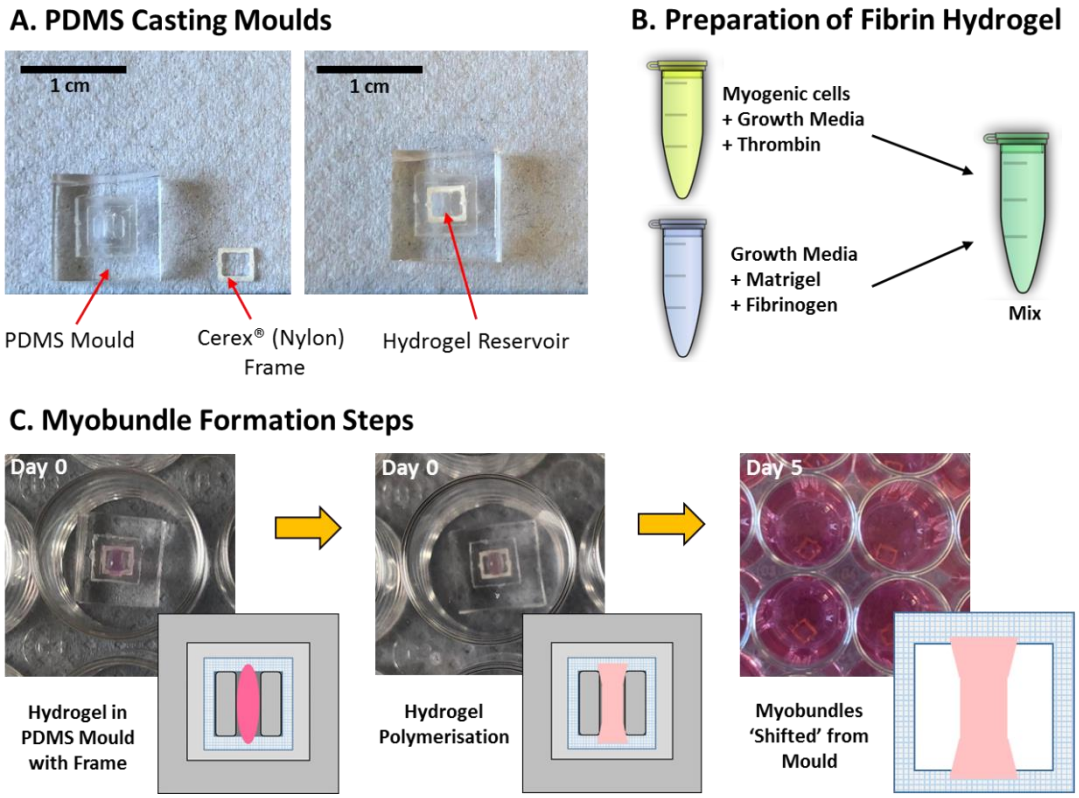

Figure 3.2 Schematic representation of the myobundle generation process (Madden *et al*., 2015).

The cell/hydrogel mixture was polymerised at 37 °C for 25 minutes followed by incubation in complete growth media supplemented with 1.5 mg/mL 6-aminocaproic acid (ACA) for 5 days to allow the hydrogel structure to compact. After 5 days, the myobundles (attached to Cerex® frames) were 'shifted' from their PDMS moulds and placed into differentiation media supplemented with 2 mg/mL ACA and cultured dynamically on a fixed-angle platform rocker in suspension for a further 5 days (37 °C, 5 % (v/v) CO_2).

3.2.6 Fluorescent Imaging

3.2.6.1 Monolayers

Myoblasts were seeded on top of GFR-matrigel (5 µL/mL) coated 13 mm coverslips in 24 well plates at a density of 4500 cells/well. Cells were allowed to adhere and proliferate for 2-3 days after which they were either processed or differentiated (section 3.2.4).

Cells were rinsed with 1X PBS (-/-) before being fixed with either cold methanol for 5 minutes or 4 % (w/v) paraformaldehyde for 30 minutes. Samples were then incubated with permeabilisation buffer (1X PBS (-/-) with 0.2 % (v/v) Tween-20 and 0.5 % (v/v) Triton-X) for 30 minutes at 4 °C and blocked with 5 % (w/v) BSA reconstituted in permeabilisation buffer for a further 30 minutes at room temperature.

Primary antibodies, mouse anti-myogenin (1:50), rabbit anti-desmin (1:100) and mouse anti-vimentin (1:200) were diluted in 5 % (w/v) BSA permeabilisation buffer and incubated with the samples overnight at 4 °C. After washing, appropriate Alexa Fluor® conjugated secondary antibodies (488 nm /568 nm) were diluted 1:1000 and co-incubated with Hoechst (nuclear) and phalloidin (filamentous-actin) dyes (1:5000) for 2 hours, in the dark at room temperature.

Samples were mounted onto glass slides for imaging. 10 µL Pro-Long Gold anti-fade reagent was added to each of the samples before sealing and allowing to dry overnight at 4 °C. All images were captured using a Zeiss Axio Observer.Z1 (apotome) widefield florescent microscope and processed with Zen Blue software.

3.2.6.2 Myobundles

Differentiated myobundles were rinsed with 1X PBS (-/-) and fixed in their frames overnight with 2 % (w/v) paraformaldehyde. Myobundles were then washed and incubated with blocking/permeabilisation buffer (1X PBS (-/-) with 3 % (w/v) BSA, 0.2 % (v/v) Tween-20 and 0.5 % (v/v) Triton-X) overnight (4 °C).

Primary antibodies, mouse anti-myogenin (1:50), mouse anti-vimentin (1:200) and rabbit anti-sarcomeric alpha actinin (1:200) were diluted in 3 % BSA blocking/permeabilisation buffer and incubated with the samples overnight at 4 °C under gentle agitation. Post incubation, samples were washed before the appropriate Alexa Fluor® conjugated secondary antibodies (488 nm/568 nm) were diluted (1:1000) in 3 % BSA block/permeabilisation and co-incubated with Hoechst and phalloidin dyes (1:5000) for 2 hours, in the dark at room

temperature. All images were captured using a Zeiss Axio Observer.Z1 (Apotome) widefield florescent microscope and processed with Zen Blue Software.

3.2.7 Western Blots

Western blots were performed as previously described in Chapter 2 (section 2.2.8). Undifferentiated myobundles (day 5) and differentiated myobundles (day 12) were rinsed with 1X PBS (-/-) and lysed in 100 µL RIPA buffer via pulse sonication for 10 seconds (Soniprep 150, MSE, UK). Protein quantification was performed by BCA assay.

Briefly, 10 µg of protein lysate was mixed with 5 µL of sample loading dye. Samples were heat denatured at 95 °C for 5 minutes before loading into NuPAGE® 4-12 % Bis-Tris pre-cast gels alongside 5 µL of Precisions Plus Protein™ molecular weight marker. Loaded samples were subject to electrophoretic separation by molecular weight under reducing conditions in 1X MOPS-SDS (50 mM MOPS, 50 mM Tris-base, 0.1 % (w/v) SDS, 1 mM EDTA) running buffer supplemented with 500 µL NuPAGE® antioxidant for 1 hour (170 V).

Separated proteins were transferred onto nitrocellulose membranes using an XCell II blotting module for 1 hour (220 V). The transfer stack was submerged in 1X transfer buffer (25 mM Tris-base, 192 mM glycine, 20 % (v/v) methanol). Resultant membranes were stained with ponceau red dye to ensure transfer uniformity before blocking for 1 hour in 10 % (w/v) non-fat milk 1X TBS-T (137 mM NaCl, 2.7 mM KCl, 19 mM Tris-base, 0.01 % (v/v) Tween 20, pH 7.4).

Primary antibodies were diluted in 5 % (w/v) non-fat milk 1X TBS-T (rabbit anti-sarcomeric α-actinin (1:1000), mouse anti-myogenin (1:50) and mouse anti-actin (1:10,000)) then incubated with membranes for 16 hours (4 °C). Following washes in 1X TBS-T, appropriate HRP-conjugated secondary antibodies were diluted 1:10,000 in 5 % (w/v) non-fat milk 1X TBS-T and incubated with membranes for 2 hours at room temperature. Band signals were detected using enhanced chemiluminescent reagent (ECL) and developed on film.

3.2.8 Acute Metabolic Manipulation using Galactose Media

Myogenic cells from each donor were collected by trypsinisation and seeded into GFR-matrigel coated (5 µL/mL), flat bottomed 96-well plates in complete growth medium (20,000 cells/100 µL/well) and incubated for 24 hours (37 °C, 5 % (v/v) CO_2). Differentiation of myogenic cell cultures grown in 2D were performed as described in section 3.2.4 for 5 days. Myobundles were fabricated and differentiated as described in section 3.2.5.

Cells and myobundles were washed three times in either serum-free high-glucose (DMEM, 25 mM glucose, 4 mM L-glutamine, 1 mM sodium pyruvate and 5 mM HEPES) or galactose (DMEM, 10 mM galactose, 6 mM L-glutamine, 1 mM sodium pyruvate and 5 mM HEPES) media. Cells and myobundles were pre-incubated in glucose or galactose media (50 µL) for 2 hours (37 ºC, 5 % (v/v) CO_2).

Rotenone stock solutions were prepared in DMSO and diluted further in the appropriate media to produce a dose range between 0-10 µM for both the glucose and galactose media conditions. Diluted stock compounds were then added to each well (50 µL) for a final well volume of 100 µL and incubated for 2 hours (37 ºC, 5 % (v/v) CO_2). The final solvent concentration for all conditions was 0.5 % DMSO.

3.2.9 Combined Lactate Dehydrogenase (LDH) and ATP assays

Cells and myobundles conditioned to glucose or galactose media were incubated with rotenone for 2 hours. Supernatants were collected and cells/myobundles were lysed using 50 µL or 100 µL of somatic cell ATP releasing agent respectively. Myobundles required an additional pulse sonication for 10s to fully dissociate the micro-tissue from the Cerex® frame before commencing with the simultaneous assessment of ATP content, cell viability and protein content. Detailed assay descriptions can be found in Chapter 2 (section 2.2.4).

3.2.9.1 ATP Assay

Quantitative determination of ATP content was assessed by the addition of sample lysates (5 µL) and ATP standards to a white-walled 96-well plate. ATP reaction solution was prepared according to manufacturer's instructions by mixing ATP assay mix with ATP dilution buffer in a 1:25 ratio. 40µL of the reaction solution was added to both samples and standards then read immediately on a Varioskan™ Flash multimode plate reader with SkanIt™ software to capture the peak luminescent signal.

3.2.9.2 LDH Assay

Detection of cytotoxicity was achieved using a colorimetric LDH assay kit. LDH retention was determined by extracting 25 µL supernatant and 10 µL cell lysate for each sample and incubating them with 50 µL LDH catalyst-dye solution (1:45 ratio), according to manufacturer's instructions. After 30 minutes incubation in the dark, samples were read at 490 nm on a Varioskan Flash multimode plate reader. LDH retention was determined as:

$$\textbf{LDH Retention} = \frac{\textbf{Lysate}}{(\textbf{Supernatant} + \textbf{Lysate})}$$

3.2.9.3 BCA Assay

In order to correct for potential variance in cell number, the BCA assay was used to normalise ATP assay results. Quantification of sample protein content was determined using 10 µL sample lysate and protein standards. Assay products were read at 562 nm after 30 minutes incubation at 37 °C.

3.2.10 Extracellular Flux Analyser (XF24/XF^{e}96) Assays

Myogenic cells from each donor were collected by trypsinisation and seeded into GFR-matrigel coated (5 µL/mL), XF^{e}96 cell culture microplates in complete growth medium (25,000 cells/100 µL/well) and incubated for 24 hours (37 °C, 5 % (v/v) CO_2). Differentiation of myogenic cell cultures grown in 2D were performed as described in section 3.2.4. Myobundles were fabricated and differentiated as described in section 3.2.5. On the day of the assay, myobundles were moved to XF24 cell culture microplates coated with neat GFR-matrigel and orientated horizontally within the wells to align with the XF24 sensor cartridge probes.

Following the completion of XF assays, cells and myobundles were lysed in somatic cell ATP releasing agent (20 µL and 100 µL respectively). Lysates (10 µL) were transferred to a 96-well plate for quantification of protein content by BCA assay. Protein content per well was used as a means to normalise raw OCR and ECAR data.

3.2.10.1 Mitochondrial Stress Test

Myogenic cells and myobundles were incubated for 1 hour (37 °C, 0 % CO_2) prior to the start of the assay. Culture medium was replaced with 175 µL (XF^{e}96) or 450 µL (XF24) unbuffered XF base medium supplemented with glucose (25 mM), L-glutamine (2 mM), sodium pyruvate (1 mM), pre-warmed to 37 °C (pH 7.4).

3.2.10.1.1 Stress Test Compound Preparation

Stock mitochondrial stress test compounds were prepared and loaded into XF sensor cartridges in accordance to Table 3.1 for monolayers on the XF^{e}96 and Table 3.2 for myobundles on the XF24. Optimal stress test compound concentrations were determined empirically for each system.

Table 3.1 Mitochondrial stress test injection port locations, compound stock concentrations, dilution factors and final well concentrations for the XF^{e}96.

Injection Port	Compound	Port Dilution Factor	Final Well Concentration	Port Loading Volume
A	Oligomycin	8	1 µM	25 µL
B	FCCP	9	0.75 µM	25 µL
C	Rotenone/Antimycin A	10	1 µM	25 µL

Table 3.2 Mitochondrial stress test injection port locations, compound stock concentrations, dilution factors and final well concentrations for the XF24.

Injection Port	Compound	Port Dilution Factor	Final Well concentration	Port Loading Volume
A	Oligomycin	10	10 µM	50 µL
B	FCCP	10	6 µM	55 µL
C	FCCP	10	4 µM	62 µL
D	Rotenone/Antimycin A	10	10 µM	68 µL

Each run included a pre-programmed calibration, an equilibration step and 3 cycles of mix/measure/wait (3 mins/3 mins/0 mins) to establish a baseline OCR/ECAR prior to the injection of any compounds. Following this, a stress test was performed via the sequential injection of mitochondrial toxicants. This enabled the calculation of basal respiration (BR), maximal respiratory capacity (MRC), ATP-linked respiration (ALR), proton leak (PL) and spare respiratory capacity (SRC).

3.2.10.2 Calculation of the Proton Pumping Rate Attributable to Glycolysis (PPR_{gly})

Baseline measurements of oxygen consumption rate (OCR) and extracellular acidification rate (ECAR) were performed in the absence of any compounds for monolayers and myobundles. The OCR and ECAR measurements were then used to calculate the proton pumping rate (PPR) attributable to glycolysis (PPR_{gly}) as per the formula below:

$$\mathbf{PPR_{gly} = ECAR_{tot}/BP - (10^{(pH-pK_1)}/(1+10^{(pH-pK_1)})(max\ H^+/0_2)(OCR_{tot} - OCR_{rot/AA})}$$

Where tot = total, ECAR units = (mpH/min/µg), BP = buffering power (mpH/pmol H^+ in 2 µL (XF^{e}96) or 7 µL (XF24)), K_1 = combined equilibrium constant of CO_2 hydration and dissociation to HCO_3^- + H^+, max H^+/O_2 = the CO_2-derived acidification for the complete oxidation of glucose, OCR units = (pmol O_2/min/µg) and $OCR_{rot/AA}$ = non-mitochondrial OCR (Mookerjee and Brand, 2015).

3.2.11 Statistical Analysis

Data are representative of at least three independent experiments (n=3) and all values are expressed as mean $\pm$ standard deviation (S.D.) as appropriate. Statistical analyses were performed using GraphPad Prism® 7 software (GraphPad Software, Inc, CA, USA). Data were tested for Guassian distribution using the Shapiro-Wilk normality test before statistical significance was determined using a student's t-test with Welch's correction, one-way Analysis of Variance (ANOVA) with Dunnett's correction for multiple comparisons or two-way ANOVA with Dunnett's or Sidak's correction. Non-parametric equivalents were used as appropriate. IC_{50} values were determined using non-linear regression analysis. A p value $\leq$ 0.05 was regarded as the significance threshold.

3.3 Results

3.3.1 Participant Characteristics

A summary of clinical data for study participants and commercially sourced primary myocytes are outlined in Table 3.3. Participants and commercial myocytes were selected for the study due to their advanced age (> 45 years), statin-naïve status, lack of inherited metabolic disorders and no history of diabetes.

Table 3.3 Clinical information for recruited study participants and commercially sourced primary myocytes.

Sample ID	Age	Gender	Ethnicity	BMI (kg/m^2)	Smoking Status	Alcohol (Units/Week)	Inherited Metabolic Disorders	Medication	Biopsy Location
LMB-HI-229	85	M	Caribbean	22.7	Non-smoker	<1	No	Zemtard Betahistine Cetirizine Omeprazole	Quadriceps Femoris
LMB-PP-231	59	F	Caucasian	33.5	Previous	1-5	No	Codeine Paracetamol Ibuprofen	Quadriceps Femoris
HSKMDC	50	F	Caucasian	23	Previous	NK	No	Sertraline	Abdominal Rectus

Abbreviations: M, male; F, female; NK, not known.

3.3.2 Characterisation of Isolated and Commercial Myocytes

Proliferative cell populations from each participant were co-stained for vimentin (type III intermediate filament) and desmin (muscle specific type III intermediate filament) (Figure 3.3).

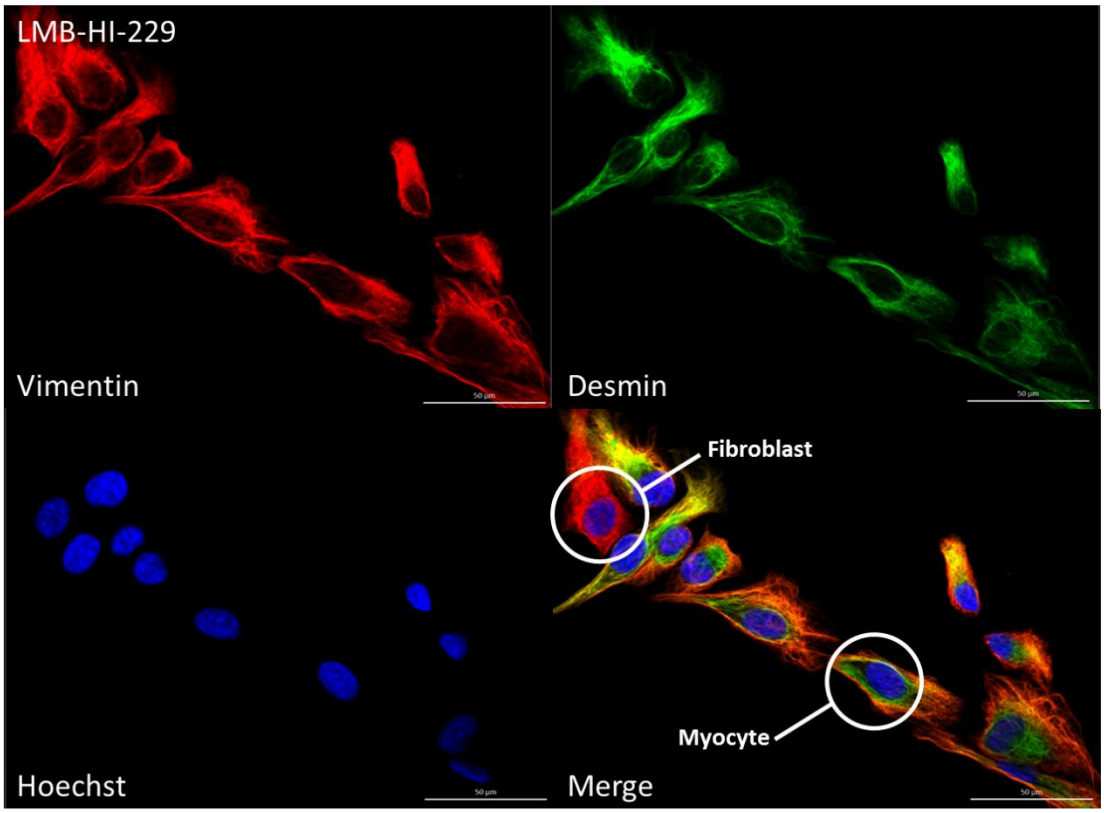

Figure 3.3 Representative image of desmin/vimentin co-staining for donor LMB-HI-229 at passage 3. Image taken on 60X oil immersion lens. Scale bar = 50 µm.

The proportion of myocytes (desmin and vimentin +ve) to fibroblasts (vimentin +ve only) were quantified for each of the cellular sources to ensure that an enriched myocyte population (>60 %) was present (Figure 3.4). In each case, the percentage of myocytes

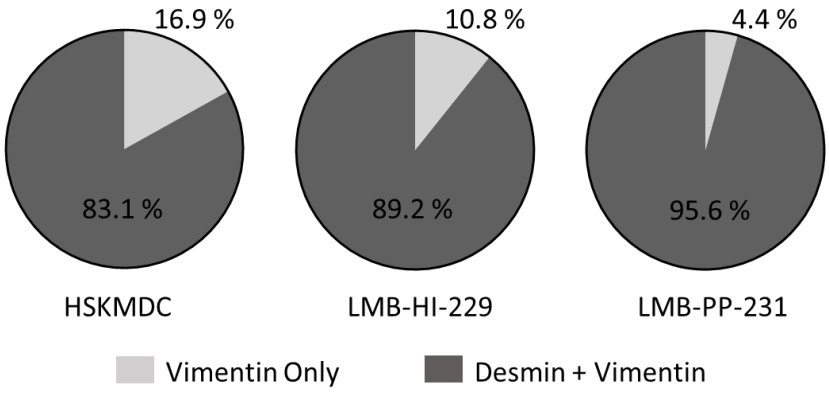

Figure 3.4 Proportion of myocytes to fibroblasts in each source culture at passage 3. Four random images per slide were taken for each slide (n=4). Average counts were performed using ImageJ 1.48 software.

exceeded the threshold, with the commercial HSKMDC culture exhibiting the least enriched stock population (83.1 %) of the sources examined.

3.3.3 Assessment of Myoblast Fusion Potential

Differentiation of myocyte cultures was assessed via visual inspection for cell fusion after the substitution of growth for differentiation medium. Commitment of cells to a myogenic fate was confirmed by probing for the expression of the myogenic regulatory factor (MRF) myogenin (MyoG). As shown in Figure 3.5 **(A)**, before initiation of differentiation myocytes were discrete, mononuclear and did not express MyoG. After differentiation (Figure 3.5 **(B)**), myocytes fused to form polynucleated myotubes and MyoG expression was present and localised to the nuclei.

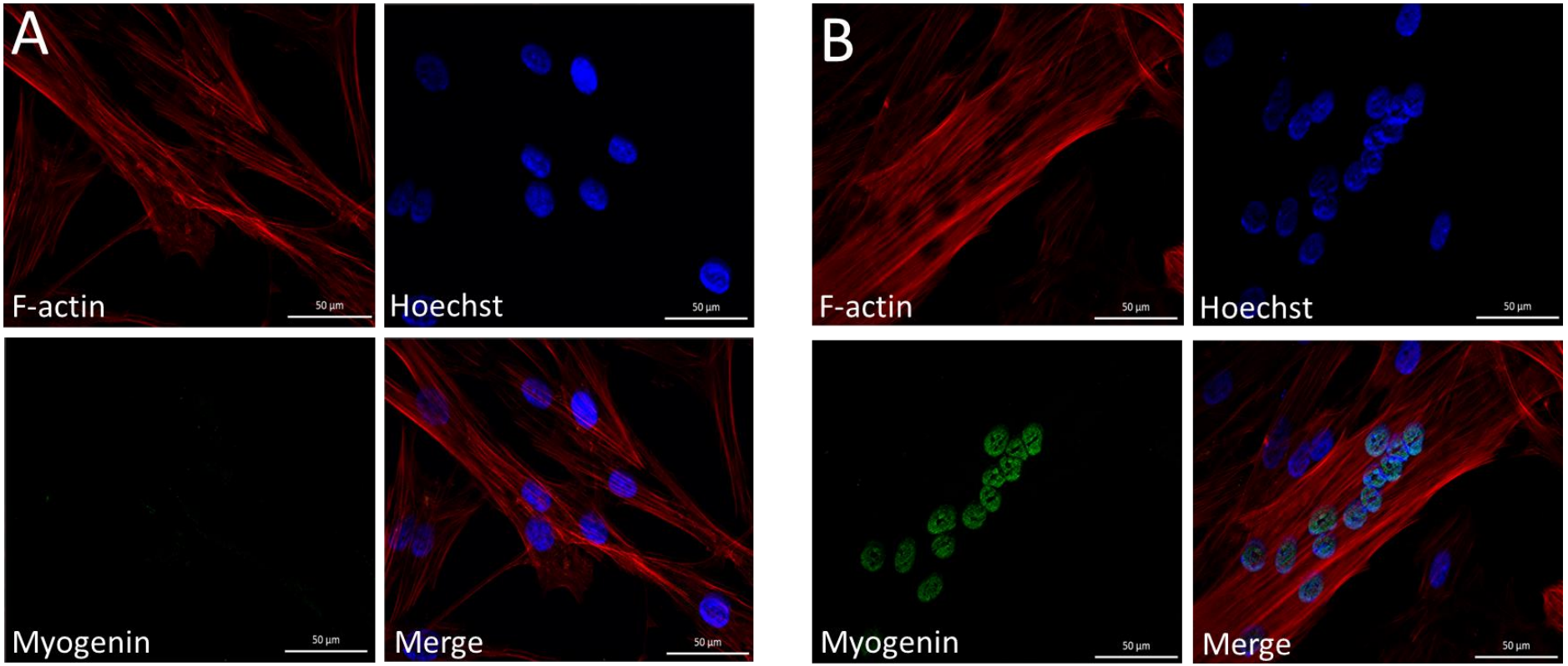

Figure 3.5 Representative images of HSKMDC MyoG staining. **(A)** Myoblasts 24 hours after seeding. **(B)** Myotubes after 5 days in differentiation media. Images taken on 40X oil immersion lens. Scale bar = 50 µm.

3.3.4 Assessment of Myobundle Architecture and Composition

Engineered skeletal 'myobundles' were generated using a fibrin hydrogel moulding technique and anchored to nylon fabric frames as previously described (Hinds *et al.*, 2011; Juhas and Bursac, 2014; Madden *et al.*, 2015) with amendments. After compaction and differentiation in dynamic suspension, myobundle constructs assumed a characteristic 'dog bone' shape, bowing due to the contraction of the seeded myocytes (Figure 3.6) (Qazi *et al.*, 2015).

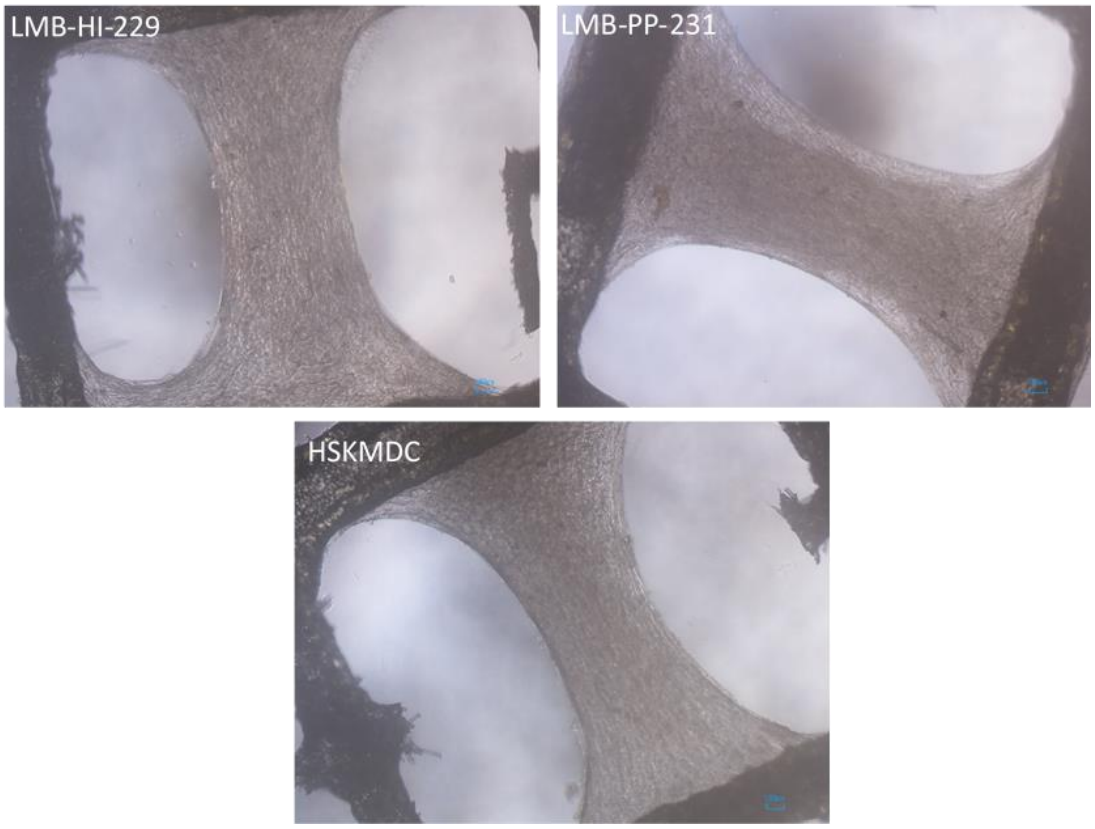

Figure 3.6 Representative images of 7.5 µL myobundles produced from each cellular source. Images taken on Nikon Digital Sight (DS-L2) imaging unit, 4X objective lens. Scale bar = 100 µm.

Differentiated myobundles exhibited extensive MyoG expression (Figure 3.7 **(A)**), showed focal accumulation of vimentin positive cells (fibroblasts) at the peripheral edge of the myobundle (Figure 3.7 **(B)**) and expressed the mature muscle protein sarcomeric α-actinin (SAA) (Figure 3.7 **(C)**). Additionally, comparisons of the expression of MyoG and SAA between pre-differentiated and differentiated myobundles showed clear differences in abundance between the two time points (Figure 3.7 **(D)**).

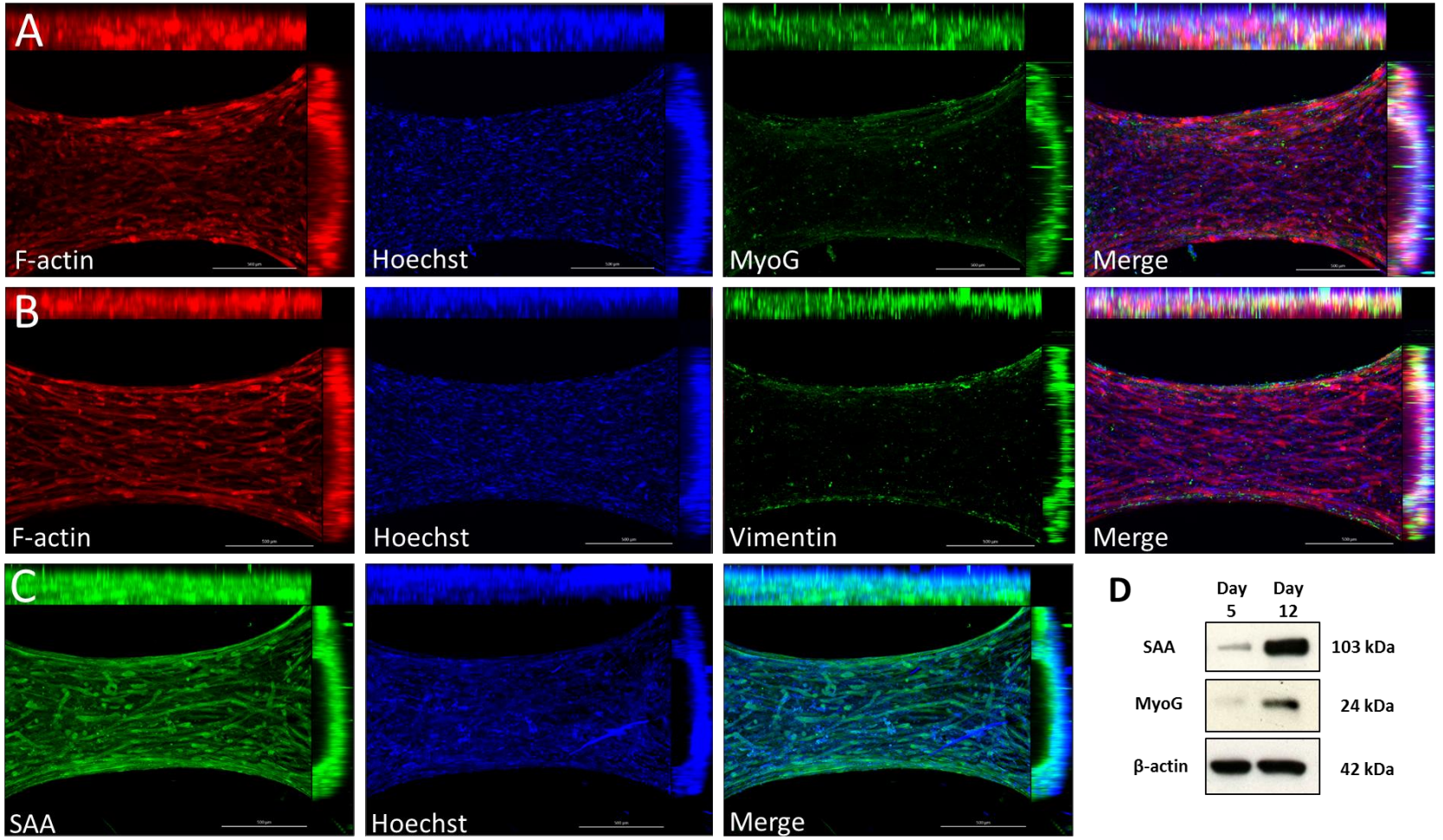

Figure 3.7 Representative HSKMDC myobundle images for **(A)** MyoG, **(B)** vimentin and **(C)** SAA staining after 7 days differentiation. Maximum intensity projection (MIP), Z-stack images (apotome) were taken using the 5X objective lens. Scale bar = 500 µm. **(D)** Differential expression of MyoG and SAA at day 5 (pre-differentiation) and day 7 (post differentiation) in HSKMDC myobundles (n=3).

3.3.5 Longitudinal Assessment of Myobundle Stability

To ensure that the cell and hydrogel components of the myobundles were not subject to degradation over time, both ATP and protein content were measured at 5 day intervals. As shown in Figure 3.8, despite small fluctuations, there was no significant change in either parameter tested, suggesting that the constructs remained stable over a 15 day period.

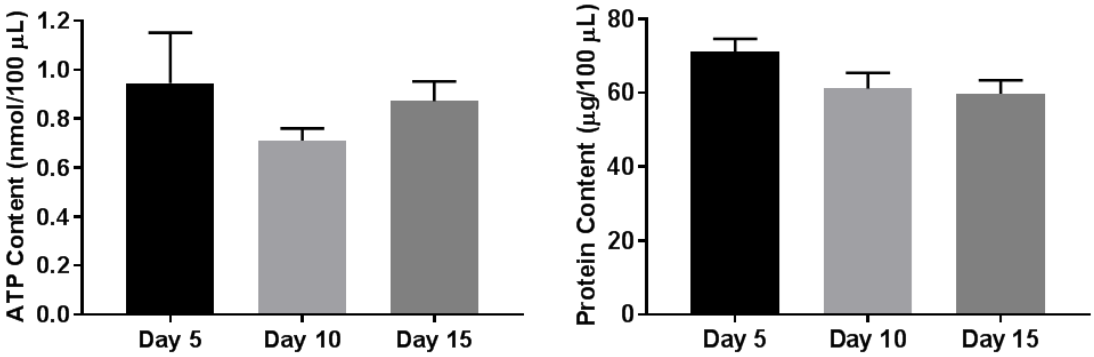

Figure 3.8 Longitudinal study of the ATP and protein content of myobundles over a 15 day period. Graphical values are displayed as mean ± S.D. and are representative of n=2 donors and n=3 myobundles per time point. Statistical significance was determined by one-way ANOVA with Dunnett's test for multiple comparisons.

3.3.6 Acute Metabolic Modification of Monolayers with Galactose Media

Differentiated myotubes, metabolically conditioned to either glucose or galactose media were exposed to rotenone, a classic mitochondrial toxin with a well-defined molecular target (complex I), for two hours as previously described (Ball *et al.*, 2016; Kamalian *et al.*, 2015). To identify compound-induced mitochondrial dysfunction in the context of cell death, cellular ATP content and LDH retention were measured simultaneously.

Exposure to rotenone for two hours did not significantly reduced the LDH retention values for any donor, in either media condition. However, ATP content values varied. Donor LMB-HI-229 (Figure 3.9 **(A)**) and the HSKMDC (Figure 3.9 **(C)**) both showed significant reductions in ATP content in glucose media, whilst LMB-PP-231 (Figure 3.9 **(B)**) appeared to be less sensitive in that respect. In all cases, there was a dramatic reduction in ATP content in myotubes conditions to galactose media. A summary of IC_{50} values for each cellular source are displayed in Table 3.4.

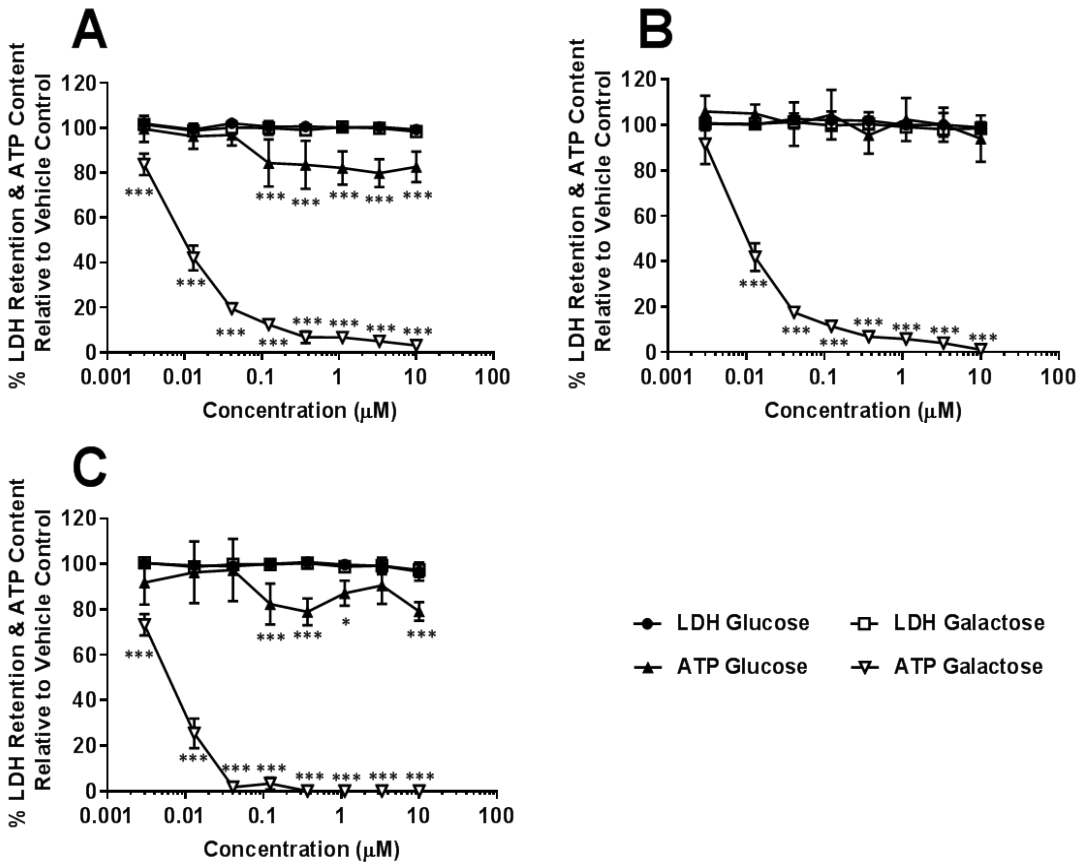

Figure 3.9 Examining the effect of rotenone (0-10 μM) exposure on ATP content and LDH retention in primary myocytes (2 Hours) compared with the vehicle control in glucose and galactose media. Results are expressed as a percentage of the corresponding media vehicle control and graphical values are displayed as mean ± S.D. (n=3). **(A)**: **LMB-HI-229**, **(B)**: **LMB-PP-231**, **(C)**: **HSKMDC**. Statistical significance was determined by one-way ANOVA with Dunnett's test for multiple comparisons. *p value < 0.05 **p value < 0.01 ***p value < 0.001.

Table 3.4 Summary of corresponding IC_{50} values for each cellular source in response to rotenone exposure (2 hours). Results are displayed as mean ± S.D. (n=3). Statistical significance was determined by un-paired t-test with Welch's correction. *p value < 0.05, **p value < 0.01, ***p value < 0.001, n/d p value not determined.

	IC_{50} ATP (μM) ± S.D.		**IC_{50} LDH (μM) ± S.D.**		**IC_{50} ATPglu/ IC_{50} ATPgal**	**IC_{50} LDHgal/ IC_{50} ATPgal**
	Glucose	Galactose	Glucose	Galactose		
LMB-HI-229	>10	0.0094 ± 0.0018	>10	>10	>1059.45 (n/d)	>1059.45 (n/d)
LMB-PP-231	>10	0.0096 ± 0.0018	>10	>10	>1039.65 (n/d)	>1039.65 (n/d)
HSKMDC	>10	0.0093 ± 0.0015	>10	>10	>1075.79 (n/d)	>1075.79 (n/d)

Mitochondrial toxicity was defined by calculating the ratio between the IC_{50} values for ATPglu versus ATPgal, whereby a ratio ≥ 2 indicated that the tested compound was a mitochondrial toxin, thus had a more pronounced effect in galactose media due to a lack of compensatory ATP generation from glycolysis. An IC_{50} ratio ≥ 2 for LDHgal versus ATPgal indicated that mitochondrial dysfunction preceded cell death, in line with previous definitions (Swiss *et al.*, 2013). In all three examples provided, both criteria were met.

3.3.7 Acute Metabolic Modification of Myobundles with Galactose Media

The assays were next performed using myobundles from each respective cellular source. In this instance, mitochondrial toxicity was defined as the lowest concentration at which the ATP level declined significantly more in galactose media than in glucose (Figure 3.10).

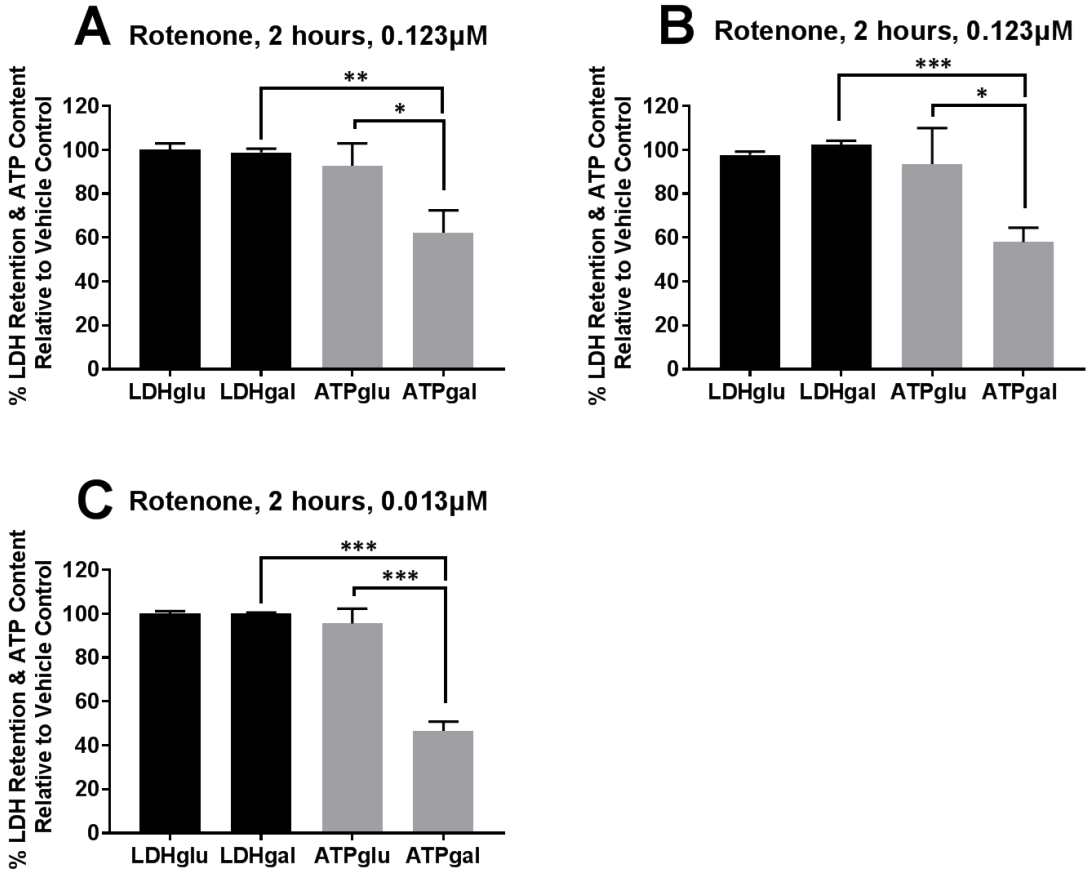

Figure 3.10 Examining the effect of rotenone exposure on ATP content and LDH retention in myobundles (2 Hours) compared with the vehicle control in glucose and galactose media. Results are expressed as a percentage of the corresponding media vehicle control and graphical values are displayed as mean ± S.D. (n=3). **(A)**: **LMB-HI-229**, **(B)**: **LMB-PP-231**, **(C)**: **HSKMDC**. Statistical significance was determined by unpaired t-test with Welch's correction. *p value < 0.05 **p value < 0.01 ***p value < 0.001.

The HSKMDC myobundles (Figure 3.10 **(C)**) were the most sensitive to rotenone exposure in galactose media, displaying a 46.9 % reduction in ATP content compare to vehicle at 0.013 µM, LMB-HI-229 (Figure 3.10 **(A)**) and LMB-PP-231 (Figure 3.10 **(B)**), required higher doses

(0.123 µM) in order to see significant reductions in ATPgal at the same time point. Nevertheless, each set of myobundles displayed differential toxicity in galactose media only without notable reductions in LDH retention compared to vehicle.

3.3.8 Examining the Oxidative and Glycolytic Profiles of Monolayers

Baseline measurements of oxygen consumption rate (OCR) and extracellular acidification rate (ECAR) in differentiated monolayers were performed in the absence of any compounds. The OCR and ECAR measurements were then used to calculate the proton pumping rate (PPR) attributable to glycolysis (PPR_{gly}). After the establishment of baseline rates, oligomycin, an ATP synthase inhibitor was acutely injected into the plates and OCR/ECAR measurements were performed again. The resultant bioenergetic profiles of each participant were plotted as phenograms and displayed in Figure 3.11. Phenograms represent the cross-points of OCR and PPR_{gly} values to describe energy derivation before and after the application of a compound (Kamalian *et al.*, 2018).

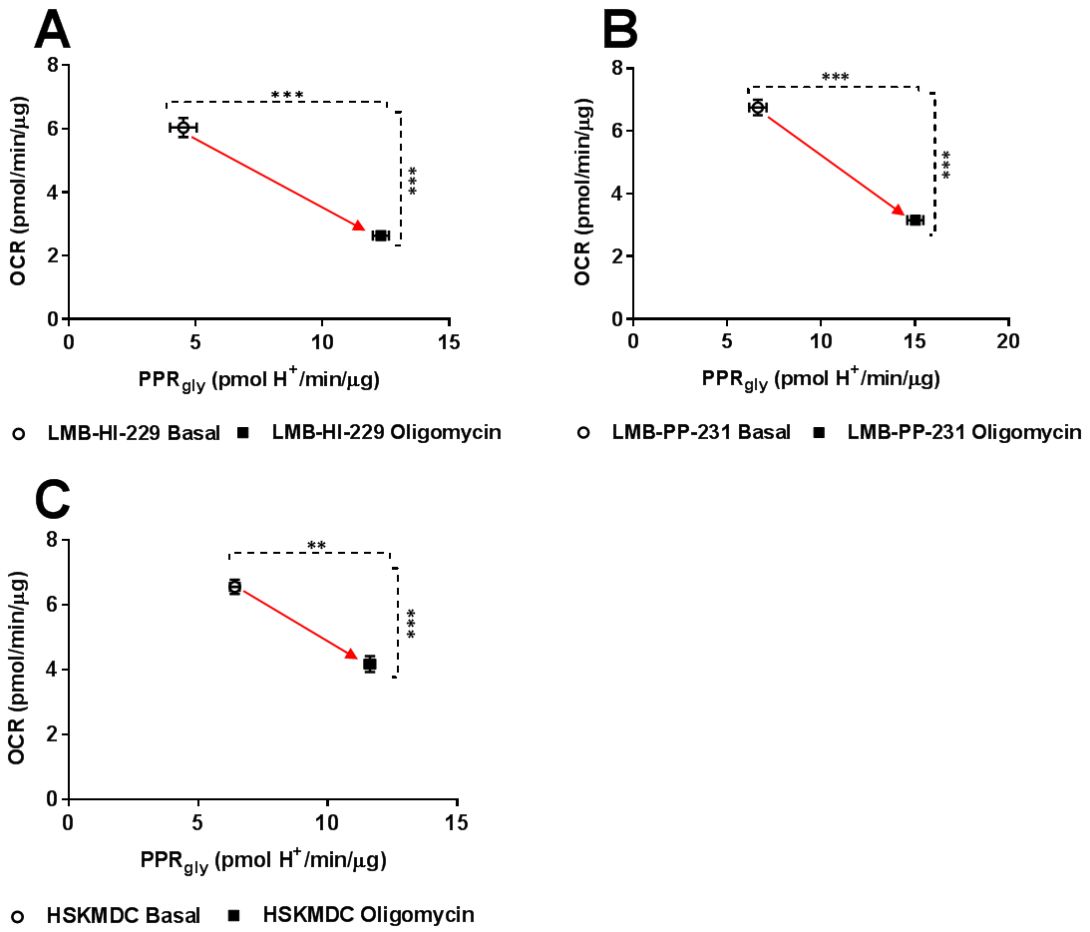

Figure 3.11 Bioenergetic phenograms for study participants in monolayer **(A) LMB-HI-229, (B) LMB-PP-231, (C) HSKMDC** before treatment **(open circles)** and after acute application of oligomycin **(closed squares)**. Graphical values are displayed as mean ± S.D. (n=3). Statistical significance was determined by unpaired t-test with Welch's correction. *p value < 0.05 **p value < 0.01 ***p value < 0.001.

The triggering of energetic dysfunction through the application of a respiratory inhibitor instigated a significant decrease in mitochondrial oxygen consumption and a rapid increase in compensatory glycolytic flux for each participant.

3.3.9 Examining the Oxidative and Glycolytic Profiles of Myobundles

The bioenergetic profile of myobundles was assessed on a XF24 instrument. PPR_{gly} was calculated using the same formula as described in section 3.2.10.2, with volumetric adjustments for buffering power (mpH/pmol H^+ in 7 µL) to account for the larger plate size. As shown in Figure 3.12, myobundles produced from the same participants exhibited higher basal OCR values than their monolayer counterparts. For example, the OCR values for LMB-PP-231 (Figure 3.12 **(B))** were 16.85 ± 5.48 pmol/min/µg for myobundles versus 6.75 ± 0.24 pmol/min/µg for monolayer (Figure 3.11 **(B)**). Conversely, basal PPR_{gly} values were greater for monolayers e.g. LMB-PP-231 were 6.64 ± 0.45 pmol H^+/min/µg versus -1.97 ± 7.58 pmol H^+/min/µg for myobundles. However, significant compensatory glycolytic flux upon administration of oligomycin was evident for each set of myobundles.

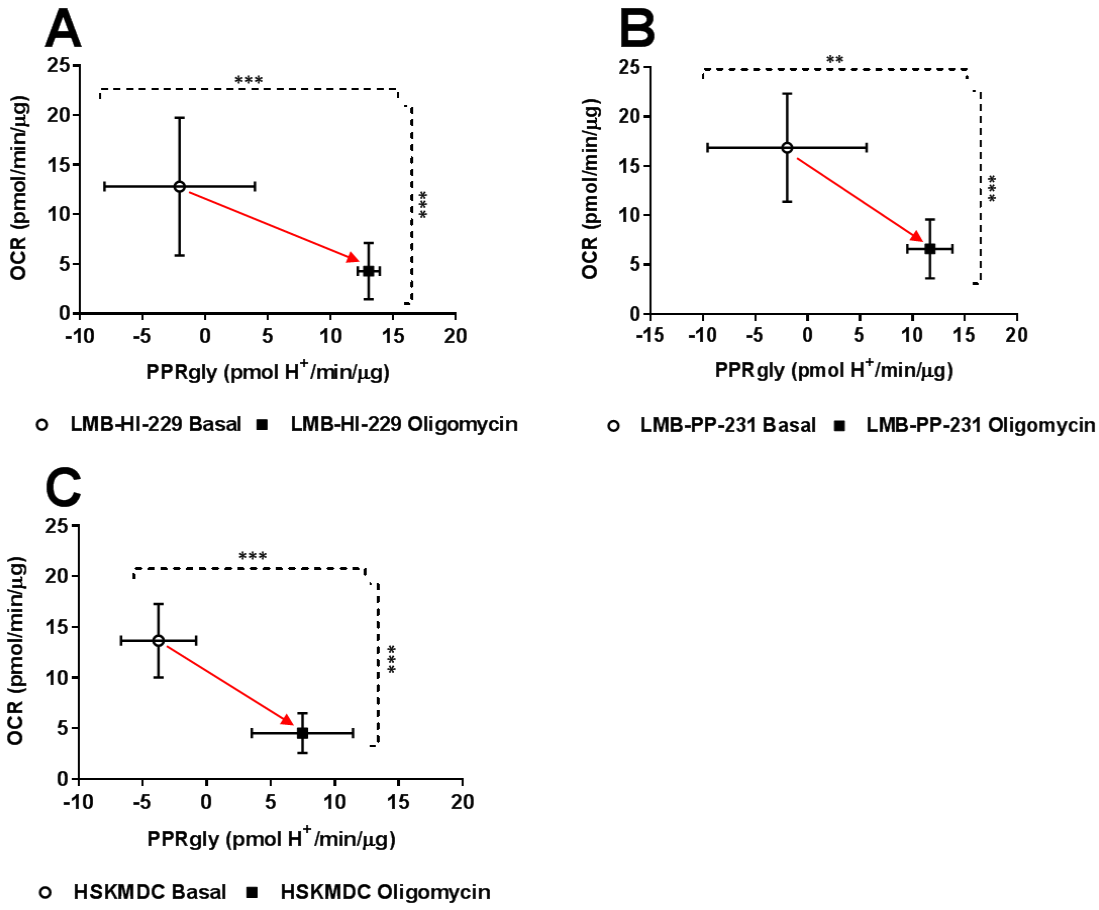

Figure 3.12 Bioenergetic phenograms for study participant myobundles **(A) LMB-HI-229, (B) LMB-PP-231, (C) HSKMDC** before treatment **(open circles)** and after acute application of oligomycin **(closed squares)**. Graphical values are displayed as mean ± S.D. (n=10). Statistical significance was determined by unpaired t-test with Welch's correction *p value < 0.05 **p value < 0.01 ***p value < 0.001.

3.3.10 Assessing Respiratory Parameters between Monolayers and Myobundles

Respiratory parameters were defined for each participant in monolayer alongside their myobundle counterparts. OCR values (pmol/min/µg) corresponding to basal respiration (BR), maximal respiratory capacity (MRC), proton leak (PL), ATP-linked respiration (ALR) and spare respiratory capacity (SRC) were calculated. Figure 3.13 depicts PL, ALR and SRC expressed as a proportion of the MRC (%) for each participant. A significant decrease in SRC for myobundles versus monolayers was observed in all cases (e.g. Figure 3.13 **(C)** HSKMDC myobundles SRC 17.72 ± 11.11 % versus HSKMDC monolayer SRC 72.54 ± 0.49 % p value <0.0001). In addition, both PL and ALR tended to occupy a greater proportion of the MRC for myobundles in comparison to monolayer.

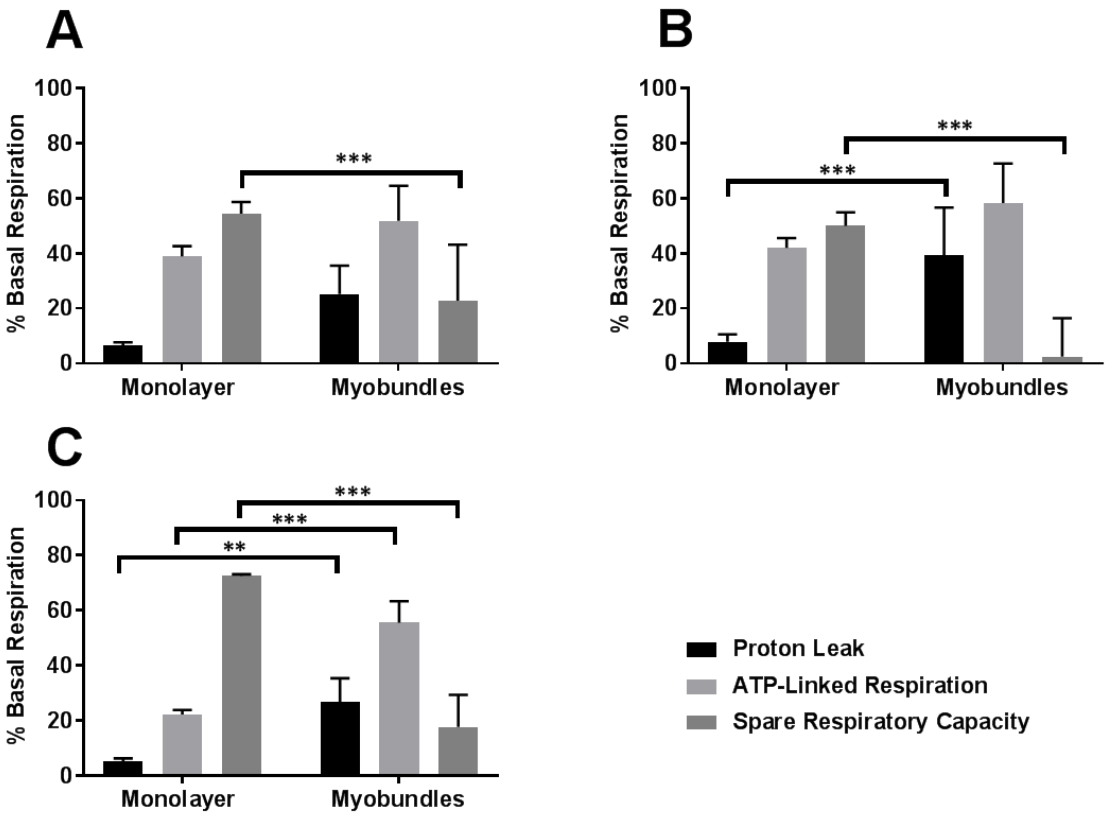

Figure 3.13 Comparison between respiratory parameters in monolayer and myobundles **(A) LMB-HI-229, (B) LMB-PP-231, (C) HSKMDC**, expressed as percentage of the maximal respiratory capacity. Graphical values are displayed as mean ± S.D. (n=3 monolayers, n=10 myobundles). Statistical significance between parameters was determined by unpaired t-test with Welch's correction *p value < 0.05 **p value < 0.01 ***p value < 0.001.

Figure 3.14 shows PL and ALR expressed as proportions of BR (%) for each participant. Myobundles exhibited a greater proportion of PL compared to that of their complimentary monolayers (LMB-HI-229 **(A)** 32.16 ± 7.46 %, LMB-PP-231 **(B)** 39.47 ± 13.98 % and HSKMDC **(C)** 32.11 ± 6.37 % respectively). Conversely, at baseline, monolayers dedicated more OCR to

ALR, implying a more efficient coupling of substrate oxidation (i.e. the proximal respiratory chain) to ATP synthesis than that observed with the myobundles.

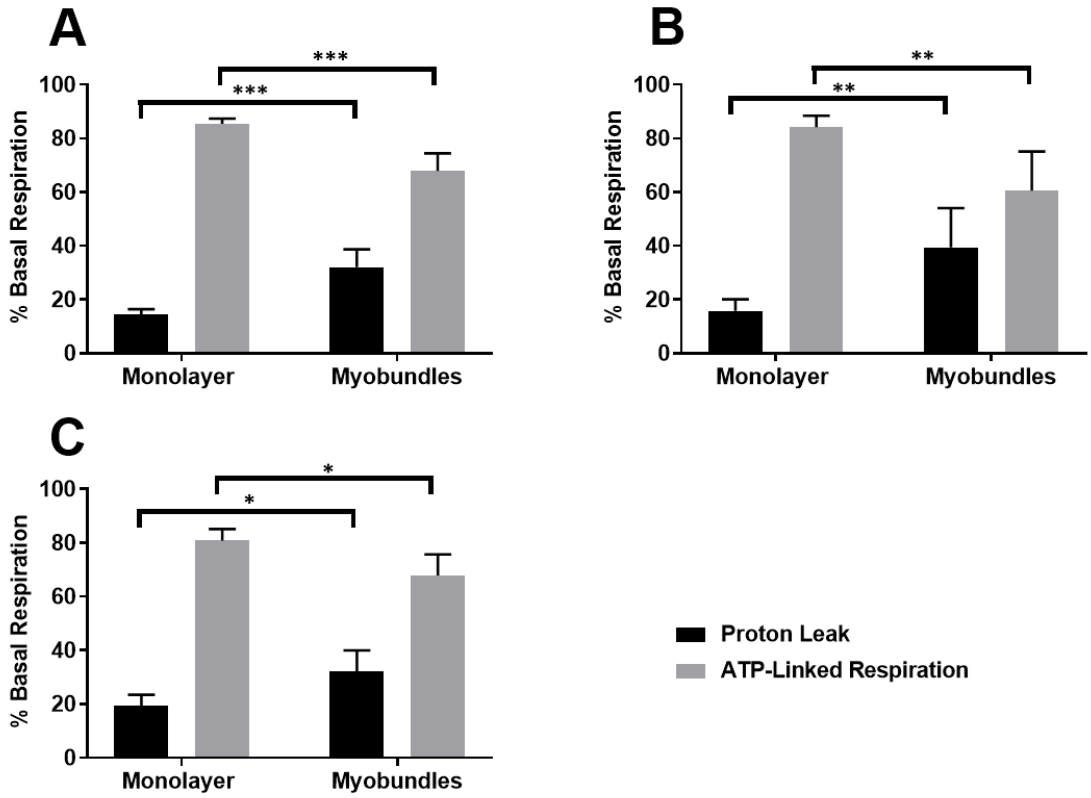

Figure 3.14 Comparison between respiratory parameters in monolayer and myobundles **(A)** LMB-HI-229**, (B)** LMB-PP-231 and **(C)** HSKMDC, expressed as a percentage of basal respiration. Graphical values are displayed as mean ± S.D. (n=3 monolayers, n=10 myobundles). Statistical significance between parameters was determined by unpaired t-test with Welch's correction *p value < 0.05 **p value < 0.01 ***p value < 0.001.

3.4 Discussion

The research described in this chapter aimed to validate a micro-physiological platform from which to measure drug-induced mitochondrial dysfunction in human skeletal muscle, with improved throughput compared to existing iterations of the model. Structural and cellular characterisation of the model showed conformity with previously published data, demonstrating that the smaller myobundles not only assumed the characteristic 'bowed' shape but also expressed key myogenic regulatory factors (MyoG) and mature structural proteins (SAA) upon serum reduction as expected (Madden *et al.*, 2015; Juhas and Bursac, 2014). Furthermore, the myobundles contained densely packed myofibers which aligned end-to-end with the Cerex® anchorage points and were surrounded at the periphery by vimentin positive fibroblasts. The presence of fibroblasts within the culture population has been reported to be pivotal for the synthesis of extracellular matrix proteins and promotion of overall myobundle integrity (Truskey, 2018). Longitudinal stability data demonstrated that the myobundle protein content did not significantly degrade over a 15 day culture period, however fluctuations in ATP content at day 10 may be explained, in part, by the changing energy demands associated with the exiting of myocytes from a state of proliferation to terminal differentiation (Davis *et al.*, 2017).

Preclinical compound screening for mitochondrial liabilities has been widely popularised due to the realisation that mitochondrial dysfunction was increasingly implicated in the aetiology of drug-induced liver injury (DILI). However, this situation can extend to other organ systems which are heavily reliant on oxidative metabolism for ATP production (Dykens and Will, 2007). Current mitochondrial toxicity screening platforms predominantly focus upon measuring alterations in the OCR or respiratory complex activities of cells grown in monoculture or in isolated mitochondria (Dott *et al.*, 2014; Hynes *et al.*, 2013; Nadanaciva *et al.*, 2007a). Whilst these methodologies have been successful in identifying compounds which possess mitochondrial liabilities, little work has been performed using micro-physiological models of skeletal muscle to date (Davis *et al.*, 2017).

Maintenance of myocytes in nutrient-limiting media has previously been proposed as a means to increase pressure for metabolic remodelling, specifically to increase basal OCR and to mediate oxidative fiber type transition *in vitro* owing to the glycolytic nature of myocytes kept under artificial culture conditions (Aguer *et al.*, 2011; Aas *et al.*, 2013; Kase *et al.*, 2013). This chapter presents the first study, to our knowledge, which utilises galactose metabolic manipulation specifically to assess compound-induced mitochondrial dysfunction in skeletal

myobundle constructs. Myobundles which had been acutely conditioned to galactose media displayed a significant reduction in ATP content, concomitantly with maintenance of LDH retention after acute (2 hours) exposure to the classic mitochondrial toxicant, rotenone. This confirmed that the myobundles were indeed capable of acute metabolic adaptation and responded appropriately when challenged with a compound that perturbed respiratory function. Furthermore, studies using primary myocytes have demonstrated their amenability to both propagation and differentiation in galactose media, this opens up the possibility of using myobundles cultured in galactose media for chronic dosing studies (Aguer *et al.*, 2011).

However, it must be noted that the HSKMDC myobundles displayed enhanced susceptibility to rotenone-mediated ATP depletion in galactose media (0.013 µM) compared to the biopsy derived myocytes (0.123 µM). One of the limitations associated with using commercially derived primary myocytes to generate myobundles is that the initial population must first be expanded to ensure sufficient cellular material for successive experiments. Consequently, the resultant cells will be of an advanced passage compared to those isolated 'in house' and may undergo phenotypic changes during the expansion phase. There is evidence to suggest that cells of an increased passage number exhibit altered mitochondrial dynamics, which in turn may confer greater susceptibility to compound-induced mitochondrial liabilities (Katajisto *et al.*, 2015). This may, in part, explain the enhanced sensitivity of the HSKMDC to rotenone. Therefore, it is of importance to use cells of the same passage number to eliminate the influence of mitochondrial aging or cellular senescence upon susceptibility to drug toxicity.

The research within this chapter aimed to define the bioenergetic profiles of primary myocytes grown in 2D vs 3D using XF analyser technology. Studies performed by Davies *et al*., first demonstrated that myobundles could be used to perform measurements of mitochondrial oxygen consumption polarographically using the Oxygraph-2k (O2k) system. It was highlighted that the myobundle model vastly improved upon the physiological relevance of the respirometry measurements being made due to enhanced *in vitro* complexity which, in turn, had profound effects upon the bioenergetic profile of the cells within the engineered constructs (Davis *et al.*, 2017). However, the O2k instrument does not have the capability to assess glycolytic flux and lacks the throughput of the plate-based XF assays, thus limiting its use for larger scale drug-screening efforts (TeSlaa and Teitell, 2014; Zhang *et al.*, 2012).

Therefore, to assess the utility of XF respirometry and gain further insight into the metabolic phenotype of the myobundles, bioenergetic parameters for OCR and PPR_{gly} were determined. At baseline, the pooled average OCR values were 2.2 times greater in the myobundles (14.43 ± 1.74 pmol/min/μg) than that of the monolayers (6.44 ± 0.30 pmol/min/μg). This is in contrast to the observations made by Davies *et al.*, who reported that baseline respiratory rates were 2.5 times higher in myocytes assayed in solution than in myobundles. However, it's important to note that measurement of oxygen consumption using Clark-type electrodes, such as the O2k, requires the removal of cells from their growth substrate and addition to a continuously stirred solution. In many adherent cell types, such as myocytes, this may result in anoikis, oxidative stress or altered oxygen consumption due to oscillatory shear, therefore the XF platform provides a physiologically more suitable environment from which to assess myocyte bioenergetics (Dranka *et al.*, 2011; Davis *et al.*, 2017). Interestingly, measurement of intrinsic NADH and FAD auto-fluorescence using label-free, non-linear optical molecular imaging (OMI) suggests that myotubes grown in 3D constructs may be more metabolically active than myotubes grown in 2D monoculture, thus supporting the data presented within this chapter (Syverud *et al.*, 2017).

In vitro myotube metabolism has been reported to be heavily reliant on glycolysis due to a combination of high glucose abundance in the culture medium and poor mitochondrial maturation (Aas *et al.*, 2013; Cheng *et al.*, 2014). Primary myotubes in monolayer exhibited higher baseline PPR_{gly}, which significantly increased upon challenge with the ATP synthase inhibitor oligomycin. Basal PPR_{gly} values were negative for the myobundles, representing no or extremely low background glycolytic activity, however myobundles demonstrated substantial PPR_{gly} reserve capacity when exposed to oligomycin. The lower baseline PPR_{gly} may be due to a change in cellular conformation from a 2D growth substrate to a 3D micro-tissue with enhanced maturation, cell-cell and cell-matrix interactions. Additionally, it has been noted that tissue-engineered skeletal muscle constructs predominantly express slow oxidative (type I) myosin heavy chain isoforms, which may support the oxidative metabolic phenotype of the myobundles (Cheng *et al.*, 2014; Martin *et al.*, 2013). Characterisation of the relative expression of MHC isoforms for each set of myobundles would, in part, address these assumptions (Vandenburgh *et al.*, 2008).

Bioenergetic parameters derived from mitochondrial interrogation on the XF instrument also showed that myobundles allocated a substantially lower proportion of their maximal respiratory capacity to SRC compared to their monolayer equivalents. This may be a by-

product of the mechanical stimulation associated with maintaining cells under passive tension on Cerex® frames. However, these observations were not in complete agreement with those made by Davies *et al.*, who stated that the maximal respiratory rates of their myobundles were more than double that of the basal respiratory rates. Whilst the SRC was not explicitly calculated, it can be inferred from their data that the myobundles had a substantial reserve capacity (Davis *et al.*, 2017). Alternatively, the differences observed between studies may be a result of donor specific variation in respiratory parameters due characteristics such as age, genetic background or environmental factors. In particular, the myobundles generated for this study were produced from participants of an advanced age (> 45 years). It has been suggested that various aspects of mitochondrial function decline with age in aerobically poised tissues such as skeletal muscle (Short *et al.*, 2005; Chabi *et al.*, 2008).

Proton leak and ATP-linked respiration were calculated as proportions of the basal metabolic rate. Both PL and ALR differed significantly between monolayer and myobundles. In myobundles, ALR made up a pooled average of 65.42 ± 3.45 % basal respiration whilst PL made up 34.58 ± 3.45 %. The higher proportion of leak respiration is in agreement with previous literature showing that basal leak can account for up to ~50 % of the basal metabolic rate of mammalian skeletal muscle at thermoneutrality (Rolfe *et al.*, 1999; Brand *et al.*, 1999; Jastroch *et al.*, 2010).

When considering the limitations of this work, the normalisation of myobundle XF data to total protein may not be the most suitable method due to the presence of artificially supplemented extracellular protein sources (i.e. fibrinogen, thrombin and matrigel). It is difficult to quantify the precise contributions of extracellular protein to the final readings, therefore the normalised OCR and PPR_{gly} values are likely to be greater than those stated. This impacts particularly upon direct comparisons between monolayer and myobundle respirometry data, especially when you consider the potential changes to the cellular proteomic profile promoted by growth within a 3D versus a 2D environment. However, previous studies performed using whole tissue sections or isolated fibers from biopsy have employed total protein normalisation as a mean for correcting skeletal muscle OCR values (Shintaku and Guttridge, 2016; Allard *et al.*, 2018).

Therefore, further work should endeavour to investigate standardised methodologies which can be used to normalise data generated from 3D cell constructs as these models become more common place in biomedical research, potentially by dissociating cells from the fibrin

construct using plasmin prior to protein quantification. Despite these potential limitations, this work represents significant advancement from the use of 2D monoculture to assess drug-induced mitochondrial dysfunction in skeletal muscle.

3.5 Conclusions

The work presented in this chapter has demonstrated the utility of the myobundle model as a novel, more physiologically relevant platform from which to assess drug-induced mitochondrial perturbations in skeletal muscle. The scaled down system, has allowed for the use of XF respirometry to assess the bioenergetic profiles of myobundles and improve throughput for the screening of muscle active-compounds. Whilst beyond the scope of this study, plasma membrane permeabiliser (PMP) could also be used to interrogate the activities of the mitochondrial respiratory complexes *in situ* by delivering complex-specific substrate mixtures to the myobundles (Divakaruni *et al.*, 2017). Furthermore, assessment of myobundle bioenergetic parameters enables a personalised approach to determining the effects of pharmaceuticals upon mitochondrial function. This may be a useful predictive tool to determine an individual's compatibility with prescribed medications to prevent adverse outcomes.

Chapter 4

Utilising Myobundles to Investigate Inter-individual Susceptibility to Statin-Induced Mitochondrial Dysfunction

Contents

4.1 Introduction 132

4.1.1 Summary of Chapter Aims 133

4.2 Materials and Methods 134

4.2.1 Materials 134

4.2.2 Satellite Cell Isolation and General Culture Maintenance 134

4.2.3 Fluorescent Imaging 135

4.2.4 Fabrication of Myobundles 136

4.2.5 Acute Metabolic Manipulation using Galactose Media 136

4.2.6 Combined Lactate Dehydrogenase (LDH) and ATP Assays 136

4.2.7 Extracellular Flux Analyser Assays (XF24) 137

4.2.8 Statistical Analysis 138

4.3 Results 139

4.3.1 Participant Characteristics 139

4.3.2 The Effect of Chronic Statin Application upon ATP Content and Viability 142

4.3.3 Functional Assessment of Patient Baseline Bioenergetic Parameters 143

4.3.4 The Effect of Atorvastatin upon Myobundle Bioenergetic Parameters 145

4.3.5 The Effect of Simvastatin upon Myobundle Bioenergetic Parameters 146

4.3.6 The Effect of Cerivastatin upon Myobundle Bioenergetic Parameters 147

4.4 Discussion 148

4.5 Conclusions 152

4.1 Introduction

The investigations detailed in the previous chapter have demonstrated the suitability of the myobundle model as a physiologically relevant platform from which to assess drug-induced mitochondrial perturbations in skeletal muscle. Furthermore, the application of the myobundle platform, using cells from specific patients or patient populations, presents an opportunity to identify functional deficits or underlying variation which may confer enhanced susceptibility to drug-mediated adverse events. This is especially relevant as inter-individual variation in response to drug treatment remains a significant clinical and public health burden, affecting both treatment efficacy and toxicity outcomes (Turner *et al.*, 2015).

Previous research has indicated that functional variation in mitochondrial respiratory parameters, as a downstream consequence of mitochondrial genome variation, can result in differential susceptibility to both complex diseases (Tanaka *et al.*, 2007; Bai *et al.*, 2007) and adverse drug reactions, as evidenced by trans-mitochondrial cybrid modelling (Canter *et al.*, 2010; Micheloud *et al.*, 2011; Kampira *et al.*, 2013). Due to the intimate link between oxidative metabolism and the physiological functioning of skeletal muscle *in vivo*, differences in baseline bioenergetic parameters between individuals may result in either enhanced resistance or susceptibility to compounds which are capable of disturbing muscular metabolic homeostasis. Proof-of-pharmacology modelling has demonstrated that simvastatin can induce subclinical mitochondrial perturbations in healthy volunteer groups with no prior metabolic defects (van Diemen *et al.*, 2017). Therefore, it could be postulated that patients with subclinical mitochondrial insufficiencies or conditions which are exacerbated by exercise are more likely to experience myopathic symptoms following statin therapy (Herbert *et al.*, 2018).

These inferences have been substantiated by Schirris *et al*., whereby muscle biopsy samples taken from symptomatic patients showed a significant decrease in respiratory complex III enzyme activity accompanied with a decrease in mitochondrial ATP production. Furthermore, there was a correlation observed between complex III activity and symptomatic severity, with patients presenting proximal weakness exhibiting the smallest reduction in CIII activity and those with rhabdomyolysis displaying the greatest (Schirris *et al.*, 2015). Although, it could be argued that reductions in CIII activity may have been, to a certain extent, due to pre-operative statin exposure rather than underlying susceptibility specifically.

Therefore, this chapter aimed to conduct a pilot study to investigate patient susceptibility to statin-mediated mitochondrial dysfunction by taking skeletal muscle samples from statin-naïve and statin tolerant control groups alongside statin-intolerance cases. Isolated proliferative myocytes derived from the tissue samples will be used to generate myobundles from which baseline respiratory measures will be made in the absence of any compounds. Lastly, the study will investigate the effects of chronic statin treatment (atorvastatin, simvastatin and cerivastatin) upon ATP content and cell viability in galactose media concomitantly with assessments of respiratory function on the XF24 instrument.

4.1.1 Summary of Chapter Aims

1) To conduct a pilot study to determine whether differences exist in baseline mitochondrial function between myobundles produced from statin-intolerant, statin-tolerant and statin-naïve patients.
2) To determine if there is differential susceptibility to statin-induced mitochondrial dysfunction between the three patient groups.

4.2 Materials and methods

4.2.1 Materials

4.2.1.1 Human Skeletal Muscle Samples

A total of five statin-naïve, five statin-tolerant and two statin-intolerant participants were recruited to the study. Surgical waste tissue (500mg-2g) was obtained from either the quadriceps femoris or gluteal muscles of participants whilst they underwent orthopaedic surgeries at the Royal Liverpool and Broadgreen University Hospital NHS Trust (RLBUHT). Tissue samples were collected by the Liverpool Musculoskeletal Biobank (LMB) in accordance with LMB approved standard operating procedures (SOPs) and covered by LMB study sponsorship (UoL001361) and ethical approval (Ref 15/NW/0661). All participants gave written informed consent. Further details of inclusion/exclusion criteria are outlined in the LMB study sponsorship protocol (Appendix I).

4.2.1.2 Reagents

All forms of DMEM, media supplements, Hoechst Fluoropure™ and AlexaFluor® conjugated secondary antibodies were purchased from Life technologies (Paisley, UK). Matrigel and growth factor reduced (GFR) matrigel were purchased from Corning GmBH (Wiesbaden, Germany). Epidermal growth factor (10 μg/mL) was purchased from PeproTech (London, UK). Anti-desmin and anti-vimentin antibodies were purchased from Abcam (Cambridge, UK). Lactate dehydrogenase cytotoxicity detection kit was purchased from Roche Diagnostics Ltd (West Sussex, UK). Extracellular flux analyser (XF24) consumables and base medium were purchased from Agilent Technologies (CA, USA). All other reagents and chemicals were purchased from Sigma Aldrich (Dorset, UK) unless otherwise stated.

4.2.1.3 Specialist Equipment

Precision milled polytetrafluoroethylene (PTFE) masters for the casting of polydimethylsiloxane (PDMS) moulds and laser cut Cerex® frames were kindly provided by Dr George Truskey, Department of Biomedical Engineering, Duke University, North Carolina. Dow Corning Sylgard 184 PDMS kit was obtained from Ellsworth Adhesives Limited (East Kilbride, Scotland).

4.2.2 Satellite Cell Isolation and General Culture Maintenance

Satellite cells were isolated from surgical waste tissue and expanded by outgrowth as described in Chapter 3 (section 3.2.2) using methods similar to those described by Blau and Webster with amendments (Blau and Webster, 1981; Madden *et al.*, 2015).

Briefly, tissue samples were collected, washed and dissected before enzymatic digestion in 0.05 % trypsin-EDTA (37 °C) for 30 minutes. Digested tissue fragments were pre-plated for two hours to dispose of remnant dermal fibroblasts prior to transfer to GFR-matrigel coated flasks (5 µL/mL). Myocyte populations were observed daily and expanded by outgrowth over a two week period. Bulk stocks were frozen using a standard cryopreservation mix which consisted of complete growth medium supplemented with 10% (v/v) DMSO at passage 3 ($1x10^6$ cells/mL).

Isolated myocytes were routinely maintained in complete growth media containing physiological glucose (5 mM) DMEM with sodium pyruvate and L-glutamine, supplemented with 8 % (v/v) FBS, 0.4 µg/mL dexamethasone, 10 ng/mL epidermal growth factor, 50 µg/mL fetuin, 0.1 % (v/v) gentamycin and amphotericin B. Cells were kept in vented T75 flasks coated in GFR-matrigel and incubated in a humidified environment (37 °C with 5 % (v/v) CO_2), media changes were performed every 48 hours. All stock cultures were maintained at sub-60% confluence and used at passage 4.

4.2.3 Fluorescent Imaging

Isolated myocytes were seeded on top of GFR-matrigel (5 µL/mL) coated 13 mm coverslips in 24 well plates at a density of 4500 cells/well. Cells were allowed to adhere and proliferate for 2-3 days before processing. The cells were rinsed with 1X PBS (-/-) before being fixed with cold methanol for 5 minutes. Samples were then incubated with permeabilisation buffer (1X PBS (-/-) with 0.2 % (v/v) Tween-20 and 0.5 % (v/v) Triton-X) for 30 minutes at 4 °C and blocked with 5 % (w/v) BSA reconstituted in permeabilisation buffer for a further 30 minutes at room temperature.

Primary antibodies, rabbit anti-desmin (1:100) and mouse anti-vimentin (1:200) were diluted in 5 % (w/v) BSA permeabilisation buffer and incubated with the samples overnight at 4 °C. After thoroughly washing, appropriate Alexa Fluor® conjugated secondary antibodies (488 nm /568 nm) were diluted 1:1000 and co-incubated with Hoechst dye (1:5000) for 2 hours, in the dark at room temperature.

Samples were mounted onto glass slides for imaging. 10 µL Pro-Long Gold anti-fade reagent was added to each of the samples before sealing and allowing to dry overnight at 4 °C. All images were captured using a Zeiss Axio Observer.Z1 (apotome) widefield florescent microscope and processed with Zen Blue software.

4.2.4 Fabrication of Myobundles

Myobundles were produced from each donor using methods described fully in Chapter 3 (section 3.2.5). Briefly, a cell solution ($1x10^5$ myocytes in 3.35 µL growth media per myobundle with 0.4 µL of 50 unit/ mL thrombin (reconstituted in 1X PBS supplemented with 0.1 % fatty acid free BSA) and a hydrogel solution (0.75 µL growth medium, 1.5 µL fibrinogen (25 mg/mL) and 1.5 µL matrigel) were prepared in separate vials on ice for up to four myobundles per vial. The two solutions were combined and pipetted vigorously on ice to mix. 7.5 µL of the resultant cell/hydrogel mixture were individually pipetted into PDMS moulds, ensuring end-to-end contact with the Cerex® frames before polymerisation at 37 °C for 25 minutes. Myobundles were maintained in complete growth media supplemented with 1.5 mg/mL ACA for 5 days before being shifted out of their moulds and incubated in differentiation media supplemented with 2 mg/mL ACA for a further 5 days in dynamic suspension (37 °C, 5 % (v/v) CO_2).

4.2.5 Acute Metabolic Manipulation using Galactose Media

Myobundles were washed three times in glucose free DMEM supplemented with 10 mM galactose, 6 mM L-glutamine, 1 mM sodium pyruvate, 5 mM HEPES, 10 nM human insulin, 0.1 % gentamycin and amphotericin B, 2 % horse serum and 2 mg/mL ACA. Myobundles were then pre-incubated in galactose media (50 µL) for 2 hours (37 °C, 5 % (v/v) CO_2) to induced metabolic adaptation.

Stock solutions for atorvastatin acid (AVA), cerivastatin acid (CVA) and simvastatin lactone (SVL) were prepared in DMSO and diluted in galactose assay media to produce final well concentrations of 0.5 µM. Diluted stock compounds were then added to each respective well (50 µL) for a final well volume of 100 µL. The solvent concentration for all conditions was 0.5 % DMSO. Myobundles were incubated with compounds for a total of 120 hours in dynamic suspension (37 °C, 5 % (v/v) CO_2), the dosing medium was refreshed every 24 hours.

4.2.6 Combined Lactate Dehydrogenase (LDH) and ATP assays

Myobundles conditioned to galactose media were incubated with their respective drug solutions for 120 hours. Supernatant samples were collected at each 24 hour time point and myobundles were sonicated in 100 µL of somatic cell ATP releasing agent at the end of the 120 hour period. ATP content, cell viability and protein content were simultaneously assessed.

4.2.6.1 ATP Assay

Quantitative determination of ATP content was assessed by the addition of lysates (5 µL) and ATP standards to a white-walled 96-well plate. ATP reaction solution was prepared according to manufacturer's instructions by mixing ATP assay mix with ATP dilution buffer in a 1:25 ratio. 40 µL of the reaction solution was added to both samples and standards then read immediately on a Varioskan™ Flash multimode plate reader with SkanIt™ software to capture the peak luminescent signal.

4.2.6.2 LDH Assay

Detection of cytotoxicity was achieved using a colorimetric LDH assay kit. LDH retention was determined by extracting 25 µL supernatant at each 24 hour time point and 10 µL lysate for each sample and incubating them with 50 µL LDH catalyst-dye solution (1:45 ratio), according to manufacturer's instructions. After 30 minutes incubation in the dark, samples were read at 490 nm on a Varioskan Flash multimode plate reader. LDH retention was determined as:

$$\textbf{LDH Retention} = \frac{\textbf{Lysate}}{(\textbf{Supernatant} + \textbf{Lysate})}$$

4.2.6.3 BCA Assay

In order to correct for potential variance in cell number, the BCA assay was used to normalise ATP assay results. Quantification of protein content was determined using 10 µL lysate and protein standards. The BCA reagent was prepared according to manufacturer's instructions by mixing bicinchoninic acid with copper (II) sulphate in a ratio of 50:1. Assay products were read at 562 nm after 30 minutes incubation at 37 °C.

4.2.7 Extracellular Flux Analyser Assays (XF24)

Myobundles were fabricated and differentiated as described in section 4.2.4, baseline metabolic parameters were determined for each donor in the absence of any compounds in accordance with Chapter 3 (section 3.2.10). In addition, myobundles produced from each donor were treated with a panel of statins. Stock solutions for AVA, CVA and SVL were prepared in DMSO and diluted in differentiation medium supplemented with 2 mg/mL ACA to produce a final concentration of 0.5 µM. Diluted compounds were added to their respective wells (100 µL). The solvent concentration for all conditions was 0.5 % DMSO. Myobundles were incubated with compounds for a total of 120 hours in dynamic suspension (37 °C, 5 % (v/v) CO_2), the dosing medium was refreshed every 24 hours. On the day of the assay, myobundles were moved to XF24 cell culture microplates coated with neat GFR-

matrigel and orientated horizontally within the wells to align with the XF24 sensor cartridge probes.

Following the completion of XF assays, myobundles were pulse sonicated (10s) in 100 µL somatic cell ATP releasing agent. Lysates (10 µL) were transferred to a 96-well plate for quantification of protein content by BCA assay. Protein content per myobundle was used as a means to normalise raw OCR and ECAR data.

4.2.7.1 Mitochondrial Stress Test

Myobundles were incubated for 1 hour (37 °C, 0 % CO_2) prior to the start of the assay. Culture medium was replaced with 450 µL unbuffered XF base medium supplemented with glucose (25 mM), L-glutamine (2 mM), sodium pyruvate 1 mM) and pre-warmed to 37 °C (pH 7.4).

4.2.7.1.1 Stress Test Compound Preparation

Stock mitochondrial stress test compounds were prepared and loaded into XF sensor cartridges in accordance with Table 4.1. Optimal stress test compound concentrations were determined empirically.

Table 4.1 Mitochondrial stress test injection port locations, compound stock concentrations, dilution factors and final well concentrations for the XF24.

Injection Port	Compound	Port Dilution Factor	Final well concentration	Port Loading Volume
A	Oligomycin	10	10 µM	50 µL
B	FCCP	10	6 µM	55 µL
C	FCCP	10	4 µM	62 µL
D	Rotenone/Antimycin A	10	10 µM	68 µL

Each run included a pre-programmed calibration, an equilibration step and 3 cycles of mix/measure/wait (3 mins/3 mins/0 mins) to establish a baseline OCR/ECAR rate prior to the injection of any compounds. Following this, a stress test was performed via the sequential injection of mitochondrial toxicants. This enabled the calculation of basal respiration, maximal respiratory capacity, ATP-linked respiration, proton leak and spare respiratory capacity.

4.2.8 Statistical Analysis

Data are representative of at least three myobundles (n=3) per donor for each condition. All values are expressed as mean ± standard deviation (S.D.). Statistical analyses were performed using GraphPad Prism® 7 software (GraphPad Software, Inc, CA, USA).

4.3 Results

4.3.1 Participant Characteristics

A summary of patient characteristics are presented in Table 4.2. A total of 12 patients were recruited to the study, with an even distribution of male and female participants. The majority of participants (83.3 %) were of a white British ethnic background with the remainder being of African (8.35 %) or Caribbean (8.35 %) descent respectively. There were no significant differences in the mean age, height, weight or BMI between the study groups (naïve, tolerant and intolerant). Patients within the statin intolerant group were classified as SRM 1, tolerable myalgia without CK elevation, in line with the Phenotype Standardization for Statin-Induced Myotoxicity definitions (Alfirevic *et al.*, 2014). In both cases, statin treatment had been withdrawn, however one participant was still experiencing muscle pain at the time of sampling. None of the participants recruited to the study had any prior history of diabetes or known underlying metabolic disorders, with the exception of one statin intolerant donor who suffered from hypothyroidism.

Table 4.2 Summary of study participant characteristics**.** Statistical significance was determined by one-way ANOVA with Dunnett's test for multiple comparisons.

	Statin Naïve (n=5)	**Statin Tolerant (n=5)**	**Statin Intolerant (n=2)**
Gender			
Male	4	2	0
Female	1	3	2
Ethnicity			
White British	3	5	2
African	1	-	-
Caribbean	1	-	-
Age (y), mean ± S.D.	67.2 ± 12.75 (NS)	71.8 ± 4.26 (NS)	64.5 ± 8.50 (NS)
Height (m), mean ± S.D.	1.708 ± 0.06 (NS)	1.634 ± 0.09 (NS)	1.585 ± 0.065 (NS)
Weight (kg), mean ± S.D.	80.54 ± 13.31 (NS)	80.66 ± 6.18 (NS)	81.65 ± 14.35 (NS)
BMI (kg/m^2), mean ± S.D.	27.65 ± 4.62 (NS)	30.49 ± 4.12 (NS)	32.19 ± 3.06 (NS)
Statins			
Atorvastatin	-	3	1
Simvastatin	-	2	1
Dose (mg/d)			
20	-	4	1[a]
40	-	-	2
80	-	1	-

SRM Classification[b]			
SRM 1[c]	-	-	2
Exercise Intolerance			
Yes	-	-	-
No	-	-	2
Statin Withdrawal	-	-	2
Symptom Resolution			
Yes	-	-	1
No	-	-	1
Smoking Status			
Non-Smoker	4	3	1
Current	-	-	1
Previous	1	2	-
Alcohol (Units/Week)			
<1	2	2	1
1-5	2	1	-
6-14	1	-	1
22-49	-	2	-
Co-medication			
Antihypertensives[d]	2	5	1
Analgesics	2	2	1
Proton Pump Inhibitors	2	5	1
Laxatives	-	3	-
Antihistamines	1	-	-
Vertigo Medication	1	-	-
NSAIDS	2	3	1
Antidepressants	-	2	-
Nutritional Supplements	1	1	1
Antimuscarinics	-	1	-
Corticosteroids	-	1	-
β_2 adrenergic agonists	-	1	-
Anti-gout	-	1	-
Hormone Replacement	-	-	1
Anti-malarial	-	-	1
Steroid Medication	-	-	1
Hypothyroidism Medication	-	-	1
Biopsy Location			
Quadriceps Femoris	3	3	2
Gluteal Muscles	2	2	0

[a] Statin dosage was dropped from 40 mg/day to 20 mg/day. [b] SRM definitions are in line with Phenotype Standardization for Statin-Induced Myotoxicity (Alfirevic *et al.*, 2014). [c] SRM 1 is defined as tolerable myalgia without creatine kinase (CK) elevation. [d] Composite drug class including angiotensin converting enzyme (ACE) inhibitors, angiotensin receptor blockers, beta blockers, calcium channel blockers, diuretics and vitamin K antagonists. Abbreviations: NS, not significant; SRM, statin-related myopathy; NSAIDS, nonsteroidal anti-inflammatory drugs.

In addition, the proportion of myocytes and fibroblasts isolated from the tissue samples of each participant were determined by fluorescent imaging to ensure that there was an enriched myocyte population for the generation of myobundles (Table 4.3).

Table 4.3 Proportion of myocytes and fibroblasts present in cultures isolated from each participant at passage 3. Four random images per slide were taken for each slide (n=4). Average counts were performed using ImageJ 1.48 software.

Patient Group	Participant ID	Vimentin only (%)	Desmin & vimentin (%)
Statin Naïve	LMB-HI-229	10.8	89.2
	LMB-PP-231	4.4	95.6
	LMB-JB-232	7.6	92.4
	LMB-TA-237	4.1	95.9
	LMB-MH-241	3.7	96.3
Statin Tolerant	LMB-JB-228	2.4	97.6
	LMB-GD-230	8.4	91.6
	LMB-DJ- 233	6.9	93.1
	LMB-DR-234	38.4	61.6
	LMB-AS-236	3.9	96.1
Statin Intolerant	LMB-RS-238	1.5	98.5
	LMB-BM-239	4.5	95.5

4.3.2 The Effect of Chronic Statin Application upon ATP Content and Viability

Patient derived myobundles conditioned to galactose media were exposed to a panel of statins for 120 hours (Figure 4.1). Exposure to atorvastatin and cerivastatin caused a significant decrease in ATP content and LDH retention in each patient group when compared with their respective vehicle controls. However, there were no significant differences between the patient groups in either of the tested parameters, an observation which was consistent across each of the statins. The statin tolerant group tended to remain marginally, albeit non-significantly, more viable than the naïve and the intolerant groups when challenged with equimolar concentrations of atorvastatin and cerivastatin. Interestingly within the statin intolerant group, ATP depletion appeared to precede loss of LDH retention, a trend which was more pronounced in the presence of cerivastatin (46.5 % LDHgal vs 25.5 % ATPgal) (Figure 4.1 **(C)**).

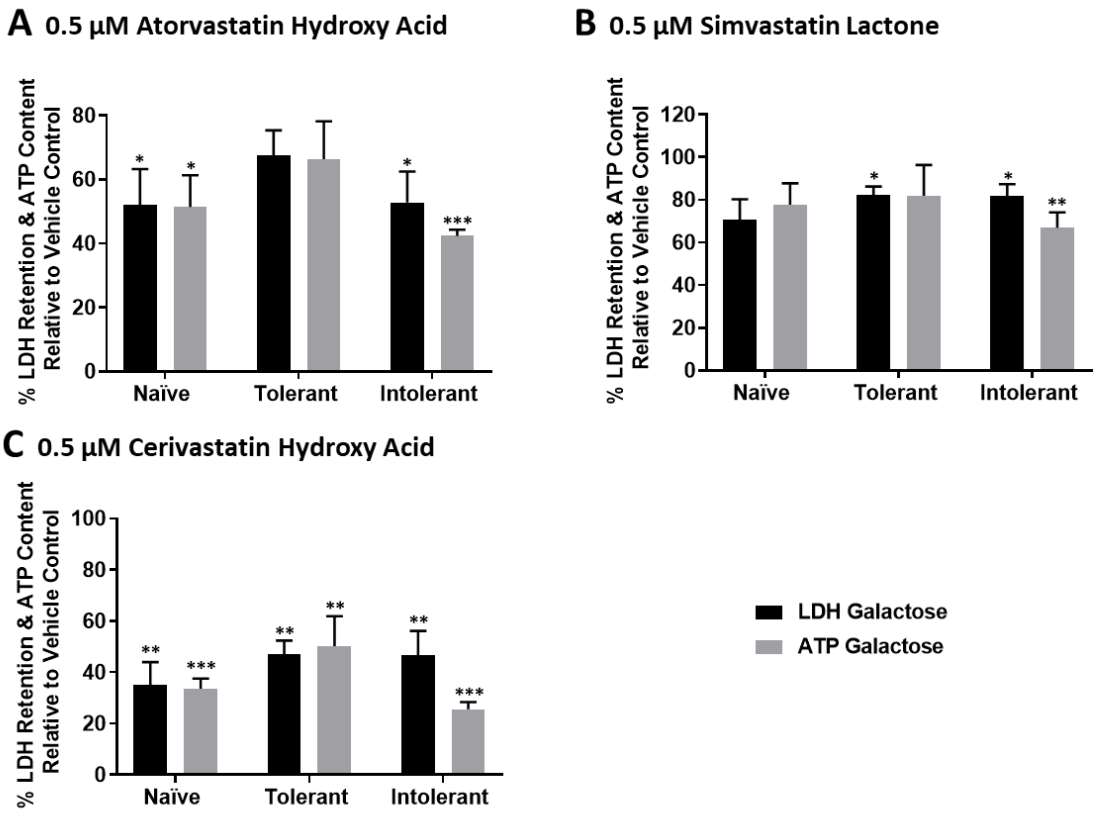

Figure 4.1 Examining the effect of chronic statin exposure upon ATP content and LDH retention in patient derived myobundles (120 hours) compared with the vehicle control in galactose media. **(A)** 0.5 µM atorvastatin hydroxy acid, **(B)** 0.5 µM simvastatin lactone and **(C)** 0.5 µM cerivastatin hydroxy acid. Results are expressed as a percentage of the vehicle control and graphical values are displayed as mean ± S.D. (n=4 myobundles per condition, per donor). Statistical significance between patient groups was determined by two-way ANOVA with Dunnett's test for multiple comparisons or t-test with Welch's correction to compare within groups back to the vehicle control (on top of bars) *p value < 0.05 **p value < 0.01 ***p value < 0.001.

4.3.3 Functional Assessment of Patient Baseline Bioenergetic Parameters

Assessment of baseline mitochondrial respiratory function using extracellular flux analysis and a mitochondrial stress test showed no significant differences between the myobundles of statin naïve, statin tolerant or statin intolerant patients in multiple bioenergetic parameters (Figure 4.2 **(A-F)**). However, the statin tolerant patients appeared to dedicate a significantly greater proportion of their maximal respiratory capacity to spare respiratory capacity when compared to the statin naïve and statin intolerant groups (23.73 % and 25.17 % difference respectively) (Figure 4.2 **(G)**). No such differences were observed for proton leak or ATP-linked respiration as proportions of maximal respiratory capacity or basal respiration (Figure 4.2 **(G-H)**).

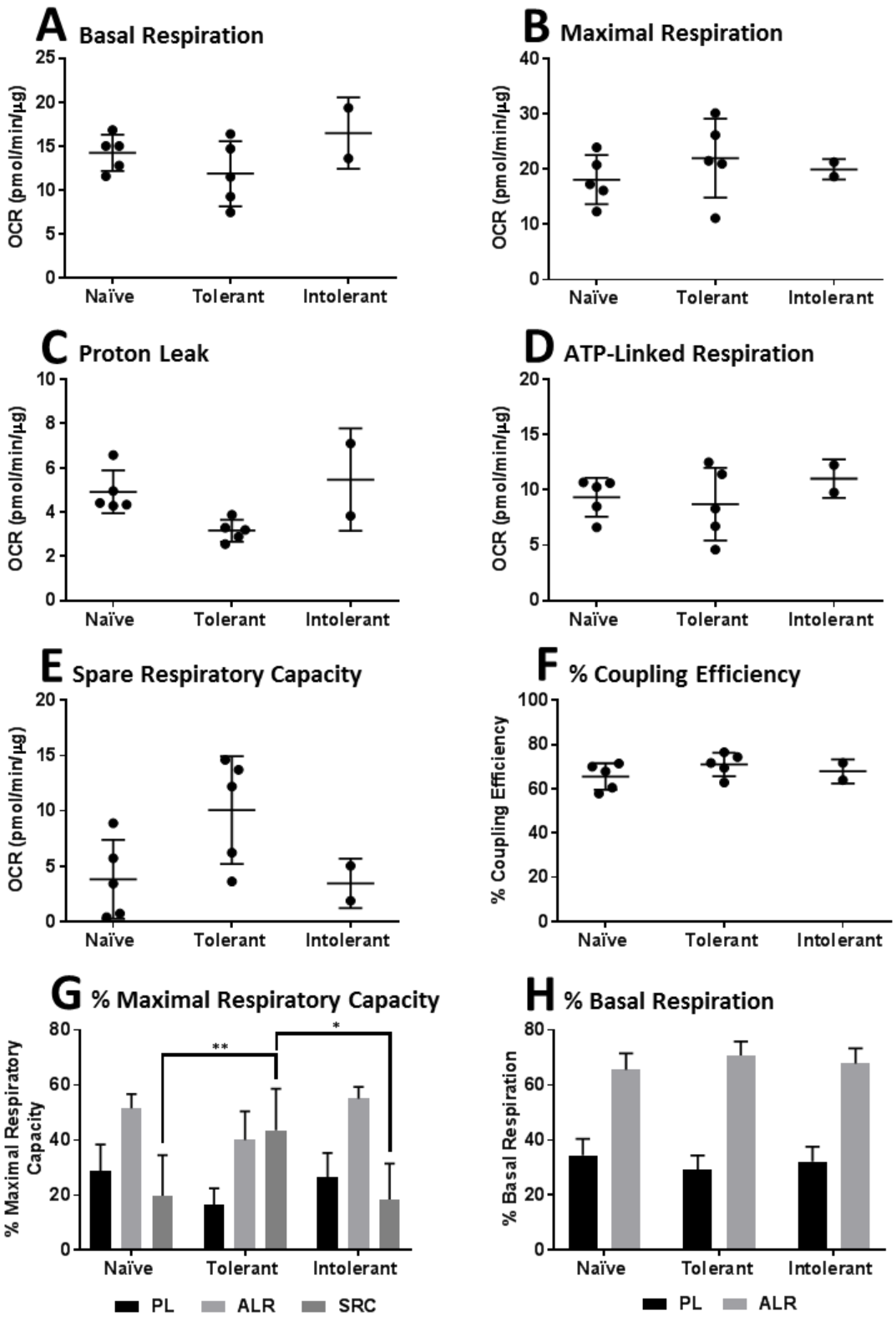

Figure 4.2 Untreated myobundles produced from the primary myocytes of statin naïve, statin tolerant and statin intolerant patients were assessed using a XF24 analyser and a mitochondrial stress test to determine: basal respiration **(A)**, maximal respiration **(B)**, proton leak **(C)**, ATP-linked respiration **(D)**, spare respiratory capacity **(E)** and % coupling efficiency **(F)**. Respiratory parameters expressed as a proportion of maximal respiratory capacity **(G)**, parameters expressed as a proportion of basal respiration **(H)**. All values are displayed as mean ± S.D. (minimum of n=5 myobundles per donor). Statistical significance was determined by one-way ANOVA with Dunnett's test for multiple comparisons *p value < 0.05 **p value < 0.01 ***p value < 0.001.

4.3.4 The Effect of Atorvastatin upon Myobundle Bioenergetic Parameters

Assessment of the respiratory integrity of patient derived myobundles was performed using XF analysis after atorvastatin exposure (Figure 4.3). There were no significant differences between the patient groups in any of the tested metabolic parameters in control or atorvastatin treated myobundles, however the statin intolerant group were the most sensitive to atorvastatin exposure.

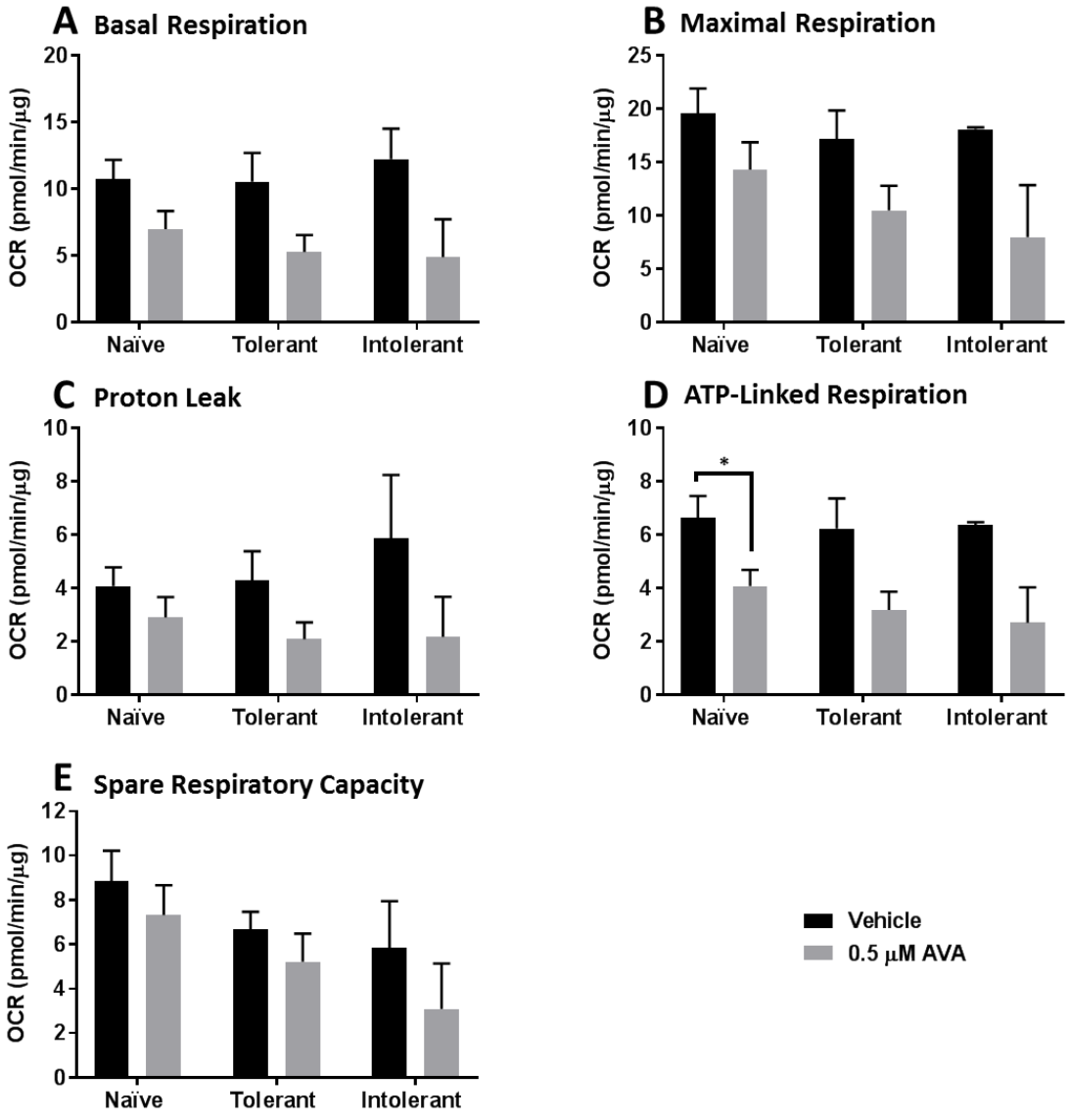

Figure 4.3 Examining the effect of chronic atorvastatin exposure upon mitochondrial function in patient derived myobundles (120 hours) compared with vehicle. **(A)** basal respiration, **(B)** maximal respiration, **(C)** proton leak, **(D)** ATP-linked respiration and **(E)** spare respiratory capacity. Graphical values are displayed as mean ± S.D. (n=5 myobundles per condition, per donor). Statistical significance was determined between patient groups by one-way ANOVA with Dunnett's test for multiple comparisons or unpaired t-test with Welch's correction within groups *p value < 0.05 **p value < 0.01 ***p value < 0.001. Abbreviations: AVA, atorvastatin hydroxy acid.

Although atorvastatin caused a ubiquitous decrease in OCR values for each metabolic parameter when compared back to the respective group controls, this only reached

statistical significance for ATP-linked respiration in the statin-naïve myobundles (Figure 4.3 **(D)**).

4.3.5 The Effect of Simvastatin upon Myobundle Bioenergetic Parameters

Parameters assessed during XF analysis did not significantly differ between the three patient groups in response to simvastatin exposure (Figure 4.4). Similarly, there were no significant differences observed between control and simvastatin treated myobundles within each of the groups despite marginal reductions in OCR values.

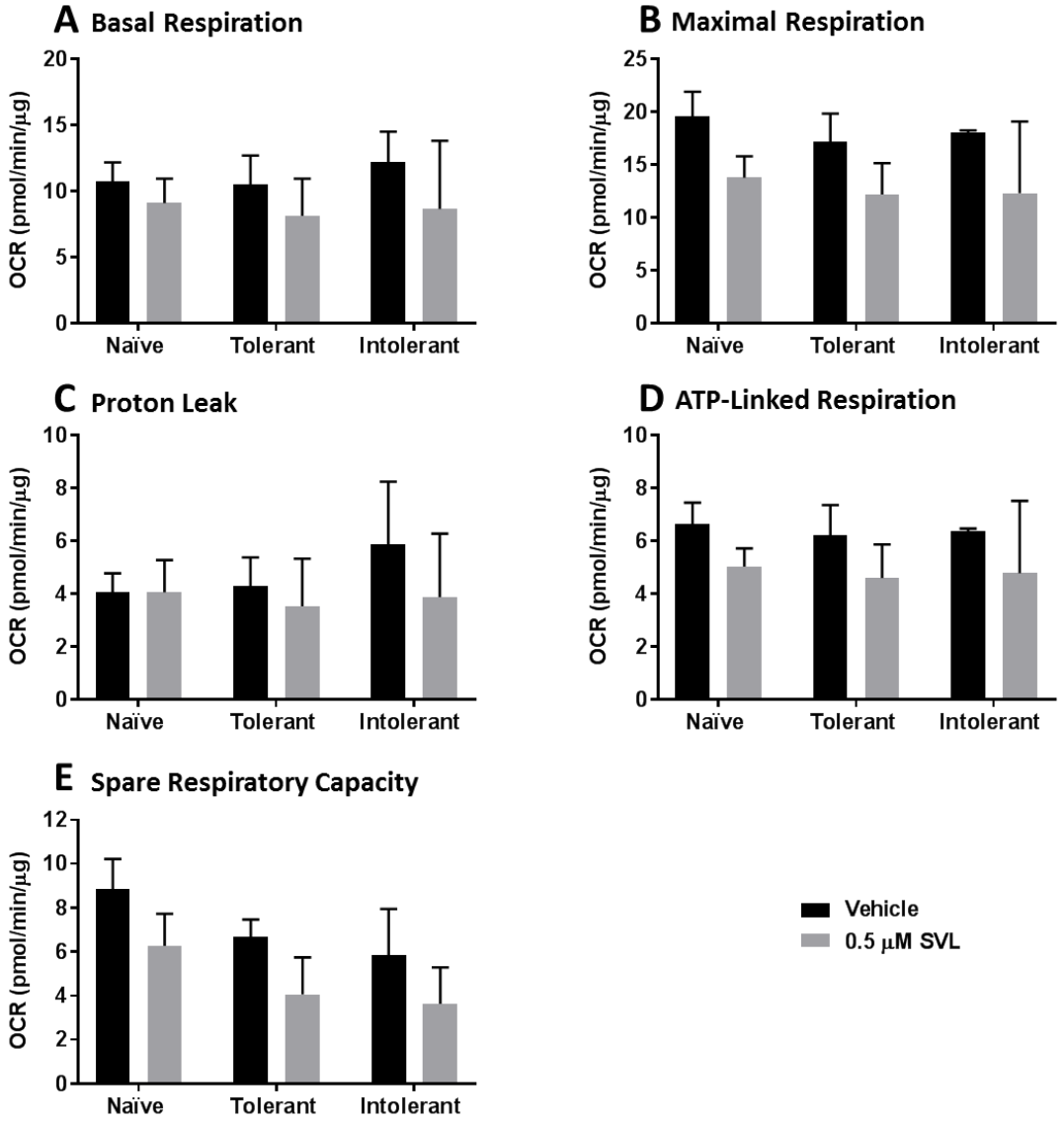

Figure 4.4 Examining the effect of chronic simvastatin exposure upon mitochondrial function in patient derived myobundles (120 hours) compared with vehicle control. **(A)** basal respiration, **(B)** maximal respiration, **(C)** proton leak, **(D)** ATP-linked respiration and **(E)** spare respiratory capacity. Graphical values are displayed as mean ± S.D. (n=5 myobundles per condition, per donor). Statistical significance was determined between patient groups by one-way ANOVA with Dunnett's test for multiple comparisons or unpaired t-test with Welch's correction within groups. Abbreviations: SVL, simvastatin lactone.

4.3.6 The Effect of Cerivastatin upon Myobundle Bioenergetic Parameters

Cerivastatin treated myobundles from each patient group exhibited a decline in bioenergetic function when compared with their controls, an effect which was particularly prominent within basal and ATP-linked respiration (Figure 4.5 **(A-D)**). There was no significant difference in spare respiratory capacity compared with control for any group (Figure 4.5 **(E)**).

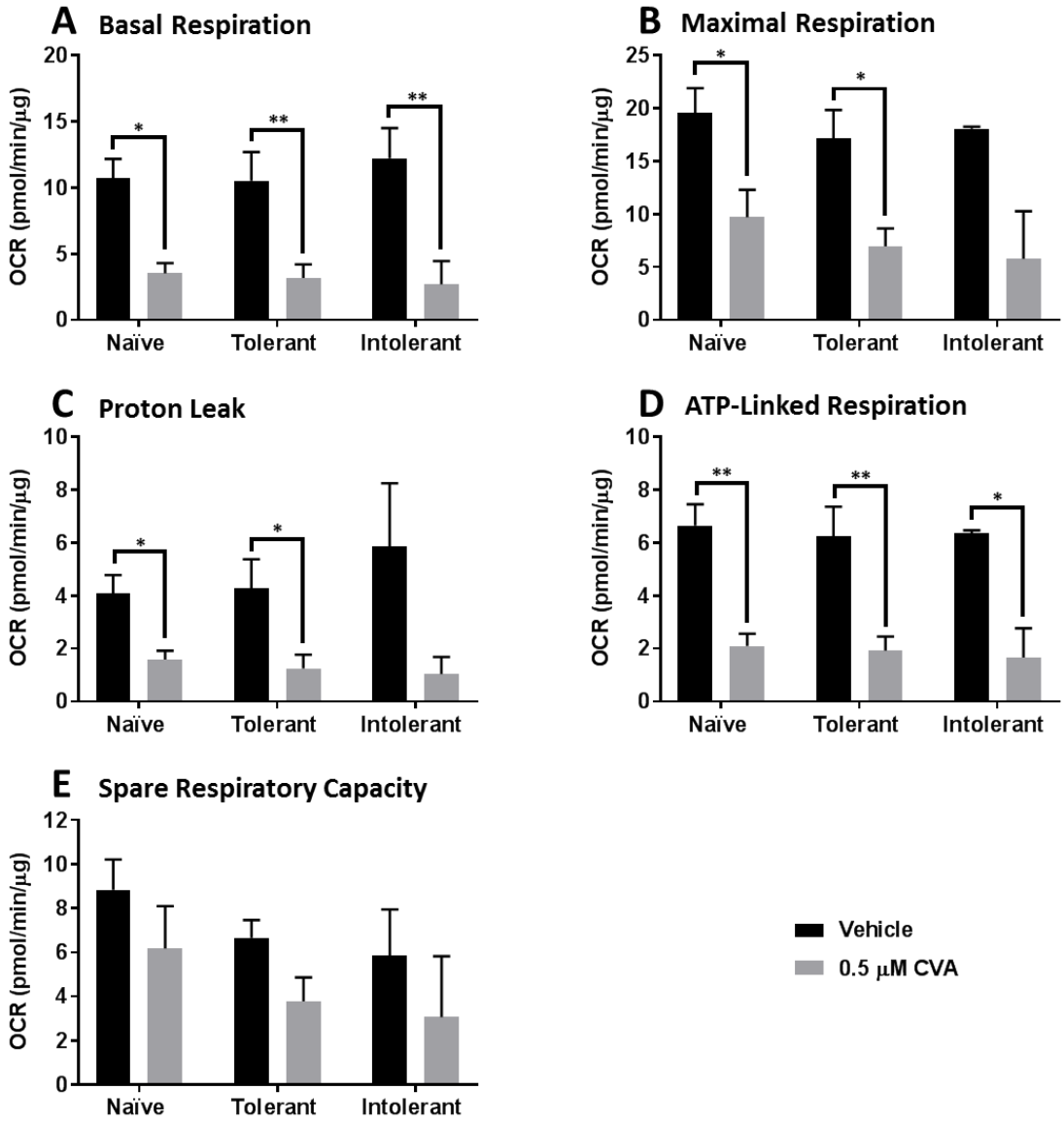

Figure 4.5 Examining the effect of chronic cerivastatin exposure upon mitochondrial function in patient derived myobundles (120 hours) compared with vehicle control. **(A)** basal respiration, **(B)** maximal respiration, **(C)** proton leak, **(D)** ATP-linked respiration and **(E)** spare respiratory capacity. Graphical values are displayed as mean ± S.D. (n=5 myobundles per condition, per donor). Statistical significance was determined between patient groups by one-way ANOVA with Dunnett's test for multiple comparisons or unpaired t-test with Welch's correction within groups *p value < 0.05 **p value < 0.01 ***p value < 0.001. Abbreviations: CVA, cerivastatin hydroxy acid.

Despite the obvious effect of cerivastatin upon respiratory function, there was no statistically significant differential toxicity observed between the three patient groups in any of the assessed parameters.

4.4 Discussion

The aim of this chapter was to generate myobundles, a biomimetic skeletal micro-tissue model, using myocytes derived from five statin naïve, five statin tolerant and two statin intolerant patients using methods described in chapter 3. As previous literature had indicated a role for subclinical mitochondrial insufficiencies in the aetiology of statin-induced myopathy, myobundles were utilised, for the first time, to conduct a small-scale pilot study to determine if variance(s) in baseline mitochondrial function exist between the three patient groups (Schirris *et al.*, 2015; Allard *et al.*, 2018; van Diemen *et al.*, 2017; Sirvent *et al.*, 2012). In addition, parallel investigations were conducted to determine if functional variation(s) in mitochondrial respiratory parameters between groups correlated with enhanced or diminished susceptibility to statin-mediated mitochondrial impairment.

All patients recruited to the study were of a similar mean age, height, weight and body mass index (BMI). In accordance with National Health Service (NHS) definitions, the mean BMI for the statin naïve group was within the overweight range (27.65) whereas the mean BMI for the statin tolerant and intolerant groups fell into the obese range (30.41 and 32.19 respectively). There is evidence to suggest that excessive nutrient consumption adversely affects skeletal muscle mitochondrial dynamics, increases ROS generation and impairs insulin-dependent glucose transport (de Mello *et al.*, 2018). Therefore, it was of importance to use patients of a similar BMI, within the statin naïve group particularly, to ensure that any phenotypic differences observed were not due to the presence of inherent pathological processes in some groups and not others (Herbert *et al.*, 2018). In order to address any further confounding effects upon mitochondrial functionality, patients receiving co-medications with known mitochondrial liabilities or patients with diagnosed metabolic disorders were excluded from the study. This was with the exception of one statin intolerant donor owing to the low number of suitable candidates encountered during the recruitment period.

In addition, due to the practicalities of recruiting patients through the Liverpool Musculoskeletal Biobank (LMB), it was not possible to collect venous blood samples to gather data on serological markers such as serum lipids (total, HDL-C, LDL-C and triglycerides), CK, and alanine aminotransferase (ALT) at the time of sampling. Any supplemental data gathered via the patient case report forms (CRF), including co-morbidities, are outlined in the appendices (Appendix II).

Initial extracellular flux analyses identified marginal differences in most baseline metabolic parameters between the patient groups, however none of these variations reached statistical significance. Concordantly, coupling efficiency, the proportion of OCR dedicated to driving ATP synthesis, did not differ between groups. When examining proton leak, ATP-linked respiration and spare respiratory capacity as proportions of the maximal respiratory capacity, the statin tolerant group dedicated a greater percentage of maximal OCR to spare capacity compared with the statin naïve and statin intolerant patients. Spare respiratory capacity has been linked to a regulated increase in substrate flux into the TCA cycle concomitantly with elevated succinate dehydrogenase (complex II) activity in response to stressors or increased functional demand. Moreover, reserve capacity, via complex II, has been shown to promote cellular survival through sirtuin-3 (SIRT3) dependent mechanisms in several cell types (Nickens *et al.*, 2013; Dhingra and Kirshenbaum, 2015; Yadava and Nicholls, 2007; Pfleger *et al.*, 2015).

Therefore, it would be of merit to investigate the putative link between statin tolerance, succinate dehydrogenase activity and spare respiratory capacity, particularly as it has been shown that complex II activity is significantly reduced in symptomatic statin users (Allard *et al.*, 2018) and sub-groups of healthy volunteers treated with high dose (80 mg/kg) simvastatin (Galtier *et al.*, 2012). Furthermore, succinate-driven respiration was impaired by simvastatin administration in L6 myocytes as evidenced in Chapter 2, providing the impetus to determine whether increased complex II activity confers enhanced resistance to statin-mediated mitochondrial dysfunction.

The effect of chronic statin application upon ATP content and LDH retention was examined in patient-derived myobundles conditioned to galactose media. This was performed to determine drug response in the absence of compensatory ATP generation from glycolysis (Marroquin *et al.*, 2007; Kamalian *et al.*, 2015). Whilst myobundle ATP content reduced, most notably with atorvastatin and cerivastatin exposure, the simultaneous loss of LDH retention was more indicative of cytotoxicity rather than mitochondrial dysfunction specifically (Swiss *et al.*, 2013). In addition, there was no significant differential toxicity observed between the patient groups when exposed to any of the test compounds. However, myobundles produced from statin tolerant patients appeared to remain slightly more viable, particularly those treated with atorvastatin.

Interestingly, within the statin intolerant group, there was a greater decline in ATP content than LDH retention. Loss of ATP before the induction of cell death in galactose media is one

of the hallmarks of mitochondrial dysfunction and aligns with the idea that changes in mitochondrial function may be an early event in the pathophysiology of statin-induced myotoxicity (Sirvent *et al.*, 2012; Allard *et al.*, 2018). This could be substantiated by performing dose responses for each statin and comparing IC_{50} values across several time points to pin point the induction of mitochondrial changes.

Whilst not considered within the present chapter, longitudinal interrogation of inter-mitochondrial dynamics (i.e. fusion and fission of mitochondrial networks) and intra-mitochondrial dynamics (i.e. the assembly of respiratory super-complexes) warrants investigation. It has been suggested that respiratory super-complex assembly modulates mitochondrial fuel utilisation and may be essential for overcoming the impact of drug-mediated perturbations upon the respiratory chain (Acin-Perez and Enriquez, 2014). Furthermore, striated muscle mitochondria establish themselves within a highly convoluted network or 'power grid' known as the mitochondrial reticulum. The reticulum is thought to mediate both proactive and reactive functions, such as the distribution of potential energy or the physical separation of malfunctioning mitochondria to limit the impact of local dysfunction (Glancy *et al.*, 2015, 2017). Indeed, a lack of mitochondrial fusion within skeletal muscle fibers is associated with a pathological profile which resembles mitochondrial myopathies associated with mtDNA depletion syndromes (Chen *et al.*, 2010; Copeland, 2008).

When the respiratory function of myobundles was measured upon treatment with the three different statins, results indicated that there were no significant differences between the patient groups for any of the tested parameters. In agreement with the LDH-ATP data (section 4.3.2), cerivastatin had the most profound effect upon respiration. Though it could be argued that some of these effects may be attributable to loss of myobundle viability rather than mitochondrial dysfunction alone. Disturbances in oxidative metabolism were also evident in both the statin naïve and statin tolerant groups after treatment, this parallels with the idea that mitochondrial impairment can also occur in patients without muscle complaints or prior exposure to statins (Allard *et al.*, 2018).

An interesting observation garnered from the respirometry data was that proton leak appeared to decrease in response to atorvastatin and cerivastatin exposure for each patient group. Dysfunctional mitochondria often have elevated proton leak due to increased uncoupling protein (UCP) activity, inner mitochondrial membrane damage, complex inhibition or electron slippage. In contrast, reduced leak is often associated with reduced

UCP activity and enhanced respiratory chain integrity (Hill *et al.*, 2012). This phenomenon may be explained by considering the bioenergetic status of the myobundles before the addition of drug. As a percentage of basal respiration, proton leak constituted a pooled average of 34.4 %, 29.2 % and 32.1 % of the statin naïve, tolerant and intolerant myobundles respectively (section 4.3.3). Native skeletal muscle is known to exhibit a high proportion of basal proton leak, a by-product of mild uncoupling to increase energy expenditure for thermogenesis, particularly in response to cold exposure or nutrient excess (Wijers *et al.*, 2008; Rolfe *et al.*, 1999). Therefore, the reduction in proton leak may be suggestive of improved coupling in an attempt to maintain energetic homeostasis after drug treatment. In order to robustly assess the kinetics of proton conductance, both respiration and mitochondrial membrane potential must be quantified simultaneously as respiration alone is an indirect and oversimplified measure (Divakaruni and Brand, 2011).

Failure to detect significant differences between patient groups, with particular reference to the statin-intolerant group, could be owing to a number of different factors. Firstly, the recruitment of patients through the LMB meant that identification of suitable candidates was performed via pre-surgical assessment. Therefore, encountering patients with a history of statin-intolerance was down to chance rather than through patient recall, resulting in lower participant numbers. Secondly, the statin-intolerant donors recruited to the study were categorised as SRM 1, tolerable myalgia without CK elevation. It may be that patients with a severe myopathy phenotype (SRM 3-5) would exhibit greater variation in metabolic parameters, though these cases are considerably rarer (Table 4.4). However, assessment of milder myopathy phenotypes is still of merit as they can lead to poor quality of life, reduced drug compliance and propagate failure to prevent adverse cardiovascular events (Alfirevic *et al.*, 2014).

Table 4.4 Statin-related myotoxicity (SRM) phenotype classifications and incidences, adapted from (Alfirevic *et al.*, 2014).

Classification	Phenotype	Incidence
SRM 0	CK elevation <4x ULN	1.5-26 %
SRM 1	Myalgia, tolerable	190/100000 patient-years; 0.3-33 %
SRM 2	Myalgia, intolerable	0.2-2/1000 patients
SRM 3	Myopathy	5/100000 patient-years
SRM 4	Severe myopathy	0.11 %
SRM 5	Rhabdomyolysis	0.1-8.4/100000 patient-years

Abbreviations: CK, creatine kinase; ULN, upper limit of normal.

In addition, the use of XF respirometry, a platform originally intended to monitor the respiratory function of cells grown in monolayer, yields inherently more variable OCR/ECAR readings when used in conjunction with three-dimensional, micro-tissue constructs. Improper or incomplete alignment of myobundles underneath the sensor cartridge probes results in measurements being taken over empty space thus precipitating variation between myobundles generated from the same donor.

The endpoint measures used within this study represent a fraction of the interrogations which could be performed to assess mitochondrial health. Particularly, optimisation of the respiratory complex assays for use with the myobundles in tandem with mitochondrial genotyping may help to reveal some of the more subtle differences in metabolic enzyme activities between the patients groups whilst providing a deeper mechanistic insight to the nature of compound-induced mitochondrial liabilities. This is especially relevant as different statins may not affect the respiratory chain in the same manner (Nadanaciva *et al.*, 2007; Herbert *et al.*, 2018; Sirvent *et al.*, 2012; Schirris *et al.*, 2015).

4.5 Conclusions

Results from this chapter indicate that impairment of mitochondrial function occurs with statin administration regardless of patient status. However, the statin intolerant participants did not appear to be any more susceptible than the naïve or tolerant groups within this study, though this may be due to a combination of mild phenotypic severity and low participant numbers. Further longitudinal studies are required to determine if changes in mitochondrial function are an early event in the aetiology of myopathy and could therefore be used as a prognostic tool or be mitigated completely by enhancing mitochondrial function (Allard *et al.*, 2018; Andreux *et al.*, 2014). Crucially, this chapter demonstrates that it is important to consider not only the factors which may confer enhanced susceptibility to adverse drugs reactions but also those which are protective.

Chapter 5

Mitochondrial DNA Haplogroup-Disease Association Study for Statin-Related Myopathy

Contents

5.1 Introduction 155

5.1.1 Summary of Chapter Aims 157

5.2 Methods 158

5.2.1 Cohort 158

5.2.2 DNA Extraction 158

5.2.3 DNA Quality Control 159

5.2.4 DNA Quantification 159

5.2.5 Sequencing Preparation 159

5.2.6 Mitochondrial Genome Sequencing 165

5.2.7 Bioinformatics Analysis 165

5.2.8 Statistical Analysis 166

5.3 Results 167

5.3.1 MtDNA Haplogroup Assignment 167

5.3.2 MtDNA Haplogroup Calling Concordance 169

5.3.3 Comparison of mtDNA Haplogroup Distribution to an Online Database 170

5.3.4 MtDNA Haplogroup Distribution Between Statin Myopathy Cases and Statin Tolerant Controls 170

5.3.5 Patient Stratification Based upon Statin Type 172

5.3.6 Sample Size Calculations 174

5.4 Discussion 175

5.5 Conclusions 178

5.1 Introduction

The principle aim of personalised medicine is to predict the clinical outcome of a given drug treatment in different patients with view to tailoring treatment regimens to the individual. Pharmacogenomics, the branch of science concerned with the interaction between genetic factors and drug response, forms one of the core components of personalised medicine (Schwab and Schaeffeler, 2012). By its very definition, pharmacogenomics encompasses the study of both the nuclear and mitochondrial genomes. However, the contribution of mitochondrial genome variation upon differential susceptibility to adverse drug reactions has, so far, been studied considerably less within the field (Chapter 1, section 1.6.8).

Throughout human history the mitochondrial genome has accumulated single nucleotide polymorphisms (SNPs) which, in the absence of bi-parental recombination, have formed a nested phylogenetic tree (Neiman and Taylor, 2009). The major subdivisions of the global phylogeny are known as mtDNA haplogroups. Greater than 95 % of Europeans belong to one of ten macro-haplogroups, H, J, T, U, K (subgroup of U), M, I, V, W and X, each of which are defined by specific set of sequence variations. mtDNA haplogroups affect the assembly, stability and functionality of the mitochondrial respiratory chain, therefore mitochondrial genome variation has the propensity to confer enhanced or diminished risk of mitochondrial dysfunction under certain pathological conditions (Chinnery *et al.*, 2010). Indeed there is a growing body of evidence indicating that mitochondrial dysfunction, as a downstream consequence of mitochondrial genome variation, is a critical component in the aetiology of a number of complex traits and diseases (Hudson *et al.*, 2014).

Prior research concerning potential genetic determinants of statin-related myopathy (SRM) have been conducted extensively in the context of the nuclear genome. Early investigations focussed upon candidate genes hypothesised to play a role in SRM by virtue of their implication in the metabolism, transport or action of statins (Table 5.1) (Brunham *et al.*, 2018). However, whilst these studies have been successful in identifying potential associations between candidate genes and the development of SRM, most have not been widely replicated with the exception of the coding variant rs4149056 (p.Val174Ala) in the *SLCO1B1* gene (Link *et al.*, 2008).

Table 5.1 Examples of genetic variants, encoded by the nuclear genome, associated with elevated or diminished risk of statin-related myopathy. Table adapted from Brunham *et al.*, 2018.

Gene	Variant	Function of Encoded Protein	References
SLCO1B1	rs4149056	Solute carrier organic anion transporter (liver)	(Voora *et al.*, 2009; Carr *et al.*, 2013; Brunham *et al.*, 2012; Link *et al.*, 2008)
COQ2	rs4693075	Ubiquinone biosynthesis	(Ruano *et al.*, 2011; Oh *et al.*, 2007)
HTR7	rs1935349	Serotonin receptor	(Ruano *et al.*, 2007)
RYR1	rs118192172	Calcium channel (skeletal muscle)	(Vladutiu *et al.*, 2011)
GATM	rs9806699	Creatine biosynthesis	(Luzum *et al.*, 2015; Mangravite *et al.*, 2013; Floyd *et al.*, 2014)
CYP3A4	rs2740574	Drug metabolism	(Becker *et al.*, 2010)
CYP2D6	*4	Drug metabolism	(Mulder *et al.*, 2001; Frudakis *et al.*, 2007)
UGT1A3	*2	Drug metabolism	(Riedmaier *et al.*, 2010)
ABCC2	rs717620	ATP-binding cassette transporter	(Becker *et al.*, 2013)
RYR2	rs2819742	Calcium channel (cardiac muscle)	(Feng *et al.*, 2012; Hubacek *et al.*, 2015; Marciante *et al.*, 2011)
CLCN1	rs55960271	Voltage-dependent chloride channel	(Neroldova *et al.*, 2016)
VDR	rs731236	Vitamin D3 receptor	(Ovesjo *et al.*, 2016)
ABCG2	rs2231142	ATP-binding cassette transporter	(Mirosevic Skvrce *et al.*, 2015)

To date there have been no large scale case-control studies examining the influence of mitochondrial genome variation upon susceptibility to statin-related myopathy. Small *in vitro* studies have demonstrated that fibroblasts isolated from patients with complex III deficiencies were more sensitive to statin lactones than those from healthy controls (Schirris *et al.*, 2015). However, whilst complex III deficiencies are commonly associated with mutations in the mtDNA *MT-CYB* (cytochrome *b* subunit) gene, insufficiencies can also arise from mutations in one of several genes encoded by the nuclear genome (e.g. *BCS1L* and *QP-C*) (Bénit *et al.*, 2009). In addition, *in vitro* studies using trans-mitochondrial, cytoplasmic hybrid (cybrid) modelling have shown that an individual's mtDNA background, specifically mutations in cytochrome c oxidase subunit 1 (*COX1*, T6124C, Met74Thr), affect the degree to which simvastatin affects prostate cancer progression (Sun *et al.*, 2015). Therefore, given the role of mitochondrial dysfunction in the aetiology of statin-related myopathy, there is rationale behind the hypothesis that inter-individual variation in the mitochondrial genome may contribute, at least in part, to an enhanced or diminished susceptibility to myopathic symptoms in patients.

The present chapter aimed to use a combination of next-generation sequencing (NGS) technology and bioinformatics analyses to identify and compare sequence variation across the entire mitochondrial genomes of both a healthy volunteer cohort consisting of 342 individuals and a statin myopathy, case-control cohort consisting of 555 patients. The use of NGS allowed for the identification of genome wide heteroplasmic variants in > 1 % of mtDNA copies; in contrast with other currently used mitochondrial sequencing methodologies such as Sanger sequencing that can only detect variants that are present in > 10 % of mtDNA copies (Kloss-Brandstatter *et al.*, 2015).

To achieve this, genomic DNA was extracted from the whole blood of 264 statin myopathy cases (SRM 3-6), 291 statin-tolerant controls and 342 healthy volunteers prior to the use of multiplexed amplicon tagging (Fluidigm Access Array) to enable the simultaneous sequencing of samples (Illumina MiSeq). Concordance between four different variant calling methods were assessed after inputting data into HaploGrep2 for the classification of samples into their macro- and sub-haplogroups. Haplogroup frequencies were compared across groups to determine if there was a putative association between mitochondrial haplogroup and statin-related myopathy.

5.1.1 Summary of Chapter Aims

1. To perform next-generation whole mitochondrial genome sequencing of cohort samples.
2. To perform classification of mitochondrial DNA variants into both macro- and sub-haplogroups using HaploGrep2 software.
3. To conduct an mtDNA haplogroup-disease association study for statin-related myopathy.

5.2 Methods

5.2.1 Cohort

The analysed statin myopathy case and tolerant control cohort were recruited as part of the PREDICTION-ADR consortium, funded by the EU Seventh Framework Programme, with study approval granted by the North West of England Research Ethics Committee: STAGE (REC reference number: 09/H1001/38) and MOLGEN (REC reference number: 09/H1005/28) . All participants gave written informed consent. Study eligibility and inclusion criteria have been published previously (Siddiqui *et al.*, 2017a; Siddiqui *et al.*, 2017b).

Briefly, 555 patients (264 statin-related myopathy cases and 291 statin-tolerant controls) were recruited from four European centres (Liverpool, Dundee, Uppsala and Utrecht). The cohort consisted of 35 % female and 65 % male participants with a mean age of 71 years (range 39-93 years). All patients were of Caucasian descent. Most patients were receiving simvastatin (n=339) followed by atorvastatin (n=162), pravastatin (n=28), rosuvastatin (n=20), fluvastatin (n=5) and drug unknown (n=1).

The analysed healthy volunteer cohort were selected from a study published by Faulkner *et al.*, during which 1000 volunteers were recruited from the North West of England and 100 mL whole blood was collected for DNA extraction (Faulkner *et al.*, 2016; Alfirevic *et al.*, 2012). The study was approved by the North West of England Research Ethics Committee and all participants gave written informed consent (REC reference number: 09/H1005/10). The most recently collected 342 samples of Caucasian descent were selected for analysis. The volunteer cohort was 63.7 % female and 36.3 % male with a mean age of 29 years (range 18-60 years).

Volunteers were eligible to take part in the study if they were healthy, aged between 18 and 60 years and willing to donate one or more blood samples. Volunteers were excluded from participation if they had: donated blood to the transfusion services in the last four months, had any medical problems; inclusive of asthma, diabetes, epilepsy and anaemia or taken medicinal or recreation drugs within the last 6 weeks. Women were excluded if pregnant.

5.2.2 DNA Extraction

Genomic DNA was extracted from whole blood samples using the Chemagen magnetic separation module 1 (PerkinElmer, Buckinghamshire, UK). Briefly, the Chemagen module enables the separation of nucleic acids from biological samples through highly specific binding to M-polyvinyl alcohol (PVA) magnetic beads. The PVA beads are attracted to

magnetised rods that are inserted into the samples. The magnetised rods transfer the bead bound DNA through several washing and elution steps. The rod rotation, switched on after the deactivation of the electromagnet, efficiently resuspends the beads after each step.

5.2.3 DNA Quality Control

Quality control of the resultant DNA samples was performed using nanodrop spectrophotometry (Thermo Fisher Scientific, Loughborough, UK). Samples with an $A_{260/230}$ >1.8 and $A_{260/280}$ >1.9 were deemed acceptable for downstream processing. Sample quality was also monitored using 2 % E-gel electrophoresis (Invitrogen, UK), with reference DNA ladder, Quick-Load 1 Kb DNA ladder (New England BioLabs, MA, USA) to ensure the absence of contaminants such as RNA (< 200 bp smear).

5.2.4 DNA Quantification

Sample DNA concentrations were determined by PicoGreen dsDNA Assay Kit (Life Technologies, UK) in accordance with the manufacturer's instructions. PicoGreen is a fluorescent dye that binds to double–stranded DNA (dsDNA) and forms a luminescent complex when compared to the free dye in solution. Once bound, the DNA intercalation and electrostatic interactions immobilize the dye molecule resulting in a > 1000-fold increase in its fluorescent signal (Dragan *et al.*, 2010).

The DNA content of each sample was derived by reference to a DNA standard curve (2 µg/mL - 0 µg/mL in Tris-EDTA (TE) buffer). Black-walled plates were read on a VarioSkan plate reader (excitation ~480 nm/ emission ~520 nm). All samples were then diluted to 100 ng/µL using TE buffer (10 mM Tris, 0.1 mM EDTA, pH 8.0).

5.2.5 Sequencing Preparation

Next-generation, whole mitochondrial genome sequencing and all associated preparations were performed by the Centre for Genome Research (CGR) at the University of Liverpool.

5.2.5.1 Multiplex Primer Stock Plate

In a DNA-free hood, a multiplex primer stock plate was prepared by combining six stock primer plates of individual primer pairs (60 µM) as depicted in Figure 5.1 (Fluidigm, CA, USA). 5 µL from each of the 12 columns of the source plate were transferred into a corresponding single column in the destination plate to produce primer concentrations of 5 µM. Each well contained up to 12 forward and 12 reverse primers in a final volume of 60 µL per well. Three daughter plates were prepared from this plate each containing 20 µL. The plates were stored at -80 °C

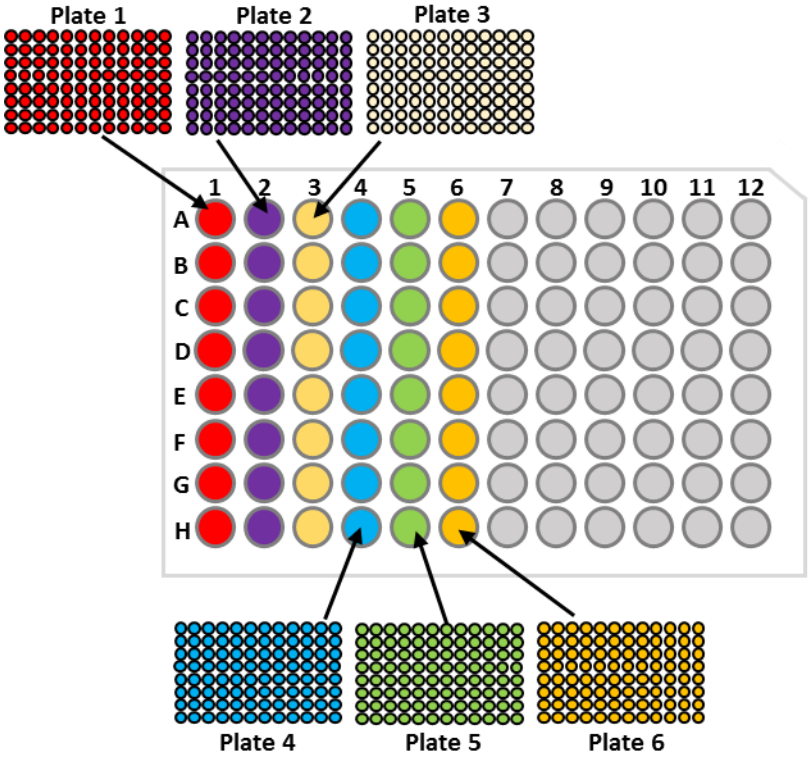

Figure 5.1 Preparation of multiplex primer stock plates by combining six stock primer plates of individual primer pairs. Image adapted from Fluidigm user guide.

5.2.5.2 20X Primer Solutions

In 96-well plates, 75 µL polymerase chain reaction (PCR)-grade water was combined with 20 µL of the stock multiplex primer mix (5 µM) and 5 µL 20X Access Array Loading Reagent for a final primer concentration of 1 µM. Multiple copies of these working plates were produced and stored at -20 °C to reduce exposing primers to repeated freeze thaw cycles.

5.2.5.3 Access Array Integrated Fluidic Circuit (IFC)

In 96-well plates, each patient sample (1 µL of 100 ng/µL DNA) was added to 4 µL of Pre-sample mastermix solution, the constituents of which are outlined in Table 5.2.

Table 5.2 Access Array IFC pre-sample mastermix solution constituents.

Reagent	Volume per Reaction (µL)	Final Concentration
10X FastStart High fidelity Reaction Buffer without $MgCl_2$ (Roche)	0.5	1X
25 mM $MgCl_2$ (Roche)	0.9	4.5 mM
DMSO (Roche)	0.25	5 %
10 mM dNTP Mix (Roche)	0.1	200 µM
5 units/µL FastStart High Fidelity Enzyme Blend (Roche)	0.05	0.05 units/µL
20X Access Array Loading Reagent	0.25	1X
PCR Grade Water	1.95	N/A

Abbreviations: $MgCl_2$, magnesium chloride; DMSO, dimethyl sulfoxide; dNTP, deoxynucleotide; PCR, polymerase chain reaction.

5.2.5.4 Priming the Access Array

Prior to adding samples and primers, the integrated fluidic circuit (IFC) (Figure 5.2) was loaded with reagents in accordance with Table 5.3 and placed into the pre-PCR IFC controller before the Prime 151x script was run.

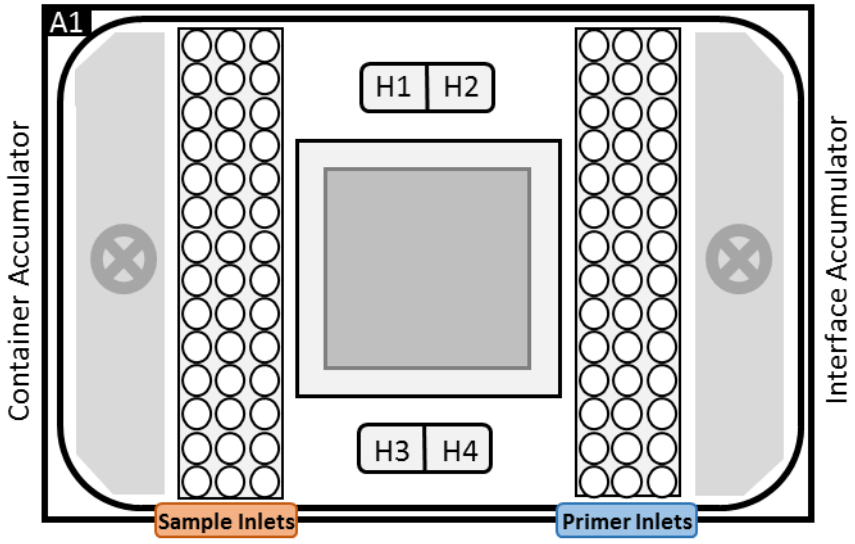

Figure 5.2 The Access Array Integrated Fluidics Circuit (IFC) holds up to 48 samples and 48 groups of primers within its inlets. The IFC must also be loaded with harvesting and hydration solutions and control-line fluid. Image adapted from the Fluidigm user guide.

Table 5.3 Integrated Fluidics Circuit (IFC) reagent loading positions and volumes.

Position	Reagent	Volume (µL)
Accumulators	Control-line fluid	300
H1	1X Access Array Harvest Solution	700
H2, H3	1X Access Array Harvest Solution	500
H4	1X Access Array Hydration Solution v2	500
Primer Inlets	20X Primer Solution	4
Sample Inlets	Sample Mastermix	4

Once priming of the Access Array cassette was complete, 4 µL of the prepared samples were loaded into the ICF samples inlets and 4 µL of 20X primer solution mix was added to the primer inlets as displayed in Figure 5.2. The cassette was returned to the Pre-PCR IFC and the Load Mix (151x v7) script was run, this procedure draws primer and samples from the inlets to the centre of the IFC ready for PCR. Upon completion of the script, the IFC was transferred to the Fluidigm FC1 cycler and the protocol AA48x 48 standard v1 was performed as described in Table 5.4.

Table 5.4 FC1 thermal cycler protocol AA48x 48 standard v1

	Temperature (°C)	Time (sec)	Cycles
Thermal Mix	50	120	1
	70	1200	
Hot Start	95	600	1
PCR	95	15	10
	60	30	
	72	60	
C0t Cycle	95	15	2
	80	30	
	60	30	
	72	60	
PCR Cycle	95	15	8
	60	30	
	72	60	
C0t	95	15	2
	80	30	
	60	30	
	72	60	
PCR Cycle	95	15	8
	60	30	
	72	60	
C_0t	95	15	5
	80	30	
	60	30	

	72	60	
Extension	72	180	1
Cool Down	10	hold	-

Abbreviations: C_0t, PCR amplicon normalisation cycle.

5.2.5.5 Sample Harvesting

Following the amplification of samples in the FC1 thermal cycler, the IFC was removed and the remaining fluids in ports H1-4 were removed. An additional 700 µL 1X Access Array harvest solution was added to port H1 and 600 µL to ports H2-H4. 2 µL of 1X harvest solution was also loaded into each of the sample inlets. The IFC was then placed into the post-PCR IFC controller and the script harvest (151 v7) was run. Upon completion of the run, the IFC was removed and the harvested samples (~10-12 µL) were transferred to a new 96-well plate. The harvested sample plate was stored at -20 °C.

5.2.5.6 Attaching Sequence Barcodes

A mastermix solution was prepared for the harvested samples (Table 5.5). 15 µL of Pre-Mix mastermix was combined with illumina barcodes (4 µL; Illumina, CA, USA) and 1 µL of a 100-fold dilution of the harvested PCR product for a total reaction volume of 20 µL. The resultant 96-well plates were then run on a thermal cycler in accordance to Table 5.6.

Table 5.5 Mastermix constituents.

Reagent	**Volume per Reaction (µL)**	**Final Concentration**
10X FastStart High fidelity Reaction Buffer without $MgCl_2$ (Roche)	2.0	1X
25 mM $MgCl_2$ (Roche)	3.6	4.5 mM
DMSO (Roche)	1.0	5 %
10 mM dNTP Mix (Roche)	0.4	200 µM
5 units/µL FastStart High Fidelity Enzyme Blend (Roche)	0.2	0.05 units/µL
PCR Grade Water	7.8	N/A

Abbreviations: $MgCl_2$, magnesium chloride; DMSO, dimethyl sulfoxide; dNTP, deoxynucleotide; PCR, polymerase chain reaction.

Table 5.6 Thermal cycler protocol for the incorporation of sample specific Illumina barcodes and adaptor sequences for the identification of individual amplicons.

Time (sec)	Temperature (°C)	Cycles
600	95	1
15	95	15
30	60	
60	72	
180	72	1

5.2.5.7 Purification of PCR Products

All barcoded amplicon produced by the Access Array IFC underwent further quality control measures using a Fragment Analyser™ (Thermo Fisher Scientific, MA, USA). The Fragment Analyser™ accelerates nucleic acid workflow through the automation of gel loading and sample injection. Each sample is injected into parallel capillaries which contain a pre-loaded, intercalating fluorescent dye. During gel electrophoresis, nucleic acid fragments migrate based upon size and bind to the dye. During migration, fragments pass a detection window where nucleic acid bound dye is excited by a light source and emits a fluorescent signal. When samples are compared against a calibration ladder of known size, the time required to pass the detection window and fluorescent emission can provide information on the fragment size and concentration respectively. Sample DNA concentrations were then measured using a Qubit™ dsDNA High Sensitivity Assay (Thermo Fisher Scientific, UK) according to the manufacturer's instructions and read on a Qubit™ fluorometer.

5.2.5.8 Sample Pooling

Samples were pooled using the Mosquito_X1 (TTP Labtech, UK), allowing for the rapid transfer of small volumes without further dilution requirements. 1 µL of amplicon was extracted from each well of the 96-well plates to generate one pool per plate. The resultant libraries were cleaned with Ampure beads (Beckman Coulter, CA, USA) in a 1:1 ratio. This step enables the removal of unincorporated deoxynucleotides (dNTPs), primer dimers or other contaminants whilst stabilising and efficiently recovering the DNA.

5.2.5.9 Bioanalyser Quality Control

The quality and quantity of each of the sample pools was assessed using a 2100 Bioanalyzer (Agilent, CA, USA). The 2100 Bioanalyzer simultaneously uses electrophoresis and flow cytometry to assess each sample whilst consuming minimal volume. 1 µL of PCR product was assessed using chips from the Agilent DNA 1000 kit to determine if the product pool had the

expected size. The product was expected to be the sum of the target region and the length of the incorporated Illumina barcodes.

5.2.5.10 Quantitative PCR (qPCR)

Quantitative PCR (qPCR) was performed using an Illumina Library Quantification Kit on a Roche Light Cycler LC480II (Roche, Basal, Switzerland) according the manufacturer's instructions (Kapa Biosystems, CA, USA) to determine sample pool quantity. The mastermix contains the engineered KAPA SYBER FAST DNA polymerase which amplifies GC- and AT-rich DNA fragments with similar efficiency. This enables the accurate quantification of next-generation sequencing libraries through qPCR based methods. The sample pools were then combined in equimolar ratios before performing mitochondrial genome sequencing.

5.2.6 Mitochondrial Genome Sequencing

The template DNA was denatured by combining 5 µL non-denaturing library to 5 µL of 0.1 M NaOH and 5 µL 200 mM Tris-HCl (pH 8.0). The sample-library mix (10 pM) and Read1, Read2 and Read3 sequencing primers were loaded into the MiSeq reagent cartridge (Illumina, CA, USA), pre-filled with clustering and sequencing reagents sufficient for one flow cell. Upon run initiation, libraries were transferred to the flow cell channel, a glass-based substrate from which cluster generation and the sequencing reactions are performed.

The process began with cluster generation, whereby single DNA molecules were bound to the surface of the flow cell and bridge amplified. Clusters generated within the flow cell were imaged in smaller areas called tiles. This was achieved using light-emitting diodes (LED) and filter combinations specific to each of the four fluorescently labelled dideoxynucleotides. The imaging process was repeated for each sequencing cycle. Base calling, filtering and quality scoring was performed by MiSeq reporter software.

5.2.7 Bioinformatics Analysis

5.2.7.1 Sequence Alignment Tools

Illumina sequencing generates a high volume of short reads therefore the use of fast and accurate read alignment tools are required. Sequencing reads were aligned to the revised Cambridge Reference Sequence (rCRS) (NC_012920) using the Burrows-Wheeler Alignment tool v0.7.12 (BWA-MEM algorithm) (Li and Durbin, 2009). The BWA is a fast read alignment software package which enables mapping of sequences of low divergence against a reference genome. The tool has reliable performance for 70-100 bp illumina reads.

5.2.7.2 Variant Calling Analysis

Following the alignment of sequencing reads using BWA-MEM, the resultant output was delivered in standard sequence alignment/map (SAM) format. SAMtools (v0.1.18) was used to sort and index the data so that it was suitable for use with various variant calling software packages (Li *et al.*, 2009).

Variant calling was performed with the genome analysis toolkit (GATK) v3.2.2 using haploidy, diploidy and tenploidy settings and VarScan (minimum depth = 100, supporting reads = 5, base quality = >20, mapping quality = >20) v2.3.9 (McKenna *et al.*, 2010; Koboldt *et al.*, 2009). Whilst GATK is often considered the 'gold standard' variant caller for targeted, exome and whole-genome sequencing, this is not specifically in the context of the mitochondrial genome. Therefore, multiple variant calling tools and settings were employed so that concordance between results may be assessed. Each variant caller software package generated a variant calling format (VCF) file. The average number of reads was 43,115 with 92.5 % mapped on target. The average depth (coverage) was 343.3X.

5.2.7.3 Mitochondrial Haplogroup Calling

Mitochondrial DNA haplogroups were assigned using the web application HaploGrep2 (v2.1.0) by directly inputting VCF files generated by the variant callers. HaploGrep2 mediates the automated determination of haplogroups based upon the most recent iteration of the mtDNA phylogenetic tree (Phylotree build 17) (van Oven, 2015). The software provides the user with the 50 most probable haplogroups for a given sample (Weissensteiner *et al.*, 2016). All samples with an error rate > 0 (missed 3 or more expected polymorphisms) and a low HaploGrep2 quality score < 80 % were removed from the analyses.

5.2.8 Statistical Analysis

All statistical analyses were performed using StatsDirect Version 3 (StatsDirect Ltd, UK). Statistical independence between macro-haplogroup frequencies for statin myopathy case and statin tolerant control groups was examined using a Chi-square 2-by-k contingency table (without trend). A p-value ≤ 0.05 was regarded as the significance threshold. Sample size calculations for independent case-control studies were performed using the following settings: number of controls per case (1), % power (80 %) and % alpha (5 %).

5.3 Results

5.3.1 mtDNA Haplogroup Assignment

The mitochondrial haplogroups of 264 statin myopathy cases, 291 statin tolerant controls and 342 healthy volunteers were resolved using HaploGrep2 software based upon the most recent iteration of Phylotree (build 17) (van Oven, 2015). Two variant callers were used; GATK with haploidy, diploidy and tenploidy settings and VarScan. All samples that did not meet the quality control (QC) criteria (section 5.2.7.3) were removed (error rate > 0, quality score < 80 %).

The number of samples that passed QC in the PREDICTION-ADR cohort were similar across the VarScan and GATK haploidy/diploidy analyses, whereas the GATK tenploidy settings yielded fewer high quality samples. In contrast, the number of samples that passed QC for the healthy volunteer cohort were more consistent across the different variant calling tools however GATK tenploidy still suffered the poorest yield of high quality samples (Table 5.7).

Table 5.7 Number of samples that passed quality control (QC) in different variant calling analyses for the PREDICTION-ADR cohort and healthy volunteer cohort.

	GATK haploidy	***GATK diploidy***	***GATK tenploidy***	***VarScan***
Cases	250	259	110	245
Controls	276	286	137	264
Healthy Volunteers	329	328	320	328
Total	**855**	**873**	**567**	**837**

Following QC analysis, macro-haplogroup assignment was compared between the four different variant callers for both the PREDICTION-ADR cohort and the healthy volunteer cohort (Table 5.8). Regarding the PREDICTION-ADR cohort (statin myopathy cases vs statin tolerant controls), GATK haploidy identified a total of 12 macro-haplogroups, GATK diploidy 13, GATK tenploidy 10 and VarScan 11. Amongst the healthy volunteer cohort, GATK haploidy assigned samples into 17 macro-haplogroups, GATK diploidy 17, GATK tenploidy 17 and VarScan 17. As the GATK tenploidy macro-haplogroup distribution deviated significantly from the other variant calling methods for the PREDICTION-ADR cohort specifically, it was excluded from further analyses.

Table 5.8 mtDNA macro-haplogroup distributions of analysed samples for the variant calling tools GATK (haploidy/diploidy and tenploidy settings) and VarScan.

	GATK haploidy			***GATK diploidy***			***GATK tenploidy***			***VarScan***		
Haplogroup	Myopathy Cases (%)	Tolerant Controls (%)	Healthy Volunteers (%)	Myopathy Cases (%)	Tolerant Controls (%)	Healthy Volunteers (%)	Myopathy Cases (%)	Tolerant Controls (%)	Healthy Volunteers (%)	Myopathy Cases (%)	Tolerant Controls (%)	Healthy Volunteers (%)
H	109 (43.6)	129 (46.7)	132 (40.1)	108 (41.7)	130 (45.5)	133 (40.5)	87 (79.1)	114 (83.2)	127 (39.7)	107 (44.4)	127 (48.1)	129 (39.3)
U	36 (14.4)	34 (12.3)	56 (17.0)	37 (14.3)	34 (11.9)	56 (17.1)	7 (6.4)	6 (4.4)	56 (17.5)	33 (13.7)	34 (12.9)	57 (17.4)
J	33 (13.2)	34 (12.3)	44 (13.4)	35 (13.5)	37 (12.9)	42 (12.8)	7 (6.4)	3 (2.2)	43 (13.4)	33 (13.7)	33 (12.5)	44 (13.4)
T	25 (10.0)	27 (9.8)	28 (8.5)	28 (10.8)	28 (9.8)	28 (8.5)	1 (0.9)	0 (0.0)	26 (8.1)	29 (12.0)	26 (9.8)	29 (8.8)
K	21 (8.4)	20 (7.2)	27 (8.2)	21 (8.1)	20 (7.0)	27 (8.2)	1 (0.9)	1 (0.7)	28 (8.8)	18 (7.5)	18 (6.8)	28 (8.5)
M	1 (0.4)	0 (0.0)	1 (0.3)	1 (0.4)	0 (0.0)	1 (0.3)	0 (0.0)	0 (0.0)	1 (0.3)	0 (0.0)	0 (0.0)	1 (0.3)
I	8 (3.2)	16 (5.8)	5 (1.5)	10 (3.9)	16 (5.6)	5 (1.5)	0 (0.0)	1 (0.7)	4 (1.3)	6 (2.5)	11 (4.2)	5 (1.5)
V	8 (3.2)	8 (2.9)	15 (4.6)	8 (3.1)	8 (2.8)	15 (4.6)	6 (5.5)	6 (4.4)	14 (4.4)	8 (3.3)	9 (3.4)	14 (4.3)
W	3 (1.2)	2 (0.7)	3 (0.9)	4 (1.5)	3 (1.0)	3 (0.9)	0 (0.0)	1 (0.7)	3 (0.9)	2 (0.8)	2 (0.8)	3 (0.9)
X	6 (2.4)	4 (1.4)	9 (2.7)	6 (2.3)	4 (1.4)	9 (2.7)	0 (0.0)	1 (0.7)	9 (2.8)	4 (1.7)	3 (1.1)	9 (2.7)
N	0 (0.0)	1 (0.4)	1 (0.3)	0 (0.0)	2 (0.7)	1 (0.3)	0 (0.0)	0 (0.0)	1 (0.3)	0 (0.0)	0 (0.0)	1 (0.3)
R	0 (0.0)	0 (0.0)	1 (0.3)	1 (0.4)	3 (1.0)	1 (0.3)	1 (0.9)	4 (2.9)	1 (0.3)	1 (0.4)	0 (0.0)	1 (0.3)
E	0 (0.0)	1 (0.4)	0 (0.0)	0 (0.0)	1 (0.3)	0 (0.0)	0 (0.0)	0 (0.0)	0 (0.0)	0 (0.0)	1 (0.4)	0 (0.0)
A	0 (0.0)	0 (0.0)	3 (0.9)	0 (0.0)	0 (0.0)	3 (0.9)	0 (0.0)	0 (0.0)	3 (0.9)	0 (0.0)	0 (0.0)	3 (0.9)
D	0 (0.0)	0 (0.0)	1 (0.3)	0 (0.0)	0 (0.0)	1 (0.3)	0 (0.0)	0 (0.0)	1 (0.3)	0 (0.0)	0 (0.0)	1 (0.3)
F	0 (0.0)	0 (0.0)	1 (0.3)	0 (0.0)	0 (0.0)	1 (0.3)	0 (0.0)	0 (0.0)	1 (0.3)	0 (0.0)	0 (0.0)	1 (0.3)
G	0 (0.0)	0 (0.0)	1 (0.3)	0 (0.0)	0 (0.0)	1 (0.3)	0 (0.0)	0 (0.0)	1 (0.3)	0 (0.0)	0 (0.0)	1 (0.3)
L	0 (0.0)	0 (0.0)	1 (0.3)	0 (0.0)	0 (0.0)	1 (0.3)	0 (0.0)	0 (0.0)	1 (0.3)	0 (0.0)	0 (0.0)	1 (0.3)

5.3.2 mtDNA Haplogroup Calling Concordance

Concordance in haplogroup assignment between the variant calling tools was assessed for both the PREDICTION-ADR cohort (GATK haploidy, diploidy and VarScan) and the healthy volunteer cohort (GATK haploidy, diploidy, tenploidy and VarScan) at the macro-haplogroup level (e.g. H vs J) and at the sub-haplogroup level (e.g. H1 vs H1a). Only high quality samples (error rate < 0 and HaploGrep2 quality score > 80 %) were compared. From 555 PREDICTION-ADR samples, 488 passed quality control across the three variant calling analyses (230 myopathy cases and 258 tolerant controls). Of these samples, only one discordant macro-haplogroup assignment was identified within the statin tolerant control group (Table 5.9). When examining the concordance of sub-haplogroup assignment for the same cohort, percentage matching dropped by 15.9 % and 11.8 % for the tolerant controls and myopathy cases respectively.

Table 5.9 mtDNA macro- and sub-haplogroup concordance for the PREDICTION-ADR cohort (GATK haploidly, diploidy and VarScan).

		Total Number of Samples	Concordant Calls	Match (%)
Macro-haplogroup assignment	Tolerant Controls	258	257	99.6
	Myopathy Cases	230	230	100
Sub-haplogroup Assignment	Tolerant Controls	258	216	83.7
	Myopathy Cases	230	203	88.2

From a total of 342 healthy volunteer samples, 308 passed quality control measures across the four variant calling analyses. Of these samples, four discordant macro-haplogroup assignments were identified (Table 5.10). Analysis of sub-haplogroup assignment for the same cohort resulted in a 24.1 % reduction in haplogroup matching across the four variant calling tools.

Table 5.10 mtDNA macro- and sub-haplogroup concordance for the healthy volunteer cohort (GATK haploidly, diploidy, tenploidy and VarScan).

		Total Number of Samples	Concordant Calls	Match (%)
Macro-haplogroup assignment	Healthy Volunteers	308	304	98.7
Sub-haplogroup Assignment	Healthy Volunteers	308	230	74.6

5.3.3 Comparison of mtDNA Haplogroup Distribution to an Online Database

Comparison of the five most commonly occurring macro-haplogroups to an online database of haplogroup distribution in Northern Europe showed close agreement between all observed frequencies (Eupedia, 2018). The distribution of macro-haplogroups in both cases and controls resembled that of the healthy volunteers and the Northern European population. The greatest deviation (10 %) was observed within Haplogroup H between the healthy volunteers and statin tolerant controls (Table 5.11).

Table 5.11 Comparison of mtDNA macro-haplogroup frequencies in the PREDICTION-ADR and healthy volunteer cohorts to an online database (Eupedia, 2018).

	Frequency (%)			
Haplogroup	**Eupedia Database[a]**	**Healthy Volunteers (n=304)**	**Tolerant Controls (n=257)**	**Myopathy Cases (n=230)**
H	44.9	38.6	48.6	46.1
U	16.8	17.5	13.2	14.3
J	10.7	13.3	11.7	12.6
T	9.2	8.4	9.7	10.9
K	7.8	8.8	7.0	7.8

[a]Macro-haplogroup frequency calculated from data collated from England, Scotland, Sweden and the Netherlands (Eupedia, 2018).

5.3.4 mtDNA Haplogroup Distribution between Statin Myopathy Cases and Statin Tolerant Controls

When comparing marco-haplogroup frequencies from the PREDICTION-ADR cohort, statistical analyses revealed no significant relationship between myopathy cases and controls (Table 5.12). When further stratifying the statin myopathy cases according to disease severity, SRM 3 patients (defined as CK elevation >4X ULN, <10X ULN ± muscle symptoms, complete resolution on dechallenge) also showed no significant differences in haplogroup frequency when compared with the tolerant controls (Table 5.13). Similarly, SRM 4 (CK elevation >10X ULN, <50X ULN + muscle symptoms, complete resolution on dechallenge) and SRM 5 (CK elevation >10X ULN, with evidence of renal failure + muscle symptoms or CK >50X ULN) patients examined as a compound group representing severe myopathy and rhabdomyolysis yielded statistically insignificant results (Table 5.14) (Alfirevic *et al.*, 2014).

Table 5.12 mtDNA macro-haplogroup frequencies for statin tolerant controls and myopathy cases. Statistical independence between variables was calculated by Chi-square 2-by-k (without trend) test *p value < 0.05 **p value < 0.01 ***p value < 0.001.

	Frequency (%)		
Haplogroup	**Myopathy Cases (n=230)**	**Tolerant Controls (n=257)**	**Statistics**
H	46.1	48.6	Total Chi^2 = 4.22 Chi = 2.05 (9 DF) P = 0.89
U	14.3	13.2	
J	12.6	11.7	
T	10.9	9.7	
K	7.8	7.0	
V	3.5	3.1	
I	2.2	4.3	
X	0.9	1.2	
W	1.7	0.8	
E	0.0	0.4	

Table 5.13 mtDNA macro-haplogroup frequencies for statin tolerant controls and myopathy cases (SRM 3 only). Statistical independence between variables was calculated by Chi-square 2-by-k (without trend) test *p value < 0.05 **p value < 0.01 ***p value < 0.001.

	Frequency (%)		
Haplogroup	**Cases (SRM 3) (n=139)**	**Tolerant Controls (n=257)**	**Statistics**
H	46.8	48.6	Total Chi^2 = 2.56 Chi = 1.6 (9 DF) P = 0.97
U	12.9	13.2	
J	12.2	11.7	
T	9.4	9.7	
K	7.9	7.0	
V	4.3	3.1	
I	2.9	4.3	
X	2.2	1.2	
W	1.4	0.8	
E	0.0	0.4	

Table 5.14 mtDNA macro-haplogroup frequencies for statin tolerant controls and myopathy cases (SRM 4 & 5 only). Statistical independence between variables was calculated by Chi-square 2-by-k (without trend) test *p value < 0.05 **p value < 0.01 ***p value < 0.001.

	Frequency (%)		
Haplogroup	**Cases (SRM 4 & 5) (n=84)**	**Tolerant Controls (n=257)**	**Statistics**
H	46.4	48.6	Total Chi^2 = 3.86 Chi = 1.96 (9 DF) P = 0.91
U	14.3	13.2	
J	13.1	11.7	
T	13.1	9.7	
K	8.3	7.0	
V	2.4	3.1	
I	1.2	4.3	
X	1.2	1.2	
W	0.0	0.8	
E	0.0	0.4	

5.3.5 Patient Stratification Based upon Statin Type

The PREDICTION-ADR recruited patients were next stratified based upon the statin that they had been prescribed at the time of sample collection. Analyses were performed using patients who were receiving simvastatin and atorvastatin only. This was due to the relatively low number of samples retained from participants taking pravastatin (n=26), rosuvastatin (n=17) and fluvastatin (n=4) after filtering for concordant macro-haplogroup assignment and HaploGrep2 quality score. When examining the macro-haplogroup frequencies within both the atorvastatin (Table 5.15) and simvastatin (Table 5.16) patient sub-groups, there were no statistically significant relationships observed between mtDNA haplogroup and patient status.

Table 5.15 mtDNA macro-haplogroup frequencies for statin tolerant controls and myopathy cases (atorvastatin only). Statistical independence between variables was calculated by Chi-square 2-by-k (without trend) test *p value < 0.05 **p value < 0.01 ***p value < 0.001.

	Frequency (%)		
Haplogroup	**Atorvastatin Cases (n=81)**	**Atorvastatin Controls (n=66)**	**Statistics**
H	50.0	46.9	
U	13.6	13.6	
J	18.2	13.6	
T	4.5	4.9	Total Chi^2 = 3.45
K	9.1	8.6	Chi = 1.85 (8 DF)
V	1.5	3.7	P = 0.90
I	1.5	4.9	
X	1.5	2.5	
E	0.0	1.2	

Table 5.16 mtDNA macro-haplogroup frequencies for statin tolerant controls and myopathy cases (simvastatin only). Statistical independence between variables was calculated by Chi-square 2-by-k (without trend) test *p value < 0.05 **p value < 0.01 ***p value < 0.001.

	Frequency (%)		
Haplogroup	**Simvastatin Cases (n=161)**	**Simvastatin Controls (n=131)**	**Statistics**
H	45.0	49.7	
U	14.5	13.7	
J	12.2	10.6	
T	13.7	12.4	Total Chi^2 = 2.16
K	5.3	6.8	Chi = 1.47 (7 DF)
V	3.8	3.1	P = 0.97
I	3.1	1.9	
X	1.5	0.6	

5.3.6 Sample Size Calculations

Sample size calculations were performed to determine the number of case and control samples that would be required to detect a positive correlation (odds ratio >1) at a range of different haplogroup frequencies (Table 5.17). Results indicated that the PREDICTION-ADR cohort was sufficiently sized to identify strong positive correlations between mtDNA haplogroup and patient status (odds ratio 4-5), however it was insufficiently sized to detect weaker correlations (odds ratio 2) particularly at haplogroup frequencies < 50 %.

Table 5.17 Table of sample size calculations for different haplogroup frequencies.

	Number of Required Cases and Controls		
Haplogroup Frequency (%)	**OR 5**	**OR 4**	**OR 2**
50	37	46	149
20	34	46	187
15	39	53	226
10	49	68	307
5	83	117	560

Abbreviations: OR, odds ratio.

5.4 Discussion

In this chapter, next generation, whole mitochondrial genome sequencing was performed on genomic DNA samples obtained from 342 healthy volunteers and a statin-related myopathy cohort consisting of 264 cases and 291 tolerant controls. This was followed by the comparison of several different methods of variant calling and the assignment of samples into their mtDNA sub-haplogroups using the web-based application HaploGrep2 (phylotree build 17) (van Oven, 2015; Weissensteiner *et al.*, 2016).

In the context of the nuclear genome, GATK software is often considered the 'gold-standard' for variant calling, though information regarding the tailoring of this software for the analysis of mtDNA sequencing data is limited (Liu *et al.*, 2013). Mitochondrial DNA is a haploid molecule, however there can be hundreds to thousands of copies per cell. Consequently, previous studies have relied upon variant callers that were designed for haploid genomes, such as older versions of GATK's Unified genotyper or custom designed algorithms (Guo *et al.*, 2012; DePristo *et al.*, 2011; Ye *et al.*, 2014).

Other studies, such as mtDNA SNP calling for the 1000 Genomes Project (Li *et al.*, 2010; Ye *et al.*, 2014) were performed using the diploid genotype caller GLFTools v3 (Li *et al.*, 2009; Ye *et al.*, 2014). However, using variant calling tools designed for polyploidy genomes can result in the classification of high-level heteroplasmic sites as SNPs (Ye *et al.*, 2014). Conversely, when lower mtDNA copy numbers are assumed, the likelihood that minor variants are assigned as erroneous sequence reads increases. Therefore, in order to mitigate these potential issues, GATK variant calling was performed using several 'ploidy' settings; haploidy, diploidy and tenploidy which assumes one, two and ten copies of the mitochondrial genome in addition to VarScan software (Koboldt *et al.*, 2009, 2012). Only concordant macro-haplogroup assignments with high HaploGrep2 quality scores (> 80 %) were carried forward for further analysis.

More recently, a bioinformatics pipeline called MToolBox, which implements a highly automated computational strategy for extracting data from whole exome and whole genome sequencing datasets, has become popular for the reconstruction and analysis of the human mitochondrial genome (Calabrese *et al.*, 2014). MToolBox can detect insertions and deletions (ins/dels) and assess the heteroplasmic fraction of variant alleles whilst providing a related confidence interval. In addition, it provides pathogenicity scores, profiles of genome variability and disease-associations for identified mitochondrial variants (Calabrese *et al.*, 2014). Whilst the MToolBox workflow was not used within the present study, it is

particularly useful for datasets which have a high depth of sequencing (i.e. a high number of reads at each base position). Deep sequencing increases the likelihood that minor heteroplasmic variants are detected within a sample, therefore bioinformatics tools that are capable of accurately measuring this 'heteroplasmic load' are highly desirable.

In this chapter, the use of next generation sequencing to identify SNPs from across the entire mitochondrial genome has allowed for the classification of patient samples into both their macro- and sub-haplogroups. This demonstrates progression from previous studies which have failed to assign sub-haplogroups due to the use of SNP array technologies, such as the Sequenom MassARRAY platform, to genotype samples (Guzmán-Fulgencio *et al.*, 2013). In addition, whole genome sequencing has enabled the identification of SNPs in samples which are not necessarily characteristic of the assigned haplogroup. This may be of importance if the additional SNPs are non-synonymous and effect the structure or function of a mitochondrial protein of interest.

Within this study, a significant association between mitochondrial macro-haplogroup and statin related myopathy was not identified. The distribution of mitochondrial haplogroups in both the case and control groups resembled that of the healthy volunteer cohort and the Northern European population (Eupedia, 2018). Stratification of the statin myopathy cases based upon phenotypic severity did not reveal any associations of statistical significance. Due to the genetic association between the coding variant rs4149056 (p.Val174Ala) in the *SLCO1B1* gene being more closely associated with simvastatin-related myopathy, patients were also stratified based upon the type of statin that they were prescribed (Brunham *et al.*, 2012). In the case of both simvastatin and atorvastatin, the most abundant statins within the cohort, there were no overall associations identified between macro-haplogroup and patient status.

It must be noted that haplogroup-disease association studies performed within this chapter have only considered the overarching patient macro-haplogroup (i.e. H vs J) despite each sample being assigned a higher resolution sub-haplogroup classification (i.e. H1 vs J1) by HaploGrep2 (Appendix III/IV). Clustering of samples into their respective macro-haplogroups disregards much of the diversity and mutational variation which defines each of the sub-haplogroups. For example, macro-haplogroup H is the largest and most diverse of the European haplogroups and can be divided into more than 10 major subclades, each of which can be further subdivided themselves (Roostalu *et al.*, 2007). However, within the PREDICTION-ADR cohort a total of 280 unique sub-haplogroups were identified, therefore

the frequency of each haplogroup would be exceptionally low within the sample population resulting in insufficient statistical power to detect change.

One of the most significant drawbacks of the study was the extraction of genomic DNA from whole blood instead of skeletal muscle. Whilst collection of venous blood samples is easier, quicker and less invasive than performing skeletal muscle biopsies, few studies have examined how mtDNA heteroplasmic load varies across different tissues of the same individual. It is thought that in post-mitotic cells such as myocytes, mutations can accumulate over time due to mtDNA molecules being continuously destroyed and replicated in a process called relaxed replication. In heteroplasmic cells, it is possible that a mutated mtDNA molecule may be replicated more frequently than a wild-type molecule (e.g. a pathogenic deletion will result in an mtDNA molecule which is several kilobases shorter than the wild-type molecule, allowing it replicate faster), thus changing the heteroplasmic load of a tissue over the course of a lifetime (Stewart and Chinnery, 2015; Schröder *et al.*, 2015). Conversely, in rapidly dividing hematopoietic cells, mtDNA molecules are randomly segregated between daughter cells during mitosis in a process called vegetative segregation. If heteroplasmic variants are present, each cell may receive different proportions of wild-type and mutant mtDNA molecules. Therefore, mutant molecules may be lost more readily through selection or genetic drift (Stewart and Chinnery, 2015).

It is also important to acknowledge that genomics, as a standalone approach, is insufficient as a means to aid drug development or completely resolve the mechanistic nature of adverse drug reactions. Biological networks are extremely complex and are affected by not only changes to genetic coding sequences but also transient responses to stimuli at the level of protein activity and posttranslational modification. Thus, an integrative systems pharmacology approach combining 'multi-omic' datasets as well patient history and functional *in vitro* experimentation, is necessary to achieve a better understanding of the biology behind drug response phenotypes (Schwab and Schaeffeler, 2012). This is particularly pertinent in the case of SRM given that previous genetics studies have identified multiple pathways that may lead to the development of myopathic symptoms in patients receiving statins, including altered pharmacokinetics, immunological responses, muscle regeneration, mitochondrial function and underlying susceptibility to inherited myopathy (Brunham *et al.*, 2018; Ghatak *et al.*, 2010).

In reference to the integration of *in vitro* studies, investigations concerning the effects of mitochondrial genome variation upon susceptibility to adverse drug reactions or disease

should ideally be supported by functional interrogations using trans-mitochondrial, cytoplasmic hybrid (cybrid) modelling (Figure 5.3). This technique involves the fusion of nucleated cells, which have undergone depletion of their endogenous mtDNA to form rho0 cells, with non-nucleated cytoplasts (platelets) from donors of a known mitochondrial haplogroup. The ultimate goal being to re-populate the nucleated cell with mtDNA from the cytoplast, allowing for the generation of different cellular models with an identical nuclear background but variable mtDNA haplogroup (Wilkins *et al.*, 2014).

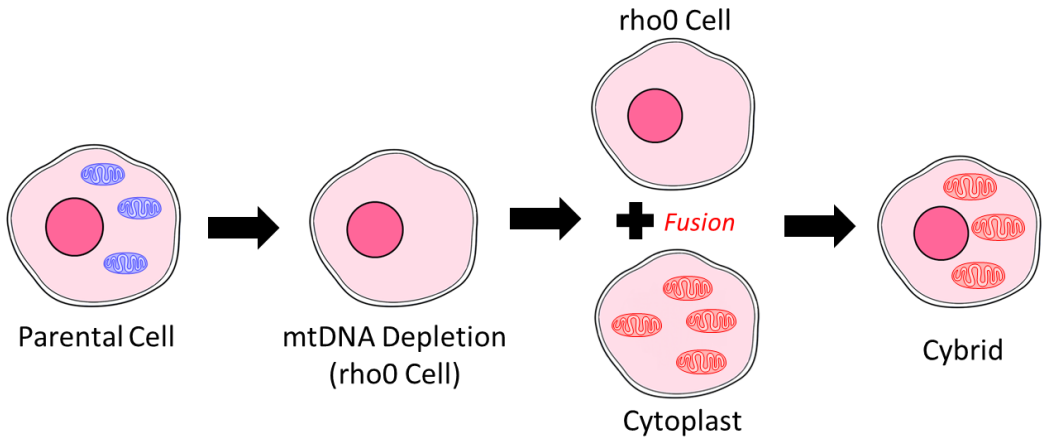

Figure 5.3 Cybrid generation technique. Cybrids are produced by combining cytoplasm from nucleated cells, depleted of their own endogenous mtDNA, with non-nucleated cells or cytoplasts.

5.5 Conclusions

In conclusion, this study represents the first mtDNA haplogroup-disease association study performed in the context of statin-related myopathy. Whilst no significant associations were identified between the clustered macro-haplogroups and patient status, differences may be detected when comparing individual sub-haplogroups. Such a study would better account for the accumulative mutations and by extension, the functional variations that are characteristic of the different mtDNA subclades, however it would require a far greater number of participants to adjust for the relatively low frequency of each sub-haplogroup. Future studies should also endeavour to compare the mtDNA haplogroup assignment concordance between whole blood and skeletal muscle biopsies from the same individuals to determine if blood is an appropriate surrogate sampling material.

Chapter 6

General Discussion

Contents

6.1 Introduction..... 181

6.2 The Mechanistic Nature of Statin-Induced Respiratory Dysfunction..... 182

6.3 Predictive *In Vitro* Skeletal Micro-Tissue Modelling 184

6.4 Studying the Effect of Mitochondrial Genotype upon Susceptibility to Drug-Induced Myopathy..... 185

6.5 Concluding Remarks..... 186

6.1 Introduction

Since their introduction, statins have been and will likely remain the pharmaceutical intervention strategy of choice for the treatment and prevention of cardiovascular and cerebrovascular disease. Indeed, it is evident that statin pharmacotherapy will continue to play a critical role in the management of CVD as the global disease burden increases, not least due to its efficacy, cost-effectiveness and firm foothold in the clinical formulary (Weintraub, 2017). When considered in conjunction with factors such as alterations to patient eligibility guidelines and the rising prevalence of obesity, a disease heavily implicated in the pathogenesis of CVD, it is unsurprising to find that statin uptake, both in the UK and indeed globally, has been increasing significantly over time (O'Keeffe *et al.*, 2016; Purcell, 2013).

As a consequence of the seemingly unwavering popularity of statins, investigations concerning the molecular and clinical determinants of statin-related myopathy, the most significant and commonly occurring barrier to atherosclerotic disease risk reduction, are both timely and absolutely necessary for the future of CVD management. This is particularly pertinent as statins are often prescribed on a 'primary prevention' basis to individuals without pre-existing atherosclerotic cardiovascular disease, thus potentiating adverse effects in otherwise 'healthy' individuals.

Therefore, the overall risk of a patient developing an adverse drug reaction must be considered when initially prescribing statins and subsequently monitoring their usage over time. In order to maximise the benefits of pharmaceutical intervention whilst concomitantly reducing the potential for myopathic outcomes, understanding the dynamic interplay between the pharmacology of the drug and an individual's underlying susceptibility to adverse effects is pivotal. However, establishment of myopathy risk is not only important for the prevention of myopathy in susceptible patients but also for the identification of factors which confer drug tolerance. This combined knowledge may help to enhance patient compliance with treatment regimens, improve quality of life and increase treatment efficacy thus helping to alleviate the absolute burden of CVD upon healthcare providers.

Drug-induced mitochondrial dysfunction has been implicated as one of several putative mechanisms by which myopathic symptoms are potentiated in some statin recipients. Therefore, the overarching aim of this research was to first establish the differential effects of statin chemical species (i.e. inactive lactones versus active β-hydroxy acids) upon the functionality of the mitochondrial respiratory chain. Based upon these findings, the

remainder of the thesis focussed upon the development of an advanced *in vitro* model of skeletal muscle to identify functional bioenergetic factors which may confer an enhanced or diminished risk of statin-mediated mitochondrial perturbations. Finally, a novel mtDNA haplogroup-disease association study was performed for a statin myopathy case-control cohort to determine if there was a link between mitochondrial genotype and patient status.

6.2 The Mechanistic Nature of Statin-Induced Respiratory Dysfunction

Investigations performed within this research identified complex II as a major, but not an exclusive site, of simvastatin-mediated respiratory dysfunction in L6 myocytes under acute and extended dosing regimens. In addition, it was noted that myobundles produced from statin-tolerant donors dedicated a greater proportion of their maximal respiratory output to spare respiratory capacity, a metabolic parameter which is thought to be partially governed by complex II activity (Pfleger *et al.*, 2015). However, in order to bridge these observations together, interrogations of complex driven respiration in myobundles would be required at baseline and post statin exposure for each donor category (i.e. statin-naïve, tolerant and intolerant). This would help to clarify if complex II activity is indeed the source of elevated spare respiratory capacity in the statin-tolerant myobundles or if it originates from alternative and/or additional sites.

It has been previously suggested that statin-induced respiratory dysfunction may be mitigated by enhancing an individual's baseline respiratory function (Allard *et al.*, 2018). This in essence forms the rationale behind the supplementation of ubiquinone (CoQ10) to statin recipients. By bolstering the mitochondrial ubiquinone pool with exogenously supplied CoQ10, endogenous biosynthetic deficits mediated by the inhibition of the mevalonate pathway may be addressed and electron transfer would, theoretically, cease to be impeded. However, in practice this yields conflicting results in patient studies, potentially due to the poor bioavailability of orally administered CoQ10 or a lack of a CoQ10 deficit in skeletal muscle all together (Bergamini *et al.*, 2012; Laaksonen *et al.*, 1996). Further *in vitro* investigations have demonstrated that by promoting convergent electron flow into the ubiquinone pool via the stimulation of glycerol-3-phosphate dehydrogenase (G3PDH) and the β-oxidation pathway, attenuation of phosphorylating respiration by several different statins can be partially reversed (Schirris *et al.*, 2015). In addition, increased spare respiratory capacity, via complex II, has been shown to promote cellular survival via sirtuin-3 (SIRT3) dependent mechanisms in a number of different cell types (Nickens *et al.*, 2013; Dhingra and Kirshenbaum, 2015; Yadava and Nicholls, 2007; Pfleger *et al.*, 2015). SIRT3 influences

multiple pathways of mitochondrial oxidative metabolism and the rate of ROS production, therefore activation of SIRT3 or the metabolic sensor AMPK may be an effective means to partially attenuate statin-mediated mitochondrial dysfunction and promote cell survival in myocytes (Figure 6.1) (Ansari *et al.*, 2017).

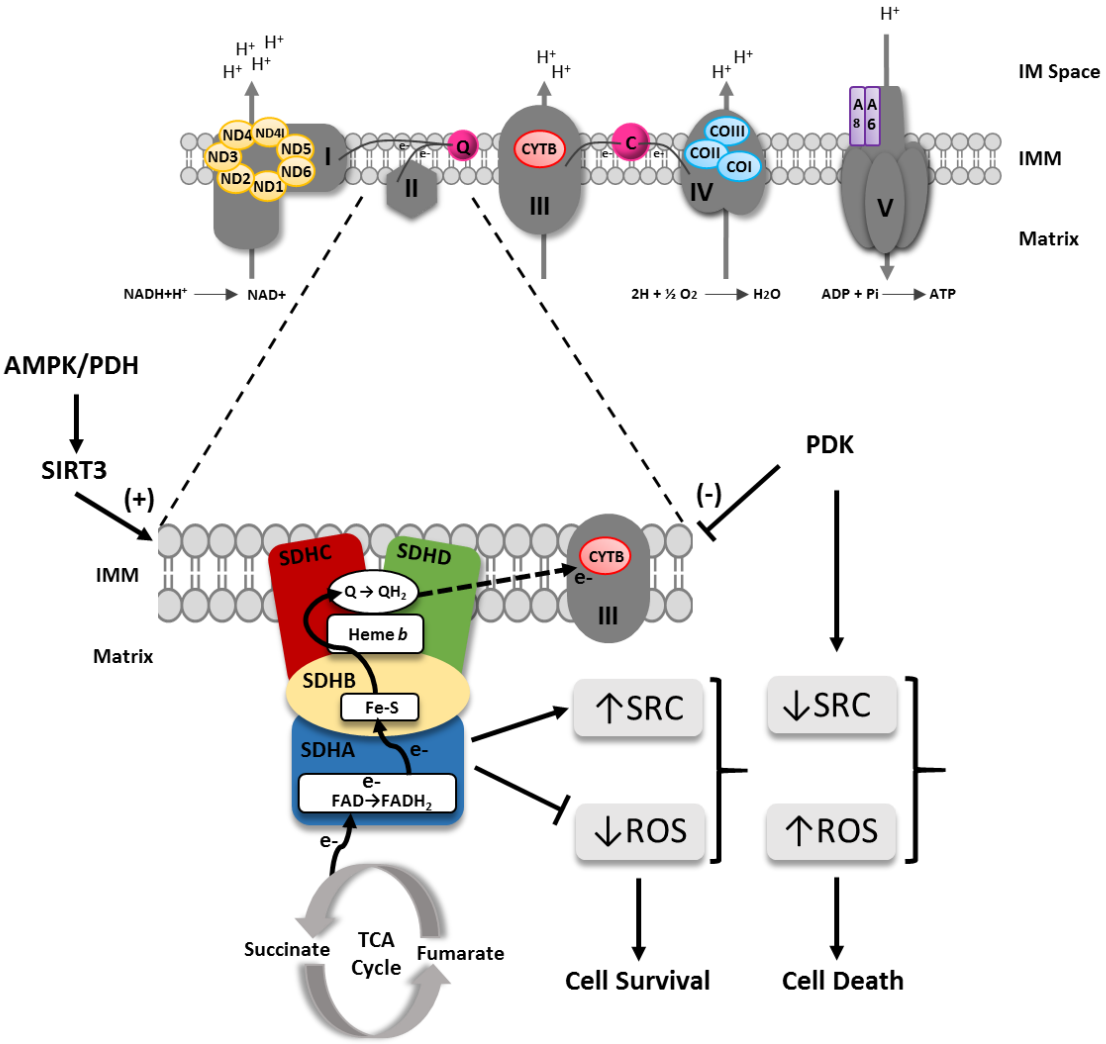

Figure 6.1 Succinate dehydrogenase (SDH), also known as complex II is comprised of four subunits (SDHA-D). Complex II regulates spare respiratory capacity (SRC) and cell survival as a functional link between the tricarboxylic acid (TCA) cycle and the electron transport chain (ETC). Complex II regulates SRC by increasing substrate flux coincident with increased metabolic demand through the TCA cycle and ETC. Pyruvate dehydrogenase kinase (PDK) negatively regulates complex II activity resulting in diminished SRC. The metabolic sensors AMP-activated protein kinase (AMPK) and metabolic regulators pyruvate dehydrogenase (PDH) and the NADH-dependent class III deacetylase Sirtuin-3 (SIRT3), positively regulate SRC (Dhingra and Kirshenbaum, 2015).

Whilst not directly addressed within this thesis, it is also important to consider the effects that mitochondrial ageing and age-related dysfunction may have upon susceptibility to statin-related myopathy. Ageing is associated with the impairment of both the capacity and control of oxidative phosphorylation in skeletal muscle, particularly impacting upon the functionality of complexes I and IV but not complexes II and III (Desler *et al.*, 2012).

Furthermore, accumulation of mtDNA mutations in post mitotic tissues, increased ROS-mediated cellular damage and altered mitochondrial dynamics have also been noted in aged tissues (Chistiakov *et al.*, 2014). A combination of these factors may contribute to the enhanced risk of statin-induced myopathies amongst the elderly (Deichmann *et al.*, 2010).

6.3 Predictive *In Vitro* Skeletal Micro-Tissue Modelling

Adaptation of established tissue-engineering methodologies to generate micro-physiological models of human skeletal muscle within this thesis demonstrates marked progression, in relation to physiological relevance, from prior *in vitro* investigations performed using conventional myocyte culture. The ability to measure functional endpoints in a population or patient specific manner allows for the performance of pharmacological time- and dose-response studies which were previously unavailable or extremely limited for isolated human skeletal muscle. Indeed, a study published after the completion of this work exemplified the utility of a myobundle model, integrated with an *in situ* force monitoring system, to examine the relationship between therapeutically relevant statin exposure (10 nM) and contractile force generation in a longitudinal, non-invasive manner (Zhang *et al.*, 2018; Truskey, 2018).

As noted, skeletal micro-tissue modelling is very much in its infancy, this provides ample scope to modify and tailor systems for a multitude of different purposes. From a pharmacological perspective, the functional integration of other human micro-physiological organ systems, such as hepatic models, with engineered skeletal muscle provides an exciting opportunity to examine the effect of xenobiotics and their metabolites upon muscular function (Vernetti *et al.*, 2017). However, in order to realise the full potential of the myobundle model, more systematic manipulations of culture conditions are required to optimise the growth and differentiation of the myocytes. Skeletal muscle constructs, particularly those produced using human pluripotent stem cells (hPSC), suffer from incomplete maturation, expressing many foetal isoforms of muscle proteins compared to native adult muscle fibers (Martin *et al.*, 2013).

In addition, supplemental methods to manipulate the development of fast- and slow- twitch muscle fibers are needed. Satellite cells derived from muscle biopsies have been shown to adopt both the contractile and metabolic properties of their parental tissue, therefore constraining their initial phenotype *in vitro* (Khodabukus and Baar, 2015). This factor is also important to consider when examining the respiratory phenotypes of myobundles generated within this thesis, since tissue biopsy location varied from patient to patient.

A combination of electrical stimulation, use of specific media formulations, co-culture with neuronal cells or microRNAs could be used to bias differentiation to fast- or slow-twitch fiber types (Truskey, 2018). The ability to manipulate the contractile properties of micro-tissue constructs, derived from a single individual, would prove particularly useful in the study of fiber type selectivity during statin myopathy (Obayashi *et al.*, 2011; Sidaway *et al.*, 2009; Piette *et al.*, 2016). For example, Westwood *et al*., have previously shown that fast-twitch muscle fibers are preferentially susceptible to statin-mediated necrosis, and the tissue distribution reflects the distribution of the plasma membrane monocarboxylate transporter isoform 4 (MCT4) (Westwood *et al.*, 2005). Bioaccumulation of statins in fast-twitch muscle fibers may increase local cytoplasmic concentrations compared to plasma levels, although it remains to be determined if statins further bioaccumulate into the mitochondria (Westwood *et al.*, 2005; Bonen, 2001; Dykens and Will, 2007).

In summary, bioengineered skeletal micro-tissues present a novel platform from which to investigate statin-induced myopathy and will be an invaluable tool for investigating the pathophysiological mechanisms underpinning xenobiotic-induced myotoxicity within a personalised medicines context. Furthermore, the modelling holds the potential to be translated to other contractile tissue types such as cardiac or smooth muscle.

6.4 Studying the Effect of Mitochondrial Genotype upon Susceptibility to Drug-Induced Myopathy

The mitochondrial genotyping performed within this thesis did not identify any significant associations between mitochondrial macro-haplogroup and patient status in the context of statin-related myopathy. However, it is important to acknowledge that this was the first study of its kind to attempt to find a link between mtDNA genotype and SRM in a case-control cohort. Furthermore, statins are not the only compounds that are capable of perpetuating mitochondrial myopathy amongst recipients e.g. nucleoside-analogue reverse transcriptase inhibitors such as zidovudine and fialuridine (Dalakas, 2009). Indeed, a limited number of studies have successfully identified an association between mitochondrial haplogroup and drug-induced adverse effects in various organ systems to date (Hendrickson *et al.*, 2009; Canter *et al.*, 2010; Kampira *et al.*, 2013; Micheloud *et al.*, 2011). With this in mind, mitochondrial genotyping, as an underrepresented branch of pharmacogenomics, may serve as a useful tool for patient stratification under circumstances where mitochondrial genotype confers an enhanced risk to adverse effects mediated by drugs with known mitochondrial liabilities.

As mentioned in the preceding chapter, studies concerning the phenotypic effects of mitochondrial genome variation are often supported by functional studies using trans-mitochondrial cybrid modelling. At present there is a distinct lack of cybrid models of musculoskeletal derivation, however previous studies have demonstrated that myocytes, particularly L6 cells and human primary myoblasts can successfully undergo partial mtDNA depletion to form respiratory deficient cells (Mercy *et al.*, 2005; Park *et al.*, 2005; Herzberg *et al.*, 1993). Optimisation of mtDNA depletion protocols in an immortalised skeletal muscle line of human origin would first be required to produce true rho0 cells for cybrid generation (Mamchaoui *et al.*, 2011; Bigot *et al.*, 2009)

As with any myocytes grown in a two-dimensional setting, the physiological relevance of the *in vitro* modelling may be improved by incorporating the cells into a 3D micro-tissue construct. Theoretically, if cybrids could be generated from an immortalised human cell line such as those described by Mamchaoui *et al*., with a proportion of remnant fibroblasts retained amongst the myocyte population, fabrication of functional myobundles with a homogeneous nuclear background and variable mtDNA genotype could be possible (Bigot *et al.*, 2009; Mamchaoui *et al.*, 2011; Wilkins *et al.*, 2014). Such a model would be particularly beneficial for the acquisition of measurable force output data in tandem with high resolution respirometry to map the metabolic and contractile profiles of myobundles against mtDNA haplogroup (Davis *et al.*, 2017a). However, the true feasibility of this is debatable due to the poor differentiation potential of myocytes which have undergone mtDNA depletion (Herzberg *et al.*, 1993). Future work should also endeavour to integrate clinical data, mitochondrial genotyping and functional interrogations of mitochondrial respiration from the same individual as this was not achieved within the confines of this thesis.

6.5 Concluding Remarks

Statin-mediated mitochondrial dysfunction has a role to play in the development of myopathic symptoms amongst susceptible patients. However, what is less clear is the relative contributions of direct respiratory inhibition and/or modulation of peripheral pathways which interact with the wider mitochondrial signalling network, to the overall pathophysiological mechanism. Some studies suggest that mitochondrial dysfunction is more of a symptom, rather than a cause, of myopathy i.e. adverse mitochondrial effects do not precede the degeneration of myofibers (Schaefer *et al.*, 2004). In contrast, others have recognised statin-induced respiratory dysfunction as an ‘initiator’ event which precipitates

the injurious effects of aberrant Ca^{2+} handling within myocytes (Sirvent, Mercier, *et al.*, 2005; Sirvent *et al.*, 2012).

Furthermore, statin-induced myopathy does not often manifest acutely in recipients, generally taking several weeks or months of continuous treatment before a clinical phenotype is evident (Laufs *et al.*, 2015). This parallels in nature with the 'biochemical threshold' theory of drug-induced mitochondrial dysfunction. According to this theory, it is possible to considerably inhibit the activity of one or several respiratory chain complexes for a period of time until a critical value is met (Rossignol *et al.*, 2003). Therefore, it could be postulated that the initial mitochondrial insult by statins is subclinical or transient in the majority of tolerant individuals, yet amplified in patients who harbour additional genetic and/or functional bioenergetic defects that differentiate them from those who can be safety treated.

Appendices

Appendix I

USB file 1: LMB study sponsorship protocol

USB file 2: LMB study approval

Appendix II

USB file 3: LMB patient clinical information table

Appendix III

Summary of concordant sub-haplogroup assignments for the PREDICTION-ADR cohort. Gender (1), male; gender (2) female. Status (1), tolerant control; status (2), statin myopathy case. SRM, statin-related myopathy classification in accordance with (Alfirevic *et al.*, 2014).

Sample ID	Age	Gender	Status	Statin	SRM	Haplogroup
446-14.56_CGTATCTCGA.fastq.gz	61	1	1	Atorvastatin	0	E1a1a1
101-STA10_0162_CAGCTATAGC.fastq.gz	49	1	1	Simvastatin	0	H
423-12.77_CTAGTCTCGT.fastq.gz	66	1	1	Pravastatin	0	H
104-STA10_0182_GCAGTATGCG.fastq.gz	58	1	1	Simvastatin	0	H
428-94228632_GACGTCTGCT.fastq.gz	77	1	1	Simvastatin	0	H+16129
440-9422570_GTACTCGCGA.fastq.gz	77	1	1	Atorvastatin	0	H+16129
109-STA10_0203_GACTCATGCT.fastq.gz	70	1	1	Simvastatin	0	H1
25-U_4140_TGTGTGCATG.fastq.gz	80	2	2	Simvastatin	SRM 5	H1
530-3095708_TACACAGTAG.fastq.gz	77	1	2	Pravastatin	SRM 4	H1
254-SRS-006_TTGTCACATC.fastq.gz	55	1	2	Simvastatin	SRM 3	H1+152

439-1919751_GCACGTAGCT.fastq.gz	59	1	1	Simvastatin	0	H1
504-15.34_AGTGTGTCTA.fastq.gz	58	1	1	Simvastatin	0	H1
179-STA10_0627_ATGTCATGCT.fastq.gz	67	1	1	Simvastatin	0	H10a
348-hdf11_ACTCAGTTAC.fastq.gz	72	1	1	Atorvastatin	0	H10e
408-1349403_GTGTATGCGT.fastq.gz	78	1	2	Simvastatin	SRM 4	H1+16189
411-1919689_GAGTGTCACT.fastq.gz	60	2	2	Simvastatin	SRM 4	H1+16239
410-1902535_CATGTCGTCA.fastq.gz	72	1	2	Simvastatin	SRM 3	H11a
57-STA15_0967_TACATCGCTG.fastq.gz	75	1	2	Simvastatin	SRM 5	H11a
28-U_4507_GAGTGCATCT.fastq.gz	61	1	2	Atorvastatin	SRM 4	H11a1
181-STA10_0640_ATACAGTCTC.fastq.gz	70	1	1	Pravastatin	0	H10e1
599-STAGE-945_GGTCAGTGTA.fastq.gz	75	2	2	Atorvastatin	SRM 4	H11a1
371-lhc147_ATCTGTCCAT.fastq.gz	70	1	1	Atorvastatin	0	H10e1
186-STA10_0665_ACGATACACT.fastq.gz	77	2	1	Pravastatin	0	H10f
123-STA10_0267_TGTACAGCGA.fastq.gz	70	1	1	Simvastatin	0	H11a2a1
307-CMS-003_GCAGATAAGT.fastq.gz	57	1	2	Rosuvastatin	SRM 4	H11a2a
451-1412838_TCACGCTATG.fastq.gz	71	1	1	Simvastatin	0	H11a2a1
489-2468936_TATCTCATGC.fastq.gz	57	1	2	Atorvastatin	SRM 3	H11a2a
373-liv192_AGTGGCAGGT.fastq.gz	81	2	1	Atorvastatin	0	H13a1a

591-NEW-6_TTGTTGCTGT.fastq.gz	0	2	2	NK	0	H11a7
442-1348383_CATGCATCAT.fastq.gz	79	2	2	Simvastatin	SRM 3	H13a1a
395-14.67_CTCTGGACGA.fastq.gz	60	1	1	Atorvastatin	0	H15a1
454-2506310_TGATCAGTCA.fastq.gz	68	2	2	Simvastatin	SRM 3	H16
323-STAGE-1039_GTACTAAGAG.fastq.gz	57	1	2	Simvastatin	SRM 3	H1a
214-STA10_0379_GGTTGGAGTT.fastq.gz	67	1	1	Simvastatin	0	H16
249-CIS-005_TGGAGCATGT.fastq.gz	74	1	2	Atorvastatin	SRM 3	H1a1
278-STA15-127_TGGATGACAT.fastq.gz	61	1	2	Simvastatin	SRM 3	H1a1
65-STA10_0722_TACTGAGCTG.fastq.gz	66	1	2	Simvastatin	SRM 3	H1a1
298-WES-002_TCTCGGATAG.fastq.gz	46	1	2	Simvastatin	SRM 3	H1a1a1
455-2782503_TGATACTCTG.fastq.gz	67	2	2	Simvastatin	SRM 3	H1ab
566-13506803_CGAGCTAGCA.fastq.gz	49	1	1	Atorvastatin	0	H1a
146-STA10_0428_GACGATCGCA.fastq.gz	82	2	1	Atorvastatin	0	T1a1
52-STA15_0943_GCTCATATGC.fastq.gz	67	1	2	Atorvastatin	SRM 3	H1ag1
538-33167893_GCTGACAGAG.fastq.gz	69	2	2	Pravastatin	SRM 4	H1am
54-STA15_0315_TAGCGCGTAG.fastq.gz	80	1	2	Simvastatin	SRM 3	H1am
183-STA10_0655_AGAGATATCA.fastq.gz	82	2	1	Simvastatin	0	H1at1a
269-STA15-922_TCGAGGTACT.fastq.gz	71	1	2	Simvastatin	SRM 3	H1ao1

351-hdf2_AGTGGTGATC.fastq.gz	84	1	1	Simvastatin	0	H1at1a
365-bvh822_AAGTACACTC.fastq.gz	53	1	1	Atorvastatin	0	H1b1+16362
561-13.55_AGACTATATC.fastq.gz	64	1	1	Simvastatin	0	H1b1+16362
120-STA10_0260_GAGACTATGC.fastq.gz	68	1	1	Pravastatin	0	H1ba
403-1413948_TACATCGCTG.fastq.gz	81	1	1	Simvastatin	0	H1bb
435-1922963_GAGTGCATCT.fastq.gz	66	1	2	Atorvastatin	SRM 3	H1ap1
571-14160844_GATATATGTC.fastq.gz	68	2	1	Simvastatin	0	H1bb
519-1352001_TGTACAGCGA.fastq.gz	57	1	1	Atorvastatin	0	H1bk
212-STA10_0361_GATGGTTGTA.fastq.gz	46	1	1	Simvastatin	0	H1bs
188-STA10_0671_ATCGCTACAT.fastq.gz	70	1	1	Simvastatin	0	H1c
13-U_3609_GAGCTAGTGA.fastq.gz	68	2	2	Simvastatin	SRM 5	H1b1
234-STA10-0079_TTGTCCTTGC.fastq.gz	60	1	2	Simvastatin	SRM 3	H1b1e
198-STA10_0198_GTGAAGGTAA.fastq.gz	62	1	1	Atorvastatin	0	H1c
427-1922786_GACTGTACGT.fastq.gz	85	2	1	Simvastatin	0	H1c
14-U_3636_CGTGCTGTCA.fastq.gz	76	1	2	Simvastatin	SRM 5	H1bs
171-STA10_0555_ACAGTCATAT.fastq.gz	55	1	1	Simvastatin	0	K1a1b1
332-BUT-003_CCAGAACAGA.fastq.gz	55	1	2	Simvastatin	SRM 3	H1c
360-yft38_CATCAACATG.fastq.gz	64	2	1	Simvastatin	0	H1c11

177-STA10_0604_ATCACTCATA.fastq.gz	67	1	1	Simvastatin	0	N1a1a1a2
579-9.46_GCGTAGACGA.fastq.gz	72	2	1	Simvastatin	0	H1c9a
39-STA15_0098_CAGTCAGAGT.fastq.gz	60	1	2	Simvastatin	SRM 4	H1c
151-STA10_0455_AGAGTCGCGT.fastq.gz	61	1	1	Atorvastatin	0	H1e1a6
169-STA10_0543_ACATAGTATC.fastq.gz	55	1	1	Simvastatin	0	H1e1b1
110-STA10_0206_GTCTGATACG.fastq.gz	70	1	1	Simvastatin	0	H1g1
508-1351728_GTGACGTACG.fastq.gz	61	2	1	Simvastatin	0	H1g1
583-14.58_ACTGATGTAG.fastq.gz	61	2	1	Atorvastatin	0	H1g1
585-2.27_TAGTACTAGA.fastq.gz	88	2	1	Simvastatin	0	H1j
541-14125416_GACTCATGCT.fastq.gz	82	1	1	Simvastatin	0	H1j7
468-3152195_GTCGTGTACT.fastq.gz	77	2	2	Simvastatin	SRM 3	H1c8
15-U_3637_GATCGTCTCT.fastq.gz	58	1	2	Simvastatin	SRM 5	H1e1b1
195-STA10_0165_TAGGTGGAAT.fastq.gz	61	1	1	Simvastatin	0	H1m
2-U_2986_GTGTATGCGT.fastq.gz	65	1	2	Atorvastatin	SRM 4	H1g
311-NEW-004_GGAACACAGG.fastq.gz	33	1	2	Atorvastatin	SRM 5	H1g1
74-STA10_0749_TAGTCTGTCA.fastq.gz	61	1	2	Simvastatin	SRM 3	H1m
64-STA10_0695_GAGATCAGTC.fastq.gz	73	2	2	Simvastatin	SRM 3	H1n+146
245-CIS-001_TGTTCGATAG.fastq.gz	63	1	2	Simvastatin	SRM 3	H1n1

356-yft53_AAGCGTAGAA.fastq.gz	83	2	1	Atorvastatin	0	H1z
128-STA10_0326_GCGAGATGTA.fastq.gz	79	1	1	Atorvastatin	0	H24a
418-1902966_TATCGATGCT.fastq.gz	55	1	1	Atorvastatin	0	H24a
96-STA10_0030_GTAGTACACA.fastq.gz	56	2	1	Simvastatin	0	H24a
29-U_4511_TGCGTAGTCG.fastq.gz	47	1	2	Simvastatin	SRM 4	H1n4
279-STA15-222_GATCCTGAGC.fastq.gz	63	1	2	Atorvastatin	SRM 3	H1o
226-STA10_0667_TATGGTAAGG.fastq.gz	39	2	1	Simvastatin	0	H27a
30-U_4602_CTGTGTCGTC.fastq.gz	73	2	2	Atorvastatin	SRM 5	H1o
483-19025711_GTGCGCTAGT.fastq.gz	62	2	1	Simvastatin	0	H27a
478-2712168_GTGATACTGA.fastq.gz	65	2	2	Simvastatin	SRM 3	H1v
18-U_3879_CATGTCGTCA.fastq.gz	55	1	2	Simvastatin	SRM 5	H27a
308-NEW-001_GTCGGCTCTA.fastq.gz	69	2	2	Atorvastatin	SRM 3	H27a
285-STA15-424_TAGCTTCACT.fastq.gz	72	1	2	Atorvastatin	SRM 4	H28
211-STA10_0344_GGTGTCTTGT.fastq.gz	62	1	1	Simvastatin	0	H2a1a
523-1418638_ACGTGCTCTG.fastq.gz	73	1	1	Atorvastatin	0	H2a1a1
6-U_3430_GCGTCGTGTA.fastq.gz	69	1	2	Simvastatin	SRM 5	H28a
207-STA10_0300_TGTGAATCTC.fastq.gz	72	1	1	Atorvastatin	0	H2a1e1a
567-14175862_CGATCGACTG.fastq.gz	77	1	1	Simvastatin	0	H2a2b1a1

87-BUT-001_GTGATACTGA.fastq.gz	65	2	2	Rosuvastatin	SRM 3	H2a1+146
103-STA10_0181_GCACGCGTAT.fastq.gz	69	2	1	Atorvastatin	0	H2a2b4
346-elh64_AATGCAGTGT.fastq.gz	68	1	1	Atorvastatin	0	H2a2b5a
524-1550080_TACATGATAG.fastq.gz	62	1	1	Atorvastatin	0	H2a3
150-STA10_0453_TAGCATACAG.fastq.gz	58	2	1	Simvastatin	0	H3
173-STA10_0568_AGCATCTATA.fastq.gz	51	1	1	Simvastatin	0	H3
487-1418960_GAGATCAGTC.fastq.gz	62	1	1	Atorvastatin	0	H3
456-2890272_GCGTCGTGTA.fastq.gz	48	1	2	Simvastatin	SRM 4	H2a1a1
134-STA10_0346_CTAGCAGATG.fastq.gz	59	2	1	Simvastatin	0	H3+152
275-STA15-946_CTGCGAATGT.fastq.gz	61	2	2	Atorvastatin	SRM 3	H2a2b1a1
121-STA10_0261_CAGAGCTAGT.fastq.gz	68	2	1	Simvastatin	0	H31a
415-1419837_GTGAGAGACA.fastq.gz	87	1	1	Simvastatin	0	H39
461-1551326_TCTCTGTGCA.fastq.gz	61	1	1	Simvastatin	0	H39
470-3872933_CTATGCGATC.fastq.gz	61	2	2	Simvastatin	SRM 3	H2a2b4
485-1350713_TACGCTGCTG.fastq.gz	48	1	1	Simvastatin	0	H3ao
119-STA10_0241_CGAGCTAGCA.fastq.gz	76	1	1	Simvastatin	0	H3b1b1
424-1927529_CTGTACGTGA.fastq.gz	62	1	2	Fluvastatin	SRM 3	H3+152
450-1351865_CACTATGTCG.fastq.gz	84	2	1	Simvastatin	0	H3g3

22-U_4024_GTCATGCGTC.fastq.gz	56	1	2	Rosuvastatin	SRM 4	H30b
600-STAGE-1062_GTAATGGAGT.fastq.gz	74	1	2	Atorvastatin	SRM 4	H39b
516-3525461_TCATATCGCG.fastq.gz	69	1	2	Atorvastatin	SRM 3	H3aa
45-STA15_0863_TATGCGCTGC.fastq.gz	53	2	2	Simvastatin	SRM 3	H3ag
237-IOW-003_CAGGTCACAT.fastq.gz	61	1	2	Simvastatin	SRM 3	M1a1i
117-STA10_0231_CACATACAGT.fastq.gz	71	1	1	Simvastatin	0	H3v+16093
41-STA15_0141_GTATGAGCAC.fastq.gz	78	1	2	Atorvastatin	SRM 3	H3b1a
317-STAGE-168_TCGAACTGCA.fastq.gz	73	2	2	Simvastatin	SRM 3	H3b1b1
88-SWB-001_CTAGATCTGA.fastq.gz	59	1	2	Rosuvastatin	SRM 3	H3b1b1
244-RNS-001_GTGGCTTCGT.fastq.gz	72	2	2	Atorvastatin	SRM 5	U4b1b1a
201-STA10_0223_GGTCAGTGTA.fastq.gz	79	1	1	Simvastatin	0	H3y
528-94226690_TACGTATAGC.fastq.gz	55	2	2	Fluvastatin	SRM 4	H3g1b
167-STA10_0538_ATCATATCTC.fastq.gz	68	2	1	Simvastatin	0	H41a
136-STA10_0349_GCAGCTGTCA.fastq.gz	82	1	1	Simvastatin	0	H45
406-1413490_TGTGTCACTA.fastq.gz	78	1	1	Simvastatin	0	H45
217-STA10_0435_TACTAGGATC.fastq.gz	67	1	1	Atorvastatin	0	H4a1a+195
507-9423813_CGCAGAGCAT.fastq.gz	75	1	1	Pravastatin	0	H4a1a1
215-STA10_0380_TGGTGTCCGT.fastq.gz	54	1	1	Atorvastatin	0	H4a1a1a1a

11-U_3598_CGCTGTAGTC.fastq.gz	79	1	2	Simvastatin	SRM 5	H3h
503-2976706_AGTCAGACGC.fastq.gz	71	1	2	Simvastatin	SRM 3	H3h
107-STA10_0197_TGCGAGACGT.fastq.gz	58	1	1	Simvastatin	0	H4a1a3
596-STAGE-241_GTGAAGGTAA.fastq.gz	62	1	2	Atorvastatin	SRM 3	H3t
580-5.3_GAGACTATGC.fastq.gz	81	2	1	Atorvastatin	0	H5
16-U_3775_GTGCTGTCGT.fastq.gz	66	1	2	Simvastatin	SRM 4	H3v+16093
259-STA15-468_GTAGCCAGTA.fastq.gz	59	1	2	Atorvastatin	SRM 3	K1c2
26-U_4429_GAGTGTCACT.fastq.gz	73	1	2	Simvastatin	SRM 4	W
92-HES-005_CTATACAGTG.fastq.gz	72	1	2	Simvastatin	SRM 3	H4a1a1
500-2661416_TATAGAGATC.fastq.gz	58	1	2	Simvastatin	SRM 4	H4a1a1a
469-3782293_GATCGTCTCT.fastq.gz	52	1	2	Atorvastatin	SRM 4	H4a1a1a1a
525-1919257_ACAGTCATAT.fastq.gz	85	2	1	Simvastatin	0	H52
357-yft60_GACAGCAAGC.fastq.gz	70	1	1	Atorvastatin	0	H58a
98-STA10_0132_AGTGTGTCTA.fastq.gz	75	1	1	Simvastatin	0	H5a1
296-IOW-004_GTGTTCGGTC.fastq.gz	73	1	2	Simvastatin	SRM 3	H4a1a3
66-STA10_0723_TAGTAGCGCG.fastq.gz	66	1	2	Simvastatin	SRM 3	H4a1a3
27-U_4441_CTAGTCTCGT.fastq.gz	65	2	2	Atorvastatin	SRM 5	U5b1e1
59-STA10_0025_GACTGTACGT.fastq.gz	67	2	2	Simvastatin	SRM 3	H4a1c

338-STAGE-377_CATACCTGAT.fastq.gz	87	1	2	Simvastatin	SRM 4	H5
274-STA15-896_TTGCAGATCA.fastq.gz	65	1	2	Atorvastatin	SRM 3	K1c2
235-TEL-002_CCTGTGTAGA.fastq.gz	74	2	2	Simvastatin	SRM 3	H5a1
250-SRS-001_GAAGGAGATA.fastq.gz	72	1	2	Atorvastatin	SRM 4	H5a1
180-STA10_0634_GCTGACAGAG.fastq.gz	70	1	1	Pravastatin	0	H5a1d
280-STA15-298_GTCGGTCTGA.fastq.gz	80	2	2	Rosuvastatin	SRM 3	H2a2b4
246-CIS-002_TCATTCAGTG.fastq.gz	87	2	2	Atorvastatin	SRM 5	H5a1c1a
283-STA15-420_GGTCGTGCAT.fastq.gz	82	2	2	Atorvastatin	SRM 4	T1a1
584-8.7_TCTACGACAT.fastq.gz	74	2	1	Atorvastatin	0	H5a1g1
89-SWB-002_TATCAGTCTG.fastq.gz	54	2	2	Rosuvastatin	SRM 3	H5a1c1a
438-1419430_GCTCATATGC.fastq.gz	80	2	1	Atorvastatin	0	H5b
288-STA10_0075_TTCGTTCCTG.fastq.gz	39	1	1	Simvastatin	0	H2a2a1
289-STA10_0239_CACTGCTTGA.fastq.gz	92	1	1	Simvastatin	0	I1f
97-STA10_0131_TGCTACATCA.fastq.gz	69	1	1	Simvastatin	0	H5b1
290-STA10_0248_TCTAGCGTGG.fastq.gz	69	1	1	Simvastatin	0	J1c2
228-STA10-0001_GGTAGAATGA.fastq.gz	77	1	2	Simvastatin	SRM 5	H5a1d
276-STA15-56_CTGTTCTAGC.fastq.gz	77	1	2	Pravastatin	SRM 3	H5a1d
133-STA10_0343_GCACTAGACA.fastq.gz	58	1	1	Simvastatin	0	H5b3

17-U_3858_TGAGCGTGCT.fastq.gz	66	1	2	Simvastatin	SRM 5	H5a8
297-WES-001_CTCAAGAAGC.fastq.gz	64	1	2	Simvastatin	SRM 3	U2e1a1
286-STA15-561_CAGATGTCCT.fastq.gz	79	1	2	Simvastatin	SRM 3	H5b1
23-U_4064_CTATGCGATC.fastq.gz	69	2	2	Atorvastatin	SRM 5	H5d
262-STA15-532_CGATCCTATA.fastq.gz	79	1	2	Atorvastatin	SRM 3	H66a
302-STA15_895_TCCTTGTTCT.fastq.gz	61	1	2	Simvastatin	SRM 3	H6a1a
243-HES-012_TCTTGTTCAC.fastq.gz	48	1	2	Rosuvastatin Ezetimibe	SRM 3	H6a1a
185-STA10_0662_AGTCAGACGC.fastq.gz	67	1	1	Simvastatin	0	H6a1a
162-STA10_0512_TCGATATCTA.fastq.gz	73	2	1	Fluvastatin	0	H6a1a3
306-BUT-006_GTATAACGCT.fastq.gz	69	1	2	Simvastatin	SRM 3	K1a1b1
149-STA10_0452_AGTCATCGCA.fastq.gz	46	1	1	Atorvastatin	0	H6a1b
55-STA15_0467_CGTCACAGTA.fastq.gz	72	1	2	Simvastatin	SRM 3	H6a1a
510-9423545_GACGATCGCA.fastq.gz	80	2	1	Simvastatin	0	H6a1b2
546-19191805_AGTCATCGCA.fastq.gz	84	1	1	Simvastatin	0	H6a1b2
106-STA10_0188_GCTACTAGCG.fastq.gz	78	1	1	Simvastatin	0	H6a1b3
202-STA10_0233_GTAATGGAGT.fastq.gz	74	1	1	Simvastatin	0	H6a1b3a
192-STA10_0102_ATCGCATAGA.fastq.gz	69	1	1	Atorvastatin	0	H6a1b4
263-STA15-685_TGACTAGCTT.fastq.gz	65	1	2	Simvastatin	SRM 3	H6a1a3

400-1902114_TGTGCTCGCA.fastq.gz	65	2	2	Simvastatin	SRM 3	H6a1a3
148-STA10_0448_ACATGTCTGA.fastq.gz	72	1	1	Simvastatin	0	H6c
319-STAGE-171_GAGCACGGAA.fastq.gz	73	1	2	Simvastatin	SRM 3	J1c2c1a
498-1417238_ACTCGATAGT.fastq.gz	68	1	1	Simvastatin	0	H7a1b
321-STAGE-974_TGCTGGCTTG.fastq.gz	72	2	2	Simvastatin	SRM 3	J1c5c1
190-STA10_0683_AGCAGTACTC.fastq.gz	65	1	1	Simvastatin	0	H7c2
63-STA10_0685_CAGCTGAGTA.fastq.gz	53	1	2	Simvastatin	SRM 3	H6a1a3
170-STA10_0550_ATGTATAGTC.fastq.gz	65	1	1	Simvastatin	0	H7c3
513-2870440_ATGTATAGTC.fastq.gz	53	1	2	Atorvastatin	SRM 3	H6a1b2e
194-STA10_0158_GTGTGGTTGT.fastq.gz	62	1	1	Simvastatin	0	H7c3
361-yft51_TGGCTACGCT.fastq.gz	86	2	1	Simvastatin	0	H7d
533-29449712_GACTAGTCAG.fastq.gz	92	2	2	Simvastatin	SRM 3	H7a1b
10-U_3594_CGCTATCAGT.fastq.gz	76	2	2	Atorvastatin	SRM 6	H7d
557-1349121_CAGAGAGTCA.fastq.gz	88	2	1	Simvastatin	0	H7d1
592-WES-5_GTGTGGTTGT.fastq.gz	74	2	2	Simvastatin	SRM 5	H89
342-STAGE-1009_AGGTAAGAGG.fastq.gz	46	1	2	Atorvastatin	SRM 3	HV0+195
277-STA15-103_CACTTGTGTG.fastq.gz	37	1	2	Atorvastatin	SRM 3	HV15
472-1551358_CAGTCAGAGT.fastq.gz	91	2	1	Simvastatin	0	H7i1

301-STA15_297_CCAAGAAGAA.fastq.gz	68	2	2	Atorvastatin	SRM 3	HV1b2
314-WES-003_GAAGCGCACT.fastq.gz	70	1	2	Simvastatin	SRM 5	HV22
232-STA10-0065_GCGTCTGAAT.fastq.gz	66	1	2	Simvastatin	SRM 3	HV5a
341-STAGE-607_TCTGGTCTCA.fastq.gz	72	1	2	Simvastatin	SRM 3	X2b+226
187-STA10_0666_AGCGAGTATG.fastq.gz	53	1	1	Atorvastatin	0	H80
344-elh53_GCACTGTTGC.fastq.gz	53	1	1	Atorvastatin	0	J2a1a1a2
496-15513540_CTGATGCAGA.fastq.gz	70	2	1	Simvastatin	0	H8c2
597-STAGE-417_TGTTGTGGTA.fastq.gz	78	2	2	Simvastatin	SRM 3	I1a1b
521-1412711_GATACACTGA.fastq.gz	82	1	1	Simvastatin	0	HV0
105-STA10_0186_TGATAGAGAG.fastq.gz	76	2	1	Simvastatin	0	HV5a
367-bvh836_ATGCCTATCA.fastq.gz	51	1	1	Atorvastatin	0	HV9
157-STA10_0486_AGTGTACTCA.fastq.gz	64	2	1	Atorvastatin	0	I1a1
142-STA10_0402_CAGAGAGTCA.fastq.gz	80	1	1	Atorvastatin	0	I1a1e
114-STA10_0224_CAGTCTACAT.fastq.gz	64	2	1	Pravastatin	0	I2
125-STA10_0280_TCACAGCATA.fastq.gz	67	1	1	Simvastatin	0	I2
131-STA10_0340_CGACGCTGAT.fastq.gz	71	1	1	Rosuvastatin	0	I2
359-yft72_CGCGACTTGT.fastq.gz	52	1	1	Atorvastatin	0	H6a1b3
602-STAGE-1087_GGAAGTAAGG.fastq.gz	55	1	2	Atorvastatin	SRM 3	I2a2

137-STA10_0369_ACGTATCATC.fastq.gz	59	2	1	Simvastatin	0	I2
362-bvh894_ACGCGGACTA.fastq.gz	64	2	1	Simvastatin	0	I5a
223-STA10_0629_GAATGGAAGA.fastq.gz	74	1	1	Pravastatin	0	I3
354-yft45_ACGCAGGAGT.fastq.gz	75	1	1	Atorvastatin	0	I5a2
320-STAGE-378_GCTCTAACAT.fastq.gz	71	1	2	Simvastatin	SRM 4	J1b1a1
238-RLS-002_GCCATGTCAT.fastq.gz	84	2	2	Atorvastatin	SRM 5	J1b1a1a
164-STA10_0522_TGAGATCATA.fastq.gz	76	2	1	Atorvastatin	0	J1b1a1
203-STA10_0254_CTCGTTATTC.fastq.gz	73	1	1	Simvastatin	0	J1b1a1+146
200-STA10_0212_GTTGATGAGT.fastq.gz	70	2	1	Simvastatin	0	J1b1a1e
486-1416484_TCGCGTGAGA.fastq.gz	53	2	1	Simvastatin	0	J1b1a1e
506-1350764_CAGTCTACAT.fastq.gz	68	1	1	Simvastatin	0	J1b2
99-STA10_0137_TCATATCGCG.fastq.gz	71	2	1	Simvastatin	0	J1b2
369-bvh843_ATAGCCGTGT.fastq.gz	61	1	1	Atorvastatin	0	J1c
582-9.43_GCAGCTGTCA.fastq.gz	72	2	1	Simvastatin	0	J1c15
299-STA15_894_CTCTGGACGA.fastq.gz	77	1	2	Simvastatin	SRM 3	J1b1a1a
86-AUS-002_CGTCTATGAT.fastq.gz	67	1	2	Atorvastatin	SRM 6	J1b1a1a
425-1348441_TATAGCACGC.fastq.gz	80	1	1	Simvastatin	0	J1c1a
481-3326934_GTGCTGTCGT.fastq.gz	53	1	2	Atorvastatin	SRM 4	J1c1a

517-3811166_TGCGAGACGT.fastq.gz	58	1	2	Atorvastatin	SRM 3	J1c1b1a
335-STAGE-741_GACAGGTGAC.fastq.gz	70	2	2	Simvastatin	SRM 5	J1c1e
526-11.17_ATGTCATGCT.fastq.gz	69	1	1	Atorvastatin	0	J1c1d
143-STA10_0412_TCGATCGACA.fastq.gz	73	2	1	Atorvastatin	0	J1c1g1
208-STA10_0303_CTAATCGTGT.fastq.gz	66	1	1	Simvastatin	0	J1c1g1
112-STA10_0215_GCGTAGACGA.fastq.gz	61	1	1	Pravastatin	0	J1c2
147-STA10_0444_TCATCATGCG.fastq.gz	73	1	1	Simvastatin	0	J1c2
443-14.33_CTATACAGTG.fastq.gz	62	1	1	Pravastatin	0	J1c2
404-1348286_TACTGAGCTG.fastq.gz	75	1	1	Simvastatin	0	J1b1a1
337-STAGE-507_CACGAAGAGC.fastq.gz	66	2	2	Simvastatin	SRM 3	J1c1e
465-2941761_CATGAGTGTA.fastq.gz	84	2	2	Simvastatin	SRM 3	J1c2
53-STA15_0150_CACTATGTCG.fastq.gz	76	1	2	Atorvastatin	SRM 3	J1c2b1
116-STA10_0230_TACACAGTAG.fastq.gz	53	1	1	Atorvastatin	0	J1c2b3
69-STA10_0730_TCTGAGCGCA.fastq.gz	77	1	2	Atorvastatin	SRM 3	J1c2b5
294-TEL-004_GGACAGATGG.fastq.gz	69	1	2	Simvastatin	SRM 3	J1c2h
158-STA10_0489_TGATGTATGT.fastq.gz	50	1	1	Atorvastatin	0	J1c2c1
484-9423349_CGCAGTCTAT.fastq.gz	79	2	1	Simvastatin	0	J1c3b
102-STA10_0179_TCGATGCGCT.fastq.gz	76	1	1	Simvastatin	0	J1c3b1a

166-STA10_0532_ATCAGTGTAT.fastq.gz	76	2	1	Atorvastatin	0	J1c3b1a
334-NWL-003_TTGTCGAGAC.fastq.gz	55	2	2	Simvastatin	SRM 3	J1c3b
42-STA15_0373_CGAGTGCTGT.fastq.gz	54	1	2	Atorvastatin	SRM 3	W5a1a
535-16660007_ACGATCACAT.fastq.gz	69	1	2	Simvastatin	SRM 3	J1c3e1
266-STA15-736_TCGCTGAACA.fastq.gz	71	1	2	Atorvastatin	SRM 5	J1c3g
520-1919808_CGACGCTGAT.fastq.gz	86	2	1	Simvastatin	0	J1c3b2
422-1419266_TCAGTGTCTC.fastq.gz	70	1	2	Simvastatin	SRM 3	J1c3g
204-STA10_0294_GGAAGTAAGG.fastq.gz	57	1	1	Atorvastatin	0	J1c5
494-1417258_CTCAGCAGTG.fastq.gz	68	2	1	Simvastatin	0	J1c5
49-STA15_0900_CTGCATGATC.fastq.gz	69	1	2	Atorvastatin	SRM 3	J1c4
587-15.39_CGAGACGACA.fastq.gz	57	2	1	Atorvastatin	0	J1c5
258-STA15-157_TTACACGTTC.fastq.gz	90	2	2	Simvastatin	SRM 5	J1c5
550-30303706_ATACAGTCTC.fastq.gz	52	1	2	Pravastatin	SRM 3	J1c5
62-STA10_0677_CGTACTACGT.fastq.gz	55	1	2	Atorvastatin	SRM 4	J1c5b
130-STA10_0339_GTGACGTACG.fastq.gz	72	1	1	Atorvastatin	0	J1c8a
218-STA10_0537_GTCTCAATGT.fastq.gz	69	2	1	Atorvastatin	0	J1c8a
512-2760345_TCGATATCTA.fastq.gz	64	2	2	Simvastatin	SRM 4	J1c7a
447-14.49_TGCGTAGTCG.fastq.gz	61	1	1	Simvastatin	0	J1d1a1

562-1350455_CATAGACGTG.fastq.gz	79	2	1	Simvastatin	0	J2a1a1a
100-STA10_0149_TACGTATAGC.fastq.gz	65	2	1	Atorvastatin	0	K1a
83-HES-003_TAGAGTCTGT.fastq.gz	71	2	2	Simvastatin	SRM 3	J1c8a
457-3164036_CGTGCTGTCA.fastq.gz	55	1	2	Simvastatin	SRM 4	J2a2a1a1
60-STA10_0159_GCACGTAGCT.fastq.gz	52	2	2	Simvastatin	SRM 5	J2b1a
73-STA10_0748_CGTATGATGT.fastq.gz	63	1	2	Atorvastatin	SRM 3	J2b1a
358-yft68_CTGACCGAGA.fastq.gz	77	1	1	Atorvastatin	0	K1a+150
421-1418027_CGCTGTAGTC.fastq.gz	78	2	2	Simvastatin	SRM 3	J2b1b1
495-1417002_CAGAGCTAGT.fastq.gz	80	1	1	Simvastatin	0	K1a+195
577-2.72_ATCTAGATCA.fastq.gz	86	2	1	Simvastatin	0	K1a+195
295-TEL-005_CTTACGTTGC.fastq.gz	57	2	2	Atorvastatin	SRM 3	K1a+150
363-bvh812_AGAGGTCGGA.fastq.gz	69	1	1	Simvastatin	0	K1a10a
576-13.28_AGAGATATCA.fastq.gz	65	2	1	Atorvastatin	0	K1a1b2a1a
127-STA10_0316_CGATCGACTG.fastq.gz	80	2	1	Simvastatin	0	K1a3a1b
191-STA10_0684_ATCTAGATCA.fastq.gz	66	1	1	Atorvastatin	0	K1a4a1
210-STA10_0307_GGATAGGATC.fastq.gz	70	2	1	Atorvastatin	0	K1a4a1e
24-U_4098_TGCTATGCTG.fastq.gz	44	1	2	Atorvastatin	SRM 3	K1a+195
537-26046556_ACATATACGT.fastq.gz	64	1	2	Fluvastatin	SRM 4	K1a+195

449-1550253_TATGCGCTGC.fastq.gz	71	2	1	Simvastatin	0	K1a4a1f
399-1550575_TGTGTGCATG.fastq.gz	67	2	2	Atorvastatin	SRM 3	K1a4a1
420-1412729_TGCTCGTAGT.fastq.gz	56	2	2	Simvastatin	SRM 4	K1a4a1
539-14.37_ATCGCTACAT.fastq.gz	62	1	1	Atorvastatin	0	K1a4d
257-SRS-009_GTTCTTCGTA.fastq.gz	74	1	2	Simvastatin	SRM 5	K1a4a1a2a
518-14204883_TACTGCAGCG.fastq.gz	77	2	1	Simvastatin	0	K1b1a1d1
304-STA15_501_TGGACTCAGA.fastq.gz	74	2	2	Pravastatin	SRM 3	K1a4a1b2
140-STA10_0388_GACTAGTCAG.fastq.gz	59	2	1	Simvastatin	0	K2a
324-STAGE-308_GAAGTCAAGC.fastq.gz	68	1	2	Simvastatin	SRM 3	K1a4a1e
466-3058235_CGTCTATGAT.fastq.gz	54	1	2	Simvastatin	SRM 3	K1a4a1f
248-CIS-004_GTAGAAGTGG.fastq.gz	75	1	2	Atorvastatin	SRM 3	K1c1
273-STA15-889_CTAAGTCATG.fastq.gz	77	1	2	Atorvastatin	SRM 3	K1c1
549-31580991_AGCATCTATA.fastq.gz	45	2	2	Pravastatin	SRM 4	K1c1
129-STA10_0328_CTGATGCAGA.fastq.gz	69	1	1	Simvastatin	0	K2a6
588-11.35_ATGCTGCGCT.fastq.gz	68	2	1	Simvastatin	0	K2a6
475-1350481_CAGCTGAGTA.fastq.gz	75	2	1	Simvastatin	0	H
460-15507730_GTCTACTGTC.fastq.gz	81	2	1	Simvastatin	0	K2b1a1a
551-35695882_ATGCTAGAGA.fastq.gz	57	1	2	Pravastatin	SRM 4	K1c2

479-11.6_CTACTGATGA.fastq.gz	68	1	1	Fluvastatin	0	B5a1d
93-HES-006_TGATACTCTG.fastq.gz	59	1	2	Simvastatin	SRM 3	K1d
463-1412537_CGTACTACGT.fastq.gz	82	2	1	Simvastatin	0	T1a1
82-HES-002_TATCGATGCT.fastq.gz	61	1	2	Simvastatin	SRM 4	K2a7
480-3090330_GATGTAGCGT.fastq.gz	45	2	2	Simvastatin	SRM 3	K2b1a1
581-2.24_GCGAGATGTA.fastq.gz	88	2	1	Simvastatin	0	T1a1
222-STA10_0622_CATCTGGAGT.fastq.gz	52	2	1	Simvastatin	0	T1a1k2
462-1922104_TAGCGCGTAG.fastq.gz	71	1	1	Simvastatin	0	T2
196-STA10_0187_TGTAGGTGGA.fastq.gz	57	1	1	Simvastatin	0	T2a1a
394-1.68_TCTCGGATAG.fastq.gz	90	2	1	Atorvastatin	0	T2a1a
490-3051533_CTAGATCTGA.fastq.gz	60	2	2	Simvastatin	SRM 4	J1b1a1a
491-3643161_GTAGTACACA.fastq.gz	62	2	2	Simvastatin	SRM 3	I1a1
492-3684114_TGCTACATCA.fastq.gz	42	1	2	Simvastatin	SRM 3	I1a1
284-STA15-423_CAGGCTCAGT.fastq.gz	80	1	2	Atorvastatin	SRM 4	T1a1
326-STAGE-989_GTCCAGACAT.fastq.gz	71	1	2	Simvastatin	SRM 4	T1a1
256-SRS-008_TGTCAGCTTA.fastq.gz	69	1	2	Simvastatin	SRM 4	T2a1a
396-1412062_GTATCGTCGT.fastq.gz	67	1	2	Simvastatin	SRM 3	T2a1a2
138-STA10_0382_AGTATCGTAC.fastq.gz	89	1	1	Simvastatin	0	T2b

499-1.5_CACGAGATGA.fastq.gz	91	2	1	Simvastatin	0	H2a2b3
5-U_3429_GTGCGTGTGT.fastq.gz	70	0 (2 plink)	2	Simvastatin	SRM 4	T2b
81-HES-001_TGTGTCACTA.fastq.gz	70	1	2	Pravastatin	SRM 3	T2a1b1a1a2
84-HES-004_CATGCATCAT.fastq.gz	68	2	2	Simvastatin	SRM 4	T2a1b1a1b
242-HES-011_TTGCTTAGTC.fastq.gz	66	1	2	Simvastatin	SRM 4	T2b
416-1550626_TAGTAGCGCG.fastq.gz	79	2	1	Simvastatin	0	T2b
251-SRS-002_CGAATGTATG.fastq.gz	60	2	2	Simvastatin	SRM 6	T2b
260-STA15-502_TGAGAAGGTA.fastq.gz	70	1	2	Atorvastatin	SRM 3	T2b
558-1349883_TAGCATACAG.fastq.gz	75	1	1	Simvastatin	0	T2b
430-1349088_TAGAGTCTGT.fastq.gz	81	2	2	Atorvastatin	SRM 3	T2b
467-3079482_TCAGCGATAT.fastq.gz	73	2	2	Simvastatin	SRM 4	T2b
8-U_3434_GATGTAGCGT.fastq.gz	57	0 (2 plink)	2	Simvastatin	SRM 5	T2b
509-1348220_AGTATCGTAC.fastq.gz	79	1	1	Simvastatin	0	H2a2a1
229-STA10-0003_TTCTCATCGT.fastq.gz	81	1	2	Rosuvastatin	SRM 3	T2b13
340-STAGE-875_ATTGTGGAGT.fastq.gz	91	1	2	Simvastatin	SRM 4	T2b16
132-STA10_0341_CTACGATCAG.fastq.gz	61	1	1	Simvastatin	0	T2b19
315-WES-004_GCATGCCAGT.fastq.gz	65	1	2	Simvastatin	SRM 3	T2b17a
572-19198989_ATCATATCTC.fastq.gz	89	1	1	Simvastatin	0	T2b21

505-762806_GCTACTAGCG.fastq.gz	60	1	2	Simvastatin	SRM 3	T2b19
570-19191508_AGAGTCGCGT.fastq.gz	85	1	1	Simvastatin	0	T2b24a
122-STA10_0262_CGCAGAGCAT.fastq.gz	84	1	1	Simvastatin	0	T2b2b
206-STA10_0299_CGTCTTCTTA.fastq.gz	73	2	1	Simvastatin	0	T2b2b
375-lth87_AGGAGAAGGA.fastq.gz	56	1	1	Atorvastatin	0	T2b2b
563-1902283_AGCAGTACTC.fastq.gz	81	2	1	Simvastatin	0	T2b2b
398-1420561_TGAGCGTGCT.fastq.gz	61	1	2	Simvastatin	SRM 3	T2b2b1
265-STA15-707_TCGAATGTGC.fastq.gz	68	1	2	Rosuvastatin	SRM 4	T2b3+151
160-STA10_0495_TAGTACTAGA.fastq.gz	62	1	1	Simvastatin	0	T2b33
542-14.48_CACATACAGT.fastq.gz	61	1	1	Pravastatin	0	T2b35
477-2385599_TGTCGTCATA.fastq.gz	56	2	2	Simvastatin	SRM 3	T2b33
91-IOW-001_TATGTACGTG.fastq.gz	21	1	2	Simvastatin	SRM 4	T2b34
458-3374947_GTCATGCGTC.fastq.gz	74	2	2	Simvastatin	SRM 3	T2b3b
434-1550142_GTGCTCATGT.fastq.gz	58	2	2	Simvastatin	SRM 3	T2b4
152-STA10_0456_TCTACGACAT.fastq.gz	60	1	1	Atorvastatin	0	T2b4a1
272-STA15-713_GGTCTGGTGT.fastq.gz	70	1	2	Rosuvastatin	SRM 3	T2b4b
417-1418404_TAGTCTGTCA.fastq.gz	62	1	1	Simvastatin	0	T2b4b
531-3259933_ACGTCAGTAT.fastq.gz	74	2	2	Simvastatin	SRM 4	J1c12a

247-CIS-003_GTGGAGAGCT.fastq.gz	62	1	2	Simvastatin	SRM 3	T2b5
322-STAGE-1021_TGCATGGAGC.fastq.gz	81	1	2	Simvastatin	SRM 5	T2b7a2
368-bvh838_ACTGTAGGAC.fastq.gz	74	1	1	Atorvastatin	0	T2b8
184-STA10_0657_ATGCTGCGCT.fastq.gz	76	1	1	Simvastatin	0	T2c1+146
111-STA10_0209_ACTAGCTGTC.fastq.gz	70	2	1	Atorvastatin	0	U2e1a1
565-14121555_ACTAGCTGTC.fastq.gz	82	1	1	Simvastatin	0	U2e2a1a
19-U_3880_TCAGTGTCTC.fastq.gz	64	0 (1 plink)	2	Simvastatin	SRM 5	U2e1a1c
253-SRS-005_GAATAGCTGA.fastq.gz	52	1	2	Atorvastatin	SRM 6	U2e1b
293-TEL-003_GAGATTGCTA.fastq.gz	71	2	2	Simvastatin	SRM 3	U2e1b1
407-13.61_TATCAGTCTG.fastq.gz	64	1	1	Atorvastatin	0	U4a
501-2762832_ACATAGTATC.fastq.gz	64	1	2	Pravastatin	SRM 3	U3a1
168-STA10_0539_AGTAGATCAT.fastq.gz	65	1	1	Simvastatin	0	U4a1b1
225-STA10_0663_TGGTGCTGGA.fastq.gz	76	1	1	Simvastatin	0	U4a1d
545-19197807_GATGACTACG.fastq.gz	55	1	1	Simvastatin	0	T1a1
153-STA10_0460_CACGAGATGA.fastq.gz	60	1	1	Simvastatin	0	U4b1b1a
559-1351716_TGATGTATGT.fastq.gz	70	1	1	Simvastatin	0	U4b1b1b
372-liv167_ACTTAGAGAG.fastq.gz	65	1	1	Atorvastatin	0	U5a1a1
595-NWL-6_TTAGTGGTGA.fastq.gz	50	1	2	Rosuvastatin	SRM 3	U4a1b

305-BUT-005_GGCATCATGC.fastq.gz	47	1	2	Simvastatin	SRM 4	U4b1b1
374-lth86_ATGAGGTCGT.fastq.gz	53	2	1	Atorvastatin	0	U5a1a1
464-1417627_TAGACGTGCT.fastq.gz	61	1	1	Atorvastatin	0	U5a1a1d
555-1419931_ACTGCGTGTC.fastq.gz	67	1	1	Simvastatin	0	J1c3a1
556-15.59_CTAGCAGATG.fastq.gz	53	1	1	Simvastatin	0	I4a1
224-STA10_0646_GGCTGTGATC.fastq.gz	67	1	1	Simvastatin	0	U5a1a1d1
436-12.72_GCGATGATGA.fastq.gz	66	1	1	Atorvastatin	0	U5a1b
327-STAGE-872_GAGACCTCTA.fastq.gz	75	2	2	Simvastatin	SRM 3	U4b1b1
598-STAGE-365_GTTGATGAGT.fastq.gz	62	1	2	Rosuvastatin	SRM 3	U4b2
339-STAGE-1018_GACGTGCTTC.fastq.gz	55	1	2	Rosuvastatin	SRM 3	U4c1
412-1919850_GATGCGAGCT.fastq.gz	54	1	2	Simvastatin	SRM 4	U4c1
564-15517418_GCACGCGTAT.fastq.gz	88	2	1	Simvastatin	0	X2b8
527-14176609_AGCGAGTATG.fastq.gz	65	2	2	Pravastatin	SRM 4	U4c1
267-STA15-890_GCGTTATTGC.fastq.gz	89	1	2	Simvastatin	SRM 3	U4c2
448-1902115_TGTCGAGTCA.fastq.gz	86	2	1	Simvastatin	0	U5a1b
497-1349653_ACGTATCATC.fastq.gz	66	1	1	Atorvastatin	0	U5a1b
213-STA10_0365_CCTCGTTGTT.fastq.gz	61	1	1	Simvastatin	0	U5a1b+16362
236-IOW-002_GATAAGAAGG.fastq.gz	77	2	2	Atorvastatin	SRM 5	U5a1a1

432-1420121_GTCGTCGTCT.fastq.gz	77	2	2	Atorvastatin	SRM 3	U5a1a1
178-STA10_0610_AGCTCTGTGA.fastq.gz	73	1	1	Simvastatin	0	U5a1b1d
155-STA10_0470_ACGTGCTCTG.fastq.gz	81	1	1	Simvastatin	0	U5a1b1d+16093
4-U_3428_GTCGTCGTCT.fastq.gz	65	1	2	Simvastatin	SRM 5	U5a1a1b
444-1551206_GTGCGTGTGT.fastq.gz	76	2	2	Simvastatin	SRM 4	U5a1a2a
364-bvh818_AATCGAGCGT.fastq.gz	47	1	1	Atorvastatin	0	U5a1b1f
471-1412699_CTGTAGTGCG.fastq.gz	63	1	1	Atorvastatin	0	U5a2c1
514-13.11_AGCTCTGTGA.fastq.gz	65	1	1	Pravastatin	0	U5b1+16189+@16192
255-SRS-007_CTGGAGGCTA.fastq.gz	54	2	2	Atorvastatin	SRM 6	U5a1a2a1
231-STA10-0063_CGCTAATGTA.fastq.gz	85	2	2	Simvastatin	SRM 3	U5a1b+16362
309-NEW-002_TTCGATAGCA.fastq.gz	58	1	2	Atorvastatin	SRM 6	U5a1b1
141-STA10_0399_GATGACTACG.fastq.gz	74	1	1	Simvastatin	0	U5b1b1+@16192
586-3.59_AGTAGATCAT.fastq.gz	84	2	1	Pravastatin	0	J2a1a1a
347-hdf1_ATATGGTGGA.fastq.gz	65	2	1	Atorvastatin	0	U5b1c1a
589-2.66_ATCGCATAGA.fastq.gz	86	2	1	Atorvastatin	0	J2a1a1a2
46-STA15_0923_TCTCTGTGCA.fastq.gz	69	2	2	Simvastatin	SRM 3	U5a1b1
529-33000015_CGATGACAGA.fastq.gz	55	1	2	Atorvastatin	SRM 3	U5a1c2a1
21-U_3959_CGTATCTCGA.fastq.gz	69	0 (2 plink)	2	Simvastatin	SRM 5	U5a1d1

310-NEW-003_GTCTAGCAGG.fastq.gz	72	1	2	Simvastatin	SRM 3	U5a1e
593-WES-6_TAGGTGGAAT.fastq.gz	79	1	2	Atorvastatin	SRM 4	I2d
292-NWL-001_GTCGTAACAC.fastq.gz	40	1	2	Simvastatin	SRM 4	U5a2b4
94-HES-007_TCAGCGATAT.fastq.gz	61	1	2	Simvastatin	SRM 3	U5a2d1a
165-STA10_0525_CTACATACTA.fastq.gz	73	1	1	Simvastatin	0	U5b2a2b1
220-STA10_0580_GGTGTTAGTG.fastq.gz	75	2	1	Simvastatin	0	U5b2b
135-STA10_0347_CATGATACGC.fastq.gz	75	1	1	Simvastatin	0	U5b2b1a1
349-yft25_AAGTGCGATG.fastq.gz	49	1	1	Simvastatin	0	U5b2b1a1
156-STA10_0481_ACGATCACAT.fastq.gz	58	1	1	Simvastatin	0	U5b2b3a1
578-7.67_GCAGTATGCG.fastq.gz	76	2	1	Simvastatin	0	U8a1a2
61-STA10_0643_TCACGCTATG.fastq.gz	65	2	2	Simvastatin	SRM 4	T2a1b1a1b
594-WES-7_TGTAGGTGGA.fastq.gz	89	2	2	Atorvastatin	SRM 3	U5b2a1a2
95-HES-008_CTACTGATGA.fastq.gz	72	1	2	Simvastatin	SRM 3	U5b2a2b
476-1412620_GTGACTCGTC.fastq.gz	66	1	1	Simvastatin	0	V+@16298
603-STAGE-1198_CGGTGTGTGT.fastq.gz	68	1	2	Simvastatin	SRM 4	U5b2b4a
77-STA10_0752_TATCATGTGC.fastq.gz	54	1	2	Simvastatin	SRM 3	U5b3g
71-STA10_0732_GTGACTCGTC.fastq.gz	61	1	2	Atorvastatin	SRM 3	U4b1a2a
72-STA10_0747_TCGAGTAGCG.fastq.gz	36	1	2	Rosuvastatin	SRM 3	T1a1

113-STA10_0221_CTCAGCAGTG.fastq.gz	62	1	1	Simvastatin	0	V+@72
370-lth37_TCACGACGAA.fastq.gz	60	1	1	Simvastatin	0	V+@72
75-STA10_0750_TGTCTCTATC.fastq.gz	79	2	2	Simvastatin	SRM3	X2b5
40-STA15_0135_CGCAGTCTAT.fastq.gz	54	1	2	Atorvastatin	SRM3	V
452-9422668_TCTGAGCGCA.fastq.gz	81	1	1	Atorvastatin	0	V10a
58-STA10_0020_GTGAGAGACA.fastq.gz	66	2	2	Simvastatin	SRM5	V+@72
271-STA15-560_TTCGAGCTAT.fastq.gz	42	1	2	Simvastatin	SRM3	V10a
401-1902376_GTATGAGCAC.fastq.gz	77	1	2	Simvastatin	SRM3	V10a
409-1350561_CGCTATCAGT.fastq.gz	81	1	2	Simvastatin	SRM3	V16
31-U_5078_CTGTAGTGCG.fastq.gz	81	2	2	Simvastatin	SRM4	V1a1
352-yft35_ACTTCTTAGC.fastq.gz	76	1	1	Atorvastatin	0	V15a
197-STA10_0195_TTAGTGGTGA.fastq.gz	71	1	1	Simvastatin	0	V1a
534-35310006_ACATGTCTGA.fastq.gz	66	2	2	Rosuvastatin	SRM3	V2
543-13516475_TCACAGCATA.fastq.gz	83	2	1	Atorvastatin	0	V2c
532-14204227_CTACGATCAG.fastq.gz	86	2	2	Pravastatin	SRM3	V24
80-TEL-001_TATCTCATGC.fastq.gz	67	1	2	Simvastatin	SRM3	W5
9-U_3593_GAGTGATCGT.fastq.gz	66	1	2	Simvastatin	SRM3	J1c2e
209-STA10_0305_CTCTTAGTTC.fastq.gz	69	2	1	Simvastatin	0	W1g

205-STA10_0298_CGGTGTGTGT.fastq.gz	82	1	1	Simvastatin	0	W3a1c
493-830046_TGATAGAGAG.fastq.gz	69	1	2	Simvastatin	SRM3	X2b4
50-STA15_0901_CGCGTATCAT.fastq.gz	58	2	2	Atorvastatin	SRM3	X2b4a1
502-2789467_ATCACTCATA.fastq.gz	55	1	2	Simvastatin	SRM3	X2b4a1
118-STA10_0236_CACAGTGATG.fastq.gz	73	1	1	Simvastatin	0	X2c1a
377-lth93_ATTAGCGAGT.fastq.gz	68	1	1	Atorvastatin	0	X2g

Appendix IV

Summary of healthy volunteer cohort concordant sub-haplogroup assignments.

Sample ID	**Gender**	**Haplogroup**
352	Male	A2+(64)
126	Male	A2v
355	Female	D1
80	Female	F1e3
159	Male	G2a5
17	Female	H
251	Male	H
165	Female	H1+16189
353	Male	H1+16189
284	Female	H1+16239
52	Female	H10e1
380	Female	H11a+152
335	Female	H11a1
336	Male	H11a1
219	Female	H11a2a
218	Female	H11a2a1
357	Male	H14b1
342	Female	H17
341	Female	H1a
144	Male	H1a1
211	Female	H1a1
178	Female	H1a1a1
272	Female	H1af1b
373	Female	H1ai

337	Female	H1am
230	Female	H1au1a
141	Female	H1b1+16362
213	Male	H1b1+16362
41	Female	H1bb
48	Female	H1bs
12	Female	H1c
210	Male	H1c
181	Female	H1c1
377	Female	H1c3
168	Male	H1e2
367	Male	H1g1
378	Female	H1g1
347	Male	H1j
365	Female	H1j
305	Female	H1m
103	Female	H1q3
287	Female	H24a
204	Female	H27c
81	Male	H2a1e1a1
112	Female	H2a2b1a1
60	Male	H3
274	Female	H31a
95	Female	H39
201	Female	H39b
195	Male	H3ap
217	Male	H3ap
13	Female	H3aq
258	Male	H3aq
319	Female	H3ar
54	Female	H42a
82	Male	H49a1
108	Male	H4a1
19	Female	H4a1a1a
107	Male	H4a1a1a
162	Male	H4a1a1a
346	Female	H4a1a2a
10	Female	H4a1c
157	Female	H5
222	Male	H56
45	Female	H58a
69	Female	H5a1
102	Female	H5a1
127	Male	H5a1
245	Male	H5a1c1a

292	Male	H5a1g1
326	Male	H5b1
320	Female	H5b4
31	Female	H5s
349	Female	H65a
55	Female	H6a1a3
42	Female	H6a1b
27	Female	H6a1b4
280	Female	H6a2a
177	Male	H6b2
194	Female	H6c
288	Male	H6c
311	Female	H7
64	Male	H7a1b
382	Male	H7b
282	Female	H8c2
207	Female	HV0+195
150	Female	HV0d
340	Male	HV0d
345	Female	HV4a1
249	Male	I1a1
370	Female	I2a2
255	Female	I5a2
100	Female	J1c+16261
53	Female	J1c1a
376	Female	J1c1a
192	Female	J1c1b2a
316	Female	J1c1c
90	Female	J1c1e
176	Female	J1c1e
225	Female	J1c2
306	Male	J1c2
359	Female	J1c2c1
38	Female	J1c2h
199	Female	J1c2l
22	Female	J1c2m
203	Female	J1c2r
114	Male	J1c3b
134	Female	J1c3b
197	Male	J1c3b
142	Female	J1c3e2
343	Female	J1c3f
3	Female	J1c3g
43	Female	J1c3g
295	Male	J1c3g

50	Male	J1c5
83	Male	J1c5
154	Female	J1c5f
329	Male	J1c8a
118	Male	J2a1a1a
158	Female	J2a1a1a
172	Female	J2a1a1a2
117	Male	J2b2
368	Female	K1a+150
202	Male	K1a+195
323	Female	K1a1b1a
236	Male	K1a1b1f
315	Female	K1a30a
79	Female	K1a3a2
314	Female	K1a4a1
224	Female	K1a4a1a2b
289	Female	K1a4a1a2b
70	Male	K1a4a1b
20	Female	K1a4a1d
85	Male	K1a4a1e
145	Female	K1b1a1d1
264	Male	K1c1
67	Female	K1c1b
209	Male	K1c2
265	Female	K1c2
309	Male	K1d
16	Male	K2a
273	Female	K2a
58	Female	K2a3
358	Female	K2a3
132	Female	N1b1b1
93	Male	R5a2
29	Male	T1a1
44	Female	T1a1
71	Male	T1a1
6	Female	T1a1a1
293	Female	T1a1a1
379	Female	T2
98	Female	T2a1b1a
331	Female	T2a1b1a
109	Male	T2b
153	Female	T2b
246	Female	T2b
348	Male	T2b
247	Female	T2b17a

61	Male	T2b21
40	Female	T2b28
171	Female	T2b2b
369	Male	T2b2b1
73	Female	T2b3
84	Male	T2b4
226	Male	T2c1+146
15	Female	T2e
235	Female	T2e
72	Female	T2e1a
14	Male	U1a1a1
36	Female	U1a1a1
310	Female	U1b3
384	Female	U2e1'2'3
366	Male	U2e1a1
381	Female	U2e2a1a
96	Female	U3a1
254	Male	U3a1
65	Male	U3a1c
2	Female	U3a1c1
228	Female	U4a2b
99	Female	U4b1a1a1
33	Male	U4b1a2b
270	Male	U4b1b1
115	Male	U4b1b1a
267	Male	U4b1b1a
317	Female	U4b1b1a
32	Female	U4b1b1b
248	Male	U5a1+@16192
11	Female	U5a1a1
18	Female	U5a1a1
188	Male	U5a1a1
304	Female	U5a1a1
51	Female	U5a1b1
239	Female	U5a1b1g
330	Male	U5a1d1
242	Female	U5a1f1a1
253	Female	U5a1f1a1
261	Female	U5a1h
299	Female	U5a1h
78	Female	U5a1i1
383	Male	U5a1i1
298	Male	U5a2+16362
283	Female	U5a2a1+152
35	Female	U5a2a2

205	Female	U5a2a2
74	Male	U5b1d1c
240	Female	U5b2a1b
105	Female	U5b2a2b1
183	Female	U5b2a3a
68	Female	U5b2b4a
215	Female	U5b3b1
56	Male	U8a1a3
25	Female	V+@16298
129	Male	V12
77	Female	V15a
234	Female	V15a
277	Female	V15a
339	Male	V15a
354	Female	V15a
268	Female	V19
37	Male	V9a2
275	Female	W1+119
47	Female	W5a1a
121	Female	W5a2
324	Female	X2+225+@16223
110	Female	X2b+226
116	Male	X2b+226
138	Female	X2b+226
257	Male	X2b5
193	Female	X2c1a

Bibliography

Aas, V. *et al.* (2013) Are cultured human myotubes far from home? *Cell Tissue Res.*, **354**, 671–682.

Acin-Perez, R. and Enriquez, J.A. (2014) The function of the respiratory supercomplexes: The plasticity model. *Biochim. Biophys. Acta - Bioenerg.*, **1837**, 444–450.

Aguer, C. *et al.* (2011) Galactose enhances oxidative metabolism and reveals mitochondrial dysfunction in human primary muscle cells. *PLoS One*, **6**.

Ahmed, T.A. *et al.* (2013) Pharmacokinetics of high-dose simvastatin in refractory and relapsed chronic lymphocytic leukemia patients. *Cancer Chemother. Pharmacol.*, **72**, 1369–1374.

Alfirevic, a *et al.* (2014) Phenotype standardization for statin-induced myotoxicity. *Clin. Pharmacol. Ther.*, **96**, 470–6.

Alfirevic, A. *et al.* (2012) In silico analysis of HLA associations with drug-induced liver injury: Use of a HLA-genotyped DNA archive from healthy volunteers. *Genome Med.*, **4**, 1–14.

Allard, N.A.E. *et al.* (2018) Statins affect skeletal muscle performance: Evidence for disturbances in energy metabolism. *J. Clin. Endocrinol. Metab.*, **103**, 75–84.

Allen, D.D. *et al.* (2005) Cell lines as in vitro models for drug screening and toxicity studies. *Drug Dev. Ind. Pharm.*, **31**, 757–768.

Andres, A. *et al.* (2017) Attenuation of Mitophagy Exacerbates the Deleterious Effects of Statins on Skeletal Muscle. *FASEB J.*, **31**, 1022.17-1022.17.

Andreux, P. a *et al.* (2014) A method to identify and validate mitochondrial modulators using mammalian cells and the worm C. elegans. *Sci. Rep.*, **4**, 5285.

Ansari, A. *et al.* (2017) Function of the SIRT3 mitochondrial deacetylase in cellular physiology, cancer, and neurodegenerative disease. *Aging Cell*, **16**, 4–16.

Anton, D. *et al.* (2015) Three-dimensional cell culture: A breakthrough in vivo. *Int. J. Mol. Sci.*, **16**, 5517–5527.

Antons, K.A. *et al.* (2006) Clinical Perspectives of Statin-Induced Rhabdomyolysis. *Am. J. Med.*, **119**, 400–409.

Apostolopoulou, M. *et al.* (2015) The role of mitochondria in statin-induced myopathy. *Eur. J. Clin. Invest.*, **45**, 745–754.

Arany, Z. (2008) PGC-1 coactivators and skeletal muscle adaptations in health and disease. *Curr. Opin. Genet. Dev.*, **18**, 426–434.

Baer, A.N. and Wortmann, R.L. (2007) Myotoxicity associated with lipid-lowering drugs. *Curr. Opin. Rheumatol.*, **19**, 67–73.

Bai, R.K. *et al.* (2007) Mitochondrial genetic background modifies breast cancer risk. *Cancer Res.*, **67**, 4687–4694.

Baker, S.K. and Tarnopolsky, M.A. (2001) Statin myopathies: Pathophysiologic and clinical

perspectives. *Clin. Investig. Med.*, **24**, 258–272.

Baker, W.L. *et al.* (2010) Differing effect of statins on insulin sensitivity in non-diabetics: A systematic review and meta-analysis. *Diabetes Res. Clin. Pract.*, **87**, 98–107.

Ball, A.L. *et al.* (2016) Identification of the additional mitochondrial liabilities of 2-hydroxyflutamide when compared with its parent compound, flutamide in HepG2 cells. *Toxicol. Sci.*, **153**, 341–351.

Bartlett, K. and Eaton, S. (2004) Mitochondrial β-oxidation. *Eur. J. Biochem.*, **271**, 462–469.

Becker, M.L. *et al.* (2013) Genetic variation in the ABCC2 gene is associated with dose decreases or switches to other cholesterol-lowering drugs during simvastatin and atorvastatin therapy. *Pharmacogenomics J.*, **13**, 251–256.

Becker, M.L. *et al.* (2010) Influence of genetic variation in CYP3A4 and ABCB1 on dose decrease or switching during simvastatin and atorvastatin therapy. *Pharmacoepidemiol. Drug Saf.*, **19**, 75–81.

Bénit, P. *et al.* (2009) Respiratory-chain diseases related to complex III deficiency. *Biochim. Biophys. Acta*, **1793**, 181–5.

Berg, J.M. *et al.* (2007) Biochemistry. In, *Biochemistry*, Biochemistry (Berg). W. H. Freeman.

Bergamini, C. *et al.* (2012) A water soluble CoQ 10 formulation improves intracellular distribution and promotes mitochondrial respiration in cultured cells. *PLoS One*, **7**, 1–11.

Bigot, A. *et al.* (2009) Large CTG repeats trigger p16-dependent premature senescence in myotonic dystrophy type 1 muscle precursor cells. *Am. J. Pathol.*, **174**, 1435–1442.

Björkhem-Bergman, L. *et al.* (2011) What is a relevant statin concentration in cell experiments claiming pleiotropic effects? *Br. J. Clin. Pharmacol.*, **72**, 164–165.

Blain, P.G. *et al.* (1985) Opiate-induced rhabdomyolysis. *Hum. Toxicol.*, **4**, 71–74.

Blau, H.M. and Webster, C. (1981) Isolation and characterization of human muscle cells. *Proc. Natl. Acad. Sci. U. S. A.*, **78**, 5623–7.

Blomberg, M.R.A. (2016) Mechanism of Oxygen Reduction in Cytochrome c Oxidase and the Role of the Active Site Tyrosine. *Biochemistry*, **55**, 489–500.

Boelsterli, U.A. and Lim, P.L.K. (2007) Mitochondrial abnormalities-A link to idiosyncratic drug hepatotoxicity? *Toxicol. Appl. Pharmacol.*, **220**, 92–107.

Bogsrud, M.P. *et al.* (2013) No effect of combined coenzyme Q10 and selenium supplementation on atorvastatin-induced myopathy. *Scand. Cardiovasc. J.*, **47**, 80–87.

Bonen, A. (2001) The expression of lactate transporters (MCT1 and MCT4) in heart and muscle. *Eur. J. Appl. Physiol.*, **86**, 6–11.

Bookstaver, D.A. *et al.* (2012) Effect of coenzyme Q10 supplementation on statin-induced myalgias. *Am. J. Cardiol.*, **110**, 526–529.

Bouitbir, J. *et al.* (2012) Opposite effects of statins on mitochondria of cardiac and skeletal muscles: A 'mitohormesis' mechanism involving reactive oxygen species and PGC-1.

Eur. Heart J., **33**, 1397–1407.

Boyer, P.D. (1993) The binding change mechanism for ATP synthase--some probabilities and possibilities. *Biochim. Biophys. Acta*, **1140**, 215–250.

Brand, M.D. *et al.* (1999) The significance and mechanism of mitochondrial proton conductance. *Int. J. Obes. Relat. Metab. Disord.*, **23 Suppl 6**, S4-11.

Brand, M.D. (2010) The sites and topology of mitochondrial superoxide production. *Exp. Gerontol.*, **45**, 466–472.

Brand, M.D.D. and Nicholls, D.G.G. (2011) Assessing mitochondrial dysfunction in cells. *Biochem. J.*, **435**, 297–312.

Breslin, S. and O'Driscoll, L. (2013) Three-dimensional cell culture: The missing link in drug discovery. *Drug Discov. Today*, **18**, 240–249.

Brunham, L.R. *et al.* (2012) Differential effect of the rs4149056 variant in SLCO1B1 on myopathy associated with simvastatin and atorvastatin. *Pharmacogenomics J.*, **12**, 233–237.

Brunham, L.R. *et al.* (2018) Role of Genetics in the Prediction of Statin-Associated Muscle Symptoms and Optimization of Statin Use and Adherence. *Cardiovasc. Res.*, 1073–1081.

Bullough, D.A. *et al.* (1985) The varied responses of different F1-ATPases to chlorpromazine. *Arch. Biochem. Biophys.*, **236**, 567–575.

Calabrese, C. *et al.* (2014) MToolBox: a highly automated pipeline for heteroplasmy annotation and prioritization analysis of human mitochondrial variants in high-throughput sequencing. *Bioinformatics*, **30**, 3115–3117.

Canter, J.A. *et al.* (2010) African Mitochondrial DNA Subhaplogroups and Peripheral Neuropathy during Antiretroviral Therapy. *J. Infect. Dis.*, **201**, 1703–1707.

Cao, P. *et al.* (2009) Statin-induced muscle damage and atrogin-1 induction is the result of a geranylgeranylation defect. *FASEB J.*, **23**, 2844–2854.

Capaldi, R.A. and Aggeler, R. (2002) Mechanism of the F1F0-type ATP synthase, a biological rotary motor. *Trends Biochem. Sci.*, **27**, 154–160.

Carr, D.F. *et al.* (2013) SLCO1B1 genetic variant associated with statin-induced myopathy: a proof-of-concept study using the clinical practice research datalink. *Clin. Pharmacol. Ther.*, **94**, 695–701.

Carvalho, M. *et al.* (2012) Toxicity of amphetamines: An update. *Arch. Toxicol.*, **86**, 1167–1231.

Caso, G. *et al.* (2007) Effect of coenzyme q10 on myopathic symptoms in patients treated with statins. *Am. J. Cardiol.*, **99**, 1409–1412.

Catapano, A.L. (2010) Pitavastatin - pharmacological profile from early phase studies. *Atheroscler. Suppl.*, **11**, 3–7.

Chabi, B. *et al.* (2008) Mitochondrial function and apoptotic susceptibility in aging skeletal muscle. *Aging Cell*, **7**, 2–12.

Chawla, J. (2011) Stepwise approach to myopathy in systemic disease. *Front. Neurol.*, **AUG**, 1–10.

Chen, H. *et al.* (2010) Mitochondrial fusion is required for mtdna stability in skeletal muscle and tolerance of mtDNA mutations. *Cell*, **141**, 280–289.

Cheng, C.S. *et al.* (2014) Physiology and metabolism of tissue-engineered skeletal muscle. *Exp. Biol. Med. (Maywood).*, **239**, 1203–14.

Chinnery, P.F. *et al.* (2010) Mitochondrial DNA haplogroups and risk of transient ischaemic attack and ischaemic stroke: a genetic association study. *Lancet. Neurol.*, **9**, 498–503.

Chinnery, P.F. and Hudson, G. (2013) Mitochondrial genetics. *Br. Med. Bull.*, **106**, 135–159.

Chistiakov, D.A. *et al.* (2014) Mitochondrial Aging and Age-Related Dysfunction of Mitochondria. *Biomed Res. Int.*, **2014**, 1–7.

Clayton, D.A. (1982) Replication of animal mitochondrial DNA. *Cell*, **28**, 693–705.

Cogen, F.C. *et al.* (1978) Phencyclidine-Associated Acute Rhabdomyolysis. 210–212.

Cogliati, S. *et al*. (2016) Mitochondrial Cristae: Where Beauty Meets Functionality. *Trends Biochem*. *Sci*. **41**, 261–273.

Copeland, W.C. (2008) Inherited mitochondrial diseases of DNA replication. *Annu. Rev. Med.*, **59**, 131–146.

Corsini, a *et al.* (1999) New insights into the pharmacodynamic and pharmacokinetic properties of statins. *Pharmacol. Ther.*, **84**, 413–428.

Crofts, A.R. (2004) The Cytochrome bc1 Complex: Function in the Context of Structure. *Annu. Rev. Physiol.*, **66**, 689–733.

Dalakas, M.C. (2009) Toxic and drug-induced myopathies. *J. Neurol. Neurosurg. Psychiatry*, **80**, 832–838.

Danesh, J. *et al.* (2007) The emerging risk factors collaboration: Analysis of individual data on lipid, inflammatory and other markers in over 1.1 million participants in 104 prospective studies of cardiovascular diseases. *Eur. J. Epidemiol.*, **22**, 839–869.

Davidson, M.H. (2002) Rosuvastatin: a highly efficacious statin for the treatment of dyslipidaemia. *Expert Opin. Investig. Drugs*, **11**, 125–41.

Davis, B.N.J. *et al.* (2017) Human, Tissue-Engineered, Skeletal Muscle Myobundles to Measure Oxygen Uptake and Assess Mitochondrial Toxicity. *Tissue Eng. Part C Methods*, **23**, ten.tec.2016.0264.

Deichmann, R. *et al.* (2010) Coenzyme q10 and statin-induced mitochondrial dysfunction. *Ochsner J.*, **10**, 16–21.

Dennis, R.G. and Kosnik, P.E. (2000) Excitability and Isometric Contractile Properties of Mammalian Skeletal Muscle Constructs Engineered in Vitro. *Vitr. Cell. Dev. Biol. - Anim.*, **36**, 327.

DePristo, M.A. *et al.* (2011) A framework for variation discovery and genotyping using next-generation DNA sequencing data. *Nat. Genet.*, **43**, 491–498.

Deschamps, D. *et al.* (1994) Inhibition by perhexiline of oxidative phosphorylation and the β-oxidation of fatty acids: Possible role in pseudoalcoholic liver lesions. *Hepatology*, **19**, 948–961.

Desler, C. *et al.* (2012) Is There a Link between Mitochondrial Reserve Respiratory Capacity and Aging? *J. Aging Res.*, **2012**, 1–9.

Dhingra, R. and Kirshenbaum, L.A. (2015) Succinate dehydrogenase/complex II activity obligatorily links mitochondrial reserve respiratory capacity to cell survival in cardiac myocytes. *Cell Death Dis*, **6**, e1956.

Diaz-Ruiz, R. *et al.* (2011) The Warburg and Crabtree effects: On the origin of cancer cell energy metabolism and of yeast glucose repression. *Biochim. Biophys. Acta - Bioenerg.*, **1807**, 568–576.

Diaz-Ruiz, R. *et al.* (2009) Tumor cell energy metabolism and its common features with yeast metabolism. *Biochim. Biophys. Acta - Rev. Cancer*, **1796**, 252–265.

van Diemen, M.P.J. *et al.* (2017) Validation of a pharmacological model for mitochondrial dysfunction in healthy subjects using simvastatin: A randomized placebo-controlled proof-of-pharmacology study. *Eur. J. Pharmacol.*, **815**, 290–297.

Diez-Juan, A. and Simón, C. (2015) Converting a problem into an opportunity: mtDNA heteroplasmy shift. *Cell Stem Cell*, **16**, 457–458.

DiMasi, J.A. *et al.* (2016) Innovation in the pharmaceutical industry: New estimates of R&D costs. *J. Health Econ.*, **47**, 20–33.

Dirks-Naylor, A.J. and Griffiths, C.L. (2009) Glucocorticoid-induced apoptosis and cellular mechanisms of myopathy. *J. Steroid Biochem. Mol. Biol. J. Steroid Biochem. Mol. Biol.*, **117**, 1–7.

Dirks, A.J. and Jones, K.M. (2006) Statin-induced apoptosis and skeletal myopathy. *Am. J. Physiol. Cell Physiol.*, **291**, C1208–C1212.

Divakaruni, A.S. *et al.* (2017) In situ measurements of mitochondrial matrix enzyme activities using plasma and mitochondrial membrane permeabilization agents. *Anal. Biochem.*, 1–6.

Divakaruni, A.S. *et al.* (2014) Measuring mitochondrial function in permeabilized cells using the seahorse XF analyzer or a clark-type oxygen electrode. *Curr. Protoc. Toxicol.*, **2014**, 25.2.1-25.2.16.

Divakaruni, A.S. and Brand, M.D. (2011) The regulation and physiology of mitochondrial proton leak. *Physiology (Bethesda).*, **26**, 192–205.

Dott, W. *et al.* (2014) Modulation of mitochondrial bioenergetics in a skeletal muscle cell line model of mitochondrial toxicity. *Redox Biol.*, **2**, 224–33.

Dragan, A.I. *et al.* (2010) Characterization of PicoGreen Interaction with dsDNA and the Origin of Its Fluorescence Enhancement upon Binding. *Biophys. J.*, **99**, 3010–3019.

Dranka, B.P. *et al.* (2011) Assessing bioenergetic function in response to oxidative stress by metabolic profiling. *Free Radic. Biol. Med.*, **51**, 1621–1635.

Duriez, P. (2003) [Mechanisms of actions of statins and fibrates]. *Therapie*, **58**, 5–14.

Dykens, J.A. *et al.* (2008) In vitro assessment of mitochondrial dysfunction and cytotoxicity of nefazodone, trazodone, and buspirone. *Toxicol. Sci.*, **103**, 335–345.

Dykens, J.A. and Will, Y. (2007) The significance of mitochondrial toxicity testing in drug development. *Drug Discov. Today*, **12**, 777–785.

Edmondson, R. *et al.* (2014) Three-Dimensional Cell Culture Systems and Their Applications in Drug Discovery and Cell-Based Biosensors. *Assay Drug Dev. Technol.*, **12**, 207–218.

Edwards, I.R. and Aronson, J.K. (2000) Adverse drug reactions: Definitions, diagnosis, and management. *Lancet*, **356**, 1255–1259.

Egom, E.E. roume A. and Hafeez, H. (2016) Biochemistry of Statins 1st ed. Elsevier Inc.

Espinosa-Diez, C. *et al.* (2015) Antioxidant responses and cellular adjustments to oxidative stress. *Redox Biol.*, **6**, 183–197.

Eupedia (2018) https://www.eupedia.com. *Date Accessed, 2018-06-05*.

Faulkner, L. *et al.* (2016) Detection of primary T cell responses to drugs and chemicals in HLA-Typed volunteers: Implications for the prediction of drug immunogenicity. *Toxicol. Sci.*, **154**, 416–429.

Fedacko, J. *et al.* (2013) Coenzyme Q(10) and selenium in statin-associated myopathy treatment. *Can. J. Physiol. Pharmacol.*, **91**, 165–170.

Feng, Q. *et al.* (2012) Individualized risk for statin-induced myopathy: current knowledge, emerging challenges and potential solutions. *Pharmacogenomics*, **13**, 579–594.

Fernández-silva, P. *et al.* (2003) Special Review Series – Biogenesis and Physiological Adaptation of Mitochondria Replication and transcription of mammalian mitochondrial DNA Experimental Physiology. *Exp. Physiol.*, **88**, 41–56.

Fernandez-Solà, J. *et al.* (2007) Molecular and cellular events in alcohol-induced muscle disease. *Alcohol. Clin. Exp. Res.*, **31**, 1953–1962.

Ferrick, D.A. *et al.* (2008) Advances in measuring cellular bioenergetics using extracellular flux. *Drug Discov. Today*, **13**, 268–274.

Flint, O.P. *et al.* (1997a) HMG CoA Reductase Inhibitor-Induced Myotoxicity: Pravastatin and Lovastatin Inhibit the Geranylgeranylation of Low-Molecular-Weight Proteins in Neonatal Rat Muscle Cell Culture. *Toxicol. Appl. Pharmacol.*, **145**, 99–110.

Flint, O.P. *et al.* (1997b) Inhibition of Cholesterol Synthesis by Squalene Synthase Inhibitors Does Not Induce Myotoxicityin Vitro. *Toxicol. Appl. Pharmacol.*, **145**, 91–98.

Flintoft, L. (2005) Mitochondria: uncovering the error of their ways. *Nat. Rev. Genet.*, **6**, 345.

Floyd, J.S. *et al.* (2014) GATM locus does not replicate in rhabdomyolysis study. *Nature*, **513**, E1.

Forouzanfar, M.H. *et al.* (2016) Global, regional, and national comparative risk assessment of 79 behavioural, environmental and occupational, and metabolic risks or clusters of risks, 1990–2015: a systematic analysis for the Global Burden of Disease Study 2015. *Lancet*, **388**, 1659–1724.

Frudakis, T.N. *et al.* (2007) CYP2D6*4 polymorphism is associated with statin-induced muscle effects. *Pharmacogenet. Genomics*, **17**, 695–707.

Fulda, S. *et al.* (2010) Targeting mitochondria for cancer therapy. *Nature*, **9**, 447–464.

Galtier, F. *et al.* (2012) Effect of a high dose of simvastatin on muscle mitochondrial metabolism and calcium signaling in healthy volunteers. *Toxicol. Appl. Pharmacol.*, **263**, 281–286.

Gazzerro, P. *et al.* (2012) Pharmacological actions of statins: a critical appraisal in the management of cancer. *Pharmacol. Rev.*, **64**, 102–46.

Ghatak, A. *et al.* (2010) The genetics of statin-induced myopathy. *Atherosclerosis*, **210**, 337–343.

Gilkerson, R. *et al.* (2013) The mitochondrial nucleoid: integrating mitochondrial DNA into cellular homeostasis. *Cold Spring Harb. Perspect. Biol.*, **5**, a011080.

Glancy, B. *et al.* (2015) Mitochondrial reticulum for cellular energy distribution in muscle. *Nature*, **523**, 617–620.

Glancy, B. *et al.* (2017) Power Grid Protection of the Muscle Mitochondrial Reticulum Cell Reports Report Power Grid Protection of the Muscle Mitochondrial Reticulum. *CellReports*, **19**, 487–496.

Goldstein, R.A. *et al.* (2009) Cocaine: History, Social Implications, and Toxicity-A Review. *Disease-a-Month*, **55**, 6–38.

Golomb, B. a. and Evans, M. a. (2008) Statin adverse effects: A review of the literature and evidence for a mitochondrial mechanism. *Am. J. Cardiovasc. Drugs*, **8**, 373–418.

Goodman, C.A. *et al.* (2015) Statin-induced increases in atrophy gene expression occur independently of changes in PGC1?? protein and mitochondrial content. *PLoS One*, **10**, 1–18.

Gorman, G.S. *et al.* (2015) Prevalence of nuclear and mitochondrial DNA mutations related to adult mitochondrial disease. *Ann. Neurol.*, **77**, 753–759.

Green, A.R. *et al.* (2004) A review of the mechanisms involved in the acute MDMA (ecstasy)-induced hyperthermic response. *Eur. J. Pharmacol.*, **500**, 3–13.

Greenberg, S.A. *et al.* (2005) Interferon-α/β-mediated innate immune mechanisms in dermatomyositis. *Ann. Neurol.*, **57**, 664–678.

Gruver-Yates, A.L. and Cidlowski, J.A. (2013) Tissue-specific actions of glucocorticoids on apoptosis: a double-edged sword. *Cells*, **2**, 202–23.

La Guardia, P.G. *et al.* (2013) Protection of rat skeletal muscle fibers by either L-carnitine or coenzyme Q10 against statins toxicity mediated by mitochondrial reactive oxygen generation. *Front. Physiol.*, **4 MAY**, 1–10.

Guengerich, F.P. (2011) Mechanisms of drug toxicity and relevance to pharmaceutical development. *Drug Metab. Pharmacokinet.*, **26**, 3–14.

Guis, S. *et al.* (2003) Drug-induced and toxic myopathies.

Guo, Y. *et al.* (2012) The use of next generation sequencing technology to study the effect of radiation therapy on mitochondrial DNA mutation. *Mutat. Res.*, **744**, 154–160.

Guzmán-Fulgencio, M. *et al.* (2013) European mitochondrial haplogroups are associated with CD41 T cell recovery in HIV-infected patients on combination antiretroviral therapy. *J. Antimicrob. Chemother.*, **68**, 2349–2357.

Hamelin, B. (1998) Hydrophilicity/ lipophilicity: relevance for the pharmacology and clinical effects of HMG-CoA reductase inhibitors. *Trends Pharmacol. Sci.*, **19**, 26–37.

Hanai, J.I. *et al.* (2007) The muscle-specific ubiquitin ligase atrogin-1/MAFbx mediates statin-induced muscle toxicity. *J. Clin. Invest.*, **117**, 3940–3951.

Harper, C.R. and Jacobson, T.A. (2007) The broad spectrum of statin myopathy: from myalgia to rhabdomyolysis. *Curr. Opin. Lipidol.*, **18**.

Hendrickson, S.L. *et al.* (2009) Mitochondrial DNA Haplogroups influence lipoatrophy after Highly Active Anti-retroviral Therapy. *J. Acquir. Immune Defic. Syndr.*, **51**, 111–116.

Herbert, E.K. *et al.* (2018) Skeletal Muscle Mitochondrial Toxicity. *Mitochondrial Dysfunct. Caused by Drugs Environ. Toxicants*.

Hermann, M. *et al.* (2005) Determination of atorvastatin and metabolites in human plasma with solid-phase extraction followed by LC–tandem MS. *Anal. Bioanal. Chem.*, **382**, 1242–1249.

Herzberg, N.H. *et al.* (1993) Differentiation and proliferation of respiration-deficient human myoblasts. *BBA - Mol. Basis Dis.*, **1181**, 63–67.

Van Den Heuvel, L. *et al.* (2010) Mitochondrial translation and beyond: Processes implicated in combined oxidative phosphorylation deficiencies. *J. Biomed. Biotechnol.*, **2010**.

Hill, B.G. *et al.* (2012) Integration of cellular bioenergetics with mitochondrial quality control and autophagy. *Biol. Chem.*, **393**, 1485–1512.

Hinds, S. *et al.* (2011) The role of extracellular matrix composition in structure and function of bioengineered skeletal muscle. *Biomaterials*, **32**, 3575–3583.

Hirst, J. (2005) Energy transduction by respiratory complex I - an evaluation of current knowledge. *Biochem. Soc. Trans.*, **33**, 525–529.

Hoffmann, M. and Nowosielski, M. (2008) DFT study on hydroxy acid-lactone interconversion of statins: the case of atorvastatin. *Org. Biomol. Chem.*, **6**, 3527–31.

Holt, I.J. *et al.* (2000) Coupled Leading- and Lagging-Strand Synthesis of Mammalian Mitochondrial DNA. *Cell*, **100**, 515–524.

Houten, S.M. and Wanders, R.J.A. (2010) A general introduction to the biochemistry of mitochondrial fatty acid β-oxidation. *J. Inherit. Metab. Dis.*, **33**, 469–477.

Hubacek, J.A. *et al.* (2015) Association between polymorphism within the RYR2 receptor and development of statin-associated myalgia/myopathy in the Czech population. *Eur. J. Intern. Med.*, **26**, 367–368.

Hudson, G. *et al.* (2014) Recent mitochondrial DNA mutations increase the risk of

developing common late-onset human diseases. *PLoS Genet.*, **10**, e1004369–e1004369.

Hur, J. *et al.* (2014) Drug-Induced Rhabdomyolysis: From Systems Pharmacology Analysis to Biochemical Flux. *Chem. Res. Toxicol.*, **27**, 421–432.

Husband, A. (2009) Managing statin-induced myopathy. *Clin. Pharm.*, **1**, 319–320.

Hüttemann, M. *et al.* (2007) Regulation of mitochondrial oxidative phosphorylation through cell signaling. *Biochim. Biophys. Acta - Mol. Cell Res.*, **1773**, 1701–1720.

Hynes, J. *et al.* (2013) A high-throughput dual parameter assay for assessing drug-induced mitochondrial dysfunction provides additional predictivity over two established mitochondrial toxicity assays. *Toxicol. Vitr.*, **27**, 560–569.

Jastroch, M. *et al.* (2010) Mitochondrial proton and electron leaks. *Essays Biochem.*, **47**, 53–67.

Jiménez-Sousa, M.A. *et al.* (2015) Mitochondrial DNA haplogroups are associated with severe sepsis and mortality in patients who underwent major surgery. *J. Infect.*, **70**, 20–29.

Johnson, T.E. (2008) Skeletal Muscle and Mitochondrial Toxicity. *Drug-Induced Mitochondrial Dysfunct.*

Jones, J.D. *et al.* (2014) The causes of drug-induced muscle toxicity. *Curr. Opin. Rheumatol.*, **26**, 697–703.

Juhas, M. and Bursac, N. (2014) Roles of adherent myogenic cells and dynamic culture in engineered muscle function and maintenance of satellite cells. *Biomaterials*, **35**, 9438–9446.

Jung, J.A. *et al.* (2012) Pharmacokinetic interaction between pitavastatin and valsartan: a randomized, open-labeled crossover study in healthy male Korean volunteers. *Clin. Ther.*, **34**, 958–965.

Kamalian, L. *et al.* (2018) The utility of HepaRG cells for bioenergetic investigation and detection of drug-induced mitochondrial toxicity. *Toxicol. Vitr.*, **53**, 136–147.

Kamalian, L. *et al.* (2015) The utility of HepG2 cells to identify direct mitochondrial dysfunction in the absence of cell death. *Toxicol. Vitr.*, **29**, 732–740.

Kampira, E. *et al.* (2013) Mitochondrial DNA subhaplogroups L0a2 and L2a modify susceptibility to peripheral neuropathy in Malawian adults on stavudine containing highly active antiretroviral therapy. *J. Acquir. Immune Defic. Syndr.*, **63**, 647–652.

Karalaki, M. *et al.* (2009) Muscle regeneration: cellular and molecular events. *In Vivo*, **23**, 779–96.

Kase, E.T. *et al.* (2013) Remodeling of Oxidative Energy Metabolism by Galactose Improves Glucose Handling and Metabolic Switching in Human Skeletal Muscle Cells. *PLoS One*, **8**.

Kashani, A. *et al.* (2006) Risks Associated With Statin Therapy: A Systematic Overview of Randomized Clinical Trials. *Circulation*, **114**, 2788–2797.

Katajisto, P. *et al.* (2015) Asymmetric apportioning of aged mitochondria between daughter cells is required for stemness. *Science (80-.).*, **348**, 340–343.

Kaufmann, P. *et al.* (2006) Toxicity of statins on rat skeletal muscle mitochondria. *Cell. Mol. Life Sci.*, **63**, 2415–2425.

Kenney, M.C. *et al.* (2014) Molecular and Bioenergetic Differences between Cells with African versus European Inherited Mitochondrial DNA Haplogroups: Implications for Population Susceptibility to Diseases. *Biochim. Biophys. Acta*, **1842**, 208–219.

Khodabukus, A. and Baar, K. (2015) Contractile and metabolic properties of engineered skeletal muscle derived from slow and fast phenotype mouse muscle. *J. Cell. Physiol.*, **230**, 1750–1757.

Kloss-Brandstatter, A. *et al.* (2015) Validation of Next-Generation Sequencing of Entire Mitochondrial Genomes and the Diversity of Mitochondrial DNA Mutations in Oral Squamous Cell Carcinoma. *PLoS One*, **10**, e0135643.

Kobayashi, M. *et al.* (2006) Inhibitory effects of statins on human monocarboxylate transporter 4. *Int. J. Pharm.*, **317**, 19–25.

Kobayashi, M. (2015) Role of Monocarboxylate Transporter in Statin-induced Cytotoxicity. *Yakugaku Zasshi*, **135**, 1227–1233.

Kobayashi, M. *et al.* (2005) Transport mechanism for L-lactic acid in human myocytes using human prototypic embryonal rhabdomyosarcoma cell line {(RD} cells). *Biol. Pharm. Bull.*, **28**, 1197–1201.

Koboldt, D.C. *et al.* (2009) VarScan: variant detection in massively parallel sequencing of individual and pooled samples. *Bioinformatics*, **25**, 2283–2285.

Koboldt, D.C. *et al.* (2012) VarScan 2: somatic mutation and copy number alteration discovery in cancer by exome sequencing. *Genome Res.*, **22**, 568–576.

Koh, K.K. *et al.* (2012) Caveats to aggressive lowering of lipids by specific statins. *Int. J. Cardiol.*, **154**, 97–101.

Kukat, A. *et al.* (2008) Generation of ρ0 cells utilizing a mitochondrially targeted restriction endonuclease and comparative analyses. *Nucleic Acids Res.*, **36**.

Kukat, C. *et al.* (2011) Super-resolution microscopy reveals that mammalian mitochondrial nucleoids have a uniform size and frequently contain a single copy of mtDNA. *Proc. Natl. Acad. Sci.*, **108**, 13534–13539.

Kuncl, R.W. and Meltzer, H.Y. (1974) Pathologic effect of phencylidine and restraint on rat skeletal muscle structure: Prevention by prior denervation. *Exp. Neurol.*, **45**, 387–402.

Kuznetsov, A. V *et al.* (2008) Analysis of mitochondrial function in situ in permeabilized muscle fibers, tissues and cells. *Nat Protoc*, **3**, 965–976.

Kwak, H.B. *et al.* (2012) Simvastatin impairs ADP-stimulated respiration and increases mitochondrial oxidative stress in primary human skeletal myotubes. *Free Radic. Biol. Med.*, **52**, 198–207.

Kwee, B.J. and Mooney, D.J. (2017) Biomaterials for skeletal muscle tissue engineering. *Curr. Opin. Biotechnol.*, **47**, 16–22.

Laaksonen, R. *et al.* (1994) Serum ubiquinone concentrations after short- and long-term treatment with HMG-CoA reductase inhibitors. *Eur. J. Clin. Pharmacol.*, **46**, 313–317.

Laaksonen, R. *et al.* (1996) The effect of Simvastatin treatment on natural antioxidants in low-density lipoproteins and high-energy phosphates and ubiquinone in skeletal muscle•. *Am. J. Cardiol.*, **77**, 851–854.

Lam, M.T. *et al.* (2009) Microfeature guided skeletal muscle tissue engineering for highly organized 3-dimensional free-standing constructs. *Biomaterials*, **30**, 1150–1155.

Larsen, S. *et al.* (2013) Simvastatin effects on skeletal muscle: Relation to decreased mitochondrial function and glucose intolerance. *J. Am. Coll. Cardiol.*, **61**, 44–53.

Larsson, N.-G. (2010) Somatic Mitochondrial DNA Mutations in Mammalian Aging. *Annu. Rev. Biochem.*, **79**, 683–706.

Laufs, U. *et al.* (2015) Treatment Options for Statin-Associated Muscle Symptoms. *Dtsch. Arztebl. Int.*, **112**, 748–755.

Leone, T.C. *et al.* (2005) PGC-1?? deficiency causes multi-system energy metabolic derangements: Muscle dysfunction, abnormal weight control and hepatic steatosis. *PLoS Biol.*, **3**, 0672–0687.

Li, H. *et al.* (2009) The Sequence Alignment/Map format and SAMtools. *Bioinformatics*, **25**, 2078–2079.

Li, H. and Durbin, R. (2009) Fast and accurate short read alignment with Burrows-Wheeler transform. *Bioinformatics*, **25**, 1754–1760.

Li, M. *et al.* (2010) Detecting heteroplasmy from high-throughput sequencing of complete human mitochondrial DNA genomes. *Am. J. Hum. Genet.*, **87**, 237–249.

Li, Y. *et al.* (2012) Mitochondrial dysfunction induced by sertraline, an antidepressant agent. *Toxicol. Sci.*, **127**, 582–591.

Liantonio, A. *et al.* (2007) Fluvastatin and Atorvastatin Affect Calcium Homeostasis of Rat Skeletal Muscle Fibers in Vivo and in Vitro by Impairing the Sarcoplasmic Reticulum / Mitochondria Ca 2 ƨ -Release System. **321**, 626–634.

Lieber, R.L. (2002) Skeletal muscle structure, function and plasticity : the physiological basis of rehabilitation 2nd ed. Lippincott Williams & Wilkins.

Lin, J. *et al.* (2005) Metabolic control through the PGC-1 family of transcription coactivators. *Cell Metab.*, **1**, 361–370.

Lin, J. *et al.* (2002) Transcriptional co-activator PGC-1α drives the formation of slow-twitch muscle fibres. *Nature*, **418**, 797–801.

Link, E. *et al.* (2008) SLCO1B1 variants and statin-induced myopathy--a genomewide study. *N. Engl. J. Med.*, **359**, 789–799.

Liu, X. *et al.* (2013) Variant Callers for Next-Generation Sequencing Data: A Comparison Study. *PLoS One*, **8**, e75619.

Luzum, J.A. *et al.* (2015) GATM polymorphism associated with the risk for statin-induced myopathy does not replicate in case-control analysis of 715 dyslipidemic individuals.

Cell Metab., **21**, 622–627.

Madden, L. *et al.* (2015) Bioengineered human myobundles mimic clinical responses of skeletal muscle to drugs. *Elife*, **2015**, 1–14.

Mamchaoui, K. *et al.* (2011) Immortalized pathological human myoblasts: towards a universal tool for the study of neuromuscular disorders. *Skelet. Muscle*, **1**, 34.

Mammen, A.L. *et al.* (2012) Increased frequency of DRB1*11:01 in anti-hydroxymethylglutaryl- coenzyme a reductase-associated autoimmune myopathy. *Arthritis Care Res.*, **64**, 1233–1237.

Mammen, A.L. (2012) Toxic myopathies. *Clin. NEUROTOXICOLOGY Syndr. Subst. Environ.*, 1634–1649.

Mangravite, L.M. *et al.* (2013) A statin-dependent QTL for GATM expression is associated with statin-induced myopathy. *Nature*, **502**, 377–380.

Marciante, K.D. *et al.* (2011) Cerivastatin, genetic variants, and the risk of rhabdomyolysis. *Pharmacogenet. Genomics*, **21**, 280–288.

Marcoff, L. and Thompson, P.D. (2007) The Role of Coenzyme Q10 in Statin-Associated Myopathy. *J. Am. Coll. Cardiol.*, **49**, 2231–2237.

Marroquin, L.D. *et al.* (2007) Circumventing the crabtree effect: Replacing media glucose with galactose increases susceptibility of hepG2 cells to mitochondrial toxicants. *Toxicol. Sci.*, **97**, 539–547.

Martin, N.R.W. *et al.* (2013a) Factors affecting the structure and maturation of human tissue engineered skeletal muscle. *Biomaterials*, **34**, 5759–5765.

Martin, N.R.W. *et al.* (2013b) Factors affecting the structure and maturation of human tissue engineered skeletal muscle. *Biomaterials*, **34**, 5759–5765.

Mastaglia, F.L. (1982) Adverse Effects of Drugs on Muscle. *Drugs*, **24**, 304–321.

Mastaglia, F.L. and Needham, M. (2012) Update on toxic myopathies. *Curr. Neurol. Neurosci. Rep.*, **12**, 54–61.

Mathur, A. *et al.* (2016) In Vitro Cardiac Tissue Models: Current Status and Future Prospects. *Adv. Drug Deliv. Rev.*, **96**, 203–213.

Matthews, A. *et al.* (2016) Impact of statin related media coverage on use of statins: interrupted time series analysis with UK primary care data. *Bmj*, **353**, 1670–1681.

McKenna, A. *et al.* (2010) The Genome Analysis Toolkit: a MapReduce framework for analyzing next-generation DNA sequencing data. *Genome Res.*, **20**, 1297–1303.

de Mello, A.H. *et al.* (2018) Mitochondrial dysfunction in obesity. *Life Sci.*, **192**, 26–32.

Meltzer, H.Y. (2000) Massive serum creatine kinase increases with atypical antipsychotic drugs: what is the mechanism and the message? *Psychopharmacology (Berl).*, **150**, 349–350.

Mercy, L. *et al.* (2005) Mitochondrial biogenesis in mtDNA-depleted cells involves a Ca2+-dependent pathway and a reduced mitochondrial protein import. *FEBS J.*, **272**, 5031–

5055.

Micheloud, D. *et al.* (2011) European mitochondrial DNA haplogroups and metabolic disorders in HIV/HCV-coinfected patients on highly active antiretroviral therapy. *J. Acquir. Immune Defic. Syndr.*, **58**, 371–8.

Mirosevic Skvrce, N. *et al.* (2015) ABCG2 gene polymorphisms as risk factors for atorvastatin adverse reactions: a case-control study. *Pharmacogenomics*, **16**, 803–815.

Mookerjee, S.A. and Brand, M.D. (2015) Measurement and Analysis of Extracellular Acid Production to Determine Glycolytic Rate. **2**, 1–9.

Morgan, J.E. and Wikstrom, M. (1991) Steady-state redox behavior of cytochrome c, cytochrome a, and CuA of cytochrome c oxidase in intact rat liver mitochondria. *Biochemistry*, **30**, 948–958.

Morgan, R.E. *et al.* (2012) Comparison of the safety, tolerability, and pharmacokinetic profile of a single oral dose of pitavastatin 4 mg in adult subjects with severe renal impairment not on hemodialysis versus healthy adult subjects. *J. Cardiovasc. Pharmacol.*, **60**, 42–48.

Mück, W. (2000) Clinical Pharmacokinetics of Cerivastatin. *Clin. Pharmacokinet.*, **39**, 99–116.

Mulder, A.B. *et al.* (2001) Association of polymorphism in the cytochrome CYP2D6 and the efficacy and tolerability of simvastatin. *Clin. Pharmacol. Ther.*, **70**, 546–551.

Mullen, P.J. *et al.* (2010) Effect of simvastatin on cholesterol metabolism in C2C12 myotubes and HepG2 cells, and consequences for statin-induced myopathy. *Biochem. Pharmacol.*, **79**, 1200–1209.

Mullen, P.J. *et al.* (2011) Susceptibility to simvastatin-induced toxicity is partly determined by mitochondrial respiration and phosphorylation state of Akt. *Biochim. Biophys. Acta - Mol. Cell Res.*, **1813**, 2079–2087.

Murphy, M.P. (2009) How mitochondria produce reactive oxygen species. *Biochem. J.*, **417**, 1–13.

Nadanaciva, S., Dykens, J.A., *et al.* (2007a) Mitochondrial impairment by PPAR agonists and statins identified via immunocaptured OXPHOS complex activities and respiration. *Toxicol. Appl. Pharmacol.*, **223**, 277–287.

Nadanaciva, S., Bernal, A., *et al.* (2007b) Target identification of drug induced mitochondrial toxicity using immunocapture based OXPHOS activity assays. *Toxicol. Vitr.*, **21**, 902–911.

Nakahara, K. *et al.* (1998) Myopathy induced by HMG-CoA reductase inhibitors in rabbits: A pathological, electrophysiological, and biochemical study. *Toxicol. Appl. Pharmacol.*, **152**, 99–106.

Navarese, E.P. *et al.* (2013) Meta-Analysis of Impact of Different Types and Doses of Statins on New-Onset Diabetes Mellitus. *Am. J. Cardiol.*, **111**, 1123–1130.

Nehlin, J.O. *et al.* (2011) Human myotubes from myoblast cultures undergoing senescence

exhibit defects in glucose and lipid metabolism. *Biogerontology*, **12**, 349–365.

Neiman, M. and Taylor, D.R. (2009) The causes of mutation accumulation in mitochondrial genomes. *Proceedings. Biol. Sci.*, **276**, 1201–1209.

Neroldova, M. *et al.* (2016) Rare variants in known and novel candidate genes predisposing to statin-associated myopathy. *Pharmacogenomics*, **17**, 1405–1414.

Neunhäuserer, D. *et al.* (2011) Human skeletal muscle: Transition between fast and slow fibre types. *Pflugers Arch. Eur. J. Physiol.*, **461**, 537–543.

Nickens, K.P. *et al.* (2013) A bioenergetic profile of non-transformed fibroblasts uncovers a link between death-resistance and enhanced spare respiratory capacity. *Mitochondrion*, **13**, 662–667.

O'Keeffe, A.G. *et al.* (2016) Time trends in the prescription of statins for the primary prevention of cardiovascular disease in the United Kingdom: a cohort study using The Health Improvement Network primary care data. *Clin. Epidemiol.*, **8**, 123–132.

Obayashi, H. *et al.* (2011) Cerivastatin induces type-I fiber-, not type-II fiber-, predominant muscular toxicity in the young male F344 rats. *J. Toxicol. Sci.*, **36**, 445–452.

Oh, J. *et al.* (2007) Genetic determinants of statin intolerance. *Lipids Health Dis.*, **6**, 7.

Ostrovidov, S. *et al.* (2013) Micro- and Nanoengineering Approaches to Developing Gradient Biomaterials Suitable for Interface Tissue Engineering. *Micro Nanotechnologies Eng. Stem Cells Tissues*.

Ostrovidov, S. *et al.* (2014) Skeletal Muscle Tissue Engineering: Methods to Form Skeletal Myotubes and Their Applications. *Tissue Eng. Part B Rev.*, **20**, 403–436.

van Oven, M. (2015) PhyloTree Build 17: Growing the human mitochondrial DNA tree. *Forensic Sci. Int. Genet. Suppl. Ser.*, **5**, e392–e394.

Ovesjo, M.-L. *et al.* (2016) Low Vitamin D Levels and Genetic Polymorphism in the Vitamin D Receptor are Associated with Increased Risk of Statin-Induced Myopathy. *Basic Clin. Pharmacol. Toxicol.*, **118**, 214–218.

Paiva, H. *et al.* (2005) High-dose statins and skeletal muscle metabolism in humans: a randomized, controlled trial. *Clin. Pharmacol. Ther.*, **78**, 60–68.

Park, S.Y. *et al.* (2005) Depletion of mitochondrial DNA causes impaired glucose utilization and insulin resistance in L6 GLUT4myc myocytes. *J. Biol. Chem.*, **280**, 9855–9864.

Pasnoor, M. *et al.* (2014) Toxic Myopathies. *Neurol. Clin.*, **32**, 647–670.

Pasternak, R.C. *et al.* (2002) ACC / AHA / NHLBI Clinical Advisory on Statins ACC / AHA / NHLBI Clinical Advisory on the Use and Safety of Statins. *J. Am. Coll. Cardiol.*, **40**, 1024–1028.

Patel, R. *et al.* (1979) Myoglobinuric Acute Renal Failure Associated With Phencyclidine Abuse. *West. J. Med.*, **131**, 244–247.

Pereira, C. V *et al.* (2012) Mitochondrial bioenergetics and drug-induced toxicity in a panel of mouse embryonic fibroblasts with mitochondrial DNA single nucleotide polymorphisms. *Toxicol. Appl. Pharmacol.*, **264**, 167–181.

Perry, C.G.R. *et al.* (2013) Methods for assessing mitochondrial function in diabetes. *Diabetes*, **62**, 1041–1053.

Perry, S.W. *et al.* (2011) Mitochondrial membrane potential probes and the proton gradient: A practical usage guide. *Biotechniques*, **50**, 98–115.

Pette, D. and Staron, R.S. (1990) Cellular and molecular diversities of mammalian skeletal muscle fibers.

Pette, D. and Staron, R.S. (2000) Myosin isoforms, muscle fiber types, and transitions. *Microsc. Res. Tech.*, **50**, 500–509.

Pfleger, J. *et al.* (2015) Mitochondrial complex II is a source of the reserve respiratory capacity that is regulated by metabolic sensors and promotes cell survival. *Cell Death Dis*, **6**, e1835.

Phillips, P.S. *et al.* (2002) Statin-associated myopathy with normal creatine kinase levels. *Ann. Intern. Med.*, **137**, 581–585.

Pierno, S. *et al.* (1995) Potential risk of myopathy by HMG-CoA reductase inhibitors: a comparison of pravastatin and simvastatin effects on membrane electrical properties of rat skeletal muscle fibers. *J. Pharmacol. Exp. Ther.*, **275**, 1490–1496.

Pierno, S. *et al.* (2009) Statins and fenofibrate affect skeletal muscle chloride conductance in rats by differently impairing ClC-1 channel regulation and expression. *Br. J. Pharmacol.*, **156**, 1206–1215.

Piette, A.B. *et al.* (2016) A short-term statin treatment changes the contractile properties of fast-twitch skeletal muscles. *BMC Musculoskelet. Disord.*, **17**, 1–7.

De Pinieux, G. *et al.* (1996) Lipid-lowering drugs and mitochondrial function: effects of HMG-CoA reductase inhibitors on serum ubiquinone and blood lactate/pyruvate ratio. *Br. J. Clin. Pharmacol.*, **42**, 333–337.

Pohjoismäki, J.L.O. *et al.* (2010) Mammalian mitochondrial DNA replication intermediates are essentially duplex, but contain extensive tracts of RNA/DNA hybrid. *J. Mol. Biol.*, **397**, 1144–1155.

Prueksaritanont, T., Tang, C., *et al.* (2002) Effects of fibrates on metabolism of statins in human hepatocytes. *Drug Metab. Dispos.*, **30**, 1280–1287.

Prueksaritanont, T., Subramanian, R., *et al.* (2002) Glucuronidation of statins in animals and humans: A novel mechanism of statin lactonization. *Drug Metab. Dispos.*, **30**, 505–512.

Purcell, H. (2013) Cardiovascular consequences of obesity: how will the UK cope? *Drugs Context*, **2013**, 212247.

Qazi, T.H. *et al.* (2015) Biomaterials based strategies for skeletal muscle tissue engineering: Existing technologies and future trends. *Biomaterials*, **53**, 502–521.

Rahman, S. *et al.* (2001) Decrease of 3243 ArG mtDNA Mutation from Blood in MELAS Syndrome: A Longitudinal Study.

Rajpathak, S.N. *et al.* (2009) Statin Therapy and Risk of Developing Type 2 Diabetes: A Meta-Analysis. *Diabetes Care*, **32**, 1924 LP-1929.

Rana, P. *et al.* (2011) Toxicology in Vitro Mitochondrial membrane potential measurement of H9c2 cells grown in high-glucose and galactose-containing media does not provide additional predictivity towards mitochondrial assessment. *Toxicol. Vitr.*, **25**, 580–587.

Rebelo, A.P. *et al.* (2011) Mitochondrial DNA transcription regulation and nucleoid organization. *J. Inherit. Metab. Dis.*, **34**, 941–951.

Reitzer, L.J. *et al.* (1979) Evidence that glutamine, not sugar, is the major energy source for cultured HeLa cells. *J. Biol. Chem.* , **254**, 2669–2676.

Richards, J.R. (2000) Rhabdomyolysis and drugs of abuse. *J. Emerg. Med.*, **19**, 51–56.

Richter, E.A. and Hargreaves, M. (2013) Exercise, GLUT4, and Skeletal Muscle Glucose Uptake. *Physiol. Rev.*, **93**, 993–1017.

Riedmaier, S. *et al.* (2010) UDP-glucuronosyltransferase (UGT) polymorphisms affect atorvastatin lactonization in vitro and in vivo. *Clin. Pharmacol. Ther.*, **87**, 65–73.

Robinson, N.C. (1993) Functional binding of cardiolipin to cytochrome c oxidase. *J. Bioenerg. Biomembr.*

Rodríguez-Enríquez, S. *et al.* (2001) Multisite control of the Crabtree effect in ascites hepatoma cells. *Eur. J. Biochem.*, **268**, 2512–2519.

Rolfe, D.F. *et al.* (1999) Contribution of mitochondrial proton leak to respiration rate in working skeletal muscle and liver and to SMR. *Am. J. Physiol.*, **276**, C692–C699.

Roostalu, U. *et al.* (2007) Origin and expansion of haplogroup H, the dominant human mitochondrial DNA lineage in west Eurasia: The Near Eastern and Caucasian perspective. *Mol. Biol. Evol.*, **24**, 436–448.

Rossignol, R. *et al.* (2003) Mitochondrial threshold effects. *Biochem. J.*, **370**, 751–62.

Ruano, G. *et al.* (2011) Mechanisms of statin-induced myalgia assessed by physiogenomic associations. *Atherosclerosis*, **218**, 451–456.

Ruano, G. *et al.* (2007) Physiogenomic association of statin-related myalgia to serotonin receptors. *Muscle Nerve*, **36**, 329–335.

Russo, M.W. *et al.* (2009) Drug-induced liver injury associated with statins. *Semin. Liver Dis.*, **29**, 412–422.

Rutter, J. *et al.* (2010) Succinate Dehydrogenase—Assembly, Regulation and Role in Human Disease. *Mitochondrion*, **10**, 393–401.

Sacher, J. *et al.* (2005) Delineation of Myotoxicity Induced by 3-Hydroxy-3- methylglutaryl CoA Reductase Inhibitors in Human Skeletal Muscle Cells. *Pharmacology*, **314**, 1032–1041.

Sahni, V. *et al.* (2008) Unusual complications of heroin abuse: Transverse myelitis, rhabdomyolysis, compartment syndrome, and ARF. *Clin. Toxicol.*, **46**, 153–155.

Sakamoto, K. and Kimura, J. (2013) Mechanism of Statin-Induced Rhabdomyolysis. *J. Pharmacol. Sci.*, **123**, 289–294.

Salabei, J.K. *et al.* (2014) Comprehensive measurement of respiratory activity in

permeabilized cells using extracellular flux analysis. *Nat. Protoc.*, **9**, 421–38.

Salway, J.G. (2004) Metabolism at a glance 3rd ed. Blackwell Pub.

Sanuki, Y. *et al.* (2017) A rapid mitochondrial toxicity assay utilizing rapidly changing cell energy metabolism. **42**, 349–358.

Sathasivam, S. (2012) Statin induced myotoxicity. *Eur. J. Intern. Med.*, **23**, 317–24.

Sattar, N. *et al.* (2010) Statins and risk of incident diabetes: a collaborative meta-analysis of randomised statin trials. *Lancet (London, England)*, **375**, 735–742.

Sattar, N. and Taskinen, M.-R. (2012) Statins are diabetogenic--myth or reality? *Atheroscler. Suppl.*, **13**, 1–10.

Scaduto, R.C. and Grotyohann, L.W. (1999) Measurement of Mitochondrial Membrane Potential Using Fluorescent Rhodamine Derivatives. **76**, 469–477.

Scatena, R. *et al.* (2007) The role of mitochondria in pharmacotoxicology: a reevaluation of an old, newly emerging topic. *AJP Cell Physiol.*, **293**, C12–C21.

Schachter, M. (2005) Chemical, pharmacokinetic and pharmacodynamic properties of statins: An update. *Fundam. Clin. Pharmacol.*, **19**, 117–125.

Schaefer, W.H. *et al.* (2004) Evaluation of ubiquinone concentration and mitochondrial function relative to cerivastatin-induced skeletal myopathy in rats. *Toxicol. Appl. Pharmacol.*, **194**, 10–23.

Scheffler, I.E. (2008) Basic Molecular Biology of Mitochondrial Replication. *Drug-Induced Mitochondrial Dysfunct.*

Schick, B. a *et al.* (2007) Decreased skeletal muscle mitochondrial DNA in patients treated with high-dose simvastatin. *Clin. Pharmacol. Ther.*, **81**, 650–653.

Schirris, T.J.J. *et al.* (2015) Statin-Induced Myopathy Is Associated with Mitochondrial Complex III Inhibition. *Cell Metab.*, **22**, 399–407.

Schirris, T.J.J. *et al.* (2015) Statin Lactonization by Uridine 5'-Diphospho-glucuronosyltransferases (UGTs). *Mol. Pharm.*, **12**, 4048–4055.

Schmitt, S. *et al.* (2013) A semi-automated method for isolating functionally intact mitochondria from cultured cells and tissue biopsies. *Anal. Biochem.*, **443**, 66–74.

Schönfeld, P. and Wojtczak, L. (2016) Short- and medium-chain fatty acids in energy metabolism: the cellular perspective. *J. Lipid Res.*, **57**, 943–954.

Schröder, R. *et al.* (2015) Extensive tissue-related and allele-related mtDNA heteroplasmy suggests positive selection for somatic mutations. *Proc. Natl. Acad. Sci.*, **112**, 2491–2496.

Schwab, M. and Schaeffeler, E. (2012) Pharmacogenomics: a key component of personalized therapy. *Genome Med.*, **4**, 93.

Scruggs, E.R. and Dirks Naylor, A.J. (2008) Mechanisms of zidovudine-induced mitochondrial toxicity and myopathy. *Pharmacology*, **82**, 83–88.

Shintaku, J. and Guttridge, D.C. (2016) Analysis of Aerobic Respiration in Intact Skeletal Muscle Tissue by Microplate-Based Respirometry. *Methods Mol. Biol.*, **1460**, 337–343.

Shitara, Y. and Sugiyama, Y. (2006) Pharmacokinetic and pharmacodynamic alterations of 3-hydroxy-3-methylglutaryl coenzyme A (HMG-CoA) reductase inhibitors: Drug-drug interactions and interindividual differences in transporter and metabolic enzyme functions. *Pharmacol. Ther.*, **112**, 71–105.

Short, K.R. *et al.* (2005) Decline in skeletal muscle mitochondrial function with aging in humans. *Proc. Natl. Acad. Sci.*, **102**, 5618–5623.

Sidaway, J. *et al.* (2009) Statin-induced myopathy in the rat: relationship between systemic exposure, muscle exposure and myopathy. *Xenobiotica.*, **39**, 90–98.

Siddiqui, M. *et al.* (2017) A common missense variant of LILRB5 is associated with statin intolerance and myalgia. *Eur. Heart J.*, **38**, 3569–3575.

Siddiqui, M.K. *et al.* (2017) CKM Glu83Gly Is Associated With Blunted Creatine Kinase Variation, but Not With Myalgia. *Circ. Cardiovasc. Genet.*, **10**.

Sieb, J.P. and Gillessen, T. (2003) Iatrogenic and toxic myopathies. *Muscle and Nerve*, **27**, 142–156.

Silber, T.J. (2005) Ipecac syrup abuse, morbidity, and mortality: Isn't it time to repeal its over-the-counter status? *J. Adolesc. Heal.*, **37**, 256–260.

Silva, M.A. *et al.* (2006) Statin-related adverse events: A meta-analysis. *Clin. Ther.*, **28**, 26–35.

Sirvent, P. *et al.* (2012) Muscle mitochondrial metabolism and calcium signaling impairment in patients treated with statins. *Toxicol. Appl. Pharmacol.*, **259**, 263–268.

Sirvent, P., Bordenave, S., *et al.* (2005a) Simvastatin induces impairment in skeletal muscle while heart is protected. *Biochem. Biophys. Res. Commun.*, **338**, 1426–1434.

Sirvent, P., Mercier, J., *et al.* (2005b) Simvastatin triggers mitochondria-induced Ca2+ signaling alteration in skeletal muscle. *Biochem. Biophys. Res. Commun.*, **329**, 1067–1075.

Skarlovnik, A. *et al.* (2014) Coenzyme Q10 supplementation decreases statin-related mild-to-moderate muscle symptoms: a randomized clinical study. *Med. Sci. Monit.*, **20**, 2183–2188.

Skottheim, I.B. *et al.* (2008) Statin induced myotoxicity: The lactone forms are more potent than the acid forms in human skeletal muscle cells in vitro. *Eur. J. Pharm. Sci.*, **33**, 317–325.

Song, S. *et al.* (2005) DNA precursor asymmetries in mammalian tissue mitochondria and possible contribution to mutagenesis through reduced replication fidelity. *Proc. Natl. Acad. Sci.*, **102**, 4990–4995.

du Souich, P. *et al.* (2017) Myotoxicity of statins: Mechanism of action. *Pharmacol. Ther.*

Stefano, B. *et al.* (2004) Safety of Statins. *Circulation*, **109**, III-50-III-57.

Stewart, J.B. and Chinnery, P.F. (2015) The dynamics of mitochondrial DNA heteroplasmy:

implications for human health and disease. *Nat. Rev. Genet.*, **16**, 530–42.

Stringer, H.A.J. *et al.* (2013) Decreased skeletal muscle mitochondrial DNA in patients with statin-induced myopathy. *J. Neurol. Sci.*, **325**, 142–147.

Stroes, E.S. *et al.* (2015) Statin-associated muscle symptoms: impact on statin therapy - European Atherosclerosis Society Consensus Panel Statement on Assessment, Aetiology and Management. *Eur. Heart J.*, **36**, 1012–1022.

Strohman, R.C. *et al.* (1990) Myogenesis and histogenesis of skeletal muscle on flexible membranes in vitro. *Vitr. Cell. Dev. Biol.*, **26**, 201–208.

Sultana, J. *et al.* (2013) Clinical and economic burden of adverse drug reactions. *J. Pharmacol. Pharmacother.*, **4**, S73–S77.

Sun, Q. *et al.* (2015) A mitochondrial DNA mutation influences the apoptotic effect of statins on prostate cancer. *Prostate*, **75**, 1916–1925.

Sutovsky, P. *et al.* (2004) Degradation of paternal mitochondria after fertilization: implications for heteroplasmy, assisted reproductive technologies and mtDNA inheritance. *Reprod. Biomed. Online*, **8**, 24–33.

Swiss, R. *et al.* (2013) Validation of a HTS-amenable assay to detect drug-induced mitochondrial toxicity in the absence and presence of cell death. *Toxicol. Vitr.*, **27**, 1789–1797.

Syverud, B.C. *et al.* (2017) Quantitative, Label-Free Evaluation of Tissue-Engineered Skeletal Muscle Through Multiphoton Microscopy. *Tissue Eng. Part C Methods*, **23**, 616–626.

Taha, D.A. *et al.* (2017) Hyperlipidaemia alone and in combination with acidosis can increase the incidence and severity of statin-induced myotoxicity. *Eur. J. Pharm. Sci.*, **100**, 163–175.

Taha, D.A. *et al.* (2016) The role of acid-base imbalance in statin-induced myotoxicity. *Transl. Res.*, **174**, 140–160.e14.

Tam, E.W.Y. *et al.* (2008) A novel mitochondrial DNA mutation in COX1 leads to strokes, seizures, and lactic acidosis. *Neuropediatrics*, **39**, 328–334.

Tanaka, M. *et al.* (2007) Women with mitochondrial haplogroup N9a are protected against metabolic syndrome. *Diabetes*, **56**, 518–521.

Taylor, B.A. *et al.* (2015) A randomized trial of coenzyme Q10 in patients with confirmed Statin Myopathy. *Atherosclerosis*, **238**, 329–335.

Temperley, R. *et al.* (2010) Hungry Codons Promote Frameshifting in Human Mitochondrial Ribosomes. *Science (80-.).*, **327**, 301 LP-301.

Terada, H. (1990) Uncouplers of oxidative phosphorylation. *Environ. Health Perspect.*, **87**, 213–218.

TeSlaa, T. and Teitell, M.A. (2014) Techniques to monitor glycolysis. *Methods Enzymol.*, **542**, 91–114.

Thapaliya, S. *et al.* (2014) Alcohol-induced autophagy contributes to loss in skeletal muscle mass. *Autophagy*, **10**, 677–690.

Thapar, M. *et al.* (2013) Statins and liver injury. *Gastroenterol. Hepatol. (N. Y).*, **9**, 605–606.

Thompson, P.D. *et al.* (2003) Statin-associated myopathy. *JAMA*, **289**, 1681–1690.

Thompson, W.E. *et al.* (2003) Ubiquitination of Prohibitin in Mammalian Sperm Mitochondria: Possible Roles in the Regulation of Mitochondrial Inheritance and Sperm Quality Control1. *Biol. Reprod.*, **69**, 254–260.

Tiwari, V. and Khokhar, M. (2014) Mechanism of action of anti-hypercholesterolemia drugs and their resistance. *Eur. J. Pharmacol.*, **741**, 156–170.

Tricarico, P. *et al.* (2015) Mevalonate Pathway Blockade, Mitochondrial Dysfunction and Autophagy: A Possible Link. *Int. J. Mol. Sci.*, **16**, 16067–16084.

Truskey, G.A. *et al.* (2013) Design considerations for an integrated microphysiological muscle tissue for drug and tissue toxicity testing. *Stem Cell Res. Ther.*, **4**, S10.

Truskey, G.A. (2018) Development and application of human skeletal muscle microphysiological systems. *Lab Chip*, 3061–3073.

Trusler, D. (2011) Statin prescriptions in UK now total a million each week. *BMJ*, **343**, d4350.

Tuppen, H.A.L. *et al.* (2010) Mitochondrial DNA mutations and human disease. *Biochim. Biophys. Acta - Bioenerg.*, **1797**, 113–128.

Turner, R.M. *et al.* (2015) Parsing interindividual drug variability: An emerging role for systems pharmacology. *Wiley Interdiscip. Rev. Syst. Biol. Med.*, **7**, 221–241.

Turrens, J.F. (2003) Mitochondrial formation of reactive oxygen species. *J. Physiol.*, **552**, 335–344.

Underhill, G.H. and Khetani, S.R. (2018) Bioengineered Liver Models for Drug Testing and Cell Differentiation Studies. *Cell. Mol. Gastroenterol. Hepatol.*, **5**, 426–439.e1.

Vainshtein, A. *et al.* (2015) The role of PGC-1α during acute exercise-induced autophagy and mitophagy in skeletal muscle. *Am. J. Physiol. - Cell Physiol.*, ajpcell.00380.2014.

Vaklavas, C. *et al.* (2009) Molecular basis of statin-associated myopathy. *Atherosclerosis*, **202**, 18–28.

Valiyil, R. and Christopher-Stine, L. (2010) Drug-related myopathies of which the clinician should be aware. *Curr. Rheumatol. Rep.*, **12**, 213–220.

Vandenburgh, H. *et al.* (2008) Drug-screening platform based on the contractility of tissue-engineered muscle. *Muscle Nerve*, **37**, 438–447.

Vaughan, R. a. *et al.* (2013) Ubiquinol rescues simvastatin-suppression of mitochondrial content, function and metabolism: Implications for statin-induced rhabdomyolysis. *Eur. J. Pharmacol.*, **711**, 1–9.

Vernetti, L. *et al.* (2017) Functional Coupling of Human Microphysiology Systems: Intestine, Liver, Kidney Proximal Tubule, Blood-Brain Barrier and Skeletal Muscle. *Sci. Rep.*, **7**, 44517.

Villalba Garcia, M. V *et al.* (1994) Rhabdomyolysis in acute intoxications. *An. Med. Interna*,

11, 119–122.

Vladutiu, G.D. *et al.* (2006) Genetic risk factors associated with lipid-lowering drug-induced myopathies. *Muscle and Nerve*, **34**, 153–162.

Vladutiu, G.D. *et al.* (2011) Genetic risk for malignant hyperthermia in non-anesthesia-induced myopathies. *Mol. Genet. Metab.*, **104**, 167–173.

Voora, D. *et al.* (2009) The SLCO1B1*5 genetic variant is associated with statin-induced side effects. *J. Am. Coll. Cardiol.*, **54**, 1609–1616.

Vuda, M. and Kamath, A. (2016) Drug induced mitochondrial dysfunction: Mechanisms and adverse clinical consequences. *Mitochondrion*.

Vye, M. V. (1976) The ultrastructure of striated muscle. *Ann. Clin. Lab. Sci.*, **6**, 142–151.

Wallace, D.C. (2013) Bioenergetics in human evolution and disease: implications for the origins of biological complexity and the missing genetic variation of common diseases. *Philos. Trans. R. Soc. B Biol. Sci.*, **368**, 20120267–20120267.

Wallace, D.C. and Chalkia, D. (2013) Mitochondrial DNA genetics and the heteroplasmy conundrum in evolution and disease. *Cold Spring Harb. Perspect. Biol.*, **5**, a021220.

Wallace, K.B. and Starkov, A.A. (2000) MITOCHONDRIAL TARGETS OF DRUG TOXICITY. *Annu. Rev. Pharmacol. Toxicol*, **40**, 353–88.

Warburg, O. (1956) Injuring of Respiration the Origin of Cancer Cells. *Science (80-.).*, **123**, 309–14.

Wei, Q. and Paterson, B.M. (2001) Regulation of MyoD function in the dividing myoblast. *FEBS Lett.*, **490**, 171–178.

Weintraub, W.S. (2017) Perspective on Trends in Statin Use. *JAMA Cardiol.*, **2**, 11–12.

Weissensteiner, H. *et al.* (2016) HaploGrep 2: mitochondrial haplogroup classification in the era of high-throughput sequencing. *Nucleic Acids Res.*, **44**, W58–W63.

Welch, R.D. *et al.* (1991) Incidence of cocaine-Associated rhabdomyolysis. *Ann. Emerg. Med.*, **20**, 154–157.

Wende, A.R. *et al.* (2007) A role for the transcriptional coactivator PGC-1α in muscle refueling. *J. Biol. Chem.*, **282**, 36642–36651.

Westerblad, H. *et al.* (2010) Skeletal muscle: Energy metabolism, fiber types, fatigue and adaptability. *Exp. Cell Res.*, **316**, 3093–3099.

Westwood, F.R. *et al.* (2005) Statin-Induced Muscle Necrosis in the Rat: Distribution, Development, and Fibre Selectivity. *Toxicol. Pathol.*, **33**, 246–257.

White, C.M. (2002) A review of the pharmacologic and pharmacokinetic aspects of rosuvastatin. *J. Clin. Pharmacol.*, **42**, 963–970.

White, J. *et al.* (2016) Association of Lipid Fractions With Risks for Coronary Artery Disease and Diabetes. *JAMA Cardiol.*, **1**, 692–699.

Wijers, S.L.J. *et al.* (2008) Human skeletal muscle mitochondrial uncoupling is associated

with cold induced adaptive thermogenesis. *PLoS One*, **3**, 2–6.

Wilkins, H.M. *et al.* (2014) Cytoplasmic hybrid (cybrid) cell lines as a practical model for mitochondriopathies. *Redox Biol.*, **2**, 619–631.

Wojtczak, L. and Zabłocki, K. (2008) Basic Mitochondrial Physiology in Cell Viability and Death. In, *Drug-Induced Mitochondrial Dysfunction*.

Wu, M. *et al.* (2007) Multiparameter metabolic analysis reveals a close link between attenuated mitochondrial bioenergetic function and enhanced glycolysis dependency in human tumor cells. *Am. J. Physiol. Physiol.*, **292**, C125–C136.

Yadava, N. and Nicholls, D.G. (2007) Spare Respiratory Capacity Rather Than Oxidative Stress Regulates Glutamate Excitotoxicity after Partial Respiratory Inhibition of Mitochondrial Complex I with Rotenone. *J. Neurosci.*, **27**, 7310–7317.

Yaffe, D. (1968) Retention of differentiation potentialities during prolonged cultivation of myogenic cells. *Proc. Natl. Acad. Sci. U. S. A.*, **61**, 477–483.

Yaffe, D. and Saxel, O. (1977) Serial passaging and differentiation of myogenic cells isolated from dystrophic mouse muscle. *Nature*, **270**, 725–727.

Yang, Y. *et al.* (2008) Mitochondrial DNA haplogroup R predicts survival advantage in severe sepsis in the Han population. *Genet. Med.*, **10**, 187–192.

Yasukawa, T. *et al.* (2006) Replication of vertebrate mitochondrial DNA entails transient ribonucleotide incorporation throughout the lagging strand. *EMBO J.*, **25**, 5358–5371.

Ye, F. *et al.* (2014) High-throughput sequencing in mitochondrial DNA research. *Mitochondrion*, **17**, 157–163.

Young, J.M. *et al.* (2007) Effect of coenzyme Q(10) supplementation on simvastatin-induced myalgia. *Am. J. Cardiol.*, **100**, 1400–1403.

Zhang, J. *et al.* (2012) Measuring energy metabolism in cultured cells, including human pluripotent stem cells and differentiated cells. *Nat. Protoc.*, **7**, 1068–1085.

Zhang, X. *et al.* (2018) A system to monitor statin-induced myopathy in individual engineered skeletal muscle myobundles. *Lab Chip*, 2787–2796.

Zorlutuna, P. *et al.* (2012) Microfabricated biomaterials for engineering 3D tissues. *Adv. Mater.*, **24**, 1782–1804.